RAA 2015 Vol. **15** No. **12**, 1945–2140 doi: 10.1088/1674–4527/15/12/001
http://www.raa-journal.org *http://www.iop.org/journals/raa*

Research in Astronomy and Astrophysics

Thirty Meter Telescope Detailed Science Case: 2015 *

Warren Skidmore on behalf of the TMT International Science Development Teams & TMT Science Advisory Committee

Thirty Meter Telescope International Observatory, 100 West Walnut Street, Pasadena, California 91105, USA; *was@tmt.org*

Received 2015 April 29; accepted 2015 May 5

Abstract The TMT Detailed Science Case describes the transformational science that the Thirty Meter Telescope will enable. Planned to begin science operations in 2024, TMT will open up opportunities for revolutionary discoveries in essentially every field of astronomy, astrophysics and cosmology, seeing much fainter objects much more clearly than existing telescopes. Per this capability, TMT's science agenda fills all of space and time, from nearby comets and asteroids, to exoplanets, to the most distant galaxies, and all the way back to the very first sources of light in the universe. More than 150 astronomers from within the TMT partnership and beyond offered input in compiling the new 2015 Detailed Science Case. The contributing astronomers represent the entire TMT partnership, including the California Institute of Technology (Caltech), the Indian Institute of Astrophysics (IIA), the National Astronomical Observatories of the Chinese Academy of Sciences (NAOC), the National Astronomical Observatory of Japan (NAOJ), the University of California, the Association of Canadian Universities for Research in Astronomy (ACURA) and US associate partner, the Association of Universities for Research in Astronomy (AURA).

Key words: instrumentation and method — cosmology and nongalactic astrophysics — Earth and planetary astrophysics — astrophysics of galaxies — high energy astrophysical phenomena

1 INTRODUCTION

This is the 2015 Detailed Science Case for the Thirty Meter Telescope (TMT) project, a public document, managed by the TMT Science Advisory Committee (SAC) and updated from the original 2007 version (RD01) with input from the TMT International Science Development Teams. It will be updated as needed during the construction and operations phases of the TMT project. The original Detailed Science Case was developed with the input of the science teams and authors of the 2006 instrument feasibility studies (RD02) and from many scientists across the collaboration. The present updated version builds on the previous work and captures the developments in the envisioned science goals and the status of the first light and future instruments.

* Cover image: artist's rendition of the TMT International Observatory on Mauna Kea opening in the late evening before beginning operations.

1.1 Purpose and Scope

The Detailed Science Case (DSC) is the highest-level statement of the TMT science case. It provides examples of the kinds of exciting, groundbreaking science that will be enabled by a 30 m telescope. Wherever possible, synergies with other major new and upcoming facilities (e.g. the Atacama Large Millimeter/submillimeter Array (ALMA), Large Synoptic Survey Telescope (LSST) and the James Webb Space Telescope (JWST)) are discussed. As appropriate, performance numbers (often conservative) are provided (e.g. sensitivities, integration times, spatial resolutions).

The DSC is not a requirements document. The Science-based Requirements Document (SRD) (RD03) is the highest-level requirements document for TMT.

This document is intended to provide a high-level overview of the TMT science case for the following audiences:

Astronomers within the TMT partnership and international scientific colleagues

Various astronomy strategic working groups and Internal TMT groups

1.2 Applicable and Reference Documents and Change Record

This high-level document has no applicable documents within the TMT Project.

Reference documents contain information complementing, explaining, detailing, or otherwise supporting the information included in the current document.

Documents can be found in the TMT Document Control Center (DCC) using their internal document number in the following URL: *https://docushare.tmt.org/docushare/dsweb/Get/Document-XXXX*.

	Name	TMT Number	Internal number
RD01	Detailed Science Case: 2007	TMT.PSC.TEC.07.003	8865
RD02	Extracted Instrument Feasibility Studies Science Cases and Operational Concepts: March 2006	TMT.PSC.COR.06.007	5625
RD03	Science-based Requirements Document	TMT.PSC.DRD.05.001	319
RD04	TMT Operations Plan	TMT.OPS.TEC.11.099	21244

Revision	Date	Section	Modifications
REL01	8 Oct 2007	All	First public release
Draft 2	6 July 2014	All	Draft version during major update process

2 OVERVIEW

The TMT will be a 30 m ground based telescope with a collecting area of 664.2 m^2. It will be able to support instruments that are sensitive through the atmospheric windows from 0.31 to 28 μm. Advanced adaptive optics (AO) capabilities will allow highly sensitive, diffraction-limited observations from wavelengths shortward of 1 μm to the mid-infrared (MIR) over most of the sky. A $20'$ diameter field of view (FOV) facilitates the deployment of wide-field, multi-object spectrographs. These capabilities will enable groundbreaking advances in a wide range of scientific areas, from the most distant reaches of the universe to our own solar system. Powerful new facilities have often opened up unimagined areas of research and made important but unanticipated discoveries. We expect the situation with TMT will be no different and hence look forward to a rich and diverse mix of both expected and unexpected scientific results.

2.1 The Big Picture

Decades of advances with ground and space-based facilities have provided a clear and convincing picture of the overall history of our universe. We now know that the observable universe began some

13.8 billion years ago when a small region of empty space became unstable and began to expand, rapidly increasing in size by some twenty or thirty orders of magnitude. This period of expansion, called inflation, lasted but a tiny fraction of a second, yet it resulted in the production of all matter and energy in our universe. When inflation ended an exceedingly hot mixture of elementary particles of all varieties pervaded space. At the same time, tiny 'quantum' fluctuations in the distribution of this energy were stretched to macroscopic scales by inflation. These fluctuations formed the seeds for the galaxies and clusters of galaxies that we see today.

Following inflation, the universe continued to expand, but at a slower rate. This expansion resulted in cooling of the plasma allowing the elementary particles to combine to form the familiar protons, neutrons, electrons, photons, neutrinos and ultimately hydrogen and helium nuclei. Also present were large quantities of what we now refer to as dark matter and dark energy. During this expansion, the gravitational attraction of the small energy fluctuations resulted in the growth of dark matter density fluctuations.

Some 400 000 years after inflation, the nuclei and electrons combined to form neutral atoms and the universe became transparent to the photons left over from the Big Bang. Today we see those photons as the cosmic microwave background (CMB). Once freed from the drag produced by interactions with those Big Bang photons, the neutral gas began to fall into the denser pockets of dark matter. In a complex process of gravitational accretion and radiative cooling, the first stars formed. The intense radiation produced by this first generation of massive stars heated the surrounding gas, creating bubbles of ionized gas. Initially, the light from these first stars was trapped in these bubbles but as more and more of the surrounding gas was re-ionized, this first light began to propagate throughout the universe.

As star formation continued and dark matter halos merged due to gravitational attraction, the first galaxies were formed. These first galaxies – relatively small collections of stars, gas, and dust caught within the gravitational potential of dark matter halos – merged to form larger more massive galaxies. The end products of this process (known as hierarchical structure formation) surround us today – from the most massive clusters of galaxies, to our home galaxy the Milky Way, and down to its dwarf galaxy neighbors.

Within many galaxies, star formation continues as clouds of gas cool and contract. Dense clouds of molecular gas form stellar nurseries that harbor newly-forming stars. These nascent stars are surrounded by disks of gas and dust within which planets develop. We now know that most stars have some form of planetary system. However we are only able to directly image a very small subset of known planets, a subset of planets that are particularly young, hot and massive compared to the range of known planets in the universe, vastly different from Earth. To attempt to characterize terrestrial exoplanets that are in the habitable zones around their stars will require the use of a 30 m class telescope.

2.2 The Big Questions

The large aperture and FOV of TMT combined with its powerful AO systems and science instruments will provide unique gains in precision astrometry, high contrast imaging and spectroscopy from the ultraviolet (UV) through the MIR to open new regions of discovery space on a number of "Big Questions" reaching from the distant universe to our own solar system:

What is the nature and composition of the universe?

The nature of dark matter and energy, the ingredients that dominate the composition of the universe, remains a complete mystery. The lower limit of the dark matter mass spectrum depends on the nature of the dark particle ("warm" vs "cold"). Diffraction-limited imaging with TMT of anomalies in strong gravitational lenses will probe this limit down to levels at least ten times smaller

than currently possible. Different dark energy models predict different rates of evolution for cosmic distances and structures, and deep spectroscopy of very distant supernovae (SNe) (up to $z = 4$) with TMT will provide a longer timeline over which these changes may be more readily detected.

When did the first galaxies form and how did they evolve?

TMT can study galaxy formation both near and far. It will be able to detect the spectroscopic signatures of metal-free star formation, i.e., of the first stars forming in the first galaxies at redshifts well beyond 10. The sensitivity of TMT will overcome the "photon starvation" plaguing existing 8 m to 10 m telescopes to produce detailed, spatially-resolved maps of morphology, chemistry, and kinematics for galaxies out to $z = 5 - 6$ with a fidelity equivalent to what is currently done at $z < 1$. The large FOV and excellent UV throughput of TMT will enable powerful surveys of stellar abundances and ages in the halo of our own Milky Way over a volume nearly 100 times larger than previously possible to build a far more complete census of the smaller fragments that were hierarchically assembled into this halo. TMT will also be able to perform photometry of spatially-resolved stellar populations in galaxies out to the distance of the Virgo Cluster to provide the first-ever "archeological" sample large enough to unambiguously show the stochastic nature of galaxy assembly.

What is the relationship between black holes and galaxies?

Black holes (BHs) with masses as high as a billion times the mass of the Sun are now known to occupy the centers of galaxies. They warp space-time in fascinating ways, and their formation process is unknown, but it must be intimately linked to galaxy formation. If mass is the link, then the BH mass function should track the galaxy mass function across the entire Hubble sequence and across time. The spatial resolution and sensitivity of TMT will make it possible to measure the BH mass function down to masses ten times smaller and make dynamical measurements in galaxies more than 20 times farther than currently possible. TMT will expand by a factor of 1000 the number of galaxies where direct BH mass measurements can be performed.

How do stars and planets form?

The birth of stars is a fundamental process closely intertwined to galaxy evolution and chemical enrichment in the universe, which ultimately results in the diverse range of planetary systems, and possibly in life itself. And yet at present, we cannot answer the very basic questions, such as what determines the stellar mass, and we are far from understanding when, where, and how planets form. Observations with TMT will play a critical role in providing answers to these questions. The initial mass functions (IMFs) will be obtained for distant young star clusters, not only in the Milky Way but also in other galaxies, in a wide range of environments, which is a necessary step toward the development of a predictive theory of star formation. Morpho-kinematical mapping of protoplanetary disks will unveil the inner 10 AU, which will yield detections of growing planets and reveal the spatial distribution of disk material including water and organic molecules.

What is the nature of extrasolar planets?

Observations made in the last few years with the Kepler space telescope suggest that most stars harbor a planetary system, that Earth-like planets in habitable zones are quite common and that the easy-to-detect hot Jupiter-type planets are the exception rather than the rule. What formation processes give rise to this variety of exoplanetary systems? Investigating the atmospheric characteristics of the closest and brightest hot Jupiter planets has just begun with existing 10 m class

facilities, and, space telescopes can only enable very limited characterization of lava-ocean rocky planets. The ability to study Earth analogs in habitable zones will therefore only come with the advent of 30 m class facilities, and a key question will be whether or not terrestrial type exoplanets have atmospheres similar to that of Earth.

Is there life elsewhere in the universe?

Are conditions on terrestrial planets conducive to the development of life? Every star has a habitable zone, where a planet would have a surface temperature similar to that of Earth. If, as expected, exoplanetary systems have populations of small icy bodies like comets, it is possible that water and organic molecules could have been delivered to such planets by impacts. If life then develops, it might be detected by signatures of biological activity in planetary atmospheres.

2.3 The Required Tools

To answer these questions, and many others, advances in technology are needed. The most progress will come from combined studies at many different wavelengths using ground and space-based facilities. Several major new telescopes will begin operation in the next decade. These include the JWST with a launch date of 2018, covering 0.6 μm to 28 μm near-infrared (NIR) and MIR wavelengths and the ground based optical LSST with commissioning science beginning mid-2022. The highly productive ALMA (0.3 to 1 mm) was completed in June 2014 and will remain the premier millimeter/submillimeter facility for the next couple of decades. The Square Kilometre Array (SKA) (80 cm to 6 m) will follow with the first phase projected for completion in 2025. The ASTRO-H and eROSITA X-ray telescopes have launch dates of 2016 and will provide survey and follow-up capabilities that will be further complemented in 2028 with the launch of the versatile ATHENA X-ray mission. The ground based submillimeter to millimeter CCAT facility, the radio JVLA (6 mm to 5 m) and the Transiting Exoplanet Survey Satellite (TESS) are other facilities with strong scientific synergies with the TMT.

Multi-wavelength observations with these powerful, next-generation facilities will undoubtedly open exciting, new frontiers. Yet they will not alone be sufficient. Much as the resolution of the Hubble Space Telescope (HST) was complemented by the greater light gathering power of the Keck 10 m telescopes, these new facilities will need a complementary large-aperture ground-based telescope that can provide high spatial and spectral resolution observations in the optical and infrared. In fact, a revolution in technical capability now makes ground-based telescopes even more effective. AO systems allow the largest optical-infrared telescopes on Earth to achieve higher resolution than telescopes in space, which necessarily have smaller apertures. By compensating atmospheric turbulence, AO allows telescopes to reach the diffraction limit, in which the angular resolution achieved is proportional to the diameter of the telescope aperture.

A useful figure of merit for telescope performance is the time required to achieve a given signal-to-noise ratio (S/N) for a particular science program or object. The reciprocal of this time is a measure of the sensitivity or productivity of the telescope. Because larger telescopes collect more light, their sensitivity typically increases in proportion to the square of the aperture diameter. In the important case of observations of faint point-like objects, the smaller angular size results in less contamination by background or foreground light from the sky, solar system and Galaxy, so the sensitivity increases in proportion to the fourth power of the diameter. This is an enormous factor, making a 30 m telescope two hundred times more sensitive[1] than an 8 m telescope.

To take advantage of these huge gains in light collection and spatial resolution, TMT will be equipped with a suite of powerful science instruments. The initial selection of first light instrument requirements from a suite of instrument concepts was made in December 2006 by the TMT SAC

[1] Sensitivity here is defined as being inversely proportional to the integration time needed to reach a particular S/N.

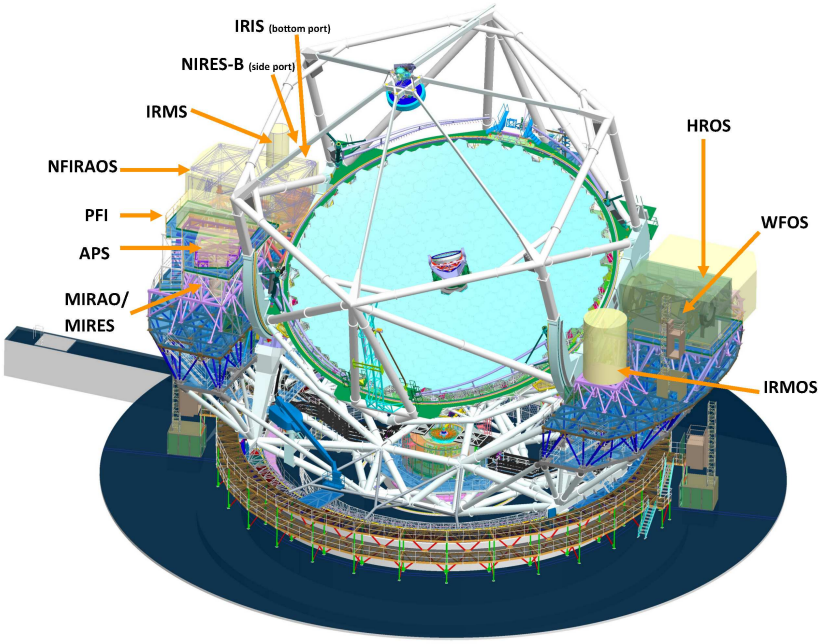

Fig. 1 The conceptual instrument suite located on the Nasmyth platforms of the latest telescope design. The conceptual instrument suite was used to derive the requirements for the observatory to ensure that the telescope was capable of supporting many different instrument types. The first light configuration includes IRIS, WFOS, and IRMS (see Sect. 2.3.1).

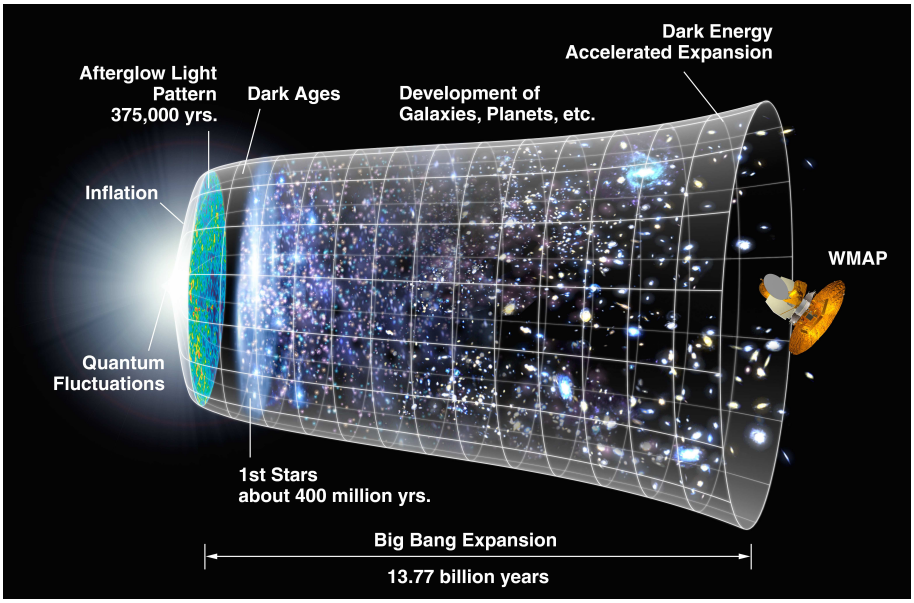

Fig. 2 Schematic history of the universe (Credit: NASA/WMAP Science Team).

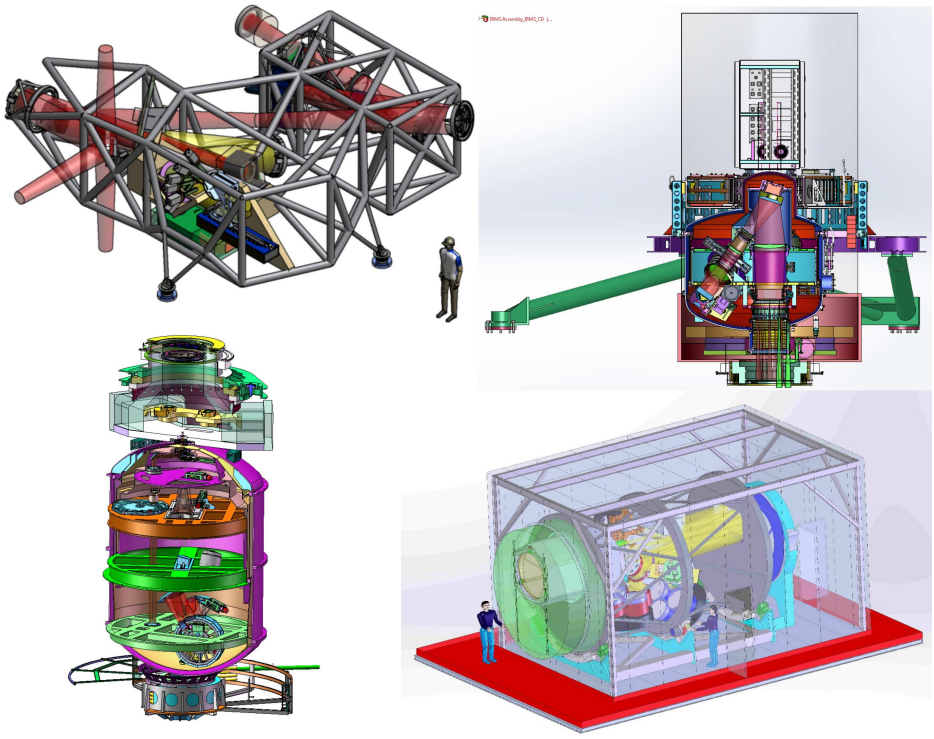

Fig. 3 The first light instrument suite that will be delivered as part of the construction project. The NFIRAOS system (*upper left*), IRMS (*upper right*), IRIS (*lower left*) and WFOS (*lower right*). Both IRIS and IRMS are NFIRAOS client instruments.

based on a careful consideration of the science programs as well as the range of capabilities essential for pursuing science areas that are currently unforeseen. Consideration was also given to technical readiness, cost and schedule. These choices were re-affirmed in 2011 at a project wide science and instrumentation workshop in Victoria. The capabilities of these instruments are summarized briefly in the next sub-sections. All instruments will be mounted and kept operationally ready at all times (except of course for periods of scheduled maintenance or upgrades). It will be possible to switch from one instrument to another in less than 10 minutes (including target acquisition).

2.3.1 First light suite

At first light, TMT plans to deploy a laser guide star supported, multi-conjugate adaptive optics (MCAO) system called NFIRAOS (Narrow Field Infrared Adaptive Optics System, pronounced "nefarious"). NFIRAOS will provide diffraction-limited resolution ($\lambda/D = 0.0055''$ and $0.017''$ at 800 nm and 2.4 μm, respectively) and high Strehl ratios[2] ($\sim 12\%$ to $\sim 77\%$ at 800 nm and 2.4 μm, respectively) over a $30''$ science field-of-view. Sky coverage is expected to be 50% at the Galactic poles. It will be possible to mount up to three instruments on NFIRAOS.

[2] Strehl ratio: When considering an unresolved point source, an AO system can be thought of as gathering a fraction of the light from the seeing disk and concentrating that fraction into an image with a diffraction limited width, superimposed over the remaining uncorrected light. The Strehl ratio is the ratio of the actual peak intensity over the theoretical diffraction limited peak intensity for a perfect image.

One of these instruments will be IRIS (InfraRed Imaging Spectrometer), a combined high-resolution imager and integral field unit (IFU) spectrometer. The direct imaging mode will provide a $34'' \times 34''$ field with 0.004 arcsec/pixel sampling. Both broadband and narrowband filters will be available. The IFU will provide spectral resolving powers of $R = 3500$, 8000 and 10 000 over the entire J, H, and K bands (one band at a time) as well as a choice of coarse and fine plate scales for different science applications. The field-of-view of the IFU ranges from $2.2'' \times 4.5''$ (coarsest scale 0.050″/spaxel) to $0.45'' \times 0.64''$ (finest scale 0.004″/spaxel).

NFIRAOS will also feed IRMS (Infrared Multi-slit Spectrometer). IRMS is a close copy of the very successful and versatile Keck/MOSFIRE instrument, and it leverages the MCAO capability provided by NFIRAOS to boost the amount of light falling within its slitlets. The heart of IRMS (and MOSFIRE) is a cryogenic slit unit that will allow up to 46 slitlets to be configured on-the-fly over a $2.3' \times 2.3'$ field. The entire Y, J, H, and K bands can be covered (one at a time) in one grating setting with a spectral resolution up to $R = 4660$. In imaging mode, IRMS covers the entire NFIRAOS field of regard with $0.06''$ sampling.

The third first-light instrument is WFOS (Wide-Field Optical Spectrometer). WFOS is a seeing-limited instrument that will cover a total spectral range from 0.31 to 1.1 μm using separate red and blue color channels. Three spectral resolution modes will be available ($R = 1000$, 5000 and 8000) with multiplexing factors up to 200 objects over a 25 arcmin^2 field. The original WFOS concept builds upon the heritage of such workhorse instruments as Keck/DEIMOS and Magellan/IMACS.

2.3.2 First light instruments Exposure Time Calculators

A comprehensive Exposure Time Calculator (ETC) covering both the spectroscopic and imaging modes of the first light instruments has been developed (*http://tmt.mtk.nao.ac.jp/ETC-e.html*). An ETC for IRMS has been developed from the existing MOSFIRE ETC (*https://drive.google.com/file/d/0B3g66sbyRdnOTzRITUFJdHEyaGc*). These ETCs are useful tools to explore the improvement in capability that TMT will bring compared to existing facilities.

2.3.3 Future instruments

The observatory has been designed to support a diverse set of instruments, and its instrument suite will evolve significantly over its 50-year lifetime. The first of the second-generation instruments is expected to be delivered two years after first light, and additional instruments should follow at the rate of one every 2.5 years thereafter. Instrument priorities will be established by the TMT SAC following community, technical and programmatic input. Future instrument concepts studied thus far as part of the observatory design include:

HROS (High-Resolution Optical Spectrometer): a single-object, seeing-limited, high-resolution ($R = 50\,000$ for $1''$ slit) optical-UV echelle spectrograph in the heritage of HIRES at Keck and UVES at the Very Large Telescope (VLT).

IRMOS (Infrared Multiobject Spectrometer): designed to use multi-object adaptive optics (MOAO) techniques over a $5'$ field of regard to feed up to 20 deployable IFUs. This future instrument combines the diagnostic power of IRIS with the multiplexing capabilities of IRMS.

MIRES (Mid-Infrared Echelle Spectrometer): is a diffraction-limited, high-resolution ($5000 < R < 10\,000$) spectrometer and imager operating at 8–18 μm. It will employ a separate AO system optimized for the MIR. A concept for a MIR high resolution spectrograph and IFU instrument called MICHI is being actively developed at this time.

NIRES (Near-Infrared Echelle Spectrometer): fed by NFIRAOS, NIRES is a diffraction-limited high-resolution ($20\,000 < R < 100\,000$) spectrometer covering 1–2.4 μm simultaneously. It is a scientific descendent of Keck/NIRSPEC and VLT/CRIRES.

PFI (Planet Formation Instrument): an extreme AO high contrast exoplanet imager with spectroscopic ($R \leq 100$) capability. The first version of the system will obtain contrasts of 10^6 (goal: 10^7) while the second version's requirement is 10^8 (goal: 10^9) in H band for $R < 8$ mag. The next design phases are greatly benefiting from all the lessons learned from GPI at Gemini and SPHERE at the VLT. There is already a large overlap between the GPI and PFI development teams and new concepts (Second Earth Imager for TMT – SEIT and Planetary Spectral Imager – PSI) are being developed.

2.3.4 Observatory operations

Both PI-directed observing and Service observing modes are planned. Each partner is free to divide up the amount of PI-directed and Service observing awarded. PI-Directed observations may use time blocks as short as an hour (see *http://www.tmt.org/observatory/operations*) but typically half or whole nights will be awarded and will involve the assignment of a support astronomer to the PI to help with planning execution and analysis of the observations. Service observing will effectively be the execution of a pre-planned queue. This will enable many varied programs to be supported including cadence and Target of Opportunity (ToO) programs as well as PI-controlled observations and eaves-dropping modes. Most observing will be carried out remotely, either from the sea level headquarters or remote observing centers in each of the partner countries.

3 FUNDAMENTAL PHYSICS AND COSMOLOGY

One of the most exciting areas of current research lies at the interface between theoretical and high-energy physics and cosmology. Indeed, the discovery of dark matter and dark energy results from astrophysical observations of the universe. It is these kinds of careful quantitative cosmological and astrophysical measurements that offer the greatest promise for constraining fundamental physical theories. TMT will contribute in this area by providing highly accurate measurements of the most distant sources, large samples of objects probing the universe at intermediate distances, and precise studies of the dark matter in nearby and distant objects.

3.1 The Nature of Dark Matter

There is now incontrovertible observational evidence that the main mass component of the universe is in the form of "dark matter" that interacts extremely weakly with atoms and photons. In the standard paradigm, non-interacting dark matter controls the clustering of dark matter, making it a tractable computational problem in which the initial conditions and the evolution equations are known once the nature of dark matter has been specified. Simulations can then be contrasted with the observed galaxy clustering pattern to shed light onto the properties of dark matter. This has led to a scenario where dark matter takes the form of elementary particles that emerge from the early universe with negligible thermal velocities and a scale-free distribution of Gaussian density fluctuations. Coupled with a "dark energy" field that governs the late expansion of the universe, this "Cold Dark Matter" (ΛCDM) paradigm has now matured into a full theory without tunable parameters, from which detailed theoretical predictions are possible. These predictions have been successfully verified on large scales (>1 Mpc), but the situation is far less clear on the scale of individual galaxies, where the ΛCDM model is challenged by a number of problems. The rotation curves of dwarf galaxies, for example, seem at face value inconsistent with the cuspy dark matter halos predicted by cosmological simulations (Sects. 3.1.1 and 7.6.2). Further, ΛCDM predicts a number of low-mass dark matter halos that far exceeds the observed number of faint galaxies (Sect. 3.1.2). Although some see these challenges as signaling the need to abandon the paradigm, others argue that observations can be accommodated within ΛCDM once the effects of baryons on the scale of dwarfs are properly included. This is a complex problem that is far from solved, and best approached by following multiple lines of inquiry. Despite its complexity, progress has been steady and breakthroughs seem within

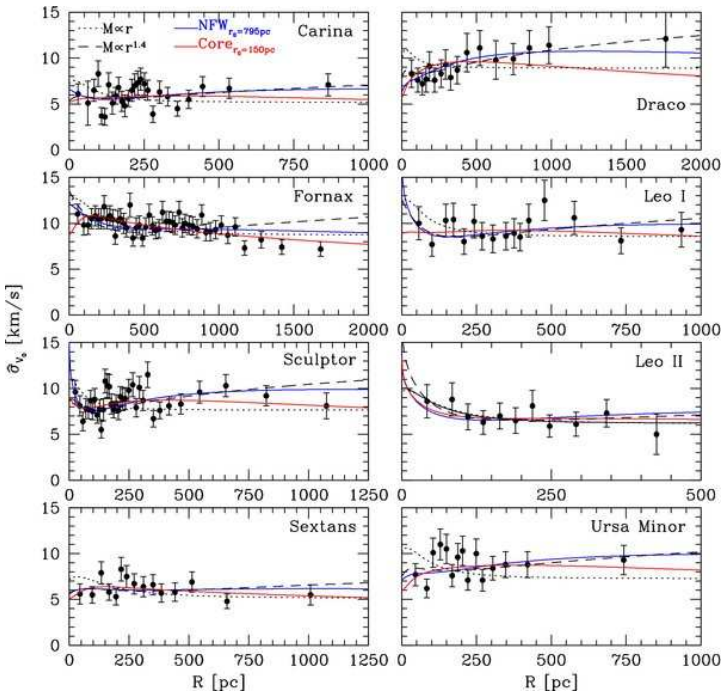

Fig. 4 Measured LOS velocity dispersion profiles in the Milky Way dSphs (Walker et al. 2009).

reach. TMT can play a key role in enabling these breakthroughs by placing definitive constraints on the mass profile of dwarf galaxies and enabling the detection of dark substructure in gravitationally lensed-systems.

3.1.1 Dwarf galaxy radial mass profiles

One of the most robust predictions of cosmological N-body simulations is that, in the absence of baryonic effects, CDM halos must have cuspy density profiles. Rotation curve studies of low surface brightness (LSB) galaxies have hinted that the actual mass profile might be shallower than predicted by simulations, fostering a lively debate regarding the meaning of these results and their consistency with ΛCDM. One possibility is that baryons may transfer energy to the dark matter as dense star-forming regions dissolve, flattening the cusps and turning them into "cores" more easily reconciled with observations (Navarro et al. 1996; Governato et al. 2010; reviewed by Pontzen & Governato 2014). This mechanism, however, can only operate in galaxies where baryons are relatively important. The dwarf spheroidal galaxies of the Local Group (dSphs) have measured line of sight (LOS) velocity dispersions that are much larger than would be inferred from their stellar content. It is believed that these are the most dark-matter-dominated galactic systems. Establishing the presence or absence of cusps/cores in dSphs is thus a direct test of one of the most distinctive predictions of the ΛCDM scenario. In addition to the cusp/core problem for the dSphs and the ultra-faint dwarfs (UFDs), there is evidence for lower central densities and smaller overall numbers of the largest satellite galaxies of the Milky Way. This is the "Too big to Fail" problem. By measuring the distribution of dark matter in these nearby satellites, TMT will make a direct test of cosmology.

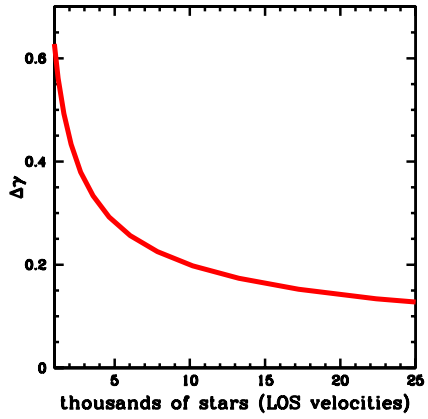

Fig. 5 Statistical uncertainty on the logarithmic-slope of the density at the half-light radius (400 pc) of a Draco-like NFW dark matter density profile as a function of the number of stars observed. This is based on a Jeans analysis of the LOS velocity dispersion, assuming 1 km s^{-1} accuracy. The Fisher matrix yields its uncertainty in a fit to a 5-parameter family of profiles. In combination with the mass within the half-light radius, in the absence of baryonic effects this measurement provides a powerful test of ΛCDM vs alternative dark matter models. Figure credit: J. Bullock (UCI).

The best constraints on dark matter profiles in these UFD galaxies are presently those based on large samples of radial velocities (RVs), see Figure 4. These analyses, however, suffer from the well-known degeneracies associated with the unknown stellar velocity anisotropy distribution (Binney & Tremaine 1987). If RVs alone are to be used, greatly increasing the sample of stars is essential to break the degeneracies. Figure 5 shows how the error on the logarithmic slope of the mass profile, γ, will be reduced as a function of the number of stars in a kinematic sample. Existing and imminent spectrographs such as Subaru's PFS will be able to efficiently measure RVs of hundreds of stars in these dwarfs. However, obtaining <5 km s^{-1} precision RVs for $> 10\,000$ stars will require reaching the main sequence in these dwarf galaxies. For Draco, that means $g \sim 23$ (Strigari et al. 2007), which will be very challenging for telescopes in the pre-TMT era. Given the relatively small core radius of these dwarf galaxies ($\sim 6'$ for Draco), TMT/WFOS will be an efficient instrument, and should allow us to greatly improve the constraints on the innermost profile of these dwarf galaxy halos (see Hayashi & Chiba 2012)

In addition to providing RVs for thousands of stars in multiple dwarf galaxies, TMT can also help to resolve the anisotropy degeneracies by providing proper motions. Strigari et al. (2007) have shown that if proper motion data could be obtained with ~ 5 km s^{-1} accuracy for just a few hundred stars per galaxy, the accuracy of current kinematic studies would be increased five fold. This is within the reach of TMT's IRIS spectro-imaging NIR camera with the NFIRAOS AO system. Relative astrometric measurement with the Keck AO system already reaches the ~ 150 μas level. IRIS is designed to obtain an accuracy of ~ 30 μas at comparable S/N. Thus, the relative positions of two measurements with respect to a reference can be determined to ~ 40 mas per star. Over a three-year baseline this corresponds to a kinematic accuracy per star of ~ 7 km s^{-1}. Doubling the time baseline would provide measurements of proper motion for stars brighter than $K \sim 18.5$ with a kinematic accuracy better than 4 km s^{-1}.

Furthermore, for red giants brighter than $V = 18$, corresponding to a G magnitude of 17.6, the Gaia mission should yield relative astrometric accuracy of ~ 70 μas (based on their revised specifications). The Sculptor dwarf contains more than 100 such stars; by combining such a Gaia and TMT

position measurement separated by ~ 10 years, proper motions with sufficient accuracy to distinguish cusp from core with a S/N of four will become available (Evslin 2015). A further TMT position measurement, several years later, could be used to measure velocity changes and thus identify binary systems with periods of years. Such binaries can contaminate the velocity dispersions of UFDs. The synergy with Gaia yields a competitive proper motion determination even in the case of the brighter but more distant Fornax dwarf, whose ecliptic latitude will provide it with more than twice the sky-averaged number of focal plane transits. The TMT will be able to definitively distinguish power-law cusps from constant density cores in many of the Milky Way's satellite galaxies.

Measuring accurate astrometry for stars covering the full tidal radius of the dwarf galaxies will not be easy, as it will require AO-assisted imaging (to get the astrometric precision) over a very large area. The tidal radius of Sculptor is nearly $75'$. Even with short (10 s) exposures (sufficient to reach $K = 22$), fully mapping the proper motions across the entire tidal radius will take some 800 hours (40 nights per epoch for two epochs) of telescope time, assuming 100% overhead for the dithering. Most other dwarfs are smaller on the sky, and their motions can be mapped with < 20 nights per dwarf of observing divided into two campaigns separated by multiple years. It will be important to observe both larger dSphs and UFDs, to control whether baryonic effects can affect the cuspiness of the mass profile (Oñorbe et al. 2015).

3.1.2 Dark matter substructure

Simulations of galaxy formation using the ΛCDM under the standard model reveal that massive galaxy halos should be associated with large numbers of small subhalos ("substructure"). On these sub-galactic scales, however, there appears to be a large discrepancy between the theory and observations of satellite galaxies. Simulations predict that there should be thousands of substructures with masses between 4×10^6 and 4×10^9 solar masses, comprising 5%–10% of the total halo mass within the virial radius (e.g. Springel et al. 2008). In contrast, observations of the Milky Way, where the most complete investigations of substructure have been conducted, have found many fewer satellites than predicted, leading to the well-known "missing satellites problem" on the low-mass end (e.g., Moore et al. 1999b; Klypin et al. 1999) and a slight tension with excess satellites on the high-mass end of the mass function (e.g., Strigari et al. 2007). Possible explanations for this discrepancy are (1) some type of astrophysical process (e.g., differences in star-formation efficiencies), (2) the Local Group is an outlier, or (3) we have an incomplete understanding of the nature of dark matter. To distinguish between these hypotheses requires a large sample of galaxies in which we can detect even non-luminous substructure. The combination of gravitational lensing with high-resolution observations by the TMT will provide exactly such a sample, and will do so via two independent techniques.

Flux ratio anomalies in lensed Active Galactic Nuclei (AGNs): The image configurations and predicted fluxes of lensed AGNs are set by the smooth mass distribution in the main halo of the lensing galaxy. Deviations from the flux ratios predicted by the smooth mass models, i.e., flux ratio anomalies, are a sign of lumpiness in the mass distribution of the lensing galaxy. This lumpiness may be due to stars in the lens (microlensing), which is the dominant contaminant in searches for dark matter substructure. However, the microlensing can be avoided if the angular size of the lensed object is larger than the lensing scale of the stars, which happens if the lensed emission is coming from a region larger than the broad line region (BLR) in the background AGN. A promising approach utilizes the narrow-line region, which is large enough to avoid microlensing. These observations require sensitive and high-resolution IFU observations, in order to obtain high-S/N spectroscopy of each of the lensed images that are typically separated by an arcsecond or less. This method was originally proposed by Moustakas & Metcalf (2003), and has recently seen a successful application by Nierenberg et al. (2014). The large gains in both sensitivity and angular resolution provided by TMT will allow this procedure to be applied to a statistically significant sample of lens systems.

Alternatively, the dusty torus that is seen in the MIR can also provide a measurement of flux ratios that is immune from microlensing and dust. Current observations of lensed QSOs have found closely separated images ($\sim 0.3''$), too faint and difficult to resolve with existing 8 m telescopes. JWST will be much more sensitive but its resolution will be significantly less than that of TMT. Diffraction-limited observations using the TMT will be essential to separate and distinguish these images, especially for the (expected) large number (100's) of small-separation lenses ($<0.3''$).

Gravitational imaging: Gravitational lensing plus sensitive high-resolution imaging provides a second path to quantifying the substructure mass function in distant galaxies. In the "gravitational imaging" technique (Koopmans 2005) the targeted systems are not lensed AGNs, but rather systems in which a background galaxy is lensed into a long arc or a ring by a massive foreground galaxy. In these systems, the radius and overall appearance of the arc is set by the smooth mass distribution in the lensing galaxy. However, the presence of dark-matter substructure can perturb the shape of the ring on small angular scales. These small astrometric perturbations to the lensed emission allow the presence of substructures to be deduced, even with no detectable luminous component. An excellent demonstration of this technique with ground-based instrumentation resulted from NIR AO observations with Keck. A 10^8 solar mass substructure in a $z \sim 0.9$ galaxy was robustly detected in three independent data sets (Vegetti et al. 2012). The substructure was detected at higher significance in the Keck AO data than in HST imaging of the same system, due to the higher angular resolution of the Keck observations, see Figure 6. With its significant improvements compared to Keck in collecting area, angular resolution, and number of systems accessible with AO, the TMT will move this technique into the regime where interesting constraints can be placed on the substructure mass functions and, furthermore, will allow these parameters to be determined as functions of, e.g., galaxy mass, redshift, and other observables.

3.1.3 Dark matter self-interaction cross-section

Many dark matter experiments are dedicated to searching for couplings of the dark matter particle to the Standard Model and can be classified into direct detection dark matter experiments (e.g. CDMS, LUX, etc), colliders (LHC) and annihilation experiments (FERMI). If, however, dark matter does not couple (or does so extremely weakly) to the Standard Model these searches will only allow us to rule out parts of a parameter space. Astrophysical experiments, however, can probe interactions between two dark matter particles via their effects on the structures and dynamics of dark-matter halos.

Interacting clusters have proven very fruitful for constraining the nature of dark matter (Clowe et al. 2006). In clusters with recent strong merger activity, the positions of dark matter halos and the main baryonic component can become separated. The separation between the X-ray emitting gas and the dark matter provides a powerful upper limit on the DM self-interaction cross section. More recently, it has also been suggested (Dawson et al. 2012) that the separation between the dark matter and the galaxies in interacting clusters can provide a lower limit to the self-interaction cross-section, $\sigma_{\rm m}$. This measurement is controversial and the significance depends on very accurate determination of the position of the weak lensing.

Current limits from studies of the Bullet Cluster (Randall et al. 2008), MACS J0025.4-1222 (Bradač et al. 2008), and DLSCLJ0916.2+2951 (Dawson et al. 2012) require $\sigma_{\rm m} < 0.7\ {\rm cm}^2\ {\rm g}^{-1}$. However they leave a considerable room for improvement. The two main observational challenges to measure both gas-DM and galaxy-DM offsets are accurate measurements of the weak lensing centroid as well as accurate determination of cluster membership and hence galaxy centroid. Even more importantly, these studies all require detailed dynamical information of the system to be included in simulations, and only TMT can provide this for a large number of faint cluster members. Furthermore, because the weak lensing centroiding accuracy is a very strong function of the number density of lensed galaxies used, this measurement requires greater depth and resolution than

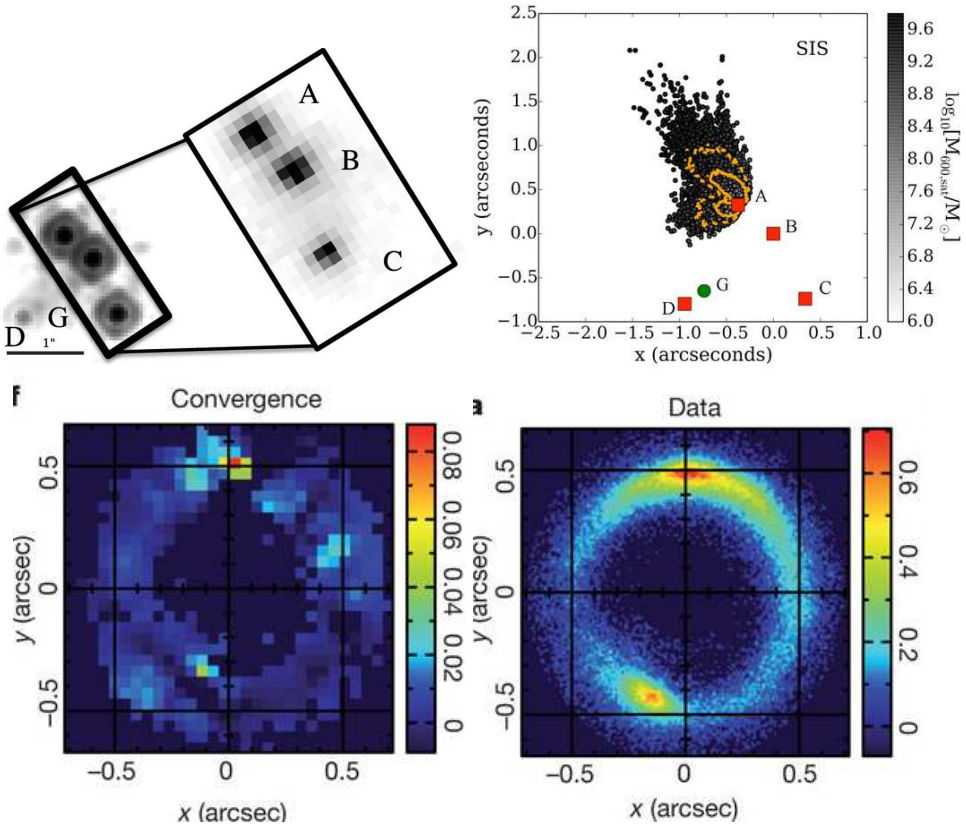

Fig. 6 Demonstration of the detection of (*dark*) substructure via gravitational lensing and Keck AO imaging. (*Top two panels*) Substructure detection via flux ratio anomalies in the B1422+231 lens system. Figures show HST (*small rectangle*) and Keck/OSIRIS imaging (*large rectangle*) and the posterior probability for the location and mass of the substructure under the assumption of a single perturbing mass and a singular isothermal sphere profile. Figures from Nierenberg et al. (2014). (*Bottom two panels*) Substructure detection via gravitational imaging in the B1938+666 system. Figures show the Keck/NIRC2 imaging of the system, with the lensing galaxy masked out, and the enhanced convergence required to fit the data. The peak in the convergence map corresponds to the location of the substructure in this system. Figures from Vegetti et al. (2012).

even HST or JWST will provide, meaning that TMT will be required if the issue of a dark matter self-interaction cross-section is to be resolved.

3.1.4 Baryonic power spectrum

The power spectrum of density fluctuations on small scales provides the strongest constraint on the fraction of hot dark matter in the universe (Hu et al. 1998) as free streaming by this matter reduces the fluctuation power on small scales. Power spectrum data can also provide constraints on a wide variety of potential low-mass particles such as sterile neutrinos, axions and thermal relics (Narayanan et al. 2000; Hannestad & Raffelt 2004; Viel et al. 2005).

Studies of the distribution of matter can also tell us details about the early inflationary period of the universe. The power spectrum of density fluctuations is predicted by theory to have arisen from

a "scale invariant" primordial spectrum that is a power law with near unity slope. Small deviations from this unity slope are expected and are related to the degree by which the universe expanded during the period of inflation and hence to the physical properties of the fields that drove inflation. By measuring the distribution of matter over a wide range of scales, one can constrain both the slope and possible deviations with high precision. Measurement of the power spectrum on large scales is limited by "cosmic variance" (there is only one universe) – the most precise measurements will necessarily come from measures on small physical scales.

In the present-day universe, the memory of the initial conditions on small scales has been erased by the formation of complex structures such as galaxies. However, by studying the details of the distribution of diffuse hydrogen gas in the intergalactic medium (IGM) at high redshift, it is possible to measure the "primordial" power spectrum of all matter. This can be achieved by studying absorption line systems along the sightlines of many different sources. Numerical simulations over the past decade (e.g. Viel et al. 2013) have further refined the power of IGM power spectrum measurements, allowing constraints to be determined even on scales that are somewhat non-linear.

The technique of measuring the power spectrum from absorption line systems has been developed over the last decade using the Sloan Digital Sky Survey (SDSS) and BOSS (McDonald et al. 2006; Busca et al. 2013; Slosar et al. 2013) using quasar spectra at fairly low resolution ($R \sim 2000$), then supplemented with smaller numbers of high resolution spectra taken with Keck, Magellan and VLT (Viel et al. 2006; Becker et al. 2011). On large scales, the most sensitive sample to date is the one studied by the BOSS survey (Lee et al. 2013b), which uses almost 55 000 quasars between $2.1 < z < 3.5$. Power spectrum measurements (combined with CMB constraints from WMAP and Planck) have placed upper mass limits of 0.23 eV for the sum of the masses of the standard model neutrinos (see Abazajian et al. 2015 for a discussion). Higher resolution and higher redshift observations (Bolton et al. 2012) have placed the current lower limit of the warm dark matter mass scale $m_{\rm wm} > 3.3$ keV. With TMT, the number of QSOs in the correct redshift range will increase by about an order of magnitude.

Absorption line studies using quasars are fundamentally limited by their angular density. However, with TMT it will be possible to use the fainter but much more abundant "normal" galaxies. By using galaxies as probes instead of quasars, TMT will allow for the first time the study of the 3-D distribution of diffuse hydrogen in the IGM, which is directly related to matter density, thereby increasing the precision of cosmological measurements by at least an order of magnitude over that possible with current telescopes. Here the distribution of matter is affected by complex physical processes, such as gas dynamics, star formation and feedback. TMT, using WFMOS and IRMS, will probe the distribution and composition of gas along the lines of sight to distant quasars and galaxies, providing unique high-quality data essential to an understanding of these processes.

3.1.5 Dark energy and modified gravity

Understanding the acceleration of the universe (Riess et al. 1998; Perlmutter et al. 1999; Eisenstein et al. 2005; Vikhlinin et al. 2009) is arguably the greatest challenge facing cosmology. In Einstein's theory of gravity, an accelerating expansion requires that the average pressure throughout space be negative. Cosmological fluids with negative pressure are called dark energy (DE). The simplest implementation of DE is a cosmological constant, which is incorporated in the concordance ΛCDM model. However ΛCDM on its own provides no explanation for the smallness of the cosmological constant relative to most scales in the theory. Observations to date are consistent with a cosmological constant but also with several distinct dark energy models. The most common way to describe any dark energy candidate is through its equation of state parameter (EOS) $w = p/\rho$, which is the ratio of its pressure (p) to its energy density (ρ). $w = -1$ is for a cosmological constant and for anything other than this, dark energy evolves with time.

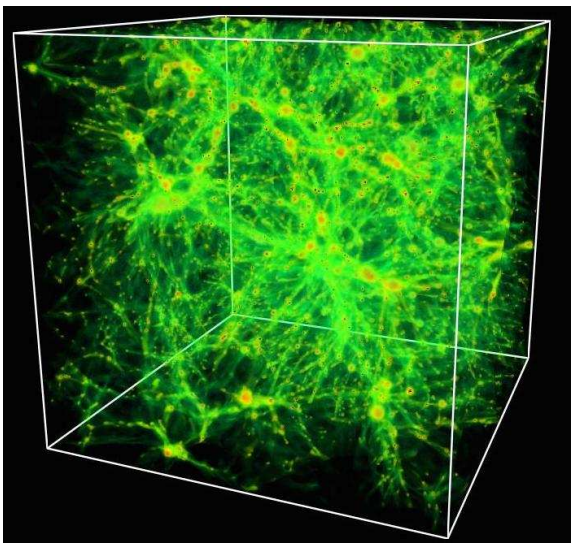

Fig. 7 Dark matter structure at $z \sim 3$. TMT will probe multiple lines of sight using WFOS and background galaxies as sources. This will provide a more complete understanding of the baryonic power spectrum and interaction of the IGM with baryonic matter in galaxies (Credit: R. Cen, Princeton U.).

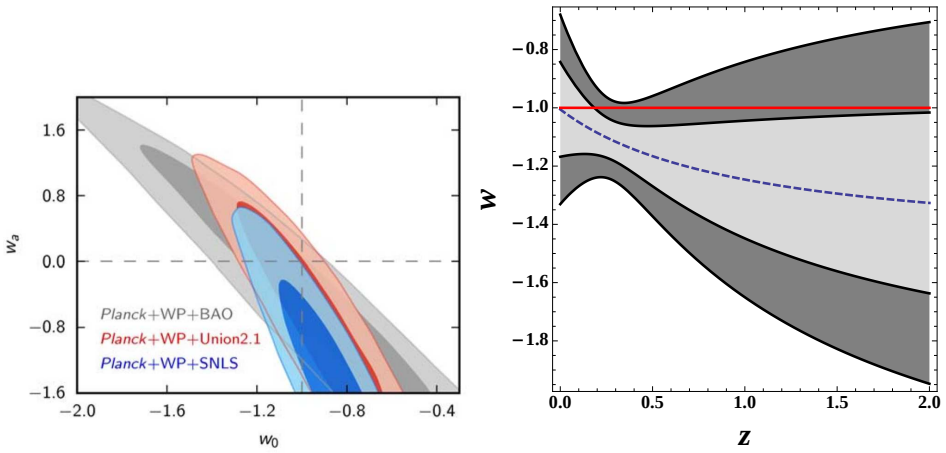

Fig. 8 *Left*: Current constraint on w_0 and w_a from different observations (Planck Collaboration 2014b); *Right*: Current constraint on behavior of $w(z)$ from different observations (Hazra et al. 2015).

Constraining w and its variation with time is one of the main goals for all present and future cosmological observations including TMT. For that, the CPL parameterization $w = w_0 + w_a(1-a)$ by Chevallier & Polarski (2001) and Linder (2003) is the widely used parameterization for the EOS. Present bounds on the evolution of w are shown in Figure 8.

Another approach to the late time acceleration is to modify the gravity at large cosmological scales without including any exotic component in the energy budget of the universe (Dvali et al. 2000; Freese & Lewis 2002; de Felice & Tsujikawa 2010; Amendola & Tsujikawa 2010). Often these

models are equivalent to dark energy models. TMT will constrain these models through the observational tests described below. Additional tests of GR involving supermassive black holes (SMBHs) are described in Section 6.1.1.

Measuring the properties of dark energy and testing alternate gravity theories is the goal of many experiments and observatories that will be operational at the same time as TMT (e.g. LSST, Euclid, WFIRST). These missions will carry out large-scale surveys in order to exploit popular dark energy diagnostics such as baryonic acoustic oscillations (BAO) or cosmic shear. TMT can be a competitive probe of dark energy and modified gravity by focusing on diagnostics that require its unique combination of sensitivity and angular resolution, like the ones described below (see also Jain et al. 2013). By measuring the anisotropy in w_0 and w_a (e.g with time delays), TMT may also be able to place competitive constraints on the speed of sound of the dark energy fluid.

3.1.6 Time-delay cosmography

Gravitational time delays between multiple images of lensed quasars have emerged as a powerful probe of dark energy (Suyu et al. 2013, 2014). A key requirement is the need to image the lensed host galaxy at sufficient resolution to chart the gravitational potential. In the next decade thousands of lensed quasars will be discovered and monitored by upcoming panoramic imaging surveys (Treu et al. 2013b), and high resolution AO imaging will be used to follow selected systems and thereby provide absolute distances to $<$1% precision. Furthermore, high resolution spectroscopy is needed to measured the redshift of the lensed quasars and the redshift and internal kinematics of the deflector. The angular diameter of the gravitational lens systems is of order $3'' - 4''$, well matched to the capabilities of IRIS. The method is particularly powerful when combined with microwave background and Type Ia supernovae (SNe Ia) experiments, as it breaks many of the residual degeneracies (e.g. between curvature and w). At the moment this method is limited by the small number of known suitable systems. However, more than an order of magnitude increase in the number of known lenses with time delays is expected with LSST (Oguri & Marshall 2010). The LSST will also find strongly lensed SNe Ia, for which we can directly measure the magnification factor to further constrain the gravitational potential (Oguri & Kawano 2003), see also Section 9.1.1. High resolution imaging and spectroscopy with TMT will transform these into high-precision cosmological probes.

3.1.7 Cosmology from clusters of galaxies

Clusters of galaxies are a very important laboratory for cosmology and fundamental physics, providing multiple probes into dark energy and its evolution, as well as the nature of dark matter and its interaction with baryons. Critical spectroscopic and astrometric measurements on lensed galaxies are only possible with the resolving power and sensitivity of an AO-fed 30 m class telescope.

3.1.7.1 Strong and weak-lensing tomography

The deflection of light due to gravitational lensing depends on the angular diameter distance ratios between the source, lens and observer. For the same lens, measuring the increase in lensing effect with source redshift provides a cosmographic measurement, whether the effect is weak lensing shear (Jain & Taylor 2003), or the position of strong lensing arcs (Golse et al. 2002). In practice, the constraint increases very strongly with the number of arcs per cluster and the number of clusters (Jullo et al. 2010), as long as the large scale structure along the LOS is known (Dalal et al. 2004). Because many arcs are observed to have characteristic widths below $0.1''$, AO-based imaging is required to resolve them, and to separate them from the background sky. At the same time, spectroscopic measurements required to securely establish arc redshifts and to identify structure along the LOS require the aperture of a 30 m class telescope. For clusters with $z > 0.5$, the entire strongly lensed region spans a $<30''$ diameter region for all but the most massive clusters (Richard et al.

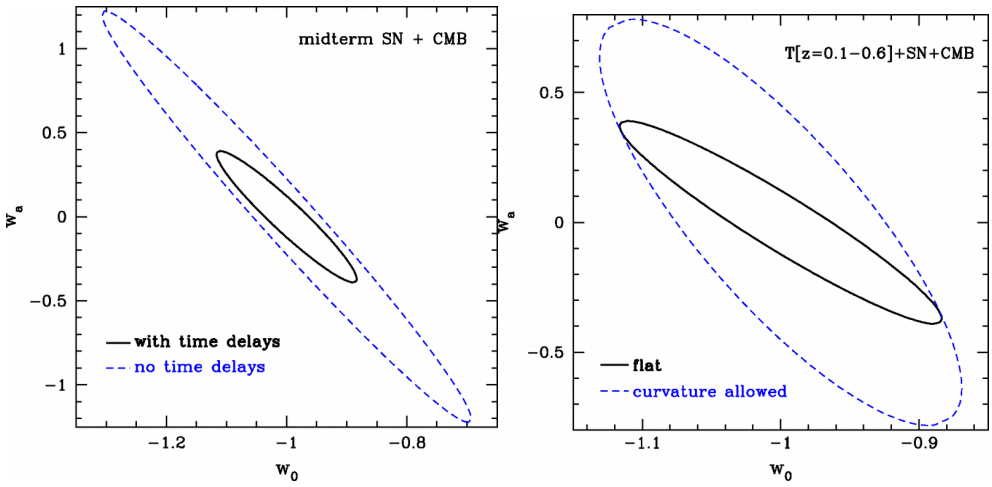

Fig. 9 *Left*: 68% confidence level constraints on the dark energy EOS parameters w_0 and w_a using midterm SN distances and CMB information with or without time delay measurements. *Right*: Similarly, 68% confidence level constraints using time delay, midterm SNe, and CMB information, assuming spatial flatness or allowing curvature. In both panels the time delay probe demonstrates strong complementarity, tightening the area of uncertainty by a factor 4.8 and 20 respectively.

2014), well-matched to the planned $34'' \times 34''$ FOV of the IRIS imager. Based on the HST WFC3 imaging of the frontier fields, TMT will be able to observe up to hundreds of multiple images per cluster field (Jauzac et al. 2014), and at a resolution (at 1 μm) $5\times$ that of ACS. For higher-redshift clusters, weak lensing tomography can be used to extend the measurements to >300 kpc, taking advantage of at least partial image correction over the entire AO-assisted FOV.

3.1.7.2 Masses for high redshift clusters

In hierarchical cluster formation scenarios, formation of clusters of galaxies occurs late in cosmic time. Therefore, detection of high mass systems at early redshifts poses a sensitive constraint on cosmological models, and may point to primordial non-Gaussian forms or complex modifications of gravity. Because the mass function is so steep, the cosmological constraining power depends critically on the ability to measure the cluster mass. Clusters at $z > 1.5$ are unlikely to be virialized, and masses derived from scaling relations from the X-ray or optical richness are unlikely to be well-calibrated at that distance. The two techniques which might have promise in determining the mass of high-z clusters both require the unique capability of a 30 m class aperture with both wide-field spectroscopic and high resolution imaging capabilities. For weak lensing, the primary difficulties are measuring shapes for enough galaxies behind the clusters to adequately measure the shear, and having sufficiently accurate redshifts to remove the huge foreground contribution (both to the galaxies and the shear). For clusters at $z \gg 1$, this requires a combination of deep optical and infrared spectroscopy (for infall measurements and foreground structure determination) and AO imaging (for shape measurements and redshift measurement of small background galaxies).

3.1.7.3 Cluster abundance and mass function: Calibrating the Mass-Observable Relations

Cosmological constraints from clusters are also derived from the evolution of the cluster mass function as a whole between $0 < z < 1.5$. Although the TMT is not a survey machine, and will not detect or measure masses for the majority of clusters for this measurement, it will play a critical role

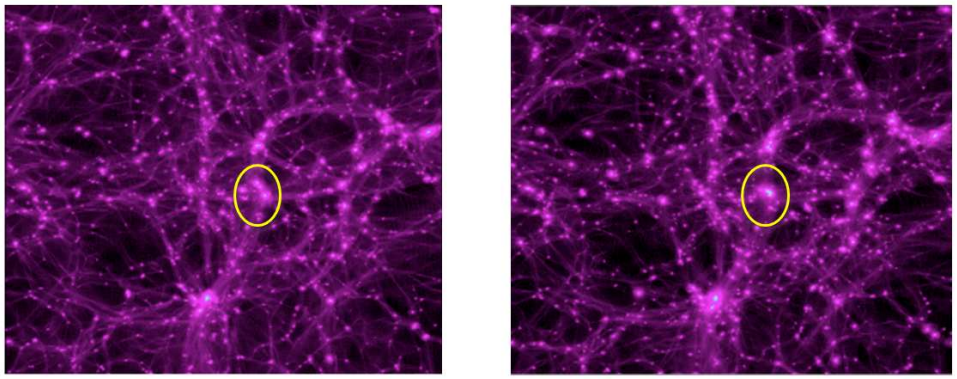

Fig. 10 Snapshots at $z = 0$ for N-body simulations of GR (*left*) and $f(R)$ gravity (*right*). 256^3 particles are simulated in a B=64 Mpc/h box. The Hu-Sawicki model (Hu & Sawicki 2007) is adopted for the $f(R)$ simulation (Zhao et al. 2011b).

in many of the steps in the calibration of the mass measurements. For example, the contribution to the uncertainty in the calibration of the mass-temperature relation that arises from uncertainty in assigning photometric redshifts for galaxies behind clusters of different redshift is already comparable to the statistical errors. This uncertainty is expected to dominate the error in the era of large surveys such as eRosita, Euclid, and LSST. Second, measurement of the relationship between the shear and the mass observable at fixed redshift requires accurate mass measurement. Defining a "golden set" of clusters with very accurate lensing measurements and especially with a dense and reliable set of redshift measurements will be key in deriving cosmological constraints from the evolution of the mass function. The angular sizes of the cluster cores are well-matched to the FOV of the AO system. However, efficient measurement of sufficient redshifts may require a second generation instrument with higher multiplexing or the use of multiple rotated grism exposures.

3.1.8 Tests of general relativity

As described in the SMBHs section, high precision determinations of the velocity and position of stars orbiting the SMBH at the center of the Milky Way provide a stringent test of General Relativity (e.g. Angélil & Saha 2011). A similar test can be performed on the scale of an entire galaxy. Even for a face-on galaxy at a fixed distance, the apparent Doppler velocity is not constant due to GR effects. The light from the central part of the galaxy will be more redshifted compared to the outer part. This is because light from the inner part has to climb out of a deeper gravitational potential. There is also the Transverse Doppler Effect that makes the kinematically-hotter center be even more redshifted. Both redshift effects are small (on the order of (0.1–1) km s^{-1}). By stacking high resolution spectra of many spatially resolved galaxies, however, the GR signal will be detectable by TMT (Zhao et al. 2013).

Alternatively, TMT can be used to test GR using the environmentally-dependent screening effect. In principle, one can modify GR so that it mimics a cosmological background expansion history similar to that in the ΛCDM model (GR plus vacuum energy as dark energy). This will automatically change the structure growth on all other scales, including the galactic, and even sub-galactic scales, which could violate the stringent solar system confirmation of GR. However, there are screening mechanisms (Khoury & Weltman 2004) in which the additional degrees of freedom (scalar fields) could be shielded to evade the solar system tests. The screening reduces the signal of modified grav-

ity (MG) on (sub-) galactic scales, Therefore the high angular resolution and sensitivity of TMT makes it ideally suited to carry out this kind of tests. For example, in modified theories, the dynamical mass and lensing mass of the same object are in general different, unlike those in GR. Based on a high-resolution N-body simulation of a $f(R)$ model (See figure 1 in Zhao et al. 2011b), it is found that the fractional difference between dynamical and lensing masses (denoted by $D_{\rm M}$) depends on the local environment (Zhao et al. 2011a).

Observationally, the lensing and dynamical masses of galaxies can be measured by TMT using strong lensing and velocity dispersion measurements (e.g. Schwab et al. 2010). Once this is done, one can similarly subdivide the samples using their lensing mass and local environment indicator, then contrast the fractional mass difference $D_{\rm M}$ of isolated low mass galaxies to those clustered massive galaxies. This can not only enhance the possible signal, but also minimize systematic effects.

3.2 Physics of Extreme Objects – Neutron Stars

Our knowledge of the strong and gravitational forces, among the four fundamental interactions conventionally recognized, is relatively incomplete. TMT can improve our understanding of both forces by constraining the EOS of extremely-dense matter and testing gravity theory with neutron star (NS) binary systems.

The measurement of NS masses provides clean and tight constraints on the state of dense matter at supranuclear density, and has profound implications on the nature of the strong interaction. However, up to now, all accurate mass measurements are from observations of binary pulsars. Gravitational microlensing has been proposed as a possible way to measure the mass of isolated NSs, and it has been highlighted that microlensing events due to pulsars could be predicted based on pulsar proper motions obtained through radio observations (Dai et al. 2010). Future large radio telescopes, such as FAST and SKA, will discover thousands of new pulsars and determine their distances and proper motions; deeper optical surveys, such as WFIRST and LSST, will provide billions of background sources. Therefore, it will become possible to predict potential microlensing events due to NSs, and further confirm and monitor them with radio telescopes (of order a few events per year can be expected from a dedicated monitoring campaign). With TMT's extremely-high sensitivity and high-precision astrometry (~ 0.1 mas), we would be able to detect weak microlensing phenomenon or provide precise measurements (see Sect. 9), and then determine isolated NS masses (Tian & Mao 2012).

White dwarf-neutron star systems provide test-beds for gravity theories. By modeling the optical spectral lines of the white dwarf (WD) and high-precision radio pulsar timing, the masses of components in WD-NS binary systems can be determined independently of gravity theory, which makes WD-NS systems unique laboratories to test theories of gravity in the strong-field regime (Freire et al. 2012; Antoniadis et al. 2013). The high spectral line sensitivity and resolution of TMT will greatly increase our sample of WD-NS systems and provide precise mass measurements of the binary components. By combining the derived masses with additional post-Keplerian parameters from radio timing, we will be able to probe various aspects of alternative gravity theories. Wide-orbit WD-NS systems are ideal systems to test strong equivalence principle, while tight-orbit WD-NS systems have proved to be extremely useful in probing the local Lorentz invariance of gravity (Shao & Wex 2012).

In addition, the optical emissions from NSs carry important information about the underlying radiation processes in strong magnetic fields and hence the nature of NSs. Normally, the optical emission is weak, and only about 20 NSs have been observed in UV/optical/IR so far. However, it has been discovered that the optical/UV fluxes exceed extrapolations of X-ray blackbody emission (Tong et al. 2011), which thus may reveal some new physical processes. Large optical telescopes, such as TMT, will be necessary to make breakthroughs in this field.

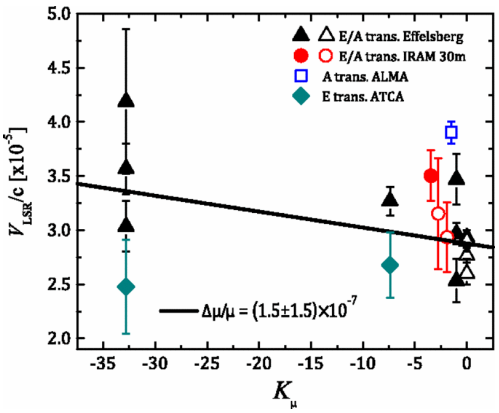

Fig. 11 Measuring alpha. Wavelength residuals seen in QSO spectra vs. sensitivity coefficient. The slope indicates a variation of the ratio of the masses of the proton and electron (Bagdonaite et al. 2013a,b, 2014).

3.3 Variation of Fundamental Physical Constants

In a large class of fundamental theories, the four-dimensional universe that we observe emerges from a higher-dimensional space-time. In such theories, the fundamental physical constants, such as the fine structure constant and the electron-to-proton mass ratio, are expected to be time dependent (see Uzan 2007 for a review). Time variation of fundamental parameters is also generic in cosmological models of quintessence. It is possible to search for and constrain any such variations of the constants by accurate measurement of wavelengths of absorption lines seen in the spectra of quasars (Webb et al. 1999). Past observations have been inconclusive. More than a decade of study using 8 and 10m telescopes to constrain evolution of the fine structure constant has yielded mixed results (e.g. Murphy et al. 2003; Chand et al. 2004; Tzanavaris et al. 2005; Reinhold et al. 2006; Molaro et al. 2013). There has been recent tantalizing evidence for a variation in the electron-to-proton mass ratio (Fig. 11). These observations have been limited both by S/N, and by identification and control of systematic errors (Murphy et al. 2007). While both of these limitations need to be addressed, it is clear that S/N provided by the current generation of 8–10 m telescopes is at best marginal. In the same amount of observing time, TMT with HROS would provide a three-fold improvement, providing a statistically definitive result. Combining TMT observations with results from other probes such as CMB power spectrum analysis (Planck Collaboration 2014b), galaxy clusters (Galli 2013), or primordial nucleosynthesis (Coc et al. 2012) promises to set limits on the order of 10^{-4} on the variation of α, and of 10^{-3} on the variation of the electron mass over the past 13 billion years.

4 EARLY UNIVERSE

The expansion of the universe stretches the wavelengths of photons, causing spectral lines to shift to longer (redder) wavelengths. The redshift of a source is thus a measure of its distance, and the epoch at which the light was emitted. The frontier for spectroscopically-confirmed galaxies is currently at a redshift of 7.5, when the universe was roughly 700 million years old, and plausible candidates have been identified as far back as $z = 11$, but have not yet been confirmed.

The motivation for finding and studying the most distant galaxies is three-fold. Firstly, astronomers are inspired to undertake a census of the first galaxies seen in the first few hundred million years after the Big Bang. This curiosity for exploration is fundamental to science and has driven as-

tronomy to major discoveries in the past; it also excites great public interest. Secondly, and more fundamentally, hydrogen in intergalactic space is ionized by a redshift of about 6, whereas it was fully neutral soon after the time the microwave radiation emerged. At some point there was a landmark event called *cosmic reionization*, akin to a phase transition in the IGM, when hydrogen became ionized. Most astronomers suspect this event was closely related to the birth of the first galactic systems that released copious amounts of ionizing UV photons. Prior to reionization, hydrogen was still in atomic form and the universe was devoid of any light emitting celestial sources – a period commonly termed the *Dark Ages*. Pinpointing when and how the Dark Ages ended, and finding the sources responsible for cosmic reionization is necessary to complete the story of galaxy evolution. Thirdly, the physical processes which accelerate or inhibit the cooling and collapse of hydrogen gas clouds into young galaxies at these early times provide the seeds from which later, more massive, galaxies such as our own Milky Way assembled. Although theory makes predictions of how these early systems grew and evolved, it is currently not directly tested by observations.

4.1 Early Galaxies and Cosmic Reionization

It is thought that the first luminous objects, forming from primordial hydrogen and helium, include giant short-lived stars, perhaps more than 200 times more massive than the Sun (Hirano et al. 2014). Their number and brightness is uncertain, but they may well be too faint to see with JWST or TMT, even if they lie in an accessible redshift range (redshift $z < 20$ for TMT; at higher redshift, Lyα shifts beyond the K band window, and there will be no light detectable by ground-based optical/infrared telescopes). As gravity inexorably forces larger hydrogen clouds to cool and collapse, low mass galaxies will begin to shine. Calculations taking into account the transfer of UV radiation from these early galaxies through the IGM suggest that "bubbles" of ionized gas will develop around each prominent source. The bubbles will enlarge and eventually overlap, completing the process of cosmic reionization.

When might this have occurred? The patterns of temperature and polarization signals from microwave background photons detected by the WMAP and Planck satellites suggest that the free electrons responsible reside in ionized gas in the redshift range 8 to 20 (Planck Collaboration 2014a). Thus it is quite likely there will be an abundance of energetic, UV-luminous, star-forming sources in this interval that are responsible for this reionization. However, it is not yet known if reionization was an instantaneous or protracted event, or whether the ionizing radiation comes from a highly abundant distribution of feeble sources, or a rarer population of brighter, more massive galaxies. Some cosmologists suspect there may also be ionizing contributions from BHs or decaying particles (e.g. Pierpaoli 2004). Only by locating and carefully studying the UV-emitting sources in this era can these important questions be answered.

Soon after the first sources emerge, the heated neutral hydrogen begins to glow more brightly than the microwave radiation. Powerful radio telescopes and interferometers now being planned should trace the topology and growth of the bubbles around these sources by mapping selected regions of the sky using the redshifted 21 cm emission line of hydrogen. However, although low frequency radio surveys may improve our knowledge of when cosmic reionization occurred, they will not detect the sources responsible. Our physical understanding of the process will thus rely crucially on observations with JWST and TMT.

JWST should certainly be able to detect the brightest sources lying within each ionized bubble. However, TMT, with AO, will be able to detect and study objects an order of magnitude fainter. The gain will be particularly dramatic if, as expected, the earliest sources are physically small. TMT may also find the signatures of the much sought-after, chemically un-evolved, "Population III" sources expected at these early epochs. In general terms, therefore, we can expect the role of TMT to be one of providing a more detailed story of the properties and influence of earliest sources on the IGM, building on the basic progress made with radio surveys and JWST.

The following subsections introduce several areas where TMT is likely to make a profound impact in its early years in addressing the physical processes in conjunction with the next generation facilities such as JWST. Inevitably, given how little is known about the properties of the early stellar systems and their contributions to cosmic reionization, the quantitative details are more speculative than in other areas of this document. Flexibility in survey strategy will be crucial as more is learned about this uncharted era. Some of the performance uncertainties are discussed in terms of both the unknown size and abundance of star-forming sources.

4.1.1 Uncovering primordial stellar systems with TMT

The earliest galaxies will contain massive stars formed from primordial gas. As these stars evolve and eject processed material from their eventual SNe, newly-formed stars containing heavy elements will become more common. Simulations consistent with the WMAP polarization results (Ciardi et al. 2006) suggest primordial (so-called Population III) stars may lie in the redshift range 8 to 20. The formation of metal-enriched Population II stars may proceed quite quickly, although this depends on how much gas is retained in the shallow gravitational potential wells of early galaxies; many of the early metals may be blown right out of galaxies by winds from massive stars and SNe. Verifying the existence of chemically primordial galaxies and determining their redshift distribution would represent a major new constraint on the first stages of galaxy formation.

The hydrogen Lyα line at 1216 Å is a characteristic signature of photoionization by massive stars, and is commonly observed in spectra of star-forming galaxies at $z < 6.5$. As much as 8% of the light of a metal-poor young galaxy can emerge in the form of Lyα, which has traditionally made it an effective tool for measuring galaxy redshifts. However Lyα is a resonance line, and is easily scattered as the IGM becomes more neutral in the early universe. The presence and strength of Lyα will depend on the size and geometry of local ionization bubbles around young galaxies that may allow Lyα photons to escape. Recent observations suggest that the fraction of Lyα-emitting galaxies drops from $z \sim 6$ to 7 (e.g., Pentericci et al. 2011; Ono et al. 2012, Schenker et al. 2012, 2014; Treu et al. 2013a). This evolution appears to steepen at $z > 7$, in clear contrast with the evolution of UV continuum emission (Konno et al. 2014, Fig. 12). Only a handful of secure Lyα lines have been detected so far at $7 < z < 7.6$, and none (yet) at $z > 8$. The disappearance of Lyα is presumed to be due to the increasing neutrality of the IGM at higher redshifts. It may be that Lyα is only detectable under rare circumstances at $z > 8$, perhaps in compact galaxy overdensities where ionization bubbles overlap, or in merging systems where peculiar motions aid the escape of Lyα photons.

For very young galaxies, the harder photoionizing spectrum from metal-poor stars should excite higher-ionization UV emission lines that are not ordinarily seen in more evolved systems. Recent observations of gravitationally lensed dwarf galaxies at redshifts 2 to 3, which may be close analogs to the galaxy population at $z > 7$ in terms of mass and metallicity, have detected moderately strong high-ionization metal lines such as CIII] 1909 Å, OIII] 1663 Å, and CIV 1549 Å, with equivalent widths (EWs) as high as 15 Å (Stark et al. 2014). In principle, these UV metal lines can be detected out to $z \sim 14$ with TMT, whose infrared spectrographs IRMS and IRIS will be more sensitive than JWST/NIRSPEC to faint, narrow line emission in compact galaxies. These high-ionization metal lines are a very promising tool for studying young star-forming galaxies, given recent evidence from ALMA that the ordinarily strong low-ionization [CII] 158 μm line can be extremely weak in galaxies at $z \approx 7$ (Ouchi et al. 2013).

For truly primordial galaxies, without metals, the last resort is observing the HeII emission line at 1640 Å (the equivalent of Hα, for ionized helium). Model atmosphere calculations by Schaerer (2002, Fig. 13) suggest this helium line could emit up to $\sim 0.8\%$ of the luminosity of a metal-poor young galaxy. Although the signal of HeII is weak, TMT would be able to see this line in galaxies

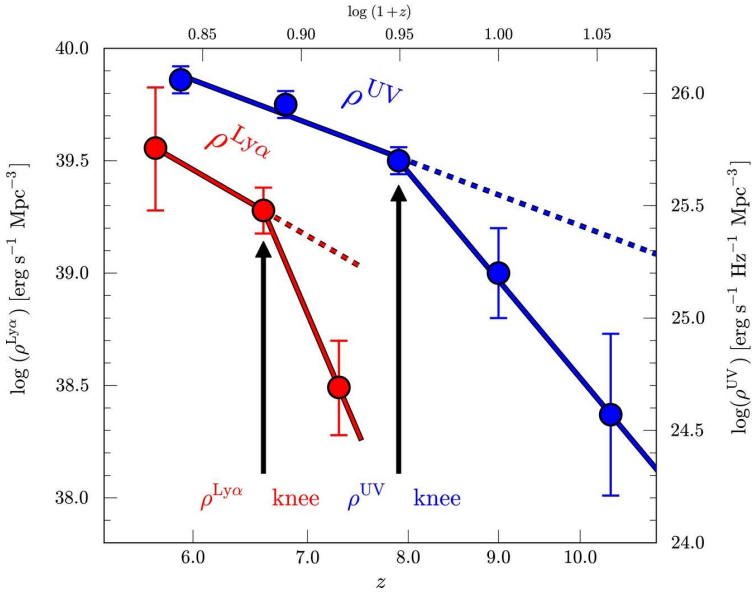

Fig. 12 Evolution of Lyα and UV luminosity densities based on recent observations (Konno et al. 2014). The red and blue circles represent the Lyα and UV luminosity densities, respectively (labeled on the left and right vertical axes, respectively). Toward high-z, the decrease of Lyα luminosity density is clearly more rapid than that of UV at $z \sim 7$, indicative of strong scattering given by neutral hydrogen gas in the IGM.

up to redshift $z \sim 14$. Assuming the sources are physically small, there will be a significant S/N advantage over JWST.

4.1.2 Detecting the sources of reionization

In the course of early galaxy formation, high-mass stars produce abundant UV photons that are believed to have been primarily responsible for cosmic reionization. Once reionization proceeds, the UV background radiation heats gas so as to suppress star formation in low-mass galaxies. Thus, early galaxy formation leads to reionization, initiating a "negative feedback loop" that actually *delays* the subsequent stellar mass build-up of the lowest mass systems. Thus, early galaxies and cosmic reionization would have a profound effect on the more recent history of galaxy formation.

At the end of the reionization era, at $z \approx 6$, galaxies that are directly detected in deep HST observations, with $M_{UV} \sim< -18$, appear to be sufficiently luminous and abundant to maintain the ionization of the IGM, provided that a substantial fraction ($\sim 30\%$) of the H-ionizing photons emitted by massive stars escapes the galaxies in which the stars are forming (the so-called "escape fraction"). However, at $z \approx 7-8$ the directly-observed galaxy population appears to fall short (e.g., Finkelstein et al. 2012) unless a large population of galaxies below the current detection limit is present. Recent observations suggest that the slope of the galaxy UV luminosity function steepens significantly between $z \sim 4$ and $z \sim 7-8$, where its slope (at observed magnitudes) approaches that expected for the dark matter halo mass function (e.g., Bouwens et al. 2015). The validity of extrapolations of the luminosity function to unobserved faint magnitudes is currently untested.

According to current theoretical models, the abundance of very faint galaxies is determined by the radiative cooling efficiency of gas within low-mass dark matter halos, which is extremely sensitive to the metallicity of the gas and (for truly zero-metallicity gas) by molecular hydrogen

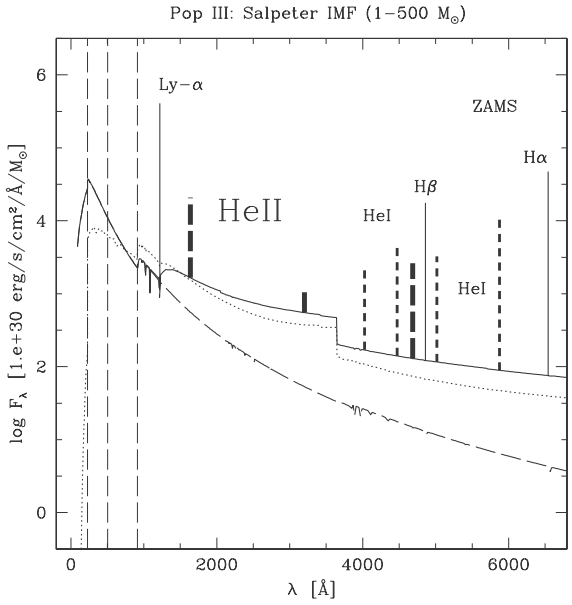

Fig. 13 Predicted spectrum of a Pop III ZAMS burst (from Schaerer 2002) based on non-LTE model atmospheres including H and He recombination lines. The dashed line shows the pure stellar continuum (neglecting nebular emission). Note the prominent He II 1640 (*thick dashed line*) and the importance of nebular continuum emission. Simulations suggest that the He II line, which decays rapidly within 2 Myr, may be a valuable tracer of metal-free stellar populations.

cooling (Jaacks et al. 2013; Boylan-Kolchin et al. 2014, Fig. 14). Moreover, the abundance of faint galaxies also depends on the effects of poorly-understood feedback processes (such as SNe) on subsequent star formation activity in the same regions. In short, the abundance of faint galaxies encodes the essential physics of star-formation and feedback in low mass dark matter halos.

Cosmic reionization models suggest that galaxies in the range $M_{UV} \sim -13$ to -18 produce more hydrogen ionizing photons than the luminous (M_{UV}) galaxies at z > 7. However, the abundance of such faint galaxies is essentially unknown and unexplored even with the deepest data in the Hubble Ultra Deep Field (Ellis et al. 2013). The on-going Hubble Frontier Fields (HFFs) initiative exploits gravitational lensing to search for still fainter galaxies behind six massive galaxy clusters. Scaling from the first HFF results, we may expect that the full HFF data set will identify a total of ~ 20 faint galaxies at $z \sim 6 - 10$, typically down to $M_{UV} \sim -16$, and typically magnified by a factor of ~ 10 (Ishigaki et al. 2015). Although this is an important step for exploring the high-z faint galaxy population, the HFF galaxy sample may be too small for robust statistical constraints on the faint end of the high-z luminosity function, and there may be lingering uncertainties on magnification factors that depend on mass models of the lensing clusters. Moreover, the Hubble imaging data alone do not provide spectroscopic information needed to evaluate the metal abundance, ionization state, or velocity fields in this important early galaxy population.

If, as expected, the very faint galaxies responsible for reionization are compact, then diffraction-limited observations with TMT will detect galaxies an order of magnitude fainter than those seen in the HFFs or that will be seen by JWST while allowing previously unstudied structures within the lensed galaxies to be resolved. An imaging campaign with TMT IRIS will unambiguously determine the abundance of high-z faint galaxies. Moreover, the combination of sensitivity and angular reso-

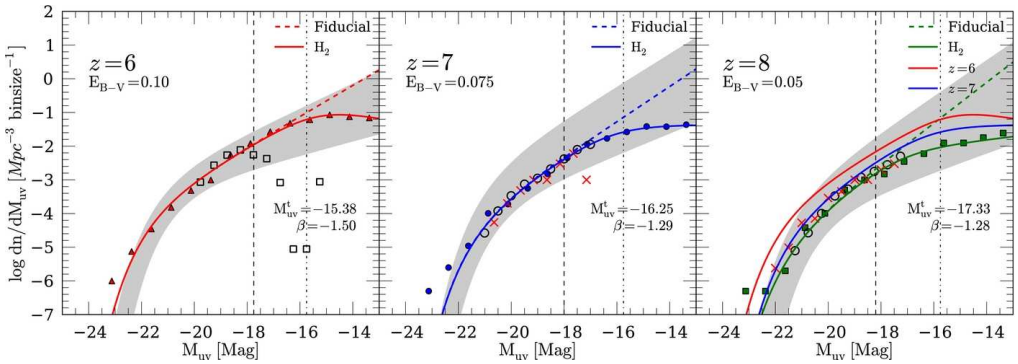

Fig. 14 UV luminosity functions at $z = 6$ (*left*), 7 (*center*), and 8 (*right*), predicted by two sets of star-formation models with different assumptions about the dominant cooling processes (Jaacks et al. 2013). The vertical dashed lines show typical deep HST observational limits, and the vertical dash-dotted lines present the approximate observational limits of JWST and HFF-source plane. TMT will probe high-z sources at the observational limits of JWST+HFF and fainter.

lution of TMT/IRIS and IRMOS will permit detailed spectroscopic studies of metal enrichment and outflow processes of these key sources.

4.1.3 The process and history of reionization

Another major open question is the *history* and *process* of reionization, i.e., how the IGM ionization develops over time and is distributed in space. Although direct observations of the 21 cm line at high redshift offer the promise of mapping the neutral IGM at the epoch of reionization, this will not be accomplished with high fidelity or angular resolution during the decade prior to TMT first light.Alternatively, one can probe neutral hydrogen gas clouds along the LOS to bright, high redshift background sources whose spectra show both Lyα and metal line absorption features. QSOs, gamma ray bursts (GRBs), and perhaps even bright galaxies can serve as the source of background illumination for this purpose.

At redshifts $z > 6$, line blanketing in the Lyα forest removes nearly all the light shortward of Lyα in the object's rest frame. Very small amounts of residual flux occasionally penetrate at $z = 6.5$ (the so-called "dark gaps"), which can be analyzed statistically to infer the structure and neutral fraction of the IGM (Songaila & Cowie 2002; Paschos & Norman 2005; Gallerani et al. 2006). Only a handful of bright quasars ($m_{\rm AB} < 20$) have been found at $z \sim 7$ and beyond, from the recent large-area NIR surveys of UKIDSS and VISTA (e.g., Venemans et al. 2013). The highest redshift quasar ULASJ1120+0641 has a redshift of 7.09. The damped Lyα line absorption profile seen in this quasar suggests that the neutral fraction of IGM was fairly large, >10%, at $z \approx 7.1$, favoring late-epoch reionization (Mortlock et al. 2011, see Fig. 15). It is also possible that IGM ionization may decline at higher redshift as intergalactic gas becomes progressively neutral; searches may then have to focus on the strong lines of low-ionizing species like OI and CII. The abundance of high-ionization CIV absorbers decreases from $z \sim 5$ to $z \sim 6$ (Ryan-Weber et al. 2009; Becker et al. 2009), possibly indicating evolution in the ionizing background consistent with the expected progress of reionization. However, high-ionization species like CIV require relatively hard-spectrum sources of ionizing photons in close proximity. Low-ionization OI, CII, and SiII absorption lines have also been observed (Becker et al. 2011). OI is of particular interest because of its strong coupling with HI via the charge exchange reaction (so that OI/HI = O/H) but interpretation depends on the unknown abundance of O. Similar absorption line studies can be conducted using GRBs as background continuum sources.

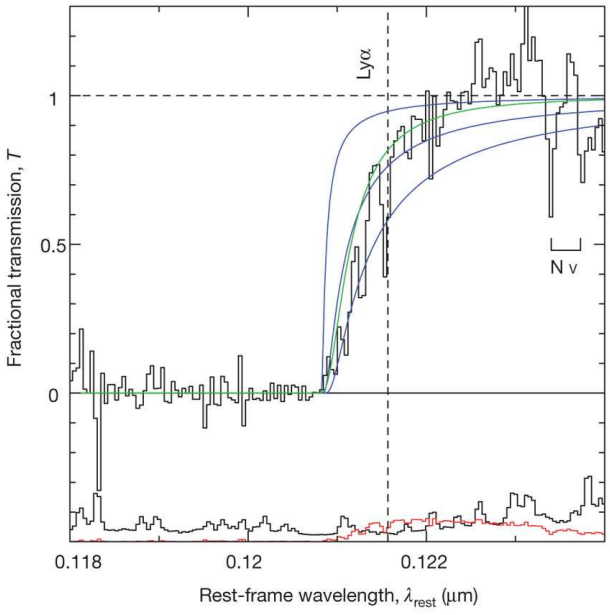

Fig. 15 The transmission profile of the $z = 7.09$ QSO ULAS J1120+0641 in the vicinity of Lyα at the emission redshift. (*black histogram*; Mortlock et al. 2011). The transmission profile is formed by dividing the observed ULAS J1120+0641 spectrum by the SDSS QSO composite spectrum, to remove the typical intrinsic Lyα emission line. At the bottom of the panel, the random and systematic uncertainties are denoted with black and red histograms, respectively. The blue curves represent model Lyα damping profiles from transmission through the IGM assuming neutral fractions of 10%, 50%, and 100% (*top to bottom*) and that the ionization front is located at a distance of 2.2 Mpc. The green curve indicates the absorption profile expected for neutral hydrogen column density of $N_{\rm HI} = 4 \times 10^{20}$ cm^{-2} located 2.6 Mpc in front of the quasar.

However, so far, there are only weak IGM constraints from observations of Lyα using GRBs at a redshift of 6.3 and below (Totani et al. 2014); progress at $z \gg 6$ has been limited by the lack of sufficiently bright GRBs (cf. the highest redshift GRB of $z = 8.2$; Tanvir et al. 2009). With its large aperture and fast response time for ToO observations, TMT will be able to obtain high-S/N spectra of faint GRBs out to very high redshifts. Nearly all of the information at these redshifts must come from Lyα damping profiles and metal lines longward of Lyα. At $z > 7$, all of these features lie at NIR wavelengths – the domain of TMT/NIRES.

As described in Section 4.1.1, recent observations suggest that Lyα damping wing absorption due to a substantially neutral IGM suppresses Lyα emission from galaxies at $z \sim 8$ and beyond. However, galaxies are also useful for probing the later progress of cosmic reionization history at $z < 8$, especially for investigating the topology of ionized bubbles in the late stages of reionization. Although neutral hydrogen in the IGM reduces the visibility of Lyα emission from distant sources, it also affects the line profile in a manner that is well understood (Miralda-Escudé 1998). Accurate observed line profiles as a function of environment and redshift can thus constrain the neutrality of the IGM, although present studies cannot discern the subtle differences in Lyα damping wing profiles expected (Ouchi et al. 2010). The measurements are challenging because of the need for high spectral resolution for individual sources, as well as the requirement to probe very faint, low-

mass systems in low-density regions, where Lyα damping wing absorption would be prominent as a result of patchy reionization. Once a large number of high redshift Lyα line emitters are located, e.g., by the on-going deep narrowband survey of Subaru Hyper Suprime-Cam, more detailed TMT spectroscopic follow-up studies will become practical. As an example, an 8 hour observation with TMT/IRIS can achieve S/N = 22 per resolution element for an emitter up to $z \sim 8$ with a Lyα luminosity of $L > 5 \times 10^{41}$ erg s^{-1}. Such systems have a star formation rate SFR of less than 10 $M_{\odot}$ yr^{-1} (Le Delliou et al. 2006) and are more representative and likely more numerous than the more luminous emitters for which such observations have been attempted so far.

4.2 Angular Sizes and the Synergy with JWST and Future Space Missions

Over the last 20 years there has been a vital synergy between HST and ground-based 8–10 m class telescopes: resolved imaging from space, and deep spectroscopy from the ground. The relationship between JWST and TMT will be somewhat different, although just as important. Both TMT and JWST have impressive imaging and spectroscopic capabilities. JWST has the advantage of a reduced NIR background in space, and its sensitivity at wavelengths longer than 2.5 microns provides sensitivity to galaxies at redshifts beyond 20. However, TMT has a much larger collecting area than JWST, and superior angular resolution (a factor of 5 higher) with AO-fed instruments, offering greater sensitivity for physically small, faint galaxies. TMT can resolve and study finer structures in galaxies than is possible with JWST. Unlike HST, JWST will offer sensitive multi-object spectroscopy with low to moderate spectral resolution (up to $R = 2700$ for JWST NIRSPEC), and at longer wavelengths, without atmospheric limitations. The higher resolution of TMT spectrometers (e.g., $R \approx 5000$ for IRMS) will improve detection limits for narrow emission and absorption lines, and offers velocity resolution that JWST cannot match.

Based on their expected timetables, TMT will see first light after the 5 year nominal lifetime of JWST operations. TMT observing programs will thus follow up galaxies detected in well-established JWST surveys, and study them in ways that JWST could not. TMT will be contemporaneous with future space missions that provide wide-field NIR survey capabilities, such as Euclid (ESA), WFIRST (NASA) and WISH (JAXA). These will also supply an abundance of distant galaxy targets for TMT follow-up.

It is very important to know how small these early galaxies are. Oesch et al. (2010) studied the morphology and size of the galaxies at $z = 7 - 8$ in the Hubble Ultra Deep Field (HUDF) and found that the galaxies with the UV absolute magnitude M(1600) = –18 to –21 ($0.2L^{\star}$ to $3L^{\star}$ for $z = 7$) are very compact, with the average size of 0.7 ± 0.3 kpc (1 kpc = 200 mas and 250 mas at $z = 7$ and 10, respectively, with the standard cosmology), but they are clearly resolved on the HST WFC3 image. Ono et al. (2013) also analyzed the images of the candidate $z = 8 - 12$ galaxies in HUDF and found that their half-light radii are extremely small, 0.3–0.4 kpc. These results suggest that the objects at $z > 7$ are small but may be resolved with the PSF size of JWST (~ 50 mas full width at half maximum (FWHM)) at 1.5 μm or TMT+AO (~ 12 mas) which corresponds to 0.15–0.25 kpc (50 mas) and 0.04–0.06 kpc at $z = 7 - 15$.

As TMT observations in this regime will be background-limited, the sensitivity is a strong function of source angular size. Figure 16 shows the S/N for spectroscopic detection of continuum emission from high-redshift galaxies observed with $R = \lambda/\Delta\lambda = 4000$ (the spectral resolution of TMT's IRIS) as a function of apparent magnitude for various spectroscopic aperture sizes. For extremely compact sources that are unresolved or only marginally resolved, corresponding to objects smaller than ~ 1 kpc (200 mas at $z = 7$) in their size, TMT will detect the continuum emission from the object with an S/N that is greater than can be achieved with JWST's NIRSPEC at $R = 1000$ and 2700 and greater than 60% of the S/N achieved with NIRSPEC for $R = 100$. Note that H_{AB} =27 corresponds to $2.3L^{\star}$ at $z = 8$, objects at the bright end of the luminosity distribution, and to $5.2L^{\star}$ at $z = 10$ if the luminosity evolution from $z = 6$ to 8 is extrapolated to $z \sim 10$. If the galaxies are

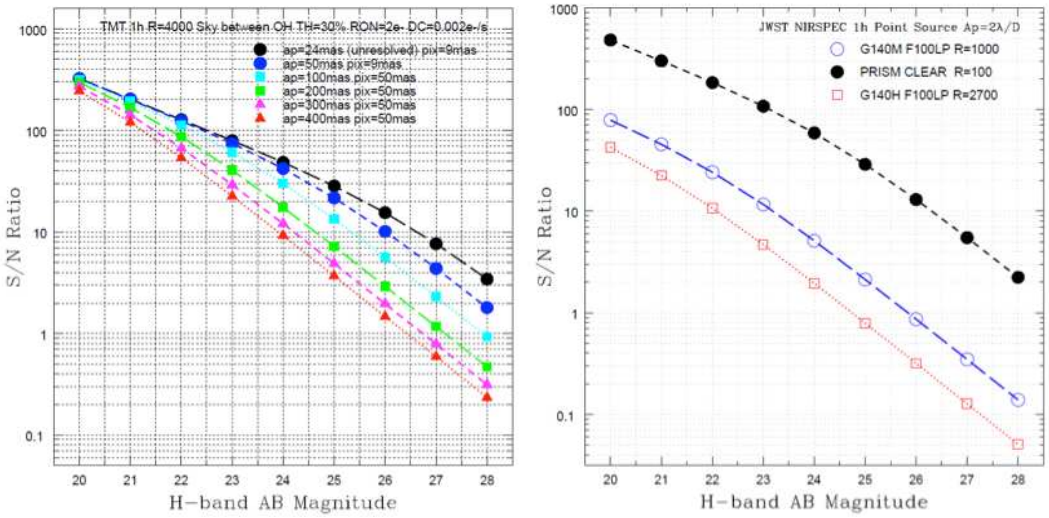

Fig. 16 Expected S/N ratio for the case of various sizes of the spectroscopic aperture estimated assuming TMT IRIS. (*Right*) Expected S/N ratio for a spatially-unresolved source with the different spectral resolution of JWST NIRSPEC obtained by NIRSPEC Exposure Time Calculator (*http://jwstetc.stsci.edu/etc/input/nirspec/spectroscopic/*).

resolved to $\sim$ 200 mas, which appears to be the case from the HUDF studies (Fig. 17), TMT will still be able to detect the continuum of $H_{AB} \sim 27$ mag source with S/N>10 in a 10 hr integration with wavelength binning to $R \sim 400$.

4.3 Gravitational Lensing

Detecting galaxies at $z > 6$ is challenging, not only due to the large distance to these objects (which makes them faint) but also due to the fact that galaxies had few stars when they first formed, meaning that they emit less light regardless of their distance. To overcome this problem one can use galaxy clusters as cosmic telescopes that, similar to ordinary glass lenses, magnify objects behind them. These cosmic telescopes allow us to find and study a unique set of faint, high-redshift galaxies, achieving an order-of-magnitude gain in sensitivity and spatial resolution over blank-field surveys. In addition, the detected sources behind a cluster lens are magnified in apparent size, allowing us to probe order of magnitude smaller physical scales. Several large campaigns are now underway to take advantage of this, particularly CLASH (Postman et al. 2012) and the HFFs. The first results from these surveys are extremely encouraging. Not only did they deliver the current record holder in redshift space ($z = 10.7$, Coe et al. 2013, see Fig. 18), these observations allow us to push the intrinsic luminosity limits further than the HUDF and study properties of representative galaxies at $z \sim 7$ and 8. For example, one can detect these galaxies with Spitzer and measure mature stellar populations as far as $z = 9.5$ (Zheng et al. 2012; Bradač et al. 2014). TMT/IRIS imaging of clusters will discover and resolve star forming regions in lensed objects more efficiently than even the HFF and CLASH (see Section 3.1.7).

Targeting sub-$L^\star$ Lyman-break galaxies (LBGs) spectroscopically at $z \sim 7$ is very difficult in blank fields due to their faintness. Indeed, the only spectroscopically detected sub-$L^\star$ galaxies at $z > 6.5$ to date are a $z = 7.045$ galaxy from Schenker et al. 2012 and a $z = 6.740$ galaxy from

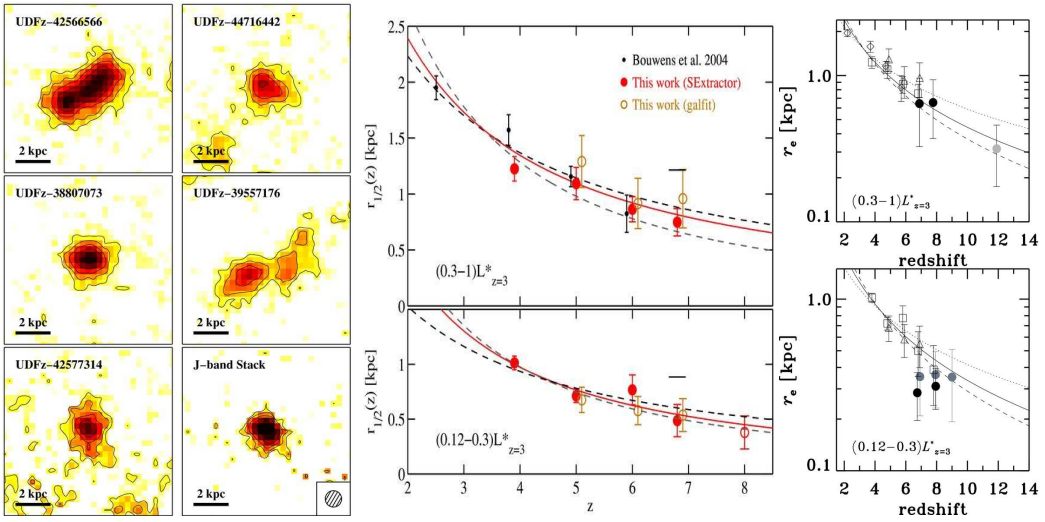

Fig. 17 Morphology (*left*) and size (*middle*) of galaxies at $z = 7-8$ (Oesch et al. 2010). *Right*: Size evolution of galaxies at $2 < z < 12$ (Ono et al. 2013).

Bradač et al. (2012). Both of these galaxies are lensed by a foreground cluster (A1703 and the Bullet Cluster, respectively), confirming the power of cosmic telescopes. Increasing the sample size is crucial, because with measurements of the EW distribution in Lyα Emitters (LAEs) we can distinguish between effects of interstellar medium (ISM) dust and neutral IGM and study the epoch of reionization (Treu et al. 2012, 2013b). We expect different EW distribution for sub-$L^\star$ and $>L^\star$ populations respectively if reionization is playing a role at these redshifts (Stark et al. 2010). The main missing observational ingredient is a measurement of the EW distribution for both luminous and sub-$L^\star$ galaxies at the redshifts of reionization. Cosmic telescopes allow us to probe the sub-$L^\star$ regime particularly efficiently. However, despite the magnification, spectroscopic redshifts have been measured for only a handful of sources close to the reionization epoch. As discussed earlier (Sect. 4.1.1), Lyα may be disappearing due to the increasing opacity of the IGM at $z > 6$. TMT detections for much weaker high-excitation emission lines like CIII] 1909 Å may be the most effective means to measure redshifts for these gravitationally lensed galaxies.

TMT will revolutionize the field and offer the best capabilities for such studies. In particular IRMOS, with its multiplexing capabilities will allow for an efficient follow up of galaxies behind cosmic telescopes. The one hour, 10-sigma TMT/IRMOS detection limit is $\sim 10^{41}$ erg s^{-1}. With assistance from lensing we can however push these limits by an order of magnitude lower and study $0.1L^\star$ Lyman Break Galaxies spectroscopically. Such systems will have an SFR of much less than 1 $1\,M_\odot$ yr^{-1}. TMT will give us an answer to whether these seeds of today's galaxies are responsible for reionizing the universe and what the topology of this process was. It will also allow us to explore galaxies and their stars in great detail from the time when the universe was only a few percent of its present age.

5 GALAXY FORMATION AND THE INTERGALACTIC MEDIUM

Tremendous progress has been made over the last decade in establishing a broad cosmological framework in which galaxies and large-scale structure develop hierarchically over time. However, there

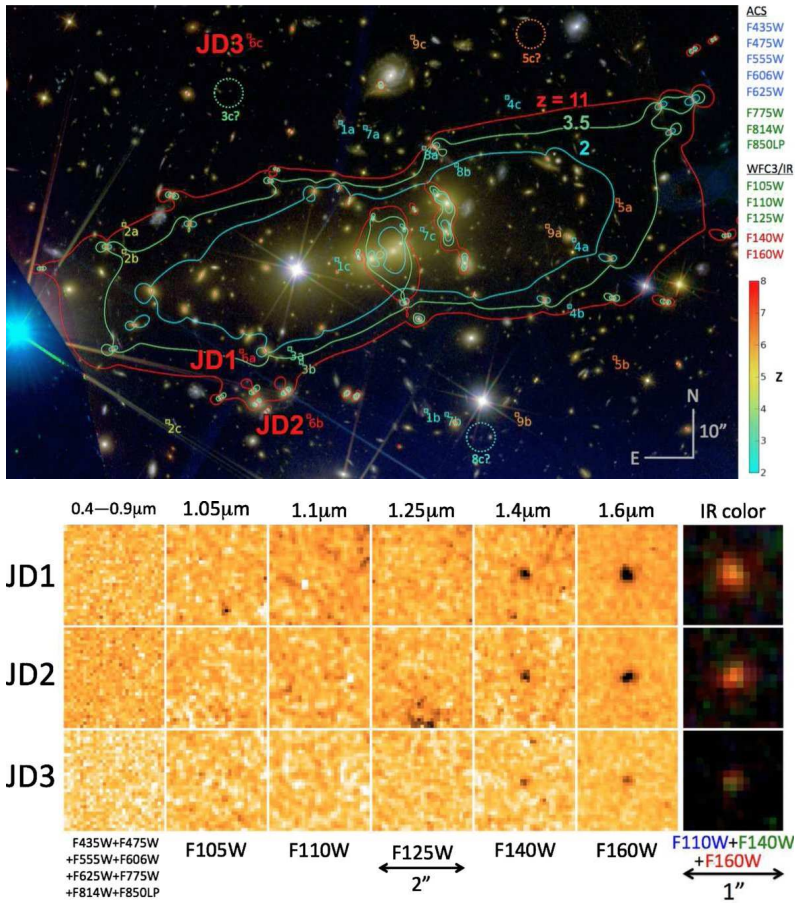

Fig. 18 A massive galaxy cluster, MACS J0647.7+7015, acts as a powerful gravitational lens, producing three highly magnified images of a background galaxy estimated to be at a redshift $z = 10.7$. Top: HST image of the cluster, from the CLASH survey, with the critical magnification lines at various redshifts (2, 3.5 and 11) indicated. The locations of the three images of the faint galaxy are marked JD1, JD2 and JD3. Bottom: Images of the three lensed images from optical through NIR wavelengths. The galaxy "drops out" at wavelengths shorter than 1.4 microns, strongly suggesting a very high redshift. From Coe et al. (2013).

remain many unanswered questions about how the observable universe of galaxies is related to the growth of the underlying distribution of dark matter; most of this uncertainty relates to our poor understanding of the complex baryonic processes that must be included in any successful theory of galaxy formation: gas cooling, star formation, feedback and merging. Understanding how these processes operate on galaxy scales is an inherently multi-wavelength observational problem that is limited at present by the sensitivity of our tools for extracting detailed physical information, for both stars and gas, as a function of cosmic time.

Observations of galaxies beyond $z \sim 1$, selected using initial surveys at UV, optical, NIR, and far-IR rest-frame wavelengths, have begun to establish in broad-brush what the universal history of star formation has been like over the last $\sim 90\%$ of the age of the universe. As Figure 19 shows,

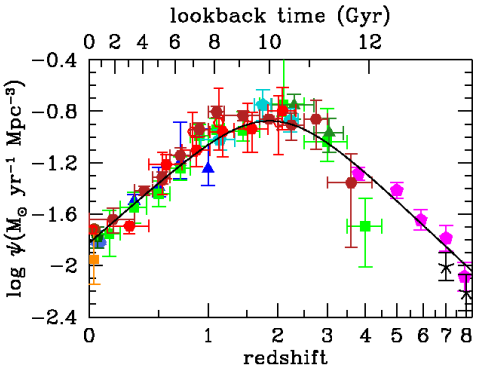

Fig. 19 Current census of the integrated SFR per unit co-moving volume since redshift $z \sim 8$. The star formation rate density (SFRD) is ~ 15 times higher at its peak near $z \sim 2$, when the universe was about 3 Gyr old, than at $z \sim 0$, and increases by a factor of ~ 25 from $z \sim 8$ to $z \sim 2$. Approximately 50% of the stars in the present day universe were formed over the ~ 2.5 billion year interval between $z \sim 1.5 - 3.5$. The history of BH mass accretion follows a surprisingly similar evolution with redshift (from Madau & Dickinson 2014).

the current census paints a picture in which the peak era for star formation in galaxies occurred in the distant past; indeed, while precise numbers remain somewhat controversial, there is now little doubt that star formation peaked at redshifts between $1.5 < z < 3$ and a large fraction of the stars observed in the present-day universe formed during a relatively brief but very intense period stretching between $z \sim 6$ and $z \sim 1.5$, corresponding to an interval of cosmic time over which the age of the universe was between 1 and 4 Gyr. Very similar behavior with cosmic time is observed for the growth of SMBHs — a broad peak near $z \sim 1.5 - 3$ with a rapid ramp-up prior to $z \sim 3$ and a rapid decline after $z \sim 1$.

What is the interplay between star formation and AGN growth? Physical understanding of galaxy formation has been limited by the observational difficulties in studying the detailed physical processes acting on high redshift galaxies, due both to their faintness and their small angular sizes. Through the recent advent of IFU spectroscopy and AO systems on ground-based 8–10 m class telescopes, however, we are just now beginning to witness the relevant processes *in situ* by resolving galaxies both spatially and kinematically; at present, however, such studies are limited to the brightest examples. TMT, with its huge light gathering power coupled with diffraction-limited angular resolution, will revolutionize our understanding of the structure of forming galaxies throughout the peak epoch of galaxy formation.

During this "peak epoch of galaxy formation", most of the baryons in the universe actually reside *outside* of galaxies, in the IGM and circumgalactic medium (CGM). The IGM/CGM is thus a vast reservoir of normal material acting as both a source of gas to fuel galaxy formation, and a "sink" of the waste products of that process. The structure of the IGM/CGM is increasingly modified by the energetic processes occurring in forming galaxies, and thereby acts as a laboratory where the most sensitive measurements of the physics of the galaxy formation process may be made. For these reasons, understanding galaxy formation in the universe requires measurements of all material, both inside and outside of galaxies. Fortuitously, observational access to both galaxies and the IGM during this crucial epoch is excellent for large-aperture telescopes placed at the very best terrestrial sites.

TMT will thus play a fundamental role in providing the detailed physical measurements necessary to understand the development of present day galaxies. TMT will provide rest-frame UV spectra of unprecedented sensitivity and depth: WFOS and HROS will together provide exquisite informa-

tion on the physics of gas associated with forming galaxies and the IGM using the rich rest-frame far-UV transitions made observable from the ground by the redshift of the sources. IRIS, IRMS, and IRMOS, all taking advantage of the diffraction-limited capabilities of TMT in the NIR, will provide spectra of extremely high sensitivity and spatial resolution, allowing the first detailed studies of galaxy structure, dynamics, and chemistry while they are in the process of forming the bulk of their stars. The NIR observations with TMT will enable studies of distant galaxies, as they are growing, using the same well-calibrated rest-frame optical diagnostic spectral features of both stars and gas, that have been established by decades of research on nearby galaxies.

5.1 The Peak Era of Galaxy Assembly

5.1.1 TMT and galaxy formation

In hierarchical structure formation, gravitationally bound structures begin on small scales, and the largest bound objects are expected to be the last to form. A universal peak in overall star-formation and BH accretion, as observed, is not necessarily expected. Neither is the observation that the most massive known galaxies appear to finish forming their stars earliest, nor that typical galaxies at redshifts $z \sim 1-3$ appear to be forming stars at rates that are 10 – 100 times higher than for typical galaxies in the local universe. The symbiotic relationship between the formation of galaxy spheroids and central BHs also does not follow directly from a cosmological framework alone. The complexity of galaxy formation requires following the behavior of dark matter *and* the astrophysics of star formation, feedback of energy, accretion and expulsion of gas, and effects of environment. Paradoxically, the former task is easier, even if we know very little of the properties of the precise nature of dark matter, because the physics of baryons are much more complex to model in a cosmological context. To make progress, observations of the baryonic component (both gas and stars) must inform theoretical developments with substantially better precision than possible today.

Among the key remaining unanswered questions in galaxy formation are:

- How does the distribution of dark matter relate to the luminous stars and gas that we see?
- Why does the growth of stellar mass and BH mass in galaxies apparently proceed in an "anti-hierarchical" fashion—that is, the largest forming earliest?
- What is the physical mechanism through which galaxies at different epochs acquire their gas, and how much cross-talk and exchange is there between galaxies and the IGM/CGM?
- What internal or environmental effects modulate the rate at which galaxy formation can occur, and what ultimately shuts down ("quenches") star formation in massive galaxies?
- How do energetic processes—massive star formation, BH accretion and SNe—influence the formation and evolution of galaxies?
- What physics are responsible for the correlation between central SMBHs and the properties of their host galaxies (which is the "chicken" and which the "egg")?
- What factors drive apparent differences between the low-redshift and high-redshift universe for galaxy scale star formation?
- How do the stellar birthrates as a function of stellar mass (the IMF) differ, and what are the ramifications of the differences?

Answers to these questions will come from detailed studies of galaxies and the IGM at high redshift. One needs to measure the distribution and metallicity of gas inside and outside of galaxies, the SFRs, internal structure, stellar content, and dynamical states of galaxies, all as a function of environment and of cosmic time. The combination of WFOS, IRIS, IRMS, and (later) IRMOS and HROS mounted on TMT provide a near ideal instrument suite for attacking the problem of structure formation in the distant universe. Across a wide wavelength range (0.3–2.4 μm), TMT complements or exceeds the spectroscopic capability of JWST while providing higher spatial resolution. In com-

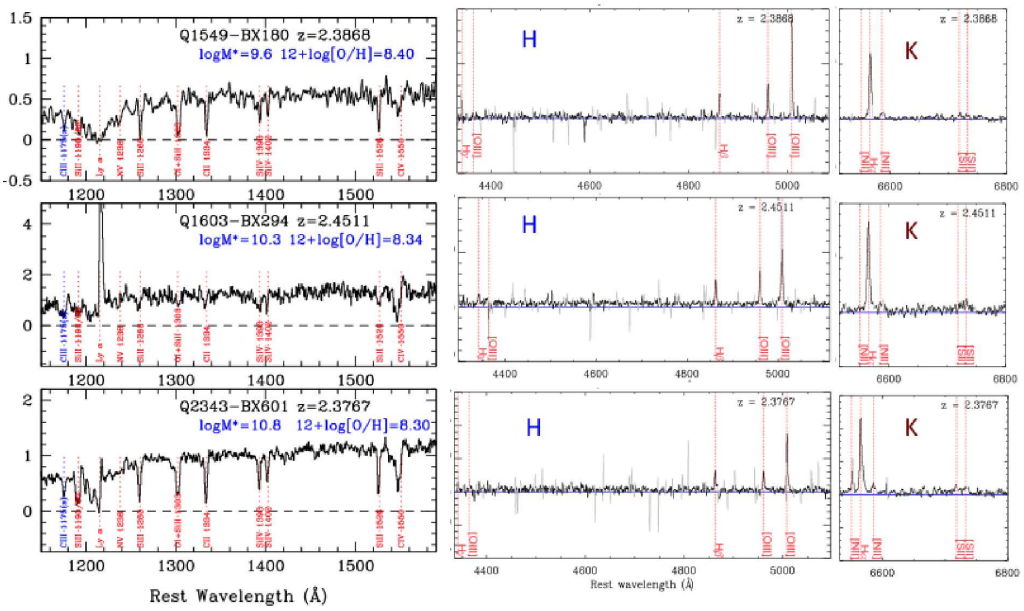

Fig. 20 Example spectra of three $z \sim 2.4$ galaxies; the left panels show the rest-frame far-UV spectra observed in the optical (0.31–0.6 μm), while the center and right panels show the rest-optical nebular emission lines observed in the H (1.6 μm) and K (2.2 μm) atmospheric windows. The rest-far-UV spectra contain a wealth of interstellar absorption features, nebular emission lines, and stellar wind and photospheric features from massive stars. The rest-optical spectra are used for measuring kinematics, gas-phase metallicities and ISM physical conditions. Credit: C. Steidel (CIT).

bination with ALMA, which tracks thermal emission from dust and provides information on the molecular gas content and kinematics of galaxies at similar spatial resolution, TMT +AO will be a powerful tool for tracking the process of galaxy formation during the most active period in the history of the universe.

Broad wavelength coverage (0.3–2.4 μm) is key to probing the critical spectral diagnostics, from the far-UV stellar, interstellar, and intergalactic lines of H and metals, to the nebular emission and stellar absorption features in the rest-frame optical. Figure 20 shows examples of low-resolution spectra obtained using current 8 m class telescopes for some of the brightest star-forming galaxies at redshift $z \sim 2$, in order to illustrate some of the spectral features of interest.

The planned TMT instrument suite (see Sect. 2.3) will play complementary roles in addressing these fundamental issues:

– WFOS is optimized both for obtaining identification-quality spectra of the faintest galaxies and AGNs throughout the epoch of galaxy formation, and for high quality rest-frame UV spectra of large samples of galaxies and AGNs that will provide diagnostics of gas and stars in galaxies, as well as the distribution, metallicity, and physical conditions of the IGM.
– IRMS allows the study of key diagnostic nebular and stellar lines in the rest-frame optical (e.g. [OIII], Hβ, Mgb and Hα). IRMS will obtain extremely sensitive multiplexed spectra in both emission lines and stellar continua in the observed frame NIR, providing information on chemistry, kinematics, and stellar populations.

– IRIS will dissect galaxies with velocity resolution of 30 km s^{-1} on physical scales as fine as 50–70 pc at any redshift in the range $z = 1 - 6$.
– IRMOS will combine the diagnostic power of IRIS and the multiplexing capabilities of IRMS, providing integral field spectroscopy in the NIR (0.8–2.5 μm) for up to 20 objects distributed over a $5'$ FOV.
– HROS, with a factor of $>$20 gain in sensitivity over the best current-generation high resolution spectroscopic capabilities, will vastly increase the number of lines of sight that can be used for the most detailed studies of the IGM and of individual galaxies and AGNs.

Below, we highlight a few of the possible science avenues that can be explored using these capabilities.

5.1.2 How does the distribution of dark matter relate to the luminous stars and gas we see?

In the present day universe, the distribution of galaxy stellar masses ($M_\star$) – the "stellar mass function"– of galaxies appears to have a different shape from that of the theoretically expected distribution of dark matter halo masses. Galaxies with small $M_\star$ have a much "flatter" distribution than (i.e., fewer galaxies with lower $M_\star$) than expected if galaxies formed with the same ratio of stellar-to-dark matter at all masses. At high $M_\star$, the stellar mass function drops exponentially with increasing halo mass, following the Schechter function (e.g. Cole et al. 2001). This behavior, where galaxy formation appears to be less efficient at low- and high-$M_\star$, is almost universally ascribed to "feedback"; the qualitative picture advocated by the majority at present is that ionizing photons, energy, and momentum produced by massive star formation and SNe are the dominant effects for lower-$M_\star$ galaxies, while AGNs (i.e., energy/momentum produced by accreting SMBHs) play the dominant role at the high-$M_\star$ end of the galaxy mass function.

While the need for feedback is universally recognized for any viable galaxy formation model, it is fair to say that we do not yet understand how, when, or where it operates, nor which of the many physical processes dominates at a given time in a given galaxy. Making progress will require observations sensitive to the details of all of the relevant physical processes, in a range of galaxy masses and over a range of cosmic times. These observations, at a minimum, must include measurement of AGN activity, massive star formation, stellar content, and gas-phase physical conditions both inside forming galaxies and in the surrounding IGM/CGM. TMT, using multiple instruments and techniques that each constitute a huge gain over existing facilities, will play a central role: extremely high spatial resolution behind AO, combined with the diagnostic power of spectroscopy (AO+IRMOS, IRIS, IRMS, and NIRES) in the NIR, and unmatched complementary sensitivity for spectroscopic observations in the observed-frame optical (WFOS, HROS), providing access to all of the astrophysical diagnostics in the rest-frame UV (Fig. 20).

5.1.3 The growth of stars: star-formation histories, dust, and chemical evolution

Fundamental to a comprehensive understanding of galaxy evolution is assessing the mechanisms by which galaxies accumulate their gas and form stars. The effect of these mechanisms (e.g., gas inflows, outflows, galaxy mergers) is imprinted on the star-formation histories of galaxies. From the theoretical side, hydrodynamical simulations suggest that galaxies living in relatively massive halos at intermediate redshifts accumulate most of their gas through relatively smooth accretion, rather than through major mergers, resulting in star-formation histories that can be well-approximated as smoothly varying functions, typically as exponentially declining or rising, or constant (e.g., Noeske et al. 2007; Reddy et al. 2012). Clustering studies and cosmological simulations suggest that star-formation histories may be more stochastic at lower stellar masses ($\leqslant 10^9 M_\odot$) at higher redshifts ($z > 1.5$). The effect is that outflows in these faint galaxies may be enhanced by short bursts of star

formation, and thus responsible for a majority of the globally-averaged metal enrichment of the IGM (Oppenheimer et al. 2012).

A promising method to deduce the level of stochasticity is to use probes that are sensitive to star formation on different timescales, such as UV continuum and Hα emission. Measuring these tracers for very faint and low mass galaxies will become routine with TMT's WFOS and IRMS instruments, and can be used for detailed studies of the "burstiness" of star formation in low mass galaxies. Combined with information from WFOS (and eventually HROS) on the CGM/IGM occupied by these objects will lead to a complete picture of IGM chemical enrichment from the outflows of faint galaxies. Further constraints on the stellar populations will come from the modeling of high-resolution spectra (e.g., from WFOS and HROS) of the stellar emission/absorption features in the rest-UV, giving detailed information on the massive star populations and the impact of binarity and mass loss on the effective temperatures, ionizing parameters, Lyman continuum escape fractions, and recombination line strengths in HII regions. Similarly, rest-optical spectroscopy of the Balmer absorption lines, Ca HK, MgB, and Fe lines will yield constraints on the star-formation history from both overall metal enrichment and measurement of metallicity ratios [α/Fe].

Critical to observations of high-redshift galaxies is the degree to which stellar light is obscured by dust. Local prescriptions for dust corrections appear to work reasonably well on average for $\sim L_\star$ galaxies at $z \sim 2$, but there are subsets of galaxies (e.g., the youngest galaxies, and the dustiest galaxies) where such relations break down (e.g., Reddy et al. 2010). At redshifts of ~ 5, there is evidence that the attenuation curve in typical LBGs may be more consistent with that found in present-day low metallicity galaxies, like the Small Magellanic Cloud (SMC) (Shim et al. 2011; Capak et al. 2015). WFOS and IRMS will enable detailed studies of the shape of the attenuation curve, potentially for individual galaxies where the intrinsic spectrum revealed through dust-free lines of sight can be spatially resolved from the dustier regions of the galaxies. The measurement of multiple Balmer line ratios (Hα/Hβ, Hβ/Hγ, Hγ/Hδ) will constrain the shape of the nebular reddening curve in individual galaxies. Together, the stellar and nebular reddening curves can be used to obtain more robust constraints on the stellar masses, ages, reddening, and star-formation rates of galaxies, as well as better understanding of the impact of nebular line emission on the stellar population modeling from photometry alone.

Aside from a better understanding of the effects of dust obscuration, dust in the gaseous phase (i.e., the metallicity) can be used as another probe of star-formation history and chemical evolution. Gas-phase metallicities measured with rest-optical emission lines, in concert with galaxy stellar masses and star-formation rates, provide important empirical constraints on the effect of galactic winds (e.g., Davé et al. 2012) on the chemical evolution of galaxies. IRMS, IRIS, and IRMOS will extend what is possible using current NIR spectrometers on 8 m class telescopes, bringing into reach diagnostics of metallicity for galaxies as faint as $L_\star/100$ at redshifts $1.4 < z < 3.8$. High spatial resolution emission line maps will reveal the variation in kinematics, excitation mechanism, stellar populations, and metallicity with spatial location within galaxies—all essential ingredients to understanding their formation and evolution.

5.1.4 The formation of passive galaxies and the birth of the Hubble Sequence

A fundamental property of galaxies that still eludes our full understanding is the Hubble Sequence, including the physical mechanisms that lead to the formation of early-type galaxies, namely the quenching of star formation. Gas removal and heating by feedback from AGN and/or star-formation have long been identified as likely mechanisms responsible for quenching, but the processes that terminate star formation on galaxy scales and prevent it from happening again on secular timescales have not been firmly identified yet.

Current facilities have identified massive and passive galaxies up to redshift $z \sim 3$ (e.g. Gobat et al. 2012, 2013; Spitler et al. 2014; Whitaker et al. 2013; Guo et al. 2012) and shown that their

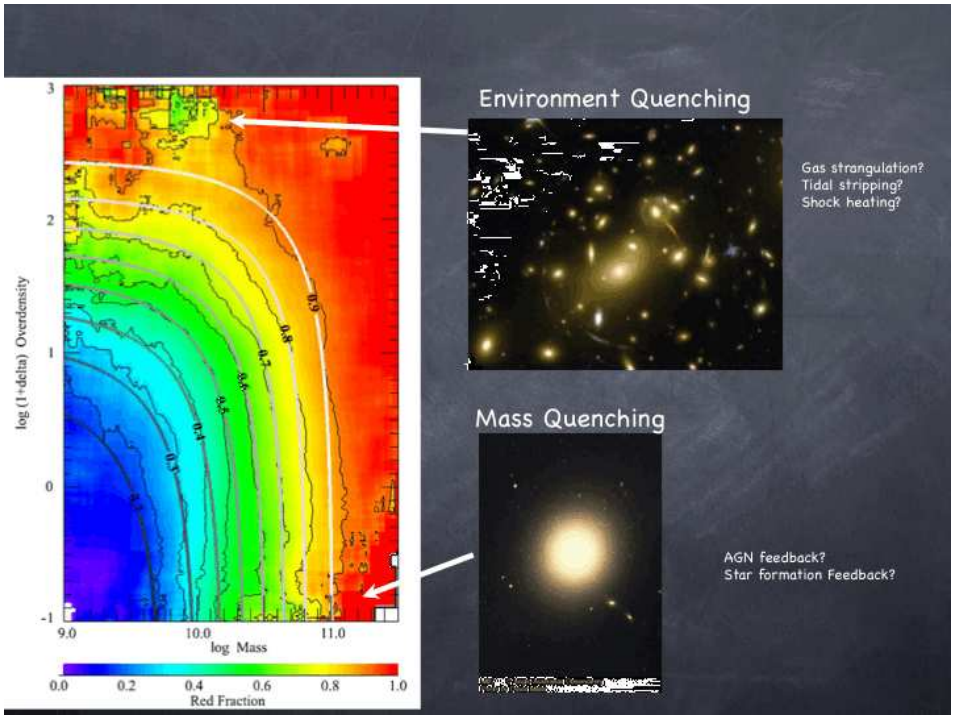

Fig. 21 The fraction of red and passive galaxies, a proxy for the probability that a galaxy's star formation has been "quenched", as a function of local overdensity and stellar mass. Evidently, processes related both to the mass of individual galaxies and to their environment cause the termination of star formation, with the former being the primary driver and the latter contributing at the $\sim 10\%$ level (from Peng et al. 2012). Which stellar mass-dependent processes control the quenching of star formation activity remains unknown.

abundance grows very rapidly afterwards (Cassata et al. 2011), suggesting that the backbone of the Hubble Sequence is in place by $z \sim 2$ (e.g. Lee et al. 2013a). At the same time most cosmological simulations suggest that, at $z > 2$, high mass galaxies can maintain high SFRs over long timescales from continuous accretion of cool gas from the IGM (e.g. Kereš et al. 2005; Dekel et al. 2009), while at lower redshift both the accretion rate and the physical state of accreted gas change at fixed stellar mass, leading to a dwindling of the gas supply available for star formation. While direct evidence that "quenching" of high mass galaxies must occur is plentiful, the processes physically responsible for it have not been clearly identified. At present, it seems that quenching depends on both galaxy mass and larger-scale environment (e.g. Peng et al. 2012, see Figure 21).

At $z > 2$ the population of galaxies in which star formation has ceased (i.e., they have become "passive") is dominated by those having very compact morphologies and large stellar masses ($M_\star > 10^{11} M_\odot$), suggesting that these systems are the first to quench and pointing to very high density of gas and stars as conditions conducive to effective "mass" quenching (Bell et al. 2012). Indeed compact, massive post-starburst galaxies have been observed with outflow speed in excess of $\sim$1000 km $^{-1}$ (Diamond-Stanic et al. 2012), significantly higher than less compact galaxies of similar stellar mass. Very deep stacks of WFC3/HST images of compact passive galaxies at $z \sim 2$ have found extremely steep light profiles ($n > 3$) and no evidence of the more diffuse component expected in merger remnants (e.g. Hopkins et al. 2008; Wuyts et al. 2010), adding support to the

notion that early massive galaxies formed more effectively via highly dissipative gas accretion than hierarchical merging of stellar sub-systems (Hopkins et al. 2008; Williams et al. 2014).

To make progress we need to explore the complex multi-dimensional manifold of galaxy properties and local environment. Diffraction limited NIR images with TMT will detail the morphology of the individual galaxies at optical rest-frame wavelengths with better spatial resolution than JWST NIRCam. TMT spectroscopy at optical and NIR wavelengths, where most of the relevant spectroscopic diagnostics of gas kinematics, stellar dynamics, star-formation, and AGN activity are found for $z < 4$, will allow detailed studies of the stars and gas of individual galaxies and of their circumgalactic gas (via absorption features of suitable background sources, as discussed in Sect. 5.2 below).

5.1.5 The stellar initial mass function, early black holes and the growth of quasars

A variety of observational data suggest the possibility of environmental dependence on the shape of the stellar IMF in galaxies over cosmic time. The clues arise from observations of the rates of high-redshift GRBs (e.g. Robertson & Ellis 2012; Chary et al. 2007), specific star-formation rates of high-redshift Lyman break galaxies (Shim et al. 2011; Davé et al. 2008) and the metal yields in Damped Lyman-alpha systems (Cooke et al. 2013, 2014). Recent observations of low metallicity dwarf galaxies in the Milky Way's neighborhood further argue in favor of an IMF which is "bottom-light" i.e. showing an underabundance of stars between $0.5 - 0.7\ M_{\odot}$ compared to a Salpeter IMF. Is there a metallicity dependence of the IMF? Does a top-heavy IMF in the first galaxies provide the intermediate mass seed BHs for the formation of quasars? These are key questions which require spectroscopic follow-up of both star-forming and AGN candidates in the distant universe identified through wide-field imaging surveys.

For example, spectroscopic measurements of the rest-frame far-UV spectra of LBGs offer direct constraints on the stellar birth rates at the "top end" of the stellar IMF, as well as the duty cycle of unusual and/or short-lived phases of high mass star formation (e.g., Pettini et al. 2000; Shapley et al. 2003; Jones et al. 2012). The same spectra provide constraints on O-star metallicity, nebular abundances and excitation, and models of massive star main sequence evolution (see Fig. 22). The most important UV features, found in the rest-wavelength range $1000 < \lambda_0 < 2000$ Å, are observationally accessible (using WFOS and IRMS) at all redshifts $1.5 < z < 7$.

Measurement of Fe-peak element abundance patterns in Damped Lyman Alpha QSO absorption line systems (DLAs; e.g. Cooke et al. 2011) have proved to be a powerful technique for tracing the nucleosynthetic yields of massive stars. At the present time, there is considerable degeneracy in the stellar population synthesis models such that the elemental yields can be fit very well by several models of intermediate mass stars ($15 - 40\ M_{\odot}$). Precision measurements of the [C, O/Fe] abundances in metal poor systems will be a powerful technique to constrain the mass and metallicity of the stars responsible for enriching the DLA systems and potentially the stellar IMF at intermediate masses.

Finally, the presence of very bright QSOs at $z > 6$ (see also Sect. 4.1.3) has come as a significant surprise, since it implies very early formation of BH masses as large as $10^{10}\ M_{\odot}$. Do these QSOs harbor significant stellar populations in their host galaxies? Are the BHs being fed via "super-Eddington" accretion on to intermediate mass black holes (IMBHs)? Are these IMBHs the end states of the earliest generations of massive stars? Measuring the metal abundances in QSO host galaxies, as well as studying the dynamics of the gas in these systems, will provide a better understanding of the formation of the most massive BHs at early times. High spatial resolution IFU observations are key to separating QSO light from host galaxy light. Clever techniques to obtain high dynamic range in the observations will likely need to be pursued while spectroscopic measurements of the gas kinematics and outflows will provide a better handle on the accretion rates of these systems.

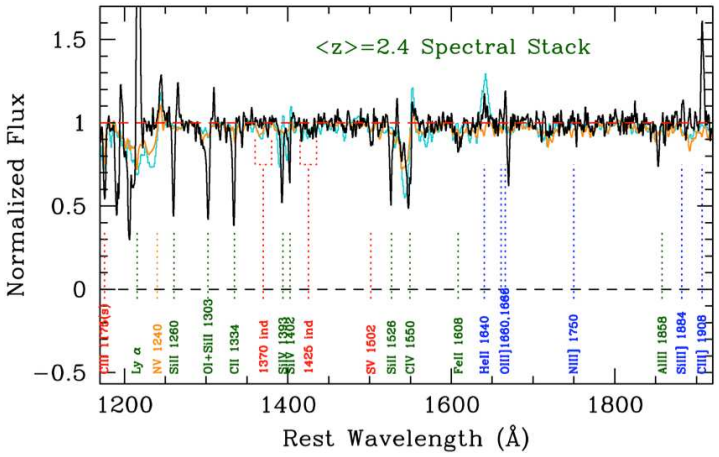

Fig. 22 Rest-UV composite spectrum of star-forming galaxies at $\langle z \rangle \sim 2.4$, obtained with $R \sim 1500$. The labeled features are color-coded according to their origin: red=stellar photospheric (O-stars); blue=nebular; green=primarily interstellar; orange: hot star wind lines. The CIV feature includes both a stellar P-Cygni emission/absorption component as well as interstellar component; HeII includes both nebular (*narrow*) and stellar (*broad*) components. Superposed on the observed spectra are population synthesis models, both assuming Salpeter IMF and 0.2 solar metal abundance: cyan: BPASS (Eldridge & Stanway 2009); light orange: Rix et al. (2004).

5.1.6 The census of baryons and the baryon cycle

Most baryonic matter, particularly during the early history of the universe, is actually outside of galaxies. Intergalactic space is filled with a tenuous gas that provides "fuel" for forming galaxies, and is a repository for material expelled by galaxies by energetic processes such as SN explosions and accretion-powered AGN activity. The interplay between the galaxies and the IGM is of prime importance for understanding the history of normal matter in the universe, the process of galaxy formation, and the effects of the "feedback" of energy produced by forming galaxies. A number of studies have found the ubiquitous presence of galaxy-scale outflows at high redshift, and the direct correspondence between HI and metal absorption systems in the inter-galactic medium (as probed by background quasars) and galaxies in the same volumes (e.g., Pettini et al. 2002; Adelberger et al. 2003; Steidel et al. 2010; Rudie et al. 2012; Hennawi & Prochaska 2013; Turner et al. 2015). The imprint of such galaxy flows can be seen most readily in the rest-UV, where the naturally dark terrestrial background in the optical (defined for the present purposes as 0.31–1 μm) makes spectroscopy of faint objects feasible for at least the brightest examples with 8–10 m telescopes. As illustrated earlier in Figure 20, the rest-UV spectra of galaxies contain a vast amount of information because of the very large number of ground-state transitions of astrophysically abundant ions at these wavelengths, including hydrogen Lyα, CII, CIII, CIV, NI, NV, OI, OVI, SiII, SiIII, SiIV, FeII, AlII, AlIII, to name a small subset. The offsets between lines arising from the nebular regions (e.g., HeII in the rest-UV, or [OII]/[OIII] and Balmer lines in the rest-optical), and those arising from the ISM allow for direct measurements of galaxy-scale outflow velocities, along with a host of other physical information including the shape of the stellar IMF at the high mass end, stellar chemical abundances, the chemistry of the interstellar gas, and the kinematics of gas motions within the galaxy. Currently, these details can be ascertained with spectral stacks or for individual bright lensed LBGs (e.g., cB58; Pettini et al. 2002).

Table 1 TMT/IRMS Predicted Sensitivity

Passband	Spec. Sky Brightness, mag arcsec^{-2} Vega (AB)	Continuum S/N = 10,1 hour, $R = 3600$ (0.23″ slit) Vega (AB)	Line flux S/N = 10, 1 hour, $R = 3600$ (0.23″ slit) (erg s^{-1} cm^{-2})
Y (0.97 to 1.13 μm)	18.8 (19.4)	23.4 (24.4)	7.4×10^{-19}
J (1.15 to 1.35 μm)	18.2 (19.1)	23.0 (24.1)	6.4×10^{-19}
H (1.48 to 1.80 μm)	17.2 (18.6)	22.7 (24.1)	5.6×10^{-19}
K (1.95 to 2.25 μm)	16.6 (18.4)	22.1 (23.9)	4.8×10^{-19}
K (2.25 to 2.40 μm)	14.2 (16.0)	20.9 (22.7)	1.9×10^{-18}

Notes: spectroscopic limits assume 0.01 e$^-$/s dark current and effective read noise of 5e$^-$/pixel, with background for spectral regions between OH lines, evaluated over a 3 pixel spectral resolution element and assuming a $0.5''$ extraction aperture.

Fortunately, spectra of the quality and diagnostic power of the cB58 spectrum will be within reach for relatively typical $\sim L_\star$ galaxies using TMT/WFOS, while obtaining spectra of high quality but lower resolution will be possible for objects significantly fainter than $L_\star$ even at $z \sim 6$ with modest ~ 1 hour integration times – the gain in sensitivity over current 8 m telescopes for spectroscopy over the 0.31–1 μm wavelength range will be a factor of at least 14. The sensitivity gain will bring intrinsically faint galaxies during the epoch of galaxy formation within spectroscopic reach for the first time, and will vastly increase the fraction of the high redshift populations for which extremely high quality spectra will be achievable, and where gas inflows and outflows can be measured in detail.

Using IRMS, it will be practical to obtain nebular spectra of hundreds of high redshift objects within a survey region, where every spectrum will be of high enough quality to measure velocity dispersion, chemical abundance, SFR, stellar excitation, and characteristic electron density — and to evaluate whether or not active AGNs are present–for galaxies at the limits of current *imaging* surveys.

NIR IFU spectroscopy will also be essential for finding evidence of outflows induced by AGN winds and jets, that are thought to provide a crucial role in preventing runaway star formation in the most massive galaxies (Fabian 2012). Current 8 m class telescopes are only capable in finding such outflows in rare, highly-luminous AGNs at $z \sim 0.5 - 2$ where these feedback effects are most important (e.g. Cano-Díaz et al. 2012). TMT will be able to observe these outflows on smaller spatial scales, and in more typical, less luminous AGNs. Together with ALMA observations of the corresponding molecular outflows, and sensitive VLA observations of the synchrotron emission from jets and outflows (even in traditionally "radio quiet" AGNs), we can build up a complete picture of the nature and energetics of AGN feedback.

5.1.7 Spatial dissection of forming galaxies

A major breakthrough scientific application will be the spatial dissection of galaxies during the peak epoch of galaxy formation. Observations of these galaxies will exploit both the light gathering power and the unique angular and spectral resolution at NIR wavelengths provided by TMT. Large samples of galaxies throughout the redshift range $z = 1 - 6$ are already known, and HST, JWST, and the current generation of 8–10 m telescopes will help us learn a great deal more in the coming decade. However, spatially resolved spectroscopy, allowing differences in chemistry, kinematics, and physical conditions to be mapped as a function of spatial position within the galaxies, is required to go beyond measurements of crude global properties, and thereby gain fresh understanding into the physics of galaxy formation.

Galaxies at $z = 1 - 5$ exhibit a variety of structures in the high spatial resolution images such as those recorded in the NIR (H band) with the HST Wide Field Camera 3 (WFC3) (see Fig. 23).

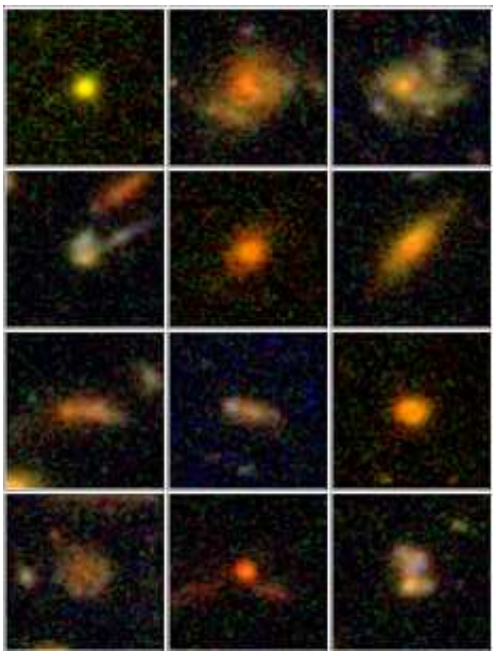

Fig. 23 Gallery of images of galaxies between redshift 1.4 and 3, from the HST CANDELS survey (ACS F814W/ WFC3/IR F125W / WFC3/IR F160W, $\sim 4.5'' \times 4.5''$; Grogin et al. 2011; Koekemoer et al. 2011). Galaxies at this epoch have diverse morphologies, including highly compact objects, dust-enshrouded disks, and highly disturbed merger candidates. With IRIS and IRMOS in both imaging and IFU modes it will be possible to observe systems of this nature with unprecedented angular resolution in the rest-frame visible.

Massive galaxies with low star-formation rates typically appear compact and smooth at these times, with sizes significantly smaller than local early type galaxies. Star-forming galaxies have a wide diversity of spatial structures, from the blue compact analogs to the quenched compact galaxies, to dusty disk-dominated systems, to highly irregular, clumpy and/or diffuse systems. Interpreting the physics underlying these varied morphologies is particularly challenging in the early universe, when frequent galaxy mergers, high gas accretion rates, and dynamically unstable disks are predicted. A key question for TMT will be to understand how the structures of distant galaxies are connected to their assembly and star-formation histories.

To maintain the typical high SFRs of $\sim 100\ M_{\odot}$ yr^{-1} observed in these galaxies without a major merger event requires rapid and semi-continuous replenishment of gas, which favors smooth accretion mechanisms such as through "cold flows" or rapid series of minor mergers (e.g., Dekel et al. 2009). Some numerical simulations predict that the gas rich heavy disks are fragmented to several clumps due to gravitational instabilities and that gas and stars in the clumps are then migrated to the center of galaxies, and they merge together and form a bulge (e.g., Hopkins et al. 2012). Despite the effort to constrain the origin and evolution of the $z \sim 2$ massive disk galaxies by numerical simulations, these evolution scenarios have not been observationally confirmed yet. To put constraints on the scenarios of galaxy assembly, it is essential to obtain the spatial distributions of stellar mass and on-going star formation activities, since past/on-going dynamical processes must be imprinted/visible in the stellar populations. Current studies with 8–10 m telescopes are limited to bright, thus massive or highly star-forming galaxies, and they need to be expanded to a much

wider domain of the SFR-$M_\star$ diagram. The key question here is how the internal structures or physical processes depend on the location in the SFR-$M_\star$ diagram, namely sSFR (burstiness) and stellar mass. In particular, we can investigate whether the compactness of star forming regions is related to the mode of star formation (burstiness/dustiness), and whether smaller galaxies undergo different formation processes from massive galaxies related to the down-sizing effect (e.g., Cowie et al. 1996). Moreover, the internal properties should also be investigated as a function of environment (such as the number density of galaxies), as some environmental impacts must also be imprinted in the spatial distribution of stellar populations, such as a centralized starburst driven by ample gas inflow during galaxy-galaxy mergers, for example.

To truly understand the physics of galaxy assembly and structure, it is essential to have maximum information about the velocity field of the gas and stars within it. As in the local universe, the most sensitive measures of galaxy kinematics come from measurements of the narrow nebular emission lines such as those illustrated in Figure 24. These lines, whose diagnostic power has been calibrated through decades of work in the local universe at rest-frame optical wavelengths, also provide information on chemistry, density, and excitation in the regions where stars are forming. Integral-field spectroscopy can be used to obtain spectral and spatial information over contiguous regions simultaneously. Initial attempts using AO-equipped 8 m class telescopes and IFU spectroscopy (e.g., Genzel et al. 2006; Law et al. 2007, 2009; Förster Schreiber et al. 2009; Wright et al. 2009; Jones et al. 2010, 2013) to observe galaxies at $z > 2$ have shown promise, but revealed the limitations, of this technique with current facilities. TMT, with IRIS and IRMOS, will represent sensitivity gains of a factor of between 10 and 100, with angular resolution gains of a factor of $> 3 – 5$, over current capabilities. The gains will vastly expand the range of targets that may be observed, making it feasible to construct the statistically representative samples needed to connect individual galaxies to the larger framework of cosmological evolution.

With TMT first-light instruments IRIS and IRMOS, the structure, velocity field, abundances, and excitation of forming galaxies may be examined at 50–100 pc resolution (8–15 mas, an order of magnitude higher than the highest resolution achieved by HST) throughout the redshift range of interest. At such scales, even individual giant HII regions and the largest rich star clusters within compact galaxies at high-redshift may be resolved and detected (see Fig. 26), providing a level of astrophysical detail currently only accessible in nearby, bright galaxies. With these extremely high resolution velocity fields, the motions of a galaxy's stars and gas may be traced within its dark-matter dominated potential, allowing astronomers to track the emergence of rotation and dispersion-dominated galaxies at early times, as well as the physics of gas flows on sub-kpc scales. By studying the evolution of these processes over cosmic time, we can see how the local correlations between galaxy structure, kinematics, and star-formation came to be.

5.2 The Age of Maturity and Quiescence

5.2.1 Morphological and kinematic growth of galaxies

More than half of the age of the universe is contained in the redshift range $z < 1.5$. During this vast time period of ~ 10 Gyr, the level of cosmic star-formation activity has declined by roughly an order of magnitude, as the number of bulge-dominated or elliptical galaxies has increased significantly. While the kinematic and morphological structure of present-day galaxies follows various well-known scaling relations, the establishment and evolution of these relations remain a poorly-understood, yet fundamental, piece in understanding the maturation of galaxies at late times. The capabilities of TMT, in particular the ability to constrain the kinematics and morphology of galaxies at $z < 1.5$, will allow the growth and development of galactic structures to be quantified at an unprecedented level of detail.

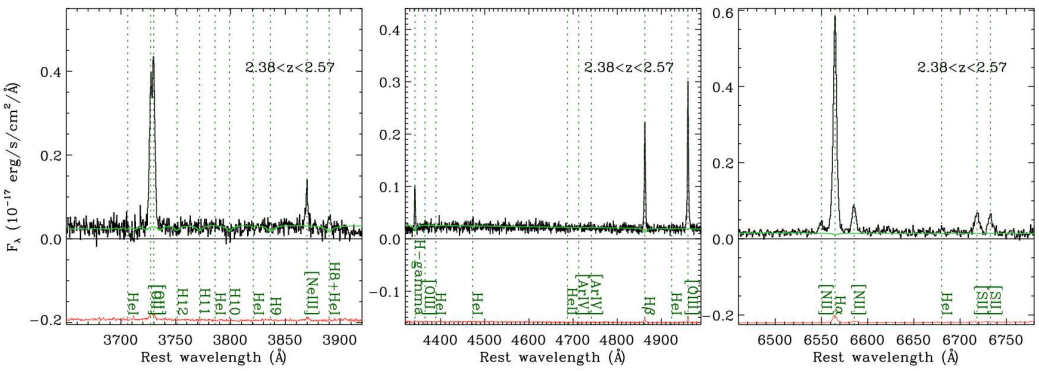

Fig. 24 The composite spectra for a sample of 70 galaxies at $\langle z \rangle \sim 2.4$, obtained in seeing-limited mode for whole galaxies using Keck/MOSFIRE. The line ratios indicate approximately 0.5 solar metallicity in the HII regions, and the ratio of the [OII] and [SII] lines indicate electron densities of $\sim$ 220 cm^{-3}. Using IRIS/IRMOS, spectra of similar quality could be obtained for positions in individual galaxies at a spatial scale of 0.1–0.2 kpc at any redshift < 4. (Credit: A. Strom and C. Steidel at CIT)

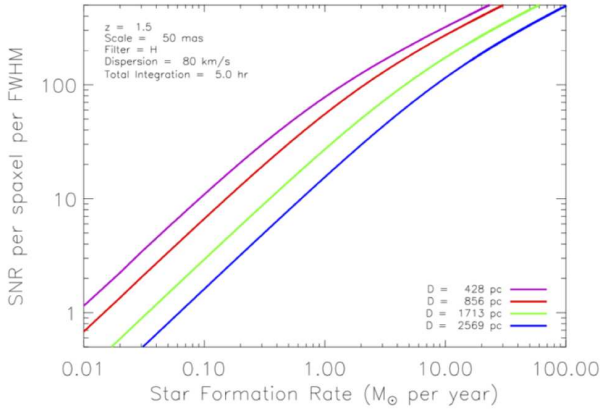

Fig. 25 Estimated S/N of the Hα emission line, per 0.004$''$ spatial element ("spaxel") per spectral resolution element, as a function of assumed SFR at $z = 1.5$ (look back time 9.3 Gyr). The curves assume a range of scales over which the flux is distributed, from angular diameters of 0.05$''$ to 0.30 and a fixed intrinsic velocity dispersion (80 km s^{-1}). A total integration time of 5 hours comprised of 20 900 second exposures (H band) was assumed (from Wright et al. 2010).

The Build-Up of Galactic Disks: Beyond $z > 1.5$ the majority of star forming galaxies have irregular or peculiar morphologies characterized by merging knots of star formation. In contrast, the most obvious feature of star forming galaxies today is the presence of a rotationally-supported disk containing gas, dust, and active star formation. The stars span a range of metallicities and ages at any given radius but HII region abundances reveal that gas-phase metallicities decrease with galactocentric radius (Zaritsky et al. 1990) suggesting that disks form from the inside out. The empirical data and semi-analytic simulations (Cole et al. 2000) suggest that the bulges of disk galaxies are comprised of old, metal-rich stars that form first though a series of major mergers followed by a more

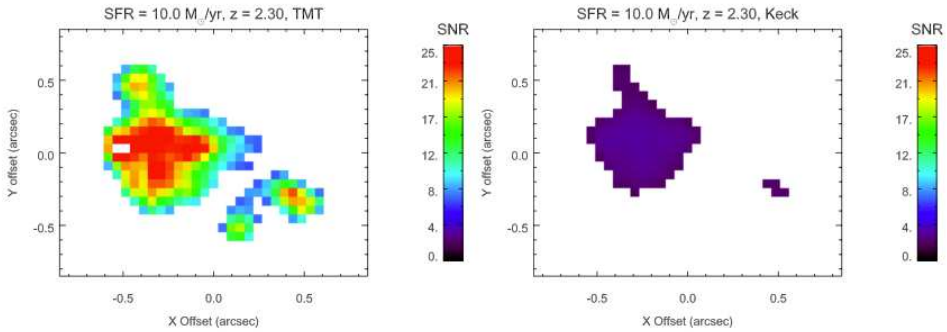

Fig. 26 A simulated $z = 2.3$ galaxy, with Hα redshifted into the K band window and an integrated SFR of 10 $M_{\odot}$ yr^{-1} (*left*). This is compared to Keck observations of the same simulated galaxy (*right*). Complex structure with multiple knots can be seen with IRIS and TMT, while only the brightest portion of the galaxy is barely detectable (S/N~ 3) with Keck.

gradual and protracted formation of a disk. The luminosity of present-day spiral galaxies correlates strongly with their rotational velocity (Tully & Fisher 1977; Tully & Pierce 2000).

The disk surface brightness is also correlated with rotational velocity; those with higher surface brightness are found in galaxies with higher rotational velocities, and there is evidence for bimodality (McDonald et al. 2009). The shapes of galaxy rotation curves are also correlated with their rotational velocities (e.g. Persic et al. 1996). Together these correlations imply that the depth of the dark matter halos of disk galaxies drive their accretion of gas and their subsequent star formation history. TMT offers an opportunity to characterize the build up of galaxy disks. This includes using kinematics to trace the build up in mass but also emission line diagnostics to trace the build up in metallicity.

Deep Keck spectroscopy of $z \sim 1$ disk galaxies has shown that the turnover in the rotation curves can be reached and the disk rotation velocity accurately measured. The Tully-Fisher (TF) relation is already in place for morphologically normal disk galaxies by $z \sim 1$ (Miller et al. 2011). The large aperture and AO capabilities of TMT will allow the characterization of disk rotation curves at higher redshifts and approaching the epoch of peak galaxy assembly ($z < 1.5$). This will require Hα emission-line kinematics with spectral resolution $R \sim 5000$. Scaling the Miller et al. (2011) results to higher redshifts suggests that disk rotational velocities can be obtained with TMT and WFOS/IRMS for moderate mass disk galaxies ($V_{\rm circ} \sim 100$ km s^{-1}) at $z \sim 1.5$ in about 4 hours. With sufficiently deep NIR surface photometry from JWST the scaling relations, metallicities, and the assembly history of disks could be characterized for the first time.

Growth and Assembly of Ellipticals: The fundamental plane (FP) of elliptical galaxies (Djorgovski & Davis 1987; Dressler et al. 1987) is thought to preserve a fossil record of their assembly history (Bender et al. 1992). This includes any differences between cluster and field samples but also differences between ellipticals within a given cluster. Data on nearby clusters suggest that the structural properties of the giant ellipticals ($L > L_{\star}$) are significantly different from the lower luminosity systems ($L < L_{\star}$; Pierce 2014). Specifically, lower luminosity galaxies appear to comprise a dissipational sequence suggestive of gaseous (wet) mergers while the most luminous galaxies form a separate family suggestive of a dry merger history. This implies that the distribution of galaxies within the FP provides a measure of the relative role of wet vs. dry mergers for a given population.

However, high redshift studies of passive galaxies and their scaling relations have been limited to small samples of the most luminous galaxies because of the heroic efforts required to obtain diagnostic spectra of the stellar light (see Fig. 28). TMT WFOS and IRMS will provide the increase

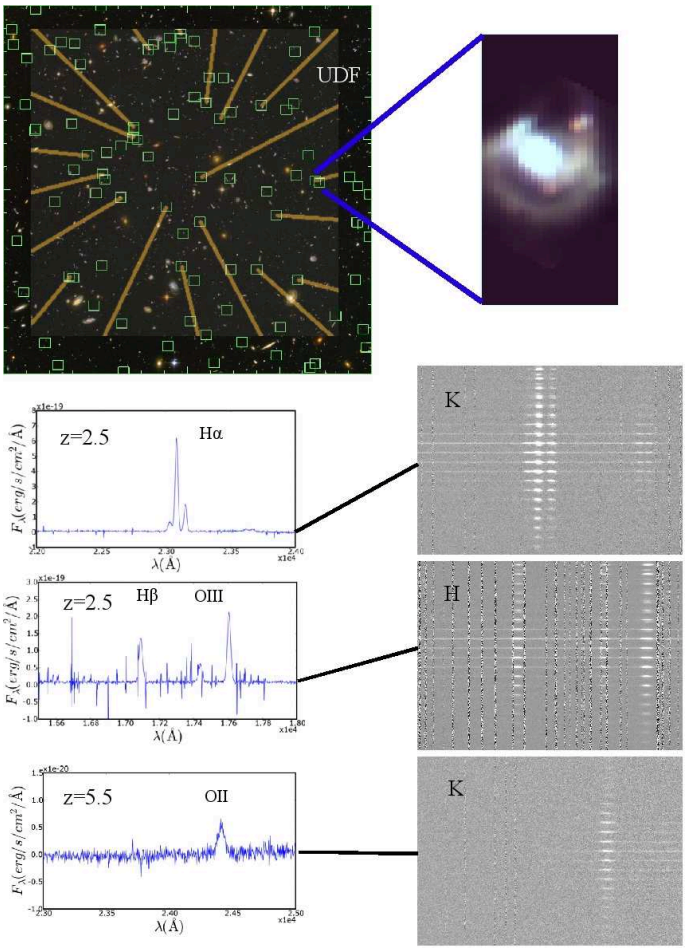

Fig. 27 Simulated IRMOS observations of a typical LBG at redshifts $z = 2.5$ and $z = 5.5$. (*Top left*) Image of the HUDF. LBG candidates at $z = 2 - 6$ are identified with green squares. The configuration of an actual MOS is shown in yellow lines. *Top right*: simulated deep NIR image of a typical LBG as seen in a single IRMOS IFU. *Lower panels*: simulated 2-D and 1-D spectra showing characteristic emission lines of LBGs at $z = 2.5$ and 5. Courtesy: IRMOS-UF/HIA team.

in sensitivity necessary to extend such diagnostic spectroscopy to lower-luminosity passive galaxies, both within and outside of distant clusters.

Accurate measurements of stellar velocity dispersions and metallicity-sensitive line indices will require S/N $\sim$ 50 spectroscopy at $R \sim 3000$. To sample 2–3 magnitudes below $L_\star$ will require exposure times of about 6 hours at $z \sim 2$.

Galactic Bars as Signposts of Disk Assembly: Half of the history of the universe is contained in the redshift range $z < 1$, over a look back time of 7 Gyr. In this time period, the star formation activity declined and disk galaxies began to mature. Previous studies of the physics of galaxy disk stability have shown that as soon as a disk is sufficiently massive, dynamically cold and rotationally-supported, it should buckle and form a bar at its center. Stellar bars thus serve as important signposts for measuring maturity of disks.

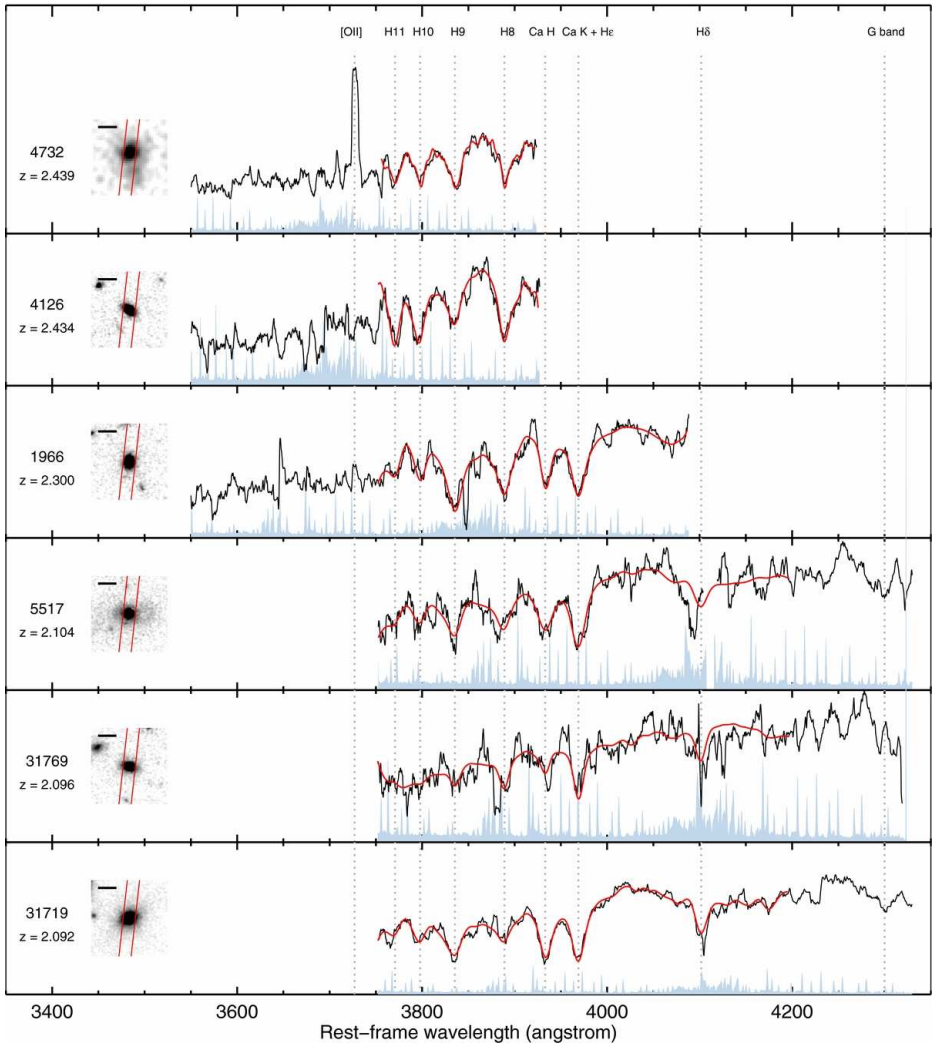

Fig. 28 Spectra of massive early type galaxies at $z > 2$ obtained using Keck/MOSFIRE with 8 hour integrations, demonstrating the ability to obtain high-quality continuum spectra of high redshift passive galaxies. IRMS and WFOS will extend such capabilities to well below $L_\star$ at similar redshifts. (from Belli et al. 2014).

Using the HST and Keck, a precise measurement of the rate of assembly for $L_\star$ and brighter disk galaxies on to the Hubble sequence has been demonstrated (see Fig. 29, Sheth et al. 2003, 2008; Cameron et al. 2010; Kraljic et al. 2012; Melvin et al. 2014). These studies have found that the decline in the bar fraction is not uniform across all galaxy types and the largest rate of evolution is seen in the low mass galaxies ($M_\star < 10^{10.5}\ M_\odot$), while redder, bulge-dominated massive disks are already in place 7 Gyr ago.

A combination of JWST and TMT will allow us to extend this type of research in three important areas: disk-wide stellar velocity dispersion measurements for $L_\star$ disks at $z < 1$, study of the bar fraction and disk stability for lower luminosity 1/10th $L_\star$ disks at $z < 1$, and study of the assembly

of massive disks from $z \sim 1-3$ using bars as a signpost for disk maturity using rest-frame optical light.

The TMT will allow us to finally measure the stellar velocity dispersion across $L_\star$ and brighter disks to $z \sim 1$. Analysis of the gas velocity dispersion from $0 < z < 1$ from the DEEP2 Keck/DEIMOS survey (Newman et al. 2013) showed that a small fraction of $L_\star$ disk galaxies may be offset from the stellar TF relation (Kassin et al. 2007), but deeper observations have countered that this is a spurious result (Miller et al. 2011). In any case, study of galactic structures in these high-redshift disks has revealed that stellar bars are only present in disks that are on the TF (see Fig. 29; Sheth et al. 2012). In other words, bars form only rotationally supported and dynamically cold disks, as in the nearby universe (Courteau et al. 2003), but not all rotationally supported and dynamically cold disks have a bar. TMT will, for the first time, allow us to probe the stellar dynamics of the disks to shed light on the role of the dark matter halo in determining the formation of structure in disk galaxies.

Another exciting capability of the TMT is to provide 2-D gas kinematics in individual galaxies at sub-kpc resolution to ascertain the gas inflows by stellar structures like bars and spiral arms. These studies will allow us to constrain how quickly the gas is being funneled to the galaxy centers, and how that impacts central starburst and AGN activity and the build up of bulges. The sub-kpc resolution observations will also allow us to measure the gas outflows by starbursts and AGN activity.

The large collecting area of TMT will allow us to probe 2.5 magnitudes deeper than currently possible with Keck. As a result we will be able to trace in detail the sub-$L_\star$ disk population. We can study the growth of structure and kinematics at $z < 1$ and connect this evolution ultimately to low mass, Magellanic disks in the nearby universe. A key question to be addressed is why the evolution of lower mass disk galaxies was delayed, and what physical process was responsible.

Finally the evolution and assembly of disks at $z > 0.85$ has been hampered by lack of high resolution, high-sensitivity NIR observations which can probe the rest-frame optical light. The time period between 7–11 Gyr of cosmic look back time is when disks are believed to have assembled. What were the disk shapes and profiles of the first objects? What were the stellar and gas kinematics and how did they affect the build up of stars? Hα spectroscopy at sub-kpc resolution with TMT will allow us to measure the velocity fields and dispersions in the earliest disks. Imaging with JWST and TMT will reveal the morphology and galactic structures of these earliest systems which can then be placed in the context of our current understanding of $L_\star$ disks at $z < 1$.

The Impact of Galaxy Mergers: The role of mergers in galaxy formation and evolution throughout cosmic time remains controversial in spite of the substantial effort, using both HST and ground-based telescopes, to understand it. Studies of high-redshift galaxies, particularly since the peak of cosmic history at $z \sim 2$, diverge on the evolution of galaxy-pair fractions (e.g. Kartaltepe et al. 2007; Lotz et al. 2008) and the dominance of mergers in fueling nuclear starbursts and AGN activities (e.g. Kocevski et al. 2012; Comerford et al. 2009). These debates necessitate a thorough understanding of the detailed physical processes occurring in the extremely energetic and dusty environments within the nuclei of galaxy mergers.

Activity transpiring in the central few hundred parsecs of a galactic nucleus may govern the properties of its host. Indeed, the observed scaling relations of the masses and kinematic properties of galactic bulges with their central SMBHs are prime examples of such an effect: $M_{\rm BH} - M_{\rm bulge}$ (Kormendy & Richstone 1995; Magorrian et al. 1998), $M_{\rm BH} - L_{\rm bulge}$ (Marconi & Hunt 2003), and $M_{\rm BH} - \sigma_\star$ (Tremaine et al. 2002; Ferrarese & Merritt 2000; Gebhardt et al. 2000). However, the possibility that the $M_{\rm BH} - \sigma_\star$ relation may evolve with redshift (e.g. Zhang et al. 2012) has led to suggestions that the scaling relation depends most directly on stellar mass (Jahnke et al. 2009; Cisternas et al. 2011); in this case, the evolution of the $M_{\rm BH} - \sigma_\star$ relation with redshift would reflect the changing fractions of mass in galaxy bulges versus disks. Cogent arguments have also been made that the growth of BHs and the stellar content of galaxies are both "self-regulated" and that

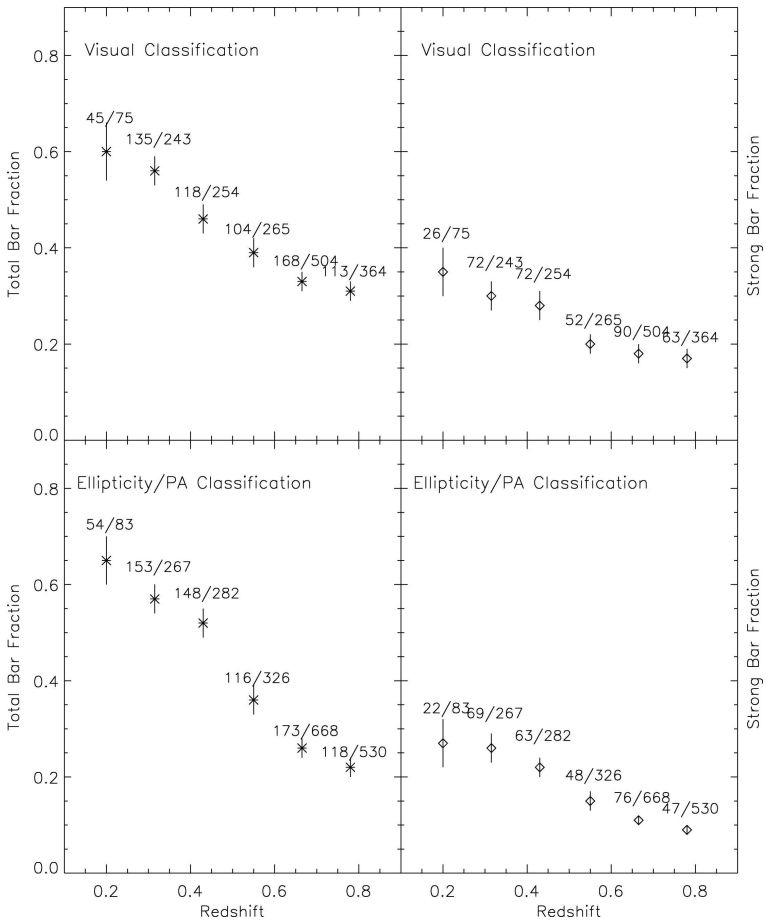

Fig. 29 Bar fraction as a function of redshift in equal time bins of 1 Gyr to a look back time of 7 Gyr. The bar fraction drops from 65% in the local universe to $\sim 20\%$ at $z \sim 0.84$. The left panels show the bar fraction for all galaxies classified as barred, whereas the right panels show the same for only the strong bars. The two rows show two independent methods for the bar classification. Numbers above each data point indicate the total number of bars (or strong bars) and total number of galaxies in the bin, and the error bars reflect the error in the measurement of the bar fraction. From Sheth et al. (2008).

ultimately it is galaxy dark matter halo mass which dictates the equilibrium state (Booth & Schaye 2010).

In any case, the coevolution of SMBHs and their host galaxies is one of the keys to understanding the driving force of galaxy evolution, as it has direct implications on the interplay between the central source and the surrounding ISM. However, this interaction has posed serious challenges to our understanding due to observational difficulties. Detailed observations of the morphology and kinematics of nuclei in interacting galaxies have been afflicted with dust extinction, making them opaque to optical telescopes, and have been impossible until the recent technological advancement of NIR integral field spectrographs with AO in the past decade (Davies et al. 2006; Nowak et al. 2008; McConnell et al. 2011; Gebhardt et al. 2011; Medling et al. 2011; U et al. 2013; Medling et al. 2014). TMT, with its nearly two order of magnitude increase in sensitivity for diffraction-limited

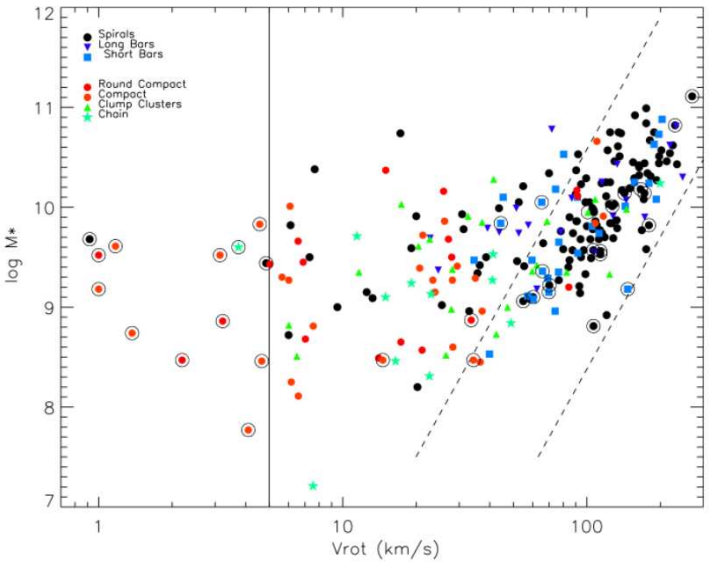

Fig. 30 Stellar mass versus rotational velocity is shown for galaxies from the DEEP2/AEGIS sample (Sheth et al. 2012). All black points are unbarred disks. Notice their scatter away from the TF which is indicated by the dashed lines. The blue points are barred spirals that tend to be on or near the TF.

imaging/spectroscopy, will undoubtedly revolutionize our understanding of processes in galactic nuclei.

The mechanism through which BH masses correlate with galaxy properties has often been associated with gas-rich galaxy mergers (e.g. Hopkins et al. 2006). Gravitational torques funnel the gas into their centers, triggering two phenomena: an intense burst of star formation to feed the bulge, and accretion of gas on to the BHs in the centers of each galaxy. It has been postulated that BH growth can regulate this process through AGN feedback (Springel et al. 2005) via massive winds that evacuate the gas from the galaxy on short timescales, cutting off star formation and future BH growth. This sense of self-regulation has been confirmed observationally by Kauffmann & Heckman (2009), who find that the Eddington ratio of a sample of AGNs depends on the supply of cold gas in the galaxy. Though the detailed mechanisms causing these correlations are still unconfirmed, star formation and BH growth are fed by the same reservoir of inflowing gas; their growth histories are intertwined. It is likely that these two processes compete for fuel in a predictable fashion.

To understand this interplay, it is critical to examine systems during the period of maximum fueling of central starbursts and SMBHs. During a merger, does the BH grow first, leaving the stars to slowly consume the remaining gas? Or is star formation quenched once the BH reaches a bright quasar phase of extreme growth? The position of a merger on BH scaling relations would indicate the relative growth timescales, and confirm whether the putative quasar-mode feedback occurs. Theoretical arguments have suggested that the starburst has preferential access to the available gas and that, therefore, a BH would grow substantially only after star formation has quenched itself and the galaxy bulge is in place (Cen 2012); this scenario would predict that these mergers fall below BH scaling relations.

Observationally, no clear verdict on the location of mergers along the $M_{\rm BH}$–galaxy scaling relations has yet to be established, as different studies have presented apparently-conflicting evidence. Kormendy & Ho (2013) show five merging galaxies falling below the $M_{\rm BH} - \sigma_\star$ and

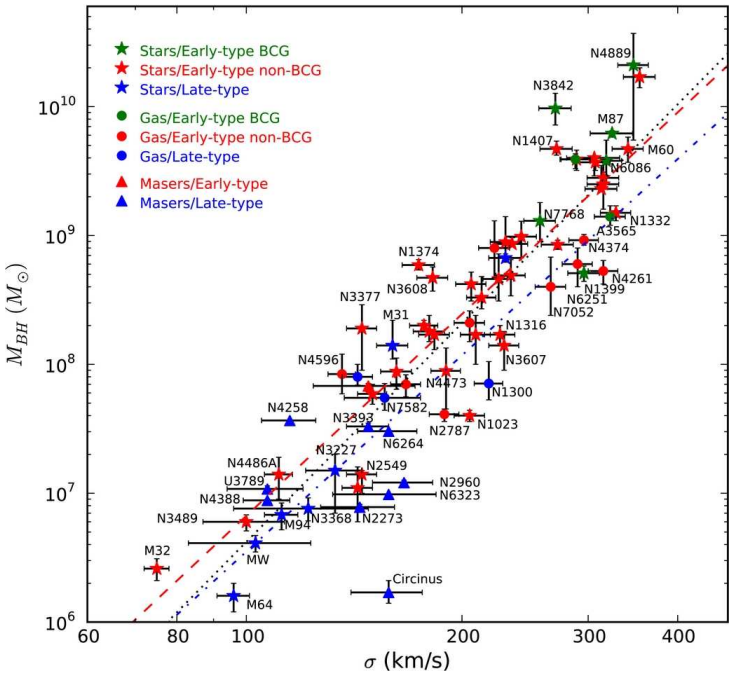

Fig. 31 Recent compilation of $M_{\rm BH} - \sigma_\star$ measurements from McConnell & Ma (2013). The BH masses are measured using the dynamics of masers (*triangles*), stars (*stars*), or gas (*circles*). Error bars indicate 68% confidence intervals. The black dotted line shows the best-fitting power law for the entire sample.

$M_{\rm BH} - L_{K,\rm bulge}$ relations and suggest that BH growth lags bulge formation in mergers; however, using the Keck/OSIRIS integral field spectrograph behind AO, Medling et al. (2014) find the BHs in a sample of gas-rich mergers at or above BH scaling relations, i.e., significantly more massive than expected given their host galaxy properties. This is contrary to the predictions of quasar-mode feedback theories, in which BH growth is delayed until the final stages of a galaxy merger, at which point energetic AGN feedback cuts off subsequent star formation.

5.2.2 Feedback and the physics of galaxy quenching

Over the last decade, observations have revealed a number of surprising discoveries about how the baryonic content of galaxies is assembled. Roughly half of the stellar mass in present-day galaxies was assembled since $z \sim 1$, over an era when the cosmic SFR steadily declined. While the stellar mass in passive, red-sequence galaxies continued to grow, the mass in star-forming galaxies remained essentially constant. Over this period, some process, yet to be securely identified, quenched star formation in massive galaxies. This quenching was not predicted by theoretical models of the underlying cosmology and the hierarchical growth of gravitationally bound structures. Understanding the growth of the baryonic component of galaxies requires following the accretion and ejection of gas from galaxies. This gas physics depends on the highly non-linear gas cooling rate and the feedback of energy, momentum, and heavy elements produced by star formation and AGNs.

Among the many new questions which these results have raised, some critical ones that can be investigated with TMT include the following:

– How exactly do the properties of the circumgalactic gas (on scales from roughly the galactic radius to the virial radius) influence the rate of baryonic accretion onto the star-forming (Toomre $Q \sim 1$) galactic disk?
– How does the mass ejection rate from star-forming galaxies vary with galaxy mass and cosmic time?
– How does the coupling among the various feedback processes (stellar winds, SNe, AGNs) shape the efficiency of mass and metal ejection from galaxies?
– Which physical processes (SN thermal energy, radiative momentum, cosmic rays, etc.) dominate the acceleration of galactic winds?
– Why is the characteristic stellar mass at which galaxies cease forming stars essentially independent of redshift?
– Why is star formation most efficient in galaxies similar in mass to the Milky Way?
– How does environment affect the cycling of matter between galaxies and their surroundings?

Progress requires more detailed studies of galaxies over the era of strongly evolving star formation activity from roughly $z \sim 1.5$ to the present. Multiple sightlines to beacons behind the halos of individual galaxies will clarify the global structure and filling factor of circumgalactic gas. Spectral imaging of galaxies will resolve metallicity gradients within galaxies and provide sensitivity to filamentary structures connecting galaxies to their surroundings.

The TMT first-light instruments offer powerful capabilities for these types of studies. The WFOS provides the blue sensitivity required to attack the halo absorption issues with observations of prominent resonance lines all the way down to $z \sim 0.1$; this science is not accessible with JWST. The IRIS instrument will generate spectral maps of star-forming structures within distant galaxies at higher resolution than JWST; and, combined with maps of molecular gas and dust obtained with ALMA, will directly reveal which regions within galaxies form stars most efficiently. IRIS and IRMS provide infrared spectroscopy of diagnostic emission lines which begin redshifting out of the optical bandpass at $z \gtrsim 0.5$, and complement JWST by offering higher spectral resolution.

Absorption-line Measurements of Galaxy Outflows: Good spectral resolution ($R \sim 5000$) is key to obtaining accurate measurements of the properties of gas outflows from galaxy spectra. Figure 32 shows examples of galaxy spectra at intermediate redshifts. The resonance absorption lines typically show a net blueshift relative to the galaxy, indicating outflowing gas along the sightlines to the star-forming regions. Each absorption trough, however, is a blend of interstellar absorption at the systemic velocity, blueshifted absorption from a galactic wind, and resonance emission (from both the near and far sides of the galactic halo). Optical spectroscopy with TMT will improve the resolution of these galaxy spectra by a factor of 9 at comparable S/N ratio per resolution element. At similar resolution (60 km s^{-1}), previous studies of lower redshift galaxies not only separate these spectral components but also derive properties of the flow as a function of the velocity (Martin & Bouché 2009).

5.2.3 The influence of local and large-scale environment

It is well established that the physical properties of galaxies strongly correlate with environment in the local universe, see Section 7.8.6. In contrast to the star-forming field galaxies, those in dense environments such as galaxy clusters are typically red and quiescent at low and intermediate redshift (Dressler 1980; Blanton et al. 2005; Cooper et al. 2006). Within these overdense environments, the galaxy population evolves strongly with redshift. Higher redshift systems have greater fractions of blue, star-forming, late-type galaxies (Butcher & Oemler 1984; Dressler et al. 1997; van Dokkum & Franx 2001; Lubin et al. 2002). Recent studies of large-scale structures at $z \sim 1$ (Lubin et al. 2009) have found that many of the infalling galaxies experience significantly increased star formation, starburst, nuclear activity, and rapid quenching of star formation (e.g. Dressler et al. 2004; Tran et al. 2003; De Lucia et al. 2004; Tanaka et al. 2005; Koyama et al. 2007; Best et al. 2003; Eastman et

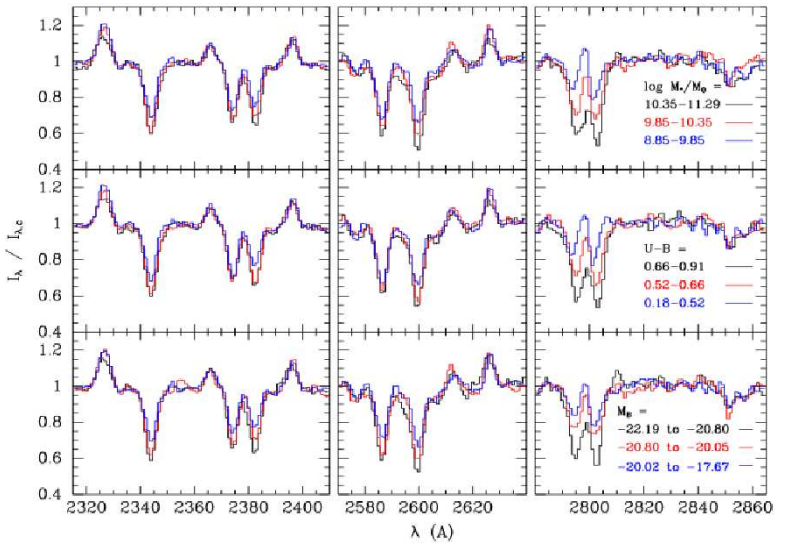

Fig. 32 Comparison of the Fe II and Mg II line profiles in average spectra of galaxies with different properties. *Top*: toward lower mass galaxies, the Mg II absorption troughs become shallower, the Mg II emission becomes stronger, and the Fe II* emission in $\lambda\lambda$2612, 2626 increases. In the highest mass tertile, the Mg II doublet ratio is not inverted, and Fe II λ2383 has a higher EW than Fe II λ2374, as it should in the absence of emission filling. *Middle*: we see similar trends with color because color is strongly correlated with stellar mass (redder galaxies are more massive on average). *Bottom*: the resonance absorption troughs become deeper in more luminous galaxies.

al. 2007; Kocevski et al. 2009). Altogether, these results imply that strong galaxy evolution occurs while galaxies assemble into clusters.

Several mechanisms had been proposed for these environmental effects. One class of mechanisms is cluster-related, such as ram-pressure stripping, galaxy harassment and strangulation (Gunn & Gott 1972; Larson et al. 1980; Balogh & Morris 2000). Other events such as galaxy interactions and galaxy mergers, which occur in both the field and in clusters, have also been suggested (Mihos & Hernquist 1994; Barnes & Hernquist 1992). We do not know which of the many possible physical mechanisms associated with the cluster environment are responsible for eventually suppressing this star formation and nuclear activity and transforming gaseous disk galaxies into passive spheroids. We *do* know that many of these mechanisms are associated *not* with the densest cluster regions, but rather with the infall regions and lower-density environments far from the cluster cores (Treu et al. 2003). We must therefore examine galaxy populations over the full range of environments to form a complete picture of galaxy evolution.

We observe strong differences in the high-mass end of the stellar mass function, even for clusters with similar dynamical (halo) masses and redshifts, implying different evolutionary histories. Thus both late quenching and merging are responsible for populating the bright end of the red sequence and that halo mass and mass specific processes play crucial roles in galaxy evolution (Lemaux et al. 2012; Wu & Zhang 2013). We also observe [OII] in many passive galaxies that is the result of nuclear emission from LINERs, not normal star formation (Lemaux et al. 2010). These observations, for instance, require a combination of rest-frame optical and IR spectroscopy, for which WFOS and IRIS are ideally suited. There is also an increasing fraction (10%–15%) of post-starburst (K+A) galaxies than the $<$3% in the distant field (Tran et al. 2004). These K+As are as massive as the passive (red) galaxies, implying a clear connection between the two populations (Wu & Zhang 2013). Their

distribution seems to be intimately connected to their environments at $z \sim 1$, indicating an important role for different processes in different environments.

Today, we require the use of the world's largest telescopes (Keck, Subaru, VLT, etc.) to study even modest samples of the brighter galaxies in these environments. The challenge increases as we approach redshifts $z > 1$, where many of the spectral features needed to measure galaxy metallicities (stellar and gas-phase), identify quenching events (post-starburst signatures), distinguish starbursts from AGNs, and determine other essential galaxy properties, all shift into the NIR. These realities necessitate multi-object NIR spectroscopy, which has just today become feasible on select facilities. But even there, large amounts of telescope time must be invested to observe modest samples at moderate resolution and S/N. Because much of the galaxy evolution at $z \sim 1-2$ occurs in the lower mass (and lower luminosity) galaxies, only TMT will be able to observe the most interesting targets. Workhorse instruments such as WFOS will enable optical spectroscopy of potentially interesting targets, identifying objects at $z \sim 1$ for follow-up rest-frame optical spectroscopy using IRMS. The most interesting candidates will be dissected using IRIS, whose extremely high spatial resolution will finally allow us to clearly see where AGNs, starbursts, mergers and tidal interactions are at play. The two infrared spectrometers will probe the most important spectral features - [OIII], Hβ, Mgb, Hα, and [NII] - that can be used to distinguish the internal processes at work during this important epoch of galaxy transformation.

Evolution of Satellite Galaxies: Over the past decade, models of galaxy formation and evolution have made significant progress in explaining the observed properties of massive galaxies as a function of cosmic time. Among other improvements, the inclusion of feedback from star formation and AGNs has aided greatly in matching the color and luminosity distributions of massive galaxies at $z < 2$ (e.g., Croton et al. 2006; Di Matteo et al. 2005). However, recent observational results have also illustrated a fundamental problem with the ability of these same models to predict the evolution of low-mass galaxies $M_\star \lesssim 10^8 M_\odot$ (Somerville et al. 2008; Weinmann et al. 2011, 2012).

The shortcomings of modern models are perhaps best illustrated by studies of the Milky Way and its satellites. Beyond the well-known missing satellites problem (Moore et al. 1999a; Klypin et al. 1999), recent work has shown that the most massive subhalos in simulated Milky Way-like systems are dramatically inconsistent with the dynamics of the brightest Milky Way satellites (otherwise known as the "Too Big To Fail" problem (Boylan-Kolchin et al. 2011, 2012). This result suggests a serious problem with our understanding of how low-mass galaxies populate dark matter halos within ΛCDM. In particular, the "Too Big To Fail" problem indicates a failure of subhalo abundance matching (SHAM) at low stellar masses ($< 10^8\ M_\odot$). Abundance matching or SHAM, a common technique for populating simulated dark matter distributions with galaxies, assumes a one-to-one relation between a galaxy's stellar mass and the mass of its parent dark matter (sub)halo (Behroozi et al. 2013; Moster et al. 2013). This simple empirical approach to modeling galaxy formation has yielded great success for massive galaxies, matching a wide range of clustering statistics as a function of cosmic time (e.g. Berrier et al. 2006; Conroy et al. 2006). The importance of this success is that it indicates that a galaxy's stellar mass is determined, to a very large extent, solely by the mass of its parent halo.

To robustly probe the dark matter content on these low-mass scales requires observations of a statistically meaningful sample of systems beyond the very local universe, ideally extending to higher redshift. Unfortunately, current kinematic constraints on the stellar mass-halo mass relation are barely able to reach the critical scales where breakdown in abundance matching arises ($M_\star < 10^8\ M_\odot$; see Fig. 33). Moreover, the required observations are very challenging, requiring 5–10 hours of integration with Keck/DEIMOS and are limited by the spatial and spectral resolution afforded by current facilities. The sensitivity of TMT combined with the spectral capabilities of IRIS and WFOS will open up the ability to constrain the dynamics (and thus dark matter halo masses) of low-mass systems far beyond current limits and across a range of environments (including both field and satellite populations).

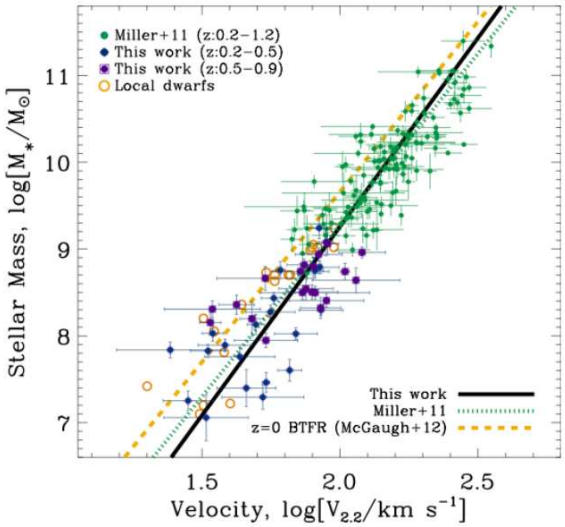

Fig. 33 Stellar-to-halo mass relation according to the abundance matching curves of Garrison-Kimmel et al. (2013; solid curve at $z = 0$) and Behroozi et al. (2013; aqua and orange curves at $z = 0.1$ and $z = 1.0$, respectively), compared to that inferred for a sample of intermediate-redshift dwarf galaxies according to deep Keck/DEIMOS kinematic measurements. Black points represent the data. TMT will extend our ability to constrain this critical stellar mass-halo mass relation to yet lower masses and to higher z.

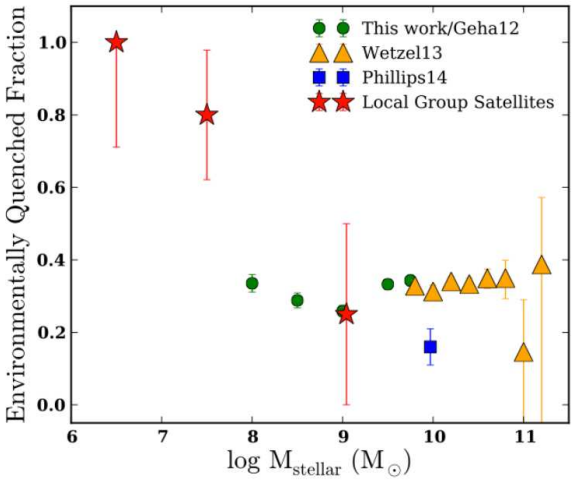

Fig. 34 The dependence of the environmentally quenched fraction on satellite stellar mass; that is, the fraction of satellites that are quenched in excess of that expected in the field, i.e. the fraction of satellites that are quenched because they are satellites, as a function of stellar mass. While environmental quenching seems to have an approximately constant efficiency of $\sim 30\%$ at stellar masses from 10^8 to 10^{11} $M_\odot$, there is a dramatic upturn in quenching at lower stellar masses (if the Local Group is typical). TMT will allow spectroscopic studies to probe this regime beyond the Local Group, measuring SFRs and kinematics for large populations of low-mass systems.

Beyond the apparent breakdown of abundance matching, the limitations in our understanding of galaxy evolution at low masses are further illustrated by the inability of current models to reproduce the number of passive or quenched satellites in the local universe, such that models overpredict the quenched satellite population locally (e.g. Weinmann et al. 2006, 2010; Kimm et al. 2009; Phillips et al. 2014). Recent observations of the quenching efficiency for satellite galaxies find that only about 25%–30% of infalling satellites are quenched in local groups and Milky Way-like systems. Moreover, this quenching efficiency is relatively independent of satellite stellar mass, such that lower mass systems ($> 10^8\ M_\odot$) are equally likely to quench as their more massive counterparts (Wetzel et al. 2013; Wheeler et al. 2014). From studies of the Local Group, however, we can conclude that this trend likely breaks down at yet lower stellar masses — below $\sim 10^8\ M_\odot$, nearly all satellites in the Local Group are quenched (see Fig. 34), potentially indicating a dramatic change in the efficiency of satellite quenching at $\sim 10^8\ M_\odot$.

The major limiting factor in understanding the quenching of satellite galaxies or more generally the evolution of low-mass systems is the limited observational information at stellar masses $< 10^8\ M_\odot$. While simulations have pushed their resolution limits down to very low masses, our observational knowledge is severely lacking. Currently, N-body simulations are able to resolve halo masses as small as $10^4 - 10^5\ M_\odot$ (e.g. Springel et al. 2008), while observations of galaxies with stellar masses of $\precsim 10^8\ M_\odot$ are limited to the few systems found in the very local universe. TMT will represent a dramatic leap forward in our observational capabilities, pushing observations of low-mass galaxies ($\sim 10^6\ M_\odot$) beyond the Local Group and more importantly out to intermediate redshift ($z \sim 1$) over a broad range of environments. In particular, TMT will place invaluable constraints on the stellar mass-halo mass relation (and its evolution), while testing models of galaxy formation (including satellite quenching) in the yet-poorly-understood low-mass regime.

Spatial distributions of stellar populations: Stellar mass functions of quiescent and star-forming galaxies evolve with time in such a way that quiescent galaxies become progressively more dominant with time. This trend is further accelerated in high-density environments, such that clusters, even those at high z, are often dominated by quiescent galaxies. The detailed physics of quenching, however, has yet to be understood and is one of the major unresolved issues in our understanding of galaxy evolution. The superb spatial resolution of TMT may give us a handle on this long-standing question.

Deep, AO-assisted, IFU spectroscopy will allow us to study the spatial distribution of stellar populations within galaxies. By examining spectral features that are sensitive to star formation on different timescales (e.g. Hδ vs. D_{4000}), we can see which part of a galaxy is quenched and on what timescale. There are a number of physical processes that are expected to shut off the star-formation activities of galaxies. Their quenching efficiencies differ between the central part and outskirts of galaxies — e.g. ram-pressure stripping first occurs in the outskirts where the potential well is shallower and star formation is expected to cease progressively from the outskirts to the center. On the other hand, strangulation suppresses star formation on a galaxy-wide scale. Together with the conventional wisdom that different processes are more or less effective in different environments (e.g. ram-pressure is most effective in dense cluster cores, while galaxy-galaxy interactions may be least effective there), mapping the spatially-resolved stellar populations may help identify the physical process(es) at work. Another clue may come from the dynamical status of the outer part of the quenched galaxies. Some processes are expected to transform star-forming galaxies into S0's instead of classical, dispersion-dominated elliptical galaxies. The E/S0 classification is notoriously difficult at high z even with HST, but they are dynamically distinct (S0 has a rotating disk, while E does not). So, if we can measure the dynamics of the outer part then that would be another important clue toward solving the problem.

The spatial distribution of stellar populations is also interesting from the point of view of the size evolution of galaxies. Current theories predict that the core of these galaxies forms at high redshifts and they are observed as the compact, massive galaxies at $z \sim 2$. Then, low-mass galaxies accrete

onto these galaxies and fill out the outer part to form an extended envelope. We can test this theory by direct observations of early-type galaxies over a range of redshifts. Low-mass galaxies are metal-poor galaxies and we expect that the metallicity gradients of massive early-type galaxies should become stronger with time. It may be challenging to measure stellar metallicity with sufficient S/N even with TMT, but a stacking analysis would make it possible.

Synergy with Large Surveys: TMT is not a survey telescope. Its field-of-view is relatively small compared to the largest panoramic telescope facilities; its power lies in spectroscopic follow-up observations. Clusters and groups of galaxies that we have discussed in this section are rare objects and one needs to survey a large volume to cover a wide enough range of environment. There are a number of on-going/future surveys such as the Hyper Suprime-Cam Survey, Dark Energy Survey, and LSST. These surveys cover more than 1000 square degrees and are highly complementary to TMT. By using cluster catalogs from these surveys, we can efficiently point TMT to interesting groups and clusters to cover a wide enough parameter space in the environment. The superb spatial resolution and depth of TMT will then allow us to gain much deeper insights into galaxy properties than these wide-area surveys can achieve.

5.3 The Intergalactic Medium

5.3.1 Background

The overwhelming majority of baryons at $z > 2$ reside in a diffuse, highly ionized plasma that lies between galaxies known as the IGM. This IGM is a fundamental prediction of hierarchical cosmology where baryons trace the underlying dark matter distribution giving rise to the Cosmic Web (Fig. 35). Observationally, this web is manifested in the spectra of distant sources as a thicket of HI Lyα absorption-lines commonly termed the Lyα forest. Because the physics of diffuse gas can be very simple, the theory has told us that the neutral hydrogen (HI) optical depth, as well as the gas temperature, is controlled by the gas density and the intensity and spectral shape of the extragalactic UV background (EUVB). This simplicity makes it possible to turn a Lyα forest spectrum, as in Figure 28, into a 1-D map of the density along the LOS, as a function of redshift. These data provide information on the spectrum of initial density fluctuations without the non-linear gravitational processing that affects denser regions of the universe, and thus the Lyα forest may offer the best means of measuring the spectrum of these perturbations on small scales where other techniques cannot.

The highest quality data on the physical properties of the IGM have been recorded for the redshift range $z = 1.6-3.5$, for several reasons: first, Lyα must be redshifted above the atmospheric UV cutoff of 0.31 μm, setting the minimum redshift; second, the Lyα forest evolves extremely rapidly with redshift, so that by $z > 3.5$, it is so dense with absorption that it loses dynamic range for measuring weak spectral features; third, QSOs bright enough for echelle observations ($m < 19$) are very rare even at their peak near $z = 2.5$, and by $z = 6$ there is only a small sample known in the entire sky. Thus, in general, our current view of the IGM is "1-D", in the sense that we do not get the picture on the lower panel of Figure 28 but only the one on the upper panel.

Indeed, experiments designed to examine the gas surrounding galaxies – their so-called CGM – reveal a substantial reservoir of cool, enriched gas. Establishing the interplay between the IGM and galaxies is a major focus of current research and bears directly on theories of galaxy formation in modern cosmology.

Nevertheless, decades of research on the IGM using high-dispersion, absorption-line spectroscopy have established the basic properties of this medium: the surface density distribution of the HI gas, the probability density function of its transmission with redshift, the fact that the gas is highly ionized, and constraints on its temperature and thermal history. These data have also revealed that portions of the IGM are enriched in heavy elements (C, Si, O). High-resolution spectra are capable of detecting trace amounts of metals, down to metallicities as low as 1/5000 of the solar

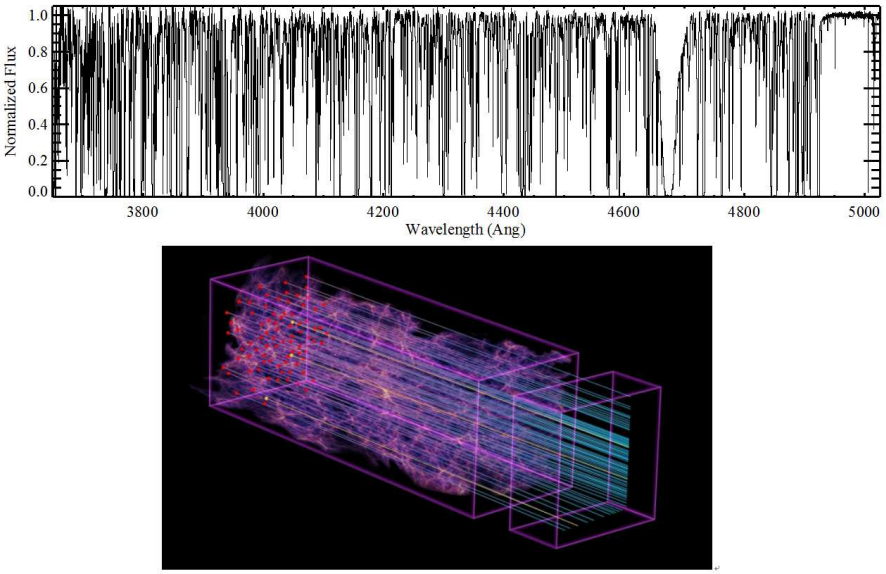

Fig. 35 The "cosmic web" of the baryon distribution in a cosmological simulation. Here, HI in the IGM traces the dark matter distribution even in regions with low density contrast. A LOS through the volume yields a 1-D map of both the HI and metallic species along the LOS, as shown in the top panel. Densely sampled sightlines through a survey volume, together with detailed maps of the galaxy distribution, will provide unprecedented views of the distribution of baryons in the universe, and their relation to the sites of galaxy formation. [Illustration Credit: Zosia Rostomian, LBNL; Nic Ross, BOSS Lyman-alpha team, LBNL; Springel et al, Virgo Consortium and the Max Planck Institute for Astrophysics]

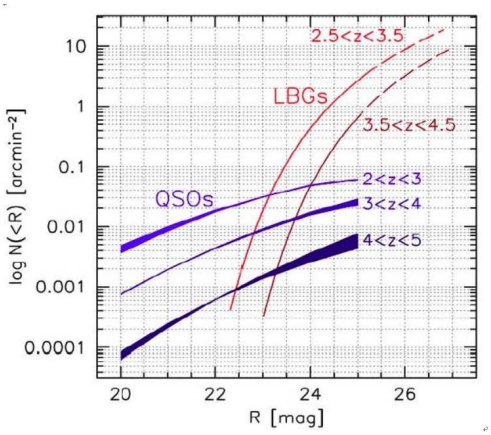

Fig. 36 The cumulative surface density of QSOs and UV-bright galaxies as a function of R mag. The surface density of suitable IGM probes increases exponentially for $R > 22$ due to the very steep rest-UV luminosity function of star forming galaxies. By $R \sim 24$, the surface density of galaxies+QSOs exceeds 1 arcmin^{-2}, sufficient for tomographic mapping of the IGM on Mpc scales.

abundances. In fact, such lines of sight provide a very high quality "core sample" of the intervening universe, from which we have learned (e.g.) that there may be no gas, anywhere in the universe, that was not "polluted" with the products of stellar nucleosynthesis at some early epoch. This enrichment implies an interplay between galaxies and the IGM throughout the early universe including, perhaps, the first stars. Current galaxy formation theory requires that the IGM provide galaxies with a nearly continuous supply of fuel for star formation.

Complementing the single-sightline, high-dispersion data, several projects have generated massive spectroscopic datasets (e.g. SDSS, BOSS) to study the IGM across large-scales and to use it as a direct probe of cosmological models. Despite the lower spectral resolution, the large sample size and sky-area-coverage offer unique analyses including measurements of the BAO in the IGM transmission field, cross-correlation of the HI gas to IGM metal absorption and high-z quasars and galaxies, and measurements of the mean free path to ionizing radiation. In the TMT era, there will be powerful synergy between the high-fidelity data one can obtain on narrow fields with these large spectroscopic datasets spanning the full sky.

5.3.2 TMT and the IGM

As emphasized above, our view of the IGM on Mpc scales is essentially 1-D, limited by the number density of luminous quasars on the sky. To resolve the Cosmic Web on scales of 1 Mpc one must obtain IGM spectra of a denser set of background sources. Figure 36 shows the space density of compact, UV-bright star forming galaxies at apparent magnitudes sufficient to yield very high quality spectra. For galaxies with $R \sim 24.5$ (~ 0.6 μJy), approximately the apparent magnitude at which TMT/WFOS can obtain a spectrum at $R \sim 5000$ with S/N ~ 30, galaxies in the appropriate redshift range ($z = 1.8 - 4$) outnumber QSOs by more than a factor of 30. This means that the IGM properties can be densely sampled on physical scales of < 1 Mpc, approximately the maximum sphere of influence of individual galaxies on the IGM and comparable to the expected coherence length of the undisturbed IGM. Thus, the 3-D IGM can be effectively reconstructed tomographically over the range $1.6 < z < 3.5$ where the Lyman-α forest can be observed from the ground with a good dynamic range.

With a sufficiently dense grid of closely-separated background sources, including faint QSOs and bright LBGs, it becomes possible to interpolate across the transverse plane to 'tomographically' reconstruct the 3-D Lyα forest absorption field. Lyα tomographic maps with $\sim$Mpc resolution will extend 3-D cosmography beyond the $z \sim 1$ currently achievable by deep galaxy redshift surveys (e.g. Davis et al. 2003; Lilly et al. 2007). In addition, as illustrated by the simulated reconstruction maps in Figure 36, Lyα tomography is far more effective at mapping out overdensities of order unity and cosmic voids. Since each Lyα forest sightline probes $\sim 500\ h^{-1}$ Mpc (comoving) along the LOS, large cosmic volumes can be efficiently mapped. The resultant maps reveal the topology of large-scale structure in the high-z universe, constrain the power-spectrum of dark matter, and resolve extrema in the density field such as proto-clusters and voids.

Our current, 1-D view of the IGM has primarily been derived from several tens of echelle spectra at high S/N ($>$30 per pixel) recorded on 10 m class telescopes. These data pale in comparison with the S/N $\gg$100 per pixel one obtains for stars in our Galaxy (and its neighbors). With an echelle spectrometer on TMT one could achieve S/N$>$1000 on the most luminous sources to give an unprecedented view of the low-density IGM. Such data could, for example, reveal the presence of a CIV 'forest', akin to the HI Lyα forest of current datasets (see Fig. 38). The spectra would establish the distribution of metals at below the mean density of the universe (i.e. the majority of the volume), testing models of pre-enrichment. These extremely high quality spectra will also place high-precision constraints on the temperature of the IGM to better resolve its thermal history. The IGM temperature with redshift is a complex balance between adiabatic cooling from cosmic expansion with photoionization heating by quasars and star-forming galaxies and (possibly) heating by

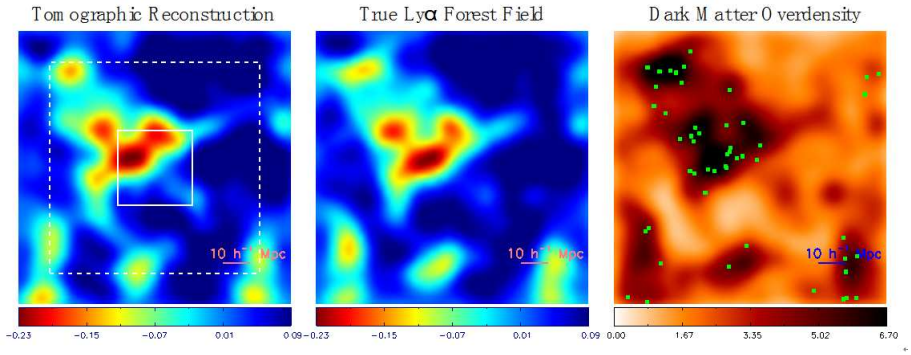

Fig. 37 Simulation slices illustrating Lyα forest tomography with map resolutions of 3.5 h^{-1} Mpc. (*Left*) A tomographic reconstruction from a set of simulated Lyα forest absorption sightlines from sources down to a survey depth of $m_{AB} = 24.5$, which include realistic modeling of spectral S/N assuming the Reddy et al. (2008) LBG UV luminosity function. The central panel shows the true underlying 3-D Lyα forest absorption field while the right panel shows the underlying dark-matter overdensity, $\Delta = \rho/\langle\rho\rangle$ (both smoothed with a 3.5 h^{-1} Mpc Gaussian to match the reconstructed map). These slices have dimensions (100 h^{-1} Mpc) 2×2 h^{-1} Mpc, and the LOS direction is into the plane of the page — in real surveys, one covers 400 h^{-1} Mpc along the LOS. The green dots overlaid on the DM field show positions of $R \leqslant 25.5$ galaxies coeval with the Lyα forest, obtained from halo abundance matching. The solid small rectangle overlaid on the left-panel shows the footprint covered by approximately 10 WFOS pointings, while the large dashed rectangle shows the area equivalent to 1 deg^2 on the sky. [Image adapted from Lee et al. 2014]

exotic sources (e.g. blazars) and structure formation. These data will also examine systematics that affect the large-field surveys of the IGM (e.g. continuum normalization).

Another emerging area of IGM research is to study the gas in emission. Once illuminated by ionizing photons from the EUVB or a nearby source, the HI gas fluoresces with approximately 60% of the photons converted to HI Lyα (Adelberger et al. 2006; Cantalupo et al. 2007; Kollmeier et al. 2010). Figure 39 shows the "Slug Nebula" surrounding the bright UM287 quasar at $z = 2.1$ which extends hundreds of kpc across, i.e. far beyond the dark matter halo hosting the source. Using the boosted ionizing radiation field of the nearby quasar, gas from the surrounding IGM may be studied in emission. Narrowband imaging and IFU spectroscopy on TMT could detect much fainter sources including optically thick gas ionized only by the EUVB. TMT's greater impact, however, would be deep optical and NIR spectra of this extended emission to diagnose properties of the IGM in an entirely complementary fashion to absorption-line techniques. The surface brightness of even the bright nebula in Figure 39 requires several night-long integrations on a 10 m telescope to sensitively study Lyα, CIV, HeII, and Hα line-emission. With TMT, one could resolve the morphology of the gas distribution and gain information on the kinematics, enrichment, density, and ionization state. If combined with an IGM tomographic study, one would gain a complete picture of the morphology and physics of the IGM on Mpc scales.

5.3.3 TMT and the CGM

One of the most exciting possibilities enabled by TMT is to combine the precision measurements of the astrophysics of the IGM using relatively bright background sources with direct observations of the luminous material — galaxies and AGNs — in the same volumes of space, providing for the first time the first 3-D view of the distribution of baryonic material in the high redshift universe. Figure 39 illustrates the connection between galaxies and the IGM, with the observed nebula span-

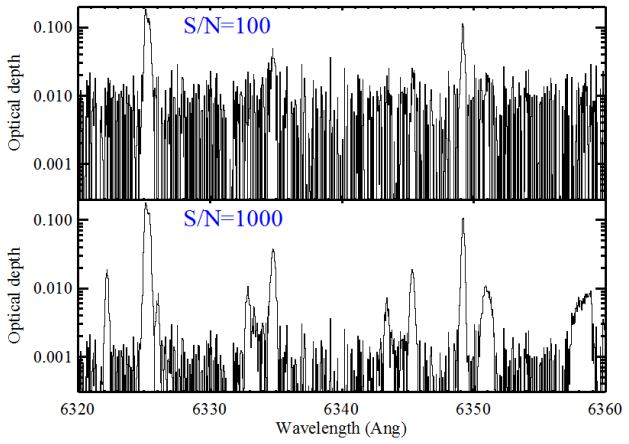

Fig. 38 Simulated optical depth plots of CIV absorption from the IGM assuming the IGM is enriched to 1/1000 solar at the mean density. The upper panel shows the highest quality spectra that one can achieve with 10 m class telescopes. With TMT, one could reach an unprecedented S/N>1000 spectra on the most luminous sources (including GRBs). These spectra would directly establish whether a CIV 'forest' exists in the $z \sim 2$ universe. In turn, the data would reveal the full distribution of metals in the high-z IGM.

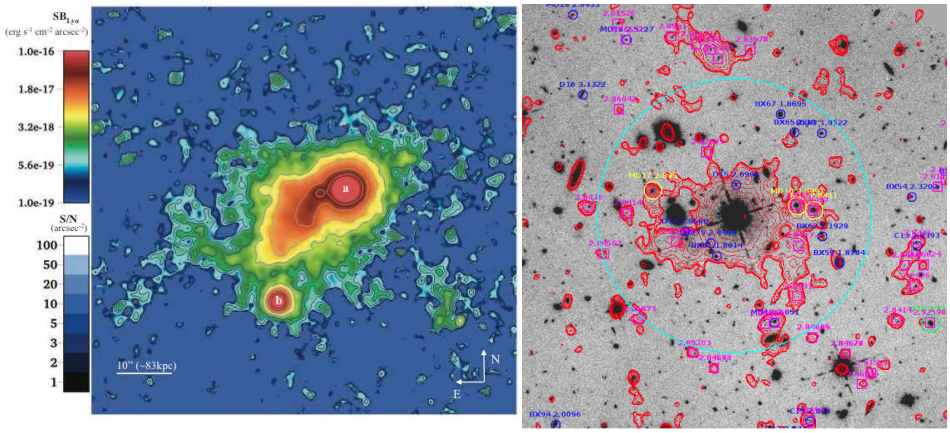

Fig. 39 (*Left*) Lyα image of the Slug Nebula surrounding UM287 (labeled "a"), obtained using narrowband imaging with Keck/LRIS-B. The color map indicates the Lyα surface brightness per arcsec^2. The extended emission spans a projected angular size of $\approx 55''$ (about 460 physical kpc), measured from $\sim 10^{-18}$ erg s^{-1} cm^{-2} arcsec^{-2} contours. The nebula appears broadly filamentary and asymmetric, extending mostly on the eastern side of quasar "a" and towards the south-east in the direction of a second, fainter quasar (labeled "b"). [Adapted from Cantalupo et al. 2014]. (*Right*) A $2'$ by $2'$ region (the cyan circle has a diameter of $1'$, or ~ 500 pkpc) surrounding the $z = 2.84$ QSO HS 1549+19; the grayscale is a deep HST WFC3 F160W image (1.6 μm) centered on the QSO; red contours are Lyα emitting regions at the same redshift, where magenta labels mark regions with Lyα spectra. (Adapted from Trainor & Steidel 2013).

Table 2 WFOS Survey of Baryonic Structure in the High-redshift Universe

Survey	Sky Area	#Targets	Exp.	λ Range	#tiles	Total
Galaxies: z = 1.6 – 3.5	4×(2°×0.56°)	120 000 @ AB < 26.5	1 hour for S/N > 5 @ R = 1000	0.32 – 0.65 μm	1000	1000 hours
IGM $z = 1.6 - 3.5$	4×(2°×0.56°)	15 000 @ AB < 24.5	4.5 hours for S/N > 35 @ R = 5000	0.31 – 0.60 μm	100	450 hours

ning the range from galactic scales (tens of kpc) to intergalactic scales (hundreds kpc). Feedback processes from galaxies and their AGNs affect the surrounding IGM, e.g. enriching the gas, ionizing the medium, and depositing heat. At the same time, gas from the IGM funnels into the galactic potential wells to fuel new stars, continuing the so-called "baryon cycle" of feedback and accretion. Present studies of the CGM are primarily limited to examining the gas in absorption in the rare cases where a quasar or luminous galaxy lies behind a foreground galaxy. One obtains single-sightline information, one galaxy at a time, and primarily at low spectral resolution with correspondingly limited constraints on the physical conditions.

The IGM tomography experiment described in the previous section may be expanded to include analysis of the CGM. Star-forming galaxies with $R < 24.5$ used to characterize the IGM absorption represent only the "tip of the iceberg" for the high redshift galaxies. The combined sensitivity of WFOS and TMT allows for spectroscopy of much fainter galaxies (to $R \sim 27$, albeit with lower spectral resolution than for the IGM probes) with a high degree of completeness. Galaxies at such apparent magnitudes have surface densities of >20 arcmin^{-2} for each interval in redshift of $\Delta z \sim 0.5$ from $z \sim 2$ to $z \sim 3.5$ (Fig. 40). Fortuitously, this redshift range also encompasses what we believe to be the most important era for galaxy growth, star formation and massive BH accretion in the history of the universe. Thus, with TMT, it will be possible to simultaneously obtain a densely sampled map of the distribution of galaxies and their CGM, in 3-D, providing the most complete possible census of all normal matter, and its relationship to dark matter. For the first time, the empirical picture of the high redshift universe would be of as high fidelity as those that currently exist only inside simulations. More importantly, the observations will reveal the inner workings of all of the poorly understood physical processes that must be incorporated in order to understand how galaxies form — feedback (both hydrodynamic and radiative) from AGNs and galaxies, gas accretion, details of the relationship between structure in diffuse gas versus that traced by galaxies.

An example of the type of ambitious survey that could be mounted with TMT would be a TMT/WFOS observing program to survey both galaxies and the IGM over a volume of the $z = 1.8 - 3.5$ universe that is as statistically representative as the SDSS redshift survey at $z \sim 0.1$, which could be accomplished in a reasonable amount of telescope time. The relationship between angular scale on the sky and co-moving scale at the targeted cosmic epoch is vastly different between $z \sim 0.1$ (SDSS) and $z \sim 2.5$ (TMT). The SDSS was carried out with a telescope+instrument combination capable of observing over an FOV with a diameter of 2.5 degrees, or a transverse scale of ~ 18 Mpc (co-moving) at the median redshift of the survey. At $z \sim 2.5$, the same 18 Mpc co-moving scale is subtended by an angle of $10.6'$ on the sky. Thus, WFOS can be thought of as a wide-field spectrograph for studies of the distant universe. A survey of a representative volume of the universe ($\sim 10^8$ co-moving Mpc^3) covers a solid angle of π steradians at $z \sim 0.1$; for the proposed TMT/WFOS baryonic structure survey, the same volume is covered by ~ 4.5 square degrees on the sky, within which there would be $\sim 650\,000$ star forming galaxies brighter than $R \sim 26.5$ in the redshift range $1.6 < z < 3.5$ that could be selected for spectroscopy using simple photometric criteria to within $\Delta z \sim 0.4$. The total number of targets with $R < 24.5$ and $1.6 < z < 3.5$ in the same volume would be ∼30 000. A summary of the observing parameters, assuming a total WFOS slit length of $8.3'$, is given in Table 2.

The WFOS survey products would also include:

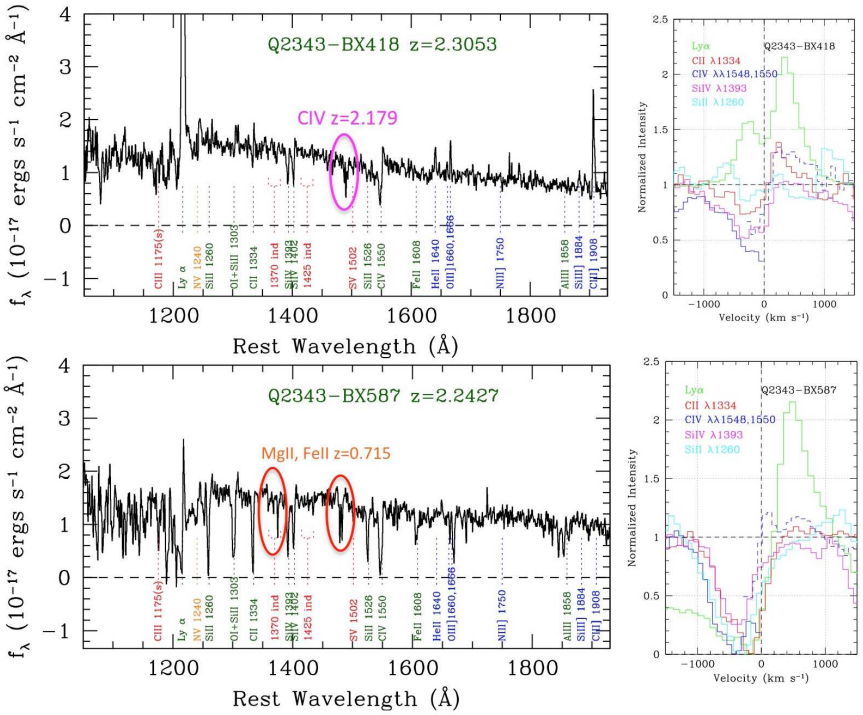

Fig. 40 (*Left*) Rest-UV spectra of $R = 24$ galaxies observed at $R = 1500$ obtained using Keck/LRIS, with 10 hour integrations. Spectra of similar galaxies could be obtained with 3–4 times higher spectral resolution; spectra with similar quality will be possible to $m_{AB} \sim 26.5$ using the $R \sim 1500$ mode of WFOS. Even at this resolution, one detects metal absorption lines from intervening material (circled feaures), as well as measurements of outflow kinematics (*right panels*), showing various interstellar transitions and Lyα emission relative to the galaxy systemic redshift.

– Identification in redshift space of ∼1000 overdense regions that will become clusters by the present-day. The physical state of potential hot gas in the proto-intracluster media can be matched against Sunyaev-Zeldovich signatures in future high resolution CMB maps, providing a complete census of baryons in all phases within the densest regions in the universe.
– Exquisite far-UV spectra of a large number of galaxies in the same redshift range for which IRIS and IRMOS can obtain rest-frame optical spectra. The far-UV spectra will provide measures of outflow kinematics, chemistry, stellar IMF, and in some cases mass outflow rate.
– The 15 000 high quality sightlines through the IGM will map intergalactic HI and metals in 3-D, to be compared with the galaxy distribution in the same cosmic volumes. Even the lower resolution galaxy spectra will allow the mapping of inhomogeneities in the UV ionizing radiation field and measurement of the lifetime of bright UV sources via the transverse proximity effect (e.g., Adelberger 2004; Trainor & Steidel 2013).
– The information content of the survey could be greatly enhanced with HROS observations of the brightest background sources in the survey regions, providing exquisite information accessible only with high S/N $R \sim 50\,000$ spectra, as well as selected IRMS/IRMOS observations of UV-faint galaxies at the same redshifts in the same survey volumes.

In addition, TMT would enable a statistically meaningful sample of high-dispersion probes of the CGM. With $R > 10\,000$ spectra, one can reliably assess the column densities of multiple ions (HI,

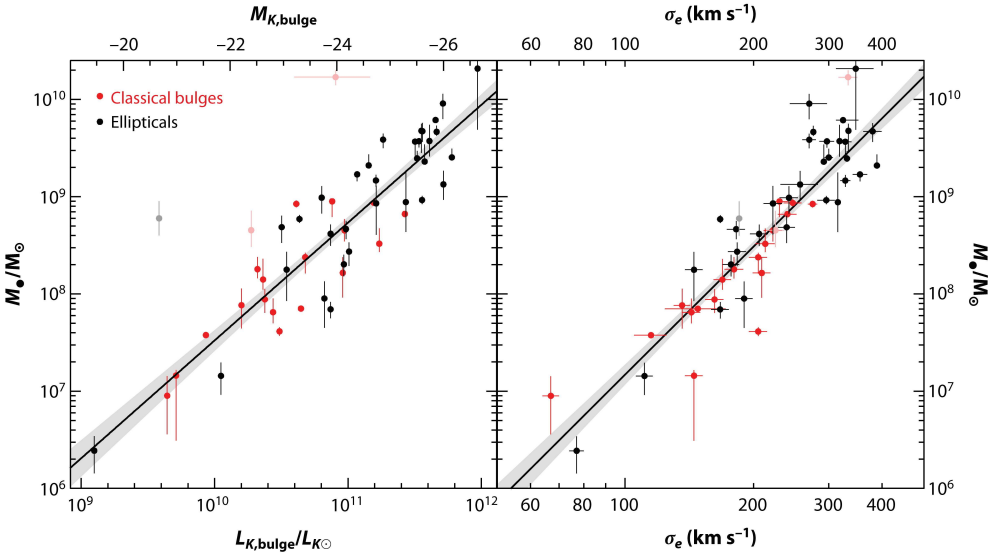

Fig. 41 Correlation between BH mass and bulge properties for nearby galaxies: (*left*) K band luminosity, and (*right*) stellar velocity dispersion (Kormendy & Ho 2013). Further studies are needed to determine the relation between BH mass and bulge properties for all kinds of galaxies.

CII, CIV, etc.) to estimate the ionization state, total surface density, metallicity, and velocity fields. Presently the astrophysics of the CGM is poorly described; TMT would fully diagnose the properties of this medium.

6 SUPERMASSIVE BLACK HOLES

SMBHs, with masses ranging from below 10^6 to above 10^{10} solar masses, are now known to be present in the centers of most and perhaps all large galaxies. The mass of the BH is correlated with the stellar mass ($M_{\rm BH}$-$M_{\rm bulge}$ relation) and velocity dispersion ($M_{\rm BH}$-σ relation) of the bulge of the galaxy (Fig. 41). These discoveries over the past 20 years have led to the popular idea that BHs and galaxies co-evolve and that feedback of AGNs during the growth phases of the BH strongly affects the gas content and star formation in the host galaxy (Ho 2004; Kormendy & Ho 2013). Understanding the formation and growth history of SMBHs, their influence on galaxy evolution, and the exotic phenomena of stellar dynamics and gas accretion in the SMBH environment has become a major theme in astronomy.

TMT's capabilities for high angular resolution imaging and ultra-deep spectroscopy will provide unprecedented opportunities to advance numerous areas of SMBH science. These will include precision measurements of BH masses spanning a range of more than four orders of magnitude in mass, examining the relationships between SMBHs and their host galaxy environments, understanding the physical processes of the fueling and feedback of BHs and their redshift evolution, determining the early growth history of SMBHs through observations of high-redshift quasars, and carrying out fundamental tests of General Relativity through high-precision measurements of stellar orbits around the Galactic Center (GC). In this section, we describe a few of the most exciting science cases for understanding the fundamental properties, accretion physics, and cosmological growth history of SMBHs.

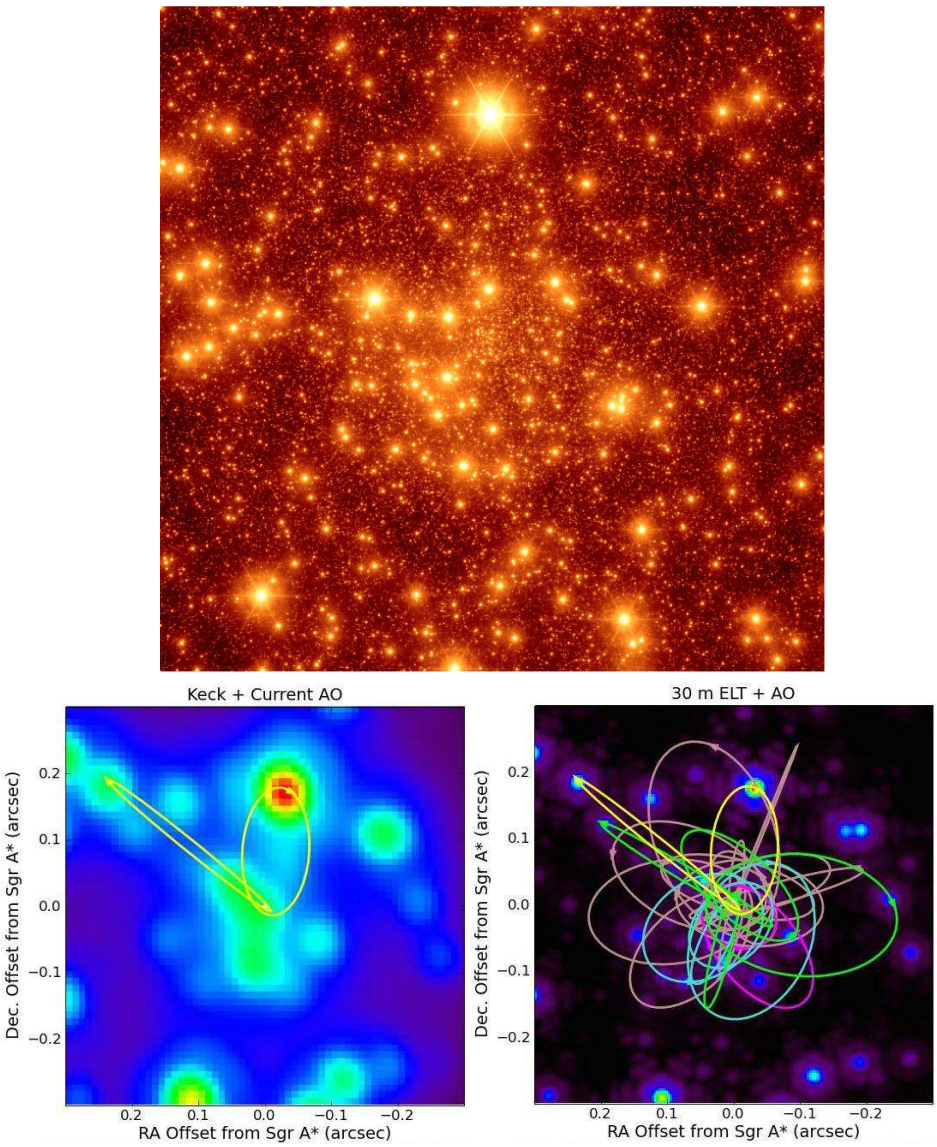

Fig. 42 (*Top*) Simulated NIR image ($t_{\rm int} = 20$s) of the central $17'' \times 17''$ of the Galaxy, centered on the SMBH, Sgr A* at the angular resolution of TMT. The image contains $\sim 2{\times}10^5$ stars down to $K \sim 24$ mag, including $\sim$2500 known stars and a theorized population based on the observed GC radial profile and the K band luminosity function of the Galactic bulge. The image includes photon, background, and read noise. (*Bottom*) Implications for short-period stars' orbits. Overlaid are all known orbits and examples of expected orbits with periods less than 23 years that are detectable both astrometrically and spectroscopically ($14 < K < 16$, yellow; $K < 17$, green; $K < 18$, cyan; $K < 19$, magenta; $K < 20$, tan). TMT/IRIS will increase the number of measurable short period orbits by an order of magnitude and also find systems that orbit the SMBH much deeper in the central potential, with orbital periods that are a factor of five smaller. These systems are particularly helpful for measurements of post-Newtonian effects (GR and extended mass distribution).

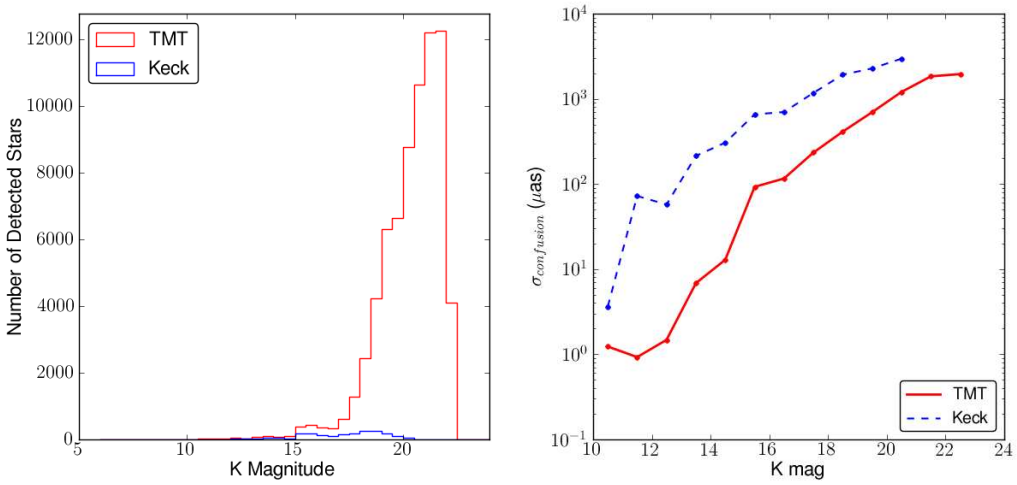

Fig. 43 (*Left*) Distribution of detected stars in the simulated images for TMT (*red*) and Keck (*blue*). The number of detected stars with TMT will be two orders of magnitude greater than Keck. (*Right*) Astrometric error resulting from confusion plotted as a function of K band magnitude of the planted star (*red solid*). Data were binned in 1-mag bins and the RMS error of the input-output positions were calculated and taken as $\sigma_{\rm confusion}$. Confusion effects in Keck data are shown for comparison (*blue dashed*).

6.1 The Galactic Center Black Hole: Our Unique Laboratory for Up-close Study

The GC's proximity makes it a unique laboratory for addressing issues in the fundamental physics of SMBHs and their roles in galaxy formation and evolution. Current AO studies have transformed our understanding of the GC. In the past decade, proper motion studies have determined the orbits of some individual stars moving within 0.04 pc of Sgr A* (Fig. 42). These provide the strongest evidence for the existence of a central BH in the GC and the best mass measurement in any galactic nuclei. However, the star density in this region is so high that source confusion has limited studies to the brightest stars, and introduces biases in astrometric and spectroscopic measurements. TMT's gains in resolution and contrast will enable detection and mapping of the orbits of stars four magnitudes fainter (Fig. 43). This will allow the detection of many stars closer to the BH than we can observe (resolve) today. The measurement of the orbits of these short period stars will be essential for tests of General Relativity in this region.

6.1.1 TMT takes General Relativity tests into an unexplored regime

Measuring the orbits of short-period stars will probe the structure of space-time very close to an SMBH in a gravitational potential 100 times stronger and a mass scale 10^5 times larger than any existing test. Current AO-equipped telescopes will make the first, but marginal, test of General Relativity by measuring the Gravitational Redshift (related to the Equivalence Principle) during the closest approach of the brightest short period star (S0-2) to the BH, in 2018. Stars with periods shorter than S0-2 are both fainter and closer to the BH. TMT's increased resolution and sensitivity will increase the number of short-period stars by an order of magnitude. As these shorter period stars are revealed, it will be possible for the first time to measure the precession of the periapse, and therefore (1) test the specific metric form of General Relativity in an unprecedented regime and

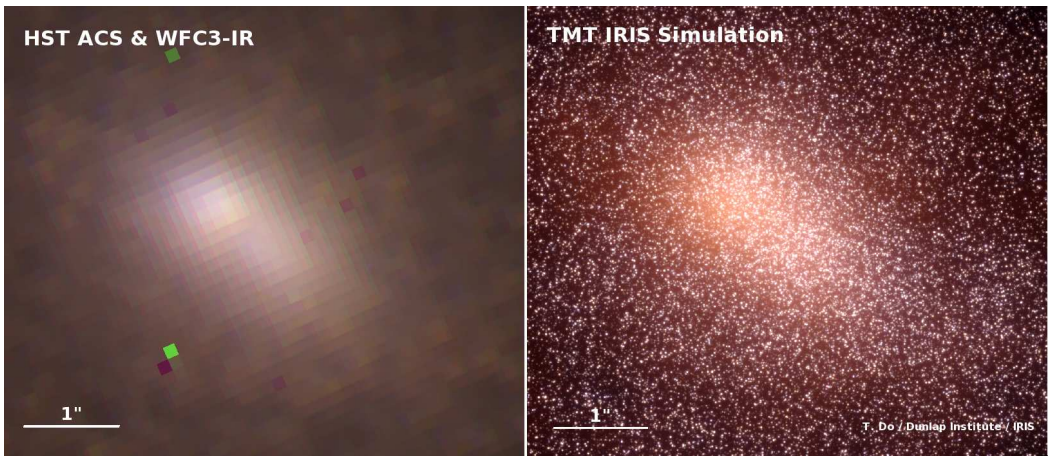

Fig. 44 TMT will enable revolutionary studies of the nucleus of Andromeda (M31). Left: A three color image of the current capabilities using HST ACS (F814W) and WFC3 (F110W, F160W). Right: A simulated image based on our current knowledge of this region, as observed with the Z, J, and K band using TMT's first light instrument IRIS with the NFIRAOS AO. TMT/IRIS will provide the necessary sensitivity and spatial resolution to understand the dynamics, stellar population, and the SMBH at M31's center.

can therefore distinguish between different metric theories of Gravity, (2) probe the distribution of dark stellar remnants and dark matter around the BH and thereby test fundamental models of galaxy evolution and N-body dynamics (Rubilar & Eckart 2001; Weinberg et al. 2005; Will 2008; Merritt et al. 2010). In addition, improved measurements of stellar orbits will dramatically improve the uncertainty in Ro, the distance from the Sun to the GC. As Ro sets the scale of the Milky Way, precise measurements with TMT will constrain the Milky Way's dark matter halo to $<1\%$ (Weinberg et al. 2005), contributing to our understanding of the origin and evolution of the Milky Way.

6.1.2 How the GC black hole interacts with its unusual environment

Outstanding puzzles include the origin of the GC's massive young star cluster, whose formation should have been suppressed by the SMBH, and an unexpected dearth of old red giants around the SMBH. These aspects challenge our notions of how SMBHs affect the formation and evolution of galaxies. The sensitivity of TMT will allow us to detect stars that are 100 times fainter than is possible today. Integral-field spectroscopy of this expanded sample will allow us to detect the pre-main sequence population for the first time at the GC, providing an important handle on the young cluster's age and IMF in this extreme environment. It will also test the idea that stellar stripping can explain the deficit of old red giants.

It was recently reported that flares in Sgr A* are highly polarized, supporting a synchrotron origin for the NIR emission (Meyer et al. 2006; Nishiyama et al. 2009). However, the spatial resolution limits our ability to draw strong conclusions. TMT's high-spatial resolution and its time-domain capabilities will enable it to perform polarimetric monitoring campaigns that will help to break model degeneracies and test relativistic effects. The NIR (1–2.5 μm) polarimetry with TMT will be sensitive enough to monitor rapid changes on timescales of less than 5 minutes, with an accuracy of 0.1%.

6.1.3 Proper motions around SMBHs in the nearest galaxies

The angular resolution and sensitivity of TMT will enable the measurement of individual stellar orbits around extragalactic SMBHs to measure precise BH masses, as well as explore the dynamics and stellar populations at a level of detail only possible in the Milky Way today. For example, the center of our nearest neighbor Andromeda (M31) is about a hundred times more distant than Sgr A* (730 kpc), but compensates by harboring an SMBH roughly 35 times larger ($1.4 \times 10^8\ M_\odot$). The resulting sphere of influence of the M31 BH subtends about 6″ in the sky, and the expected proper motion is about 6 percent of that in the GC (see E-ELT simulations in Trippe et al. 2010). Current AO NIR observations with 8–10 m telescopes of M31 are strongly confusion limited. With the D4 advantage of TMT in the confusion-limited case in addition to the ability to operate at Z band, the IRIS instrument will have both the angular resolution and sensitivity to measure both the proper motion and RVs of individual stars to reconstruct their orbits (See Fig. 44). The ability to do these observations will open a new window onto detailed dynamical studies of nearby galactic nuclei.

6.2 Dynamical Detections and Demographics of SMBHs

The mass is the most fundamental yet hard-to-measure property of BHs. The $M_{\rm BH}$-$M_{\rm bulge}$ and $M_{\rm BH}$-σ relations we observe for galaxies at $z{\approx}0$ are reasonably tight for classical bulges and elliptical galaxies (intrinsic scatter 0.29 dex), but they are not for pseudo-bulges. For redshifts $z > 1$ there are hints that both the $M_{\rm BH}$-$M_{\rm bulge}$ and $M_{\rm BH}$-σ relations evolve, in the sense that the BH tends to be over-massive with respect to the galaxy, but these findings are uncertain and controversial, depending on highly indirect estimates of $M_{\rm BH}$ and host galaxy parameters (e.g., Bennert et al. 2011; Schulze & Wisotzki 2014).

The most reliable method to measure the mass of a BH is from the orbital dynamics of gas or stars in the region within which the BH dominates the gravitational potential. This region is usually defined by the radius of the sphere of influence of the hole: $r_{\rm infl} = GM_{\rm BH}/\sigma^2 = 13$ pc $(M_{\rm BH}/10^8\ M_\odot)^{0.5}$. TMT's IRIS instrument will provide the next great leap in observational capabilities for measurement of the kinematics of galaxy nuclei on sub-arcsecond scales. TMT's AO capability will enable IRIS to achieve a spatial resolution close to the diffraction limit, 8 mas (λ/μm), which surpasses the spatial resolution of the HST by almost one order of magnitude. As illustrated in Figure 45, TMT is capable of spatially resolving the sphere of influence of a mass $M_{\rm BH}$ at an angular distance up to $D_{\rm A} = 335$ Mpc (μm/λ) $(M_{\rm BH}/10^8\ M_\odot)^{0.5}$, which corresponds to a distance of 1 Mpc for $M_{\rm BH} = 10^3\ M_\odot$ or 3 Mpc for $M_{\rm BH} = 10^4\ M_\odot$. At a redshift of $z = 0.1$, this corresponds to $M_{\rm BH} = 10^8\ M_\odot$, and at $z = 0.4$, $M_{\rm BH} = 10^9\ M_\odot$. Black holes with $M_{\rm BH} \sim 10^{10}\ M_\odot$ can be detected at any redshift, provided that suitable dynamical tracers (stellar absorption lines or emission lines from ionized or molecular gas) are accessible in wavelength ranges that can be observed using IRIS.

SMBH masses can be probed using either stars or gas as dynamical tracers. The stellar-dynamical method is more general in that it can be applied to a much larger set of targets, but modeling the full distribution of stellar orbits in a galaxy is a formidable challenge. Complications include the presence of the dark matter halo, possible triaxial structure in the bulge, and stellar population gradients. These issues can be mitigated if the SMBH sphere of influence is very well resolved by the observations, and the exquisite angular resolution provided by TMT's AO system will enable major improvements in the quality and accuracy of SMBH mass measurements even for nearby galaxies in which SMBHs have already been detected using currently available capabilities. Velocity dispersion around a $10^7\ M_\odot$ BH is ~ 67 km s^{-1} requiring a spectral resolution of $R \sim 9000$ to properly characterize it. Measurement and modeling of the kinematics of a thin gas disk in circular rotation is far simpler, but only a small fraction of galaxies contain a circumnuclear gas disk in regular rotation that also has emission lines (from ionized or molecular gas) sufficiently bright for

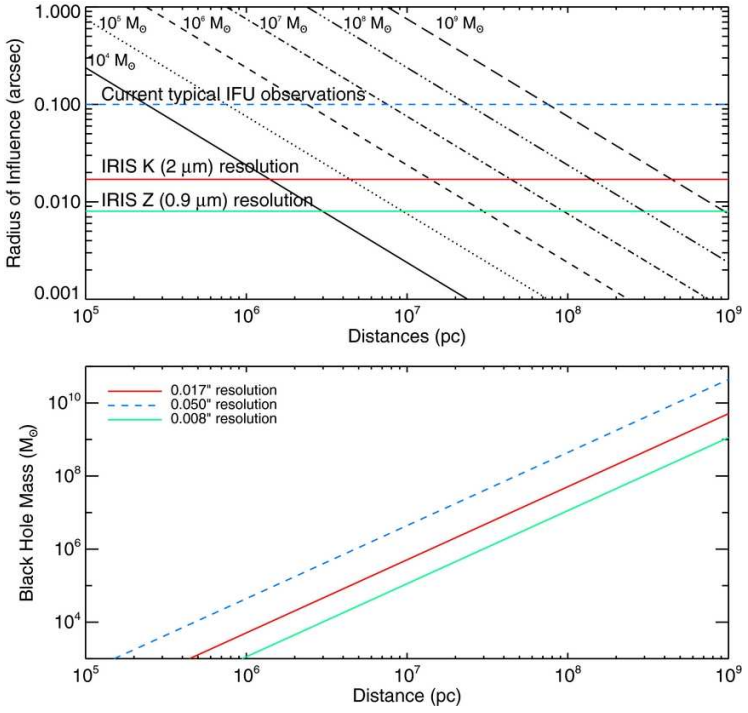

Fig. 45 (*Top*) Radius of influence for various BH masses as a function of the angular size distance using the observed M_{BH}-σ relation. We show lines for BH masses increasing from 10^4 $M_\odot$ to 10^9 $M_\odot$ (*left to right*). The increase in angular resolution will allow observations of BHs much further than possible today. (*Bottom*) Lower limits on BH mass measurements as a function of distance. Most IFS BH mass measurements today are made at a pixel scale of 50 mas (100 mas resolution; *blue, dashed*), compared to TMT, which will have angular resolution of 18 mas at K band (*red, solid*) and 8 mas at Z band (*green, solid*). (From Do et al. 2014.)

kinematic mapping. TMT and IRIS will have the capability to carry out both stellar-dynamical and gas-dynamical measurements of SMBH masses, and TMT's enormous collecting area and exquisite angular resolution will be an extremely powerful combination.

6.2.1 Towards a complete census of black holes in nearby galaxies

For some time after the discovery of the $M_{\rm BH}$-σ relation, observations suggested that this correlation had very small scatter and applied uniformly to ellipticals and spirals in a single, coherent sequence. As the number of measurements increased over time however, it was recognized that this picture was a severe oversimplification. With nearly 100 dynamical measurements of SMBH masses, it is now apparent that the $M_{\rm BH}$-σ relation shows significant scatter and clear differences between galaxy types (e.g., Kormendy & Ho 2013). In particular, the $M_{\rm BH}$-σ relation seems to hold most strongly for classical bulges, which are believed to have formed through mergers, but not for pseudo-bulges built via secular evolution processes in spiral galaxies. However, despite 20 years of observational effort, our understanding of SMBH demographics remains very incomplete. TMT will make major

contributions across this full mass spectrum by enabling SMBH searches to be expanded to areas of this parameter space that are currently inaccessible.

At the low end of the SMBH mass range ($\lesssim 10^7\ M_\odot$), where current stellar-dynamical observations cannot probe galaxies beyond a few Mpc, the overall shape of the $M_{\rm BH}$-σ relation is very poorly understood, and BH detections in H_2O megamaser galaxies indicate a strong departure from the $M_{\rm BH}$-σ relation of classical bulges (Greene et al. 2010). Do et al. (2014) show that TMT with IRIS will have the ability to detect a Milky Way equivalent SMBH ($4 \times 10^6\ M_\odot$) out to the distance of the Virgo Cluster. Such observations will open up an entirely new window on SMBH demographics, enabling surveys of statistically-meaningful samples of low-mass SMBHs to be carried out, and making it possible to explore the dependence of SMBH mass on a variety of host galaxy parameters such as the mass of a classical bulge or pseudo-bulge, or the presence or lack of a stellar bar.

Additionally, recent observations have turned up examples of galaxies with extreme and surprising properties, which demand further exploration of the full parameter space of the SMBH-host galaxy relationships. NGC 1277 is a compact lenticular galaxy in the Perseus Cluster, and observations by van den Bosch et al. (2012) found evidence for an SMBH with an astoundingly large mass of $1.7 \times 10^{10}\ M_\odot$. This is nearly 60% of the bulge's stellar mass, whereas in typical bulges the SMBH accounts for only $\sim 0.1\% - 0.2\%$ of the stellar mass. NGC 1277 serves as a powerful reminder of the need for SMBH searches to be carried out for large and complete samples of galaxies, in order to ensure that the full complexity of the SMBH-host correlations can be explored.

6.2.2 The most massive black holes in the brightest cluster galaxies

The heaviest BHs are expected to be hosted in the brightest cluster galaxies, the most massive galaxies known. These are likely the direct descendants of the most luminous quasars, which host the most massive BHs, in the distant universe. Using AO-assisted IFS on Gemini and Keck, McConnell et al. (2012) indeed succeeded in detecting such ultra-massive BHs, the largest having $M_{\rm l} = 2.1 \times 10^{10}\ M_\odot$ in NGC 4889, the brightest galaxy in the Coma Cluster. Black holes of this size have a sphere of influence that can be resolved, and thus potentially detectable, at all redshifts by TMT. Details of the orbital dynamics need to be determined, which could show whether stellar cusps form around the SMBH, and if there is evidence of mergers. The principal limitation, which places this problem beyond current telescopes and instrumentation, is the low surface brightness of the centers of massive early-type galaxies. IRIS can be used to search for very massive BHs in a complete sample of the most massive galaxies between $z = 0$ and $z = 4$, straddling the peak of quasar activity at $z = 2.5$. To date, SMBH mass measurements have been completed for only a small handful of local brightest cluster galaxies (BCGs), but TMT and IRIS will make it possible to achieve the S/N and angular resolution necessary to detect SMBHs in dozens of nearby BCGs ($D < 200$ Mpc) in just a few hours of on-source integration time per target (Do et al. 2014).

6.2.3 Intermediate mass black holes

IMBHs, with masses between 10^2 and $10^6\ M_\odot$, are a missing link between stellar-mass BHs and SMBHs. Determining the demographics of IMBHs in nearby, low-mass galaxies is of great importance since these objects are much closer to the mass scale of their original "seeds", unlike high-mass SMBHs which have essentially lost any physical "memory" of their original seed masses and environments. Theoretical models suggest that the occupation fraction and $M_{\rm BH}$-σ relation of IMBHs may contain unique clues to the distribution of BH seed masses and the efficiency of their formation (Volonteri et al. 2008). IMBHs are also of great interest as sources of gravitational waves (GWs), either from binary BH mergers or from extreme mass-ratio inspiral events (in which a stellar-mass compact object inspirals into a low-mass nuclear BH). The probable hosts of these intermediate-mass

objects are globular and other massive star clusters, and the nuclei of late-type bulgeless spirals and dwarf galaxies.

Some dynamical evidence has been reported for the existence of IMBHs in globular clusters such as G1 (Gebhardt et al. 2005). However, the existence of IMBHs is still controversial partly due to the insufficient spatial resolution and sensitivity of current telescopes. Some late-type galaxies, even those that are completely bulgeless, host a central BH with a mass as low as $M_{\rm BH} = 10^5\ M_\odot$ (Filippenko & Ho 2003; Greene & Ho 2007), but all such estimates are based on secondary methods of mass determination that rely on AGN broad emission lines. At the same time, HST stellar-dynamical observations have been used to set an astonishingly-tight upper limit of 1500 $M_\odot$ to the mass of any BH in the nucleus of the Local Group Spiral M33 (Gebhardt et al. 2001). This observation provides the best demonstration that not all galaxies contain a central BH, but the occupation fraction of BHs as a function of galaxy mass remains almost entirely unconstrained by available data for late-type and dwarf galaxies. There is tantalizing evidence for IMBHs in a small number of low-mass dwarf galaxies from X-ray observations (such as the dwarf galaxy Henize 2–10; Reines et al. 2011), but the critical confirmation via spatially resolved dynamics is still lacking. At present, direct dynamical searches for IMBHs are restricted to the Local Group and its closest neighbors.

Nuclear star clusters in dwarf and late-type galaxies are the likely homes of IMBHs (if they indeed exist), and will be high-priority targets for IMBH searches in the TMT era. These clusters typically have stellar velocity dispersions of 15–30 km s^{-1}, and the need for simultaneously high angular resolution and high spectral resolution to resolve the kinematic structure of these objects is the primary factor limiting observational progress at present. The proposed high spectral resolution mode for IRIS ($R \sim 8000 - 10\,000$) will be critically important for carrying out IMBH searches in nearby low-mass galaxies, and it will be a uniquely powerful capability for TMT. At a resolving power of $R = 8000$, it becomes possible for IRIS to deliver accurate measurements of mean velocity, velocity dispersion, and higher-order moments of the LOS velocity profile in individual spaxels for observations of central star clusters in galactic centers (Do et al. 2014) and for objects such as the M31 globular cluster G1. Other targets for IMBH searches with TMT will include ultra-compact dwarf galaxies (UCDs) in nearby groups and clusters; these objects may be the remnant nuclear clusters of tidally stripped low-mass galaxies and could host BHs in the range $10^5 - 10^7\ M_\odot$ (Mieske et al. 2013). IRIS data will revolutionize the search for IMBHs, making it possible to detect IMBHs or set highly constraining limits for targets out to a distance of several Mpc.

6.2.4 Calibration of the black hole mass scale in active galactic nuclei

Reverberation mapping (Blandford & McKee 1982) utilizes the time-delay response of the emissivity of broad emission lines to continuum variations to constrain the size of the BLR, $R_{\rm BLR}$. In combination with the velocity width of the emission lines, ΔV, we can compute the virial product $M_{\rm virial} = R_{\rm BLR}\Delta V^2/G$, which is related to the true BH mass through a normalization factor $f = M_{\rm virial}/M_{\rm BH}$ that depends on the unknown structure and kinematics of the BLR (Shen 2013). In practice, it is customary to calibrate f empirically by assuming that AGNs obey the same M-σ relation as inactive galaxies (Onken et al. 2004). This is a highly uncertain and unproven procedure. There is no guarantee that AGNs follow exactly the same M-σ relation, and it is quite likely that f differs from object to object. Yet, this is the fundamental assumption on which all current methods for estimating BH masses in AGNs and quasars are based. With IRIS, we will be able to directly calibrate f in reverberation-mapped AGNs by independently deriving $M_{\rm BH}$ through stellar-dynamical analysis. This has been attempted for a few of the nearest Seyfert 1 galaxies using AO data from 8–10 m telescopes (e.g., Davies et al. 2006; Hicks & Malkan 2008), but it is not within reach of current capabilities to expand the sample to a meaningful size. The AO capability of TMT is essential to resolve the SMBH sphere of influence, and also to reduce the size of the point-spread function of the bright central AGN point source, which otherwise completely dominates the signal from the stars.

TMT and IRIS will also make it possible to carry out a fundamental consistency check by validating stellar-dynamical SMBH measurements through direct comparison with masses measured from the dynamics of H_2O megamaser disks. NGC 4258 is the prototype megamaser disk galaxy, and its BH mass has been measured to high accuracy from the rotation of the circumnuclear molecular disk on sub-parsec scales (Miyoshi et al. 1995). In recent years, maser surveys have significantly expanded the sample of such galaxies for which precise BH mass measurements can be carried out (Kuo et al. 2011). These megamaser disk galaxies have SMBHs of order $10^7\ M_\odot$, and current capabilities are unable to resolve the stellar kinematics within the BH sphere of influence for most of these galaxies. Observations with IRIS will open up the ability to resolve the stellar kinematics within rinfl in such targets, providing a critical cross-check between different mass measurement methods applied to the same galaxies.

6.3 Coevolution of Supermassive Black Holes and Galaxies; AGN Fueling and Feedback

Measuring the host properties of AGNs is key to understanding the co-evolution of SMBHs and galaxies. However, it is also very challenging, particularly for AGNs at higher redshift. TMT's superb spatial resolution and sensitivity will bring us a major breakthrough in separating the host signatures from the bright unresolved nucleus. This can help us to better constrain the $M_{\rm BH}$-σ relation, particularly for AGNs at high redshift. Measuring the central velocity dispersion requires a strong spectral feature redshifted to an accessible wavelength. There are multiple absorption lines that can be used for this purpose. For example, the Ca II triplet at a rest-wavelength of 0.85 μm, centering it in the JHK bands corresponds to redshifts of 0.4, 0.9, and 1.6, respectively. Given the expected spatial resolution of IRIS in each of these bands, the minimum resolved radius of influence of SMBH corresponds to 60, 100, and 150 pc at these redshifts. For comparison, note that the radii of influence for M87 ($M_{\rm BH} \sim 3\times10^9\ M_\odot$) and M31 ($M_{\rm BH} \sim 7\times10^7\ M_\odot$) are approximately 100 and 12 pc, respectively. Thus, it will be possible to probe the upper end of the SMBH mass function with TMT at these redshifts.

TMT will also allow us to study in much more detail the mechanisms of feeding and feedback of AGNs. It will provide observations not only for nearby AGNs with unprecedented quality, but also to galaxies reaching redshifts out to $z \sim 2$, where galaxies are most active, and AGN feedback is suspected of playing a major role in shaping galaxy evolution. In the meantime, TMT's high-spatial-resolution spectroscopy will reveal fainter AGNs at higher redshifts, allowing us to probe the evolution of the AGN luminosity function over a far wider range of luminosities.

6.3.1 The cosmic evolution of small and moderate-size SMBHs

Nearly all work on AGNs at $z > 1$ has been restricted to the most luminous examples. However, the quasars which have been studied are quite rare and likely unrepresentative of the SMBH population as a whole. Current wide field surveys of AGNs have been identifying active 10^8 to 10^9 solar mass SMBHs during their violent growth epoch of redshift around 2. They are the most massive SMBHs in the local universe, and in order to trace the growth history of typical 10^7 to 10^8 solar mass SMBHs, it is necessary to identify at least one order of magnitude fainter AGNs, which are moderate- or low-luminosity AGNs at high-redshifts.

TMT's superb spatial resolution will bring significant improvement in this aspect. Spectroscopy done with narrower slits will be less contaminated by the light from the host, particularly for galaxies at higher redshift. This will help greatly in detecting fainter AGNs at high redshift. Surveys done with TMT WFOS and IRMS, such as the ones mentioned in Sections 5.1.3 and 5.1.7, can be used to push the luminosity functions of high-redshift AGNs orders of magnitudes fainter than currently possible with 8–10m telescopes.

Many moderate- or low-luminosity AGNs at high-redshifts are heavily-obscured by dust. Some of them can be already detected in the current ultra-deep X-ray surveys as optically-faint but NIR-bright X-ray sources. However, their natures are not well known because they are fainter than the current limit of optical and NIR spectroscopic observations with 8–10 m class telescopes. Thanks to the high sensitivity, TMT can unveil the physical nature of such X-ray-selected faint AGNs. Heavily-obscured AGNs can be missed even with the ultra-deep X-ray surveys. One possible way to identify them is to search for AGN signatures, e.g. strong high-ionization emission lines, at the centers of distant galaxies. High-spatial resolution integral field spectroscopy with TMT should identify weak AGN activity at the center of high-redshift galaxies. By identifying a statistical number of faint X-ray AGNs and weak AGN activity at the center of galaxies, TMT can trace the accretion growth history of typical SMBHs seen in the local universe.

6.3.2 The first generation of accreting MBHs

Our interests in the first generation of SMBHs have led to various surveys for high-redshift quasars. The wide-field optical surveys such as SDSS, CFHT, and Pan-STARRS1 quasar searches resulted in the discovery of a few dozens of quasars at $z \sim 6$ (e.g., Fan et al. 2000, 2001, 2003, 2004, 2006; Willott et al. 2007, 2010; Bañados et al. 2014), and recent wide-field NIR surveys such as UKIDSS and VIKING even discovered a few quasars at $z \sim 7$ (Mortlock et al. 2011; Venemans et al. 2013). However, due to the limited sensitivity of those surveys, all the discovered high-redshift quasars are already mature ones, with the mass of their SMBHs being $M_{\rm BH} \sim 10^9\ M_\odot$ and the metallicity of their BLRs is higher than the solar metallicity (e.g., Kurk et al. 2007; Juarez et al. 2009; Mortlock et al. 2011; Venemans et al. 2013). For identifying the non-matured, candidates for first generation quasars, we have to search for lower-luminosity and/or higher redshift quasars and then examine their spectroscopic properties in detail.

Upcoming deep and wide imaging surveys such as DES, HSC, LSST, and Euclid will yield many candidates of first-generation quasars at $z \sim 6-8$, in the magnitude range of $\sim 23-25$ mag (that is $\sim 2-4$ mag fainter than the SDSS limit). However, the spectroscopic characterization of those faint candidates requires very sensitive NIR spectroscopic observations that are beyond the ability of the current 8–10 m telescopes. More specifically, the determination of $M_{\rm BH}$ (and consequently the Eddington ratio, $L/L_{\rm Edd}$) requires the measurement of the CIV 1549 and MgII 2800 velocity profiles, while the determination of the chemical property requires the measurement of the NV 1240, CIV 1549, HeII 1640, CIII] 1909, MgII 2800, and FeII multiplet fluxes. For quasars at $z \sim 6-8$, those spectroscopic features are seen at $\lambda_{\rm obs} \sim 0.8-2.5$ μm, and sensitive spectroscopic observations at this wavelength range are well-suited to IRIS on TMT. Even the discovery spectrum of a true first generation quasar should reveal its much weaker metal lines. Also, quasars with low-mass SMBHs are expected to show relatively narrow (i.e., FWHM $\sim 1000-2000$ km s^{-1}) velocity profiles in emission lines as inferred from the properties of nearby narrow-line Seyfert 1 galaxies, and thus a moderately-high spectroscopic resolution of $R \sim 3000-4000$ is needed for measurements of $M_{\rm BH}$. Such a moderately high resolution is preferred also for avoiding the effects of the strong OH airglow emission that is crucial for sensitive NIR spectroscopic observations. The capability of IRIS perfectly matches the requirements in this topic.

6.3.3 Feeding and feedback of AGNs

Recent AO-assisted IFU studies in the NIR have measured non-axisymmetric structures in the central tens of parsecs of AGNs, and found significant non-circular motions in the gas velocities (Davies et al. 2014). Particularly in the most highly ionized gas (traced by coronal emission lines such as [SiVI]1.96 μm, most AGNs show biconical outflows (Müller-Sánchez et al. 2011). The estimated mass flow rates are hundreds to thousands of times higher than the inferred accretion rate onto

the central $M_{\rm BH}$. Although deceleration is observed, it is possible that most of the outflowing gas can escape the galaxy (Müller-Sánchez et al. 2011). In some but not all local AGNs, these outflows appear strong enough to provide the so-called "AGN feedback" postulated by CDM galaxy evolution theorists to restrict star formation and limit the growth of more massive galaxies. However, it is still far from clear whether the observed outflows, particularly in radio-weak AGNs, generate sufficient feedback to make these models viable.

The same NIR spectroscopic maps also trace molecular gas from H_2 emission lines (e.g. at 2.12 μm), which often show thick, turbulent disk-like structures (Hicks et al. 2009). Comparison with a control sample of non-active galactic nuclei suggests that this concentrated molecular gas is a reservoir feeding the central engine, and in some cases obscuring it in the optical (Hicks et al. 2013). Such structures are not evident in LINERs, suggesting that Low-Luminosity AGNs are not powerful enough to produce them (Müller-Sánchez et al. 2013b). Although the molecular kinematics can be complex, some AGNs show clear dynamical evidence of gas inflow, perhaps driven by bar-like deviations from an axisymmetric gravitational field (Müller-Sánchez et al. 2013a).

However current observations with IFUs on 8–10m telescopes are just able to scratch the surface of the gas dynamics in the central regions of galaxies affected by the SMBH. Observational advances will require not just much more sensitivity, but also a several-times improvement in spatial resolution, that can only be provided by AO on TMT. With IRIS observations of the centers of nearby galactic centers of all types, it will be possible for the first time to determine how SMBHs are fueled, and how they in turn control the evolution of their host galaxies.

NIR IFU spectroscopy will also be essential for finding evidence of outflows induced by AGN winds and jets, that are thought to provide a crucial role in preventing runaway star formation in the most massive galaxies at higher redshift (Fabian 2012). Current 8 m class telescopes are only capable in finding such outflows in rare, highly-luminous AGNs at $z \sim 0.5 - 2$ where these feedback effects are most important (e.g. Cano-Díaz et al. 2012; Liu et al. 2013a). TMT will be able to observe these outflows on smaller spatial scales, and in more typical, less luminous AGNs. Together with ALMA observations of the corresponding molecular outflows, and sensitive VLA observations of the synchrotron emission from jets and outflows (even in traditionally "radio quiet" AGNs), we can build up a complete picture of the nature and energetics of AGN feedback at these redshifts.

6.3.4 Distinguishing star formation in the host galaxies of AGNs

IRIS will be a powerful instrument for resolving the central bulge component of the host galaxy. A key ingredient to understanding whether the BH and galaxy grew in a synchronized manner is to be able to independently constrain the growth of the BH (accretion rate) and the host (SFR – see Sect. 7.8.8). For this purpose, it is necessary to observe not only inactive galaxies but also AGN, systems where the BH is actively accreting. Under these circumstances it is normally very challenging to disentangle the contributions from the AGN and star formation. The high angular resolution IFS capabilities of IRIS again will be a key new breakthrough (see Figure 46).

For some objects, such as ULIRGs, controversy still rages about the dominant IR emission process: either it is a very powerful AGN or a vigorous starburst component. A highly effective methodology to distinguish between emission mechanisms is the estimation of the emission surface brightness of energy sources (Imanishi et al. 2011). The energy generation efficiency of nuclear fusion inside stars is only $\sim 0.5\%$ of mc^2, and the maximum emission surface brightness of a starburst is found to be $\sim 10^{13}\ L_\odot$ kpc^{-2} through both observations and theory. However, the efficiency of an SMBH accreting matter is as high as $\sim 40\%$ of mc^2. Hence, an AGN can produce a very much higher emission surface brightness than stellar fusion ($> 10^{13} L_\odot$kpc^{-2}). Therefore, we can decisively determine the presence of a buried AGN if the emission surface brightness of the energy sources of ULIRGs is $\gg 10^{13}\ L_\odot$ kpc^{-2}. Due to the limited sensitivity and image size with 8 m class telescopes, this method has been applied to only to a limited number of ULIRGs. As ULIRGs are

more prevalent at higher redshift, probing the emission source from the local universe and constructing templates is crucial preparation for observations using space-based telescopes. Hence, MICHI on the TMT will be able to conduct key research in this area, as well as supporting subsequent observations with the JWST and SPICA at higher-z. Comprehensively understanding the evolution of ULIRGs versus redshift is a powerful way to investigate the evolution of AGNs and galaxies, and their effect on each other, which is of significant importance to cosmology.

6.3.5 Binary and merging SMBH in the nearby universe

For the later stages of the merger, the finest spatial resolution is of paramount importance. In the hierarchical paradigm of galaxy formation and evolution, galaxy mergers bring their central massive BHs together. Initially, the BHs are expected to have a separation of more than a kpc. The dynamical friction caused by stars then brings the two BHs closer on a timescale of 100 Myr, making them a gravitationally bound binary system with a separation of about a parsec (Begelman et al. 1980).

The massive binary BHs will eventually spiral in and merge to form a single central SMBH of the new galaxy (Milosavljević & Merritt 2003; Di Matteo et al. 2005). However, binary coalescence via emission of GWs requires that binary must first shrink to much smaller radii ($\sim 0.001 - 0.01$ pc) from the parsec scale separation where standard dynamical friction stops acting. Possible solutions to the so called "final parsec problem" include the interaction of the binary with the surrounding stars and gas e.g., slingshot ejection of approaching stars can shrink the binary orbit further. The resulting gravitational binding energy is released to the surrounding stars. N-body simulations show that this process can convert a steep power-law cusp into a shallow power-law cusp within the radius of gravitational influence of the BHs (Milosavljević & Merritt 2001). Successive mergers will further decrease the density in the central regions and thus form cores and result in mass that is deficit in bright elliptical galaxies (Ravindranath et al. 2002; Milosavljević et al. 2002). The density in the central regions can become very low, thus stalling the binary orbit for a few Gyrs. Thus, a large fraction of core elliptical galaxies are likely to have stalled binary BHs.

Figure 47 shows the stalling radii for nearby core elliptical galaxies in the Virgo Cluster. At present, only the total BH mass has been measured for these ellipticals. The current generation telescopes do not have the requisite spatial resolution to determine if the cores of these ellipticals have stalled binary BHs or a single merged BH. As shown in Figure 47, TMT will be able to probe down to the expected stalling radii of binary BHs and reveal dual nuclei within the cores if the nuclei are active. Also stellar orbits in the innermost regions around binary BHs are expected to be different than the orbits around single BHs. Thus, study of stellar motions in the nearest core ellipticals should also provide evidence for binary BHs even in the case of non-active nuclei.

Since the presence of an AGN is unambiguous evidence for a central massive BH, observations of double active nuclei will provide the direct evidence for the presence of binary BHs. Superior angular resolution available with Chandra and HST have enabled direct observation of a pair of active nuclei separated at ~ 1.4 kpc in the Ultra-luminous infrared galaxy (ULIRG) NGC 6240 (Komossa et al. 2003; Max et al. 2007). TMT with improved spatial resolution and sensitivity is expected to detect pairs of active nuclei in many active galaxies.

In dual AGN systems both central engines may be buried inside the obscuring dusty structure and/or host galaxy. In such cases, NIR (1–2.5 μm) polarimetry with the TMT offers a powerful way to identify obscured dual AGN systems through the conical centrosymmetric polarization pattern centered on each AGN. For example, the polarization pattern detected in the $10''$ (600 pc) central regions of NGC 1068 (Capetti et al. 1995; Simpson et al. 2002) is the signature of a central point source whose radiation is polarized by dust and/or electron scattering within the ionization cones, which if rotated by 90 degrees point directly to the illuminating source. In the case where the ionization cones can be resolved, the polarization pattern will indicate two slightly separated centers that can be identified as a dual nucleus AGN.

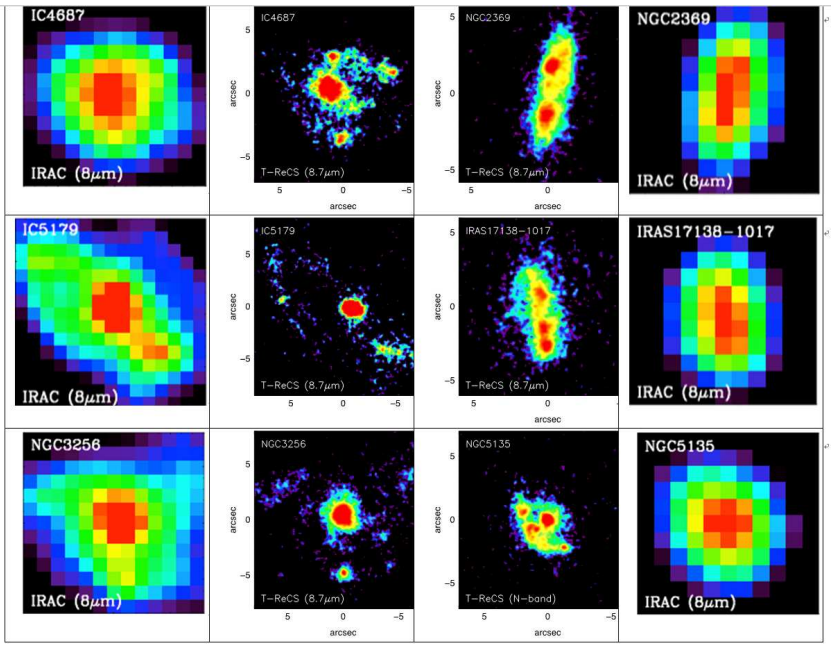

Fig. 46 Gemini North and South observations ($\sim 0.3''$ spatial resolution) of AGNs and their host galaxies (central two columns) compared to Spitzer observations at 8 μm (outer columns) of the same objects ($\sim 2.6''$ spatial resolution). We can expect similar resolution gains in the era of the TMT ($0.05''$) and JWST ($0.025''$).

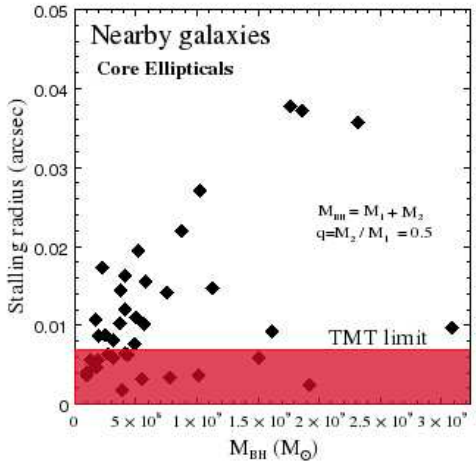

Fig. 47 The stalling radius for merging BHs in the cores of nearby galaxies in the sample of Ravindranath et al. (2002). The stalling radii were computed using the measured BH masses and the prescription given in Merritt (2006). TMT operating at the diffraction limit will be able to resolve binary BHs in a number of core ellipticals if BHs are stalled. TMT will not be able to probe stalling radii falling in the shaded region.

6.4 Dust and the Structure of the Central Engine

Some, and perhaps most, AGNs have extremely optically thick gas, which with dust can produce many magnitudes, perhaps even tens to a hundred magnitudes of visual extinction, radically altering our view (and classification) of the active nucleus. If, as suspected, much of this dust is close to the active nucleus, it will be warmed enough to produce the strong observed MIR emission. Resolving the geometry of these absorbers, possibly a 'torus' or maybe a wind covering a large solid angle of the sky, is a key goal in the field. TMT gives us our first realistic chance to do this.

Directly observing dust in galaxy centers, and the dust which constitutes the torus, is optimally achieved at MIR wavelengths, as the characteristic blackbody temperature (a few 100 K) peaks at this wavelength, and contamination from stellar emission and obscuration are greatly reduced. Through observations with 8 m telescopes, the torus in AGNs was revealed to be compact (a few pc) in moderate activity AGNs (i.e. Jaffe et al. 2004; Packham et al. 2005; Mason et al. 2006), or perhaps even absent in low activity AGNs. The torus is suspected to be a 'clumpy' distribution (Nenkova et al. 2002), rather than a homogenous distribution of dust. Tentative new results seem to show the torus structure and perhaps its presence is strongly affected by the level of activity in the AGN, which in turn is related to the fueling of the central engine. However, surveys of AGN tori using 8 m class telescopes are confined to the local universe due to the combination of flux and spatial resolution limitations.

Through the nearly four-fold increase in the spatial resolution of TMT, compared to 8 m telescopes, observations of fainter and/or more distant objects can be performed. At $z = 0.5$, the spatial resolution of JWST/MIRI is 1.5 kpc (hence heavily contaminated by galactic star forming rings, etc.), whereas the TMT spatial resolution is 330 pc (nuclear dominated) (similar comparison on spatial resolutions between Spitzer and Gemini observations is shown in Figure 46). Through careful imaging and spectral observations of the torus in $z <\sim 0.5$ objects, templates can be produced that will be of crucial importance to calibrating and interpreting observations from JWST. ALMA will probe the outermost (cold) regions of the torus structure. Only through these combined results will an accurate examination of the torus properties, effect of radio loudness, and the host galaxy versus both the level of AGN activity and redshift be probed.

NIR polarimetric studies (Young et al. 1995; Packham et al. 1997; Lumsden et al. 1999; Simpson et al. 2002; Watanabe et al. 2003; Lopez-Rodriguez et al. 2013, 2015) of few AGNs have shown that the NIR polarization is attributed to the extinction along the LOS by the passage of radiation of the central engine through hot dust ($T \sim 1500$ K) in the inner edge of the obscuring material surrounding the central engine. From a magnetohydrodynamical framework (Blandford & Payne 1982; Krolik & Begelman 1988; Emmering et al. 1992; Konigl & Kartje 1994; Kartje et al. 1999; Elitzur & Shlosman 2006), the obscuring material is part of an outflowing wind confined and accelerated by the magnetic field generated in the accretion disk. In this scheme, the hydromagnetic wind can lift the plasma from the midplane of the accretion disk to form a geometrically thick distribution of dusty clouds surrounding the central engine. The magnetic field can induce a preferential orientation of dust grains within the dusty clouds that can give rise to a measurable degree of polarization. Thus, NIR polarimetry has the advantage of providing information about the magnetic field at locations where FIR/sub-mm emission is weak.

Recent studies (Lopez-Rodriguez et al. 2013, 2015) have shown that the magnetic field strength (few mG) and geometry (aligned with the torus axis) within the obscuring material of a few AGNs can be determined through NIR (1–2.5 μm) polarimetry. However, due to the flux sensitivity of the current suite of IR polarimetric instruments in 8 m class telescopes only a few objects are observable, limiting the statistical analysis to obtain general and/or extraordinary magnetic properties. The high-angular resolution and the D^4 advantage of TMT will (1) minimize starlight dilution within the central region, important to estimate the intrinsic polarization of the AGN; and (2) increase the number of objects allowing us to measure general and/or extraordinary magnetic properties within

the torus of AGNs. This study will allow us to study the evolution, dynamics and morphology of the obscuring material and its interaction with the central engine and host galaxy from a magnetohydrodynamical framework. The NIR (1–2.5 μm) polarimetric capability of TMT should be able to obtain an accuracy of 0.1% in the degree of polarization.

An IR (1–13 μm) imaging- and spectropolarimetric capability in the TMT will be essential to study the dust properties in and around AGNs. For example, the pioneering work by Aitken et al. (1984) and Bailey et al. (1988) to study NGC 1068 using low spatial-resolution ($> 1''$) NIR (1–5 μm) imaging polarimetry and MIR (7.5–13 μm) spectropolarimetry observations showed a rotation in the position angle of polarization of $\sim 70^\circ$ between 4 and 5 μm. These results are consistent with the predicted angle change of aligned dust grains (Efstathiou et al. 1997). However, this was only attempted for few objects (Packham et al. 2007). With TMT, observations and modeling of the total (Laor & Draine 1993) and polarized (Aitken et al. 2004) IR (1–13 μm) SED of AGNs in a wide wavelength range will provide crucial probes to dust grain properties such as their sizes, shapes and compositions. They will also help investigate the fraction of thermal and non-thermal polarization mechanisms in the central regions of AGNs.

6.5 Time Variability, Probing the Structure and Processes in the Central Engine

TMT will see first light in an exciting era for time domain astronomy (see Sect. 9). Particularly exciting for the study of SMBHs is the identification and study of Tidal Disruption Events (TDEs), which occur when a star on an orbit around SMBH makes a close approach and is ripped apart by tidal forces. Once the stellar debris rains down on the BH, soft X-ray and UV radiation characterized by a 10^5 K blackbody emerges from the inner accretion region. Reprocessing of this radiation in the debris results in a fraction of the emission emerging in the optical. Large numbers of TDEs can be detected by the current big transient surveys like the Palomar Transit Factory (PTF, Arcavi et al. 2014), and many more will be found in the next generation of large-area surveys such as with the LSST. Observations of TDEs are important because they in principle provide a means of measuring the masses and spins of BHs in optically 'normal' galaxies.

The TMT will allow the detection and study of TDEs up to much higher redshifts than previously possible (see Sect. 9.8). Because of the "negative" K-correction (TDEs emitting primarily in the restframe UV with a characteristic 10^5 K blackbody) TDEs will be visible by TMT to redshifts of 6 or larger, enabling constraints on SMBH properties and evolution over a vast range of cosmic time.

The study of a large number of TDEs will help to anchor the observational signatures to precisely-measured BH masses. While analytic models and numerical simulations exist, there are still large uncertainties in the conversion from a measured light curve to a BH mass estimate – the ultimate goal of TDE studies. Finding TDEs in a nearby galaxy with an independent measurement of the BH mass, either from the M-σ relation or better yet maser disk kinematics, will provide a better calibration of the models. With current observational capabilities the probability of finding such nearby events is low, and measuring their light curves is challenging. But, with LSST and the greater follow-up sensitivity and angular resolution of the TMT, it should be possible to build up a sample of "low-z" TDEs.

Variability of AGNs provides a powerful means to explore and characterize the innermost regions. Time resolved spectroscopy and spectropolarimetry allow for highly confident identification of the excitation processes powering AGN jets. Variability studies coupled with the method of reverberation mapping discussed in Section 6.2.4 can be used to expand the present sample of a handful of AGN systems where their inner accretion disk structures and sizes can be measured up to many thousands of systems, covering the vast ranges of types and characteristics of AGNs and blazars that are observed, see also Section 9.9.

7 EXPLORATION OF THE MILKY WAY AND NEARBY GALAXIES

The stellar contents of the Milky Way and nearby galaxies make up the fossil records that were produced during galaxy formation and evolution. The spatial, temporal and abundance distributions of these stars provide important clues to the underlying astrophysical processes involved and also complement the study of galaxy formation and evolution at high redshift. We discuss a number of outstanding questions, answers to which are expected from TMT observations.

7.1 Stellar Astrophysics

There are still a number of areas important to stellar modeling and evolution that are usually ignored because it is simply unclear how to proceed – there is little observational evidence to guide theoretical models in setting the relevant parameters, hence the resulting uncertainties may be large. Here, two areas are highlighted for which TMT can make major contributions.

7.1.1 Diffusion (sinking) of heavy elements in the outer parts of stars

Diffusion is believed to occur whenever the outer parts of a star are quiet without large-scale velocity fields and are then not well mixed. Gravity and temperature will tend to concentrate the heavy elements towards the center of the star (Salaris et al. 2000). Diffusion acts very slowly with timescales $\sim 10^9$ yr, so it is most important on the main sequence, and is particularly important for metal-poor stars. Diffusion of He is important in the Sun and affects helioseismology models. Diffusion is also important in precision distance determinations based on main sequence fitting, since the abundances adopted for the model isochrone must agree with those of the stars, while the abundances deduced for the stellar atmosphere may not be those of the interior. Diffusion may also be the solution to a disagreement of a factor of ~ 2 between the Li abundances derived for halo turn off stars, assumed to be the primordial lithium abundance, and the (lower) value predicted by standard Big Bang nucleosynthesis models that adopt the baryonic density inferred from the current concordance cosmology of WMAP (Meléndez & Ramírez 2004; Korn et al. 2006; Bonifacio et al. 2007).

A key project to observe diffusion in action is to compare the elemental abundances for heavy elements near the Fe-peak of main sequence versus red giant and sub-giant stars in metal-poor globular clusters. Stars within a particular globular cluster, assuming its mass is not too high so that gas cannot have been retained beyond the first generation of star formation, are believed to have the same initial chemical inventory, and are sufficiently old that diffusion should have had time to act. The red giant branch (RGB) stars have convective envelopes, and thus whatever diffusion might have occurred on the main sequence, the surface helium and heavy elements will have been restored to very close to their initial value, while the main sequence stars will be subject to the predicted larger effects of diffusion for metal-poor stars over their entire lifetime, i.e. that of the Galactic halo, ~ 13 Gyr. Such observations require high spectral resolution spectroscopy of main sequence stars in globular clusters with S/N that is difficult or impossible to achieve with existing 8–10 m telescopes. The net efficiency gain of HROS on TMT relative to current facilities will enable the required observations of these faint stars.

7.1.2 Evolution of massive stars with low metallicity: observational probes

Massive stars contribute a large fraction of all the heavy elements through SN explosions. They provide the UV ionizing flux for the ISM and their supersonic winds help shape the ISM. They are probably linked to the re-ionization of the early universe (Bromm et al. 2001) and perhaps to the GRB phenomenon. Massive stars of very low metallicity were, until quite recently, believed not to lose very much mass through radiatively driven winds due to their weaker absorption features. This would mean that such stars might often end up as BHs, locking up their heavy element chemical

inventory in perpetuity, while a solar metallicity star of similar mass would lose enough mass to end up as an NS. However, Meynet et al. (2006) have suggested that these stars are rapid rotators that lose up to 50% of their initial mass through a rotationally driven wind. The mass loss rates they predict for the main sequence phase of a 60 $M_{\odot}$ star are more than 20 times larger than if rotation were ignored. Coupled with rotationally driven instabilities that transport both angular momentum and chemical species (Zahn 1992), this means that massive low metallicity stars can significantly enrich the ISM in H- and He-burning products.

This theoretical development is very attractive as it solves a number of problems, but the observational evidence to support this development is essentially non-existent at present. The low metallicity required to produce main sequence rotation rates of < 600 km s^{-1}, close to the breakup rate at which the effective surface gravity becomes zero, is less than that seen at any place in the Milky Way where star formation is still underway. The metal depletion of the ISM in the Large Magellanic Cloud (LMC) and in the SMC is also not sufficient. A population of young massive stars in a low metallicity galaxy is required, i.e. a very metal-poor star-forming dwarf galaxy. There are none close enough to obtain the required spectroscopy with existing 8–10 m telescopes. The most metal-poor dwarf known in the nearby universe, I Zw 18, has a distance of 18 Mpc and an oxygen abundance 1/50 that of the Sun (Skillman & Kennicutt 1993). The galaxy SBS 1415+437 with a distance of 14 Mpc is almost as metal-poor (Aloisi et al. 2005), with oxygen below 1/20 the solar value. With WFOS on TMT, it will be possible to observe the brightest supergiants in the nearest very metal-poor dwarf galaxies to determine the mass loss rate as a function of metallicity.

7.1.3 Validation of theoretical scenarios for low-mass star formation at extremely low metallicity through observations

There is still no concensus for the formation of low-mass stars from metal-free clouds. Model calculations with extremely low metallicity ([Fe/H] $<$ –5) with excess or no excess of light elements, like carbon suggest the roles of fine structure lines of these elements and of dust emission (Norris et al. 2013). Formation of multiple systems might be a key to understanding the formation processes of low-mass stars in first stars (Machida 2008). Such a study requires a large sample of extremely metal-poor stars and RV monitoring for them to obtain statistics. Metal-poor stars are extremely rare objects, which makes finding them a great challenge (Fig. 48). Large-scale systematic searches began with the HK survey by Beers et al. (1985, 1992), followed by the Hamburg/ESO Survey (Wisotzki et al. 1996; Christlieb et al. 2008) that covered $\sim$1000 square degrees of the southern sky collecting data of some 4 million point sources. More recent searches use medium resolution spectroscopy using large multi-object spectrographs (e.g. SDSS, SEGUE, LAMOST survey) or selecting metal-poor candidates from photometric survey data. The SkyMapper telescope is photometrically surveying the southern sky in specific filter sets (e.g. Bessell et al. 2011) that allow candidate selection in a very efficient way. Follow-up high resolution spectroscopy is still required for confirmation and detailed chemical abundance studies. The oldest and the most Fe deficient ([Fe/H] $<$ –7.0) star known so far, SMSS J031300.36-670839.3, is a discovery from this survey. Similar metal-poor objects to be found from this and other on-going surveys will provide observational constraints to test theoretical models for low-mass star formation at extremely low metallicity. TMT/WFOS would be useful not only to enhance the database of extremely metal-poor stars but also for conducting detailed chemical abundance studies.

7.1.4 Astrophysics of rare objects

TMT equipped with a high resolution spectrograph will provide a unique opportunity to understand the origin and evolution of rare exotic faint stellar objects through detailed chemical abundance studies. For example, observational evidence of the presence of extraordinarily strong Sr features

in the hydrogen-deficient carbon (HdC) star HE 1015–2050 from medium resolution spectroscopy (Goswami et al. 2010; Goswami & Aoki 2013) brought the issue of Sr synthesis in stellar interiors to the forefront. To acquire high resolution spectra required for detailed abundance analysis to understand the origin and evolution of such faint objects ($V_{\rm mag}$ of HE 1015–2050 ~ 16.3) is extremely difficult and time consuming with the existing 8–10 m class telescopes particularly if such objects happen to undergo significant brightness variations. Similarly, enhancement of fluorine abundance observed in the Extreme helium (EHe) and R Coronae Borealis (RCB) stars (Pandey et al. 2008) by factors of 800–8000 relative to its likely initial abundance raises questions about F synthesis mechanisms and the prevailing conditions in the stellar interiors. Measurement of fluorine abundance from the HF band in the NIR in a large sample of K and M giants covering a wide range in metallicities and ages would be essential to understand the origin and evolution of fluorine. Many such potentially interesting objects will form important targets for TMT due both to the large collecting area and more efficient spectrograph.

7.1.5 The initial-final mass relation – Version 2.0

For the past 10 years, the Keck Observatory has spearheaded an effort to measure one of the most fundamental relations of stellar astrophysics, the initial-final mass relation – IFMR v1.0. This relation connects the mass of stellar remnants, WDs, to the mass of their progenitor hydrogen-burning main sequence stars, and therefore provides a direct way to understand stellar mass loss.

The initial-final mass relation is constrained by spectroscopically measuring the masses of WDs that are members of rich star clusters. The spectroscopy yields the masses of the remnants (Balmer line fitting - Bergeron et al. 1992), and the initial masses are known given the ages of the clusters. Despite the tremendous progress, two of the biggest uncertainties in the relation today are:

- **What is the upper mass limit to WD formation (i.e., what is the lower mass limit to a Type II supernova)?** The threshold mass separating WD formation from Type II supernovae (SNe II) is a fundamental threshold for stellar astrophysics and affects several linchpins at the heart of understanding the impact of stellar evolution on galaxy evolution. For example, the transition impacts chemical evolution models and the enrichment of the ISM (and subsequent stellar populations) by setting the balance between stellar yields from lower mass stars (e.g., He, C, N) and those from SNe II (e.g., alpha elements).
- **What is the metallicity dependence of stellar mass loss?** The total amount of mass loss that a star suffers in post main sequence evolution dictates the lifetime of the star in different phases of stellar evolution, the luminosity function of those phases, the morphology of the horizontal branch, and the structure of planetary nebulae (PNe). To accurately use the initial-final mass relation to predict the evolution of mixed stellar populations with different star formation and chemical abundance histories, we need to measure how mass loss varies with metallicity. This is unconstrained from theoretical work.

The WFOS instrument on TMT offers a unique opportunity to answer these two questions. With Keck/LRIS, our current sample of target star clusters for which spectra of WD members suitable for mass determination can be obtained is limited to the nearest open star clusters within ~ 3 kpc, and the single nearest globular cluster within ~ 2 kpc. Within this volume, there is a lack of very young clusters with massive turnoffs to address the first challenge, and a lack of a metallicity spread within the clusters to address the second challenge. With TMT's light collecting area, WD spectroscopy can be pushed to systems at 10 kpc. This volume includes three dozen globular clusters with a wide range of metallicities, as well as numerous rich open clusters with ages from 30 to 100 Myr (i.e., present day evolving mass ranging from 5 to 10 $M_{\odot}$). Searching for WDs in these clusters, and linking them to their progenitor masses, will answer these fundamental questions. The key requirements for this program that would directly impact many areas of galactic and extragalactic astrophysics are ultra

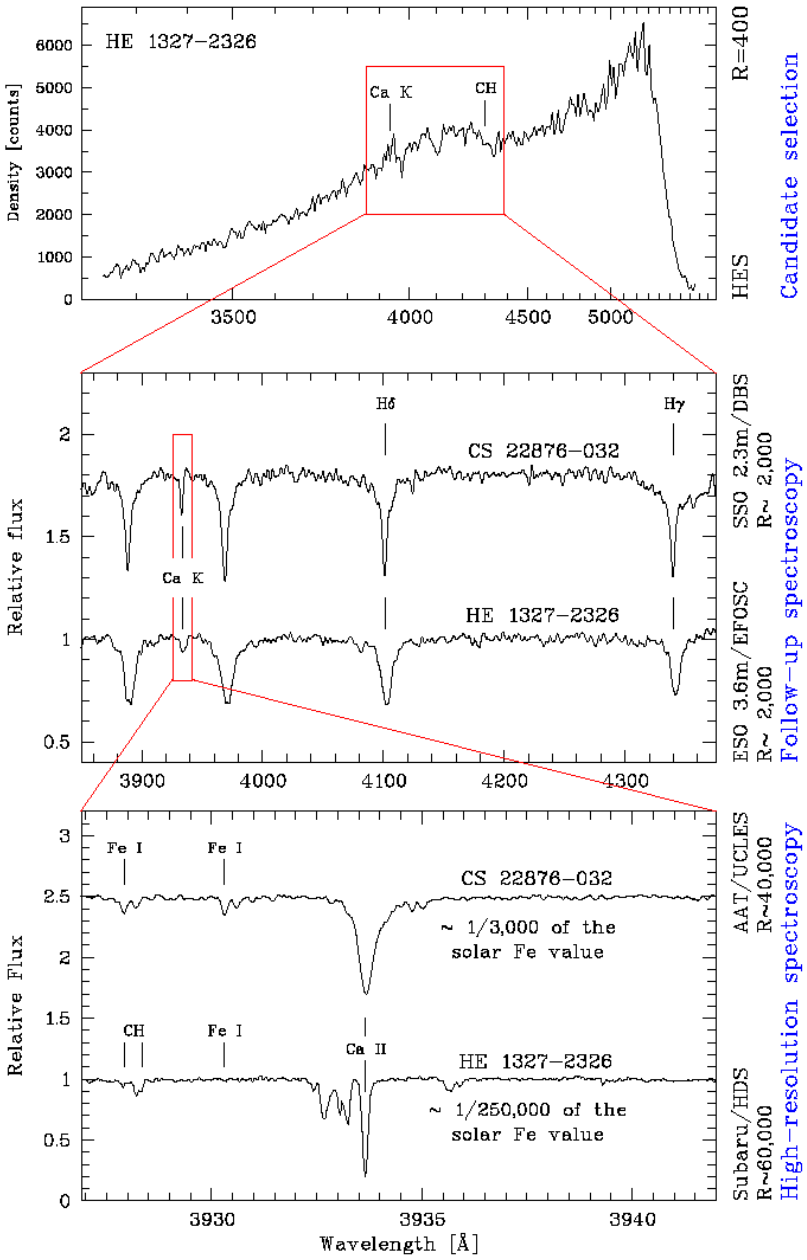

Fig. 48 The process of finding a metal-poor star. Stars with weak Ca II K lines are identified in low-resolution spectra (*top*), and are selected for follow-up with medium resolution spectroscopy (*middle*) to get a direct measure of the Ca II K line strength. The most metal-poor stars of this sample are then selected for high resolution follow-up (*bottom*), where the abundances of other elements can be determined (Source: Jacobson & Frebel 2014).

high throughput at UV wavelengths down to 3600 Å (covering the high order Balmer lines), MOS capability and low resolution spectroscopy with $R = 2000 - 4000$.

7.2 Binary Population: The Binary Frequency of Field Stars

A large fraction of stars in the Milky Way are part of binary or higher order systems, with separations < 0.04 parsecs (Larson 1995). Binaries can be identified by direct imaging or spectroscopically. The spectroscopic detection of binaries can be a laborious process that typically requires observations that span a long time baseline. Two possible imaging programs are discussed here that exploit the unprecedented angular resolution of the TMT to probe the binary frequency in very different environments:

(1) A targeted study of star clusters. A survey of targets selected according to mass, age and dynamical state will prove useful for constraining the factors that define the binary frequency. The improved angular resolution delivered by NFIRAOS will be useful for resolving multiple objects with small projected separations on the sky that might otherwise appear as a single object. Such blends will appear as erroneous points on color-magnitude diagrams (CMDs), and confuse efforts to characterize cluster properties. By measuring the brightness of the individual components of such systems as opposed to their blended light, it will be possible to obtain cleaner CMDs.
(2) A serendipitous survey of low mass binaries in the field. The TMT has the potential to become a binary-identification factory, as binary systems will be discovered serendipitously by the NFIRAOS wavefront sensors during routine target acquisition and set-up. The angular resolution of the NFIRAOS NGS probes in J is $0.01''$ FWHM, and these will guide on sources as faint as $J = 22$. Heretofore unknown binaries (as well as extragalactic objects with modest angular extensions) could be identified by the NFARIOS RTC as objects causing problematic corrections. Binary stars could be identified visually in the wavefront sensor output display during target acquisition. If pre-imaging of the field is used to identify guide stars then proper motions can be measured and thereby obtain distance information. Some of the selection biases due to separation and mass ratio inherent to imaging studies could be overcome, for example, by grouping systems according to proper motion. An interesting aspect of this investigation is that the stars that will be detected at the faintest magnitudes will have low intrinsic masses. With long term observations a binary database that spans a range of environments in the Galaxy could be sampled.

7.3 Star Clusters: Formation, Evolution and Disruption

7.3.1 Star cluster formation and evolution and their environmental dependence

Stars, and in particular the most massive stars, rarely form in isolation. In fact, it is now well established that the vast majority of active star formation occurs in clusters of some sort. Despite significant recent progress, the evolutionary connection between the recently formed young massive clusters (YMCs) in starbursts and old globular clusters in the nearby universe is still contentious. The evolution and survivability of young clusters depend crucially on their stellar IMF (see also Sect. 8.2): if the clusters are significantly depleted in low-mass stars compared to, for example, the solar neighborhood, they will likely disperse within about a Gyr of their formation. As a simple first approach, one could construct diagnostic diagrams for individual YMCs, of mass-to-light ratio (M/L; derived via dynamical mass estimates using high-resolution spectroscopy and the virial approximation) versus age (derived from spectral features), and compare the YMC locations in this diagram with models of "simple stellar populations" (SSPs) governed by a variety of IMF descriptions.

However, such an approach has serious shortcomings and suffers from a number of fundamental problems.

The essential conditions to make a major leap forward are to obtain high-resolution spectroscopy and imaging of a significantly larger cluster sample than available at present (to distinguish between trends and coincidences), covering a much more extended age range. These observations will need to be backed up by detailed N-body simulations of clusters containing both a realistic number of test particles (upwards of several $\times 10^5$) and all relevant physical processes occurring over the clusters' lifetimes. Using TMT-sized apertures will allow us to probe both the dynamics and the luminosity function of young and intermediate-age star clusters (and their host systems) out to cosmologically interesting distances, where we can obtain statistically significant samples of galaxy types spanning the entire Hubble sequence, and of their YMC systems. Using this approach, the initial conditions for cluster formation (and evolution) can be modeled fully self-consistently. This will, for the first time, provide us with the firmest handle yet on potential IMF variations in external galaxies. For the expected velocity dispersions of $\sim 7 - 15$ km s^{-1} (for masses of $\sim 10^5 - 10^6\ M_\odot$), a spectral resolution of $R > 40\,000$ is essential to efficiently sample the prevailing IMF conditions in a statistically significant number of YMCs. As long as the masses of the clusters are not too small ($M_{\rm cl} > 10^5\ M_\odot$, depending on the cluster's size), one can extract their velocity dispersions using suitably chosen cool giant and supergiant template stars (Ho & Filippenko 1996). Using $R = 40\,000$, one can resolve velocity dispersions down to $\sigma_v \sim 6.5$ km s^{-1} at a wavelength of 0.85 μm, i.e. to $M_{\rm cl} \sim 2 \times 10^5\ M_\odot$ for YMCs of globular cluster size. The spectral range around the CaII triplet ($\lambda_{\rm central} = 860$ nm) with a large number of metal lines in this spectral range can be used, and cross-correlated with a number of properly selected (super-)giant velocity template stars over the entire observed wavelength range, to obtain our velocity dispersion measurements.

Complementary imaging observations covering – ideally – at least four passbands spanning a minimum of the entire optical wavelength range will allow researchers to independently and robustly determine the cluster properties (age, mass, metallicity) using the sophisticated multi-parameter AnalySED algorithm (de Grijs et al. 2003; Anders et al. 2004), which has been shown to produce robust results.

7.3.2 Globular clusters: their origin and evolution

Research on Galactic globular clusters by many investigators over the last few decades has led to a new paradigm for the formation and evolution of these not-so-simple stellar populations. Photometric and spectroscopic evidence confirms the presence of multiple stellar populations in nearly all Galactic globular clusters. Both dynamical models of clusters and the total mass of first generation stars needed to produce the second and subsequent generations suggest that globular clusters were originally as much as 2–10 times more massive than they are today. It is believed that the less centrally concentrated first generation stars have mostly been lost to merge into the population of field halo stars, whose composition the first generation stars resemble.

This new paradigm suggests that the star formation events that created globular clusters in the early universe were significantly more luminous and more massive than star forming regions we see in the local universe today, and that the star formation process to produce a young globular cluster extended over a timescale of roughly 100 million years. At the same time, we find bimodal populations of globular clusters in external galaxies, red and blue clusters with perhaps different metallicities and/or ages, and with different spatial distributions around their host galaxies. These different cluster systems are interpreted as resulting from different formation mechanisms, either through in situ formation processes or through major or minor galaxy mergers from host galaxies that experienced different histories of star and cluster formation.

To understand the star forming regions in the early universe that may be detected with TMT, we must first learn what we can about the origin and evolution of such clusters in the local universe.

While Galactic clusters can be studied with smaller telescopes up to 8 and 10m, understanding the implications of multiple stellar populations in globular clusters beyond the Local Group will require the spatial resolution and light gathering power of TMT. Study of radial gradients in colors and spectral indices that reveal the nature of the constituent stellar populations will require spatial resolution exceeding what is possible with Hubble (which can barely resolve clusters at the distance of the Virgo Cluster) and even JWST. Such studies with TMT will help us constrain the properties of the original star forming events that produced globular clusters in different environments, and allow us to connect the clusters we observe today with the observation of high redshift cluster-forming events in the early universe observed directly with TMT.

7.3.3 Infrared counterparts of X-ray sources in globular clusters: probing IMBH candidates

X-ray sources in globular clusters are ideal candidates to look for the IMBHs that have masses intermediate between the SMBHs in AGNs and the stellar mass BHs. Some of them are ultra-luminous, known as ULX and have X-ray luminosities greater than 10^{39} ergs s^{-1}. AGNs are much more luminous and emit equally at all wavelengths with a strong correlation between the X-ray and IR luminosities from a dust torus (e.g. Krabbe et al. 2001; Lutz et al. 2004; Asmus et al. 2011; Ichikawa et al. 2012); it is important to look for similar X-ray IR correlations in ULX candidates. A study conducted for NGC 1399, using archival data from Spitzer IRAC and Chandra showed that there are two categories of bright X-ray sources, one in which, like in AGNs the MIR luminosity correlates with the X-ray, and the other where the IR and X-ray luminosities are uncorrelated (see figures 6 and 7 of Shalima et al. 2013) indicating that one has a dusty environment and the other is dust deficient. However, a major source of uncertainty is possible contamination from background AGNs. With the high spatial resolution of TMT together with spectral information on these sources, it will be possible to eliminate the background contamination and concentrate on the real IMBH candidates and their environments.

The difference in the ratio of the IR to X-ray luminosities of X-ray binaries and AGNs reflects a difference in the dusty environment of these two types of sources. With the availability of the high resolution MIR instrument MICHI on TMT it would be possible to study the dust content of these sources in detail.

7.4 The First Stars

7.4.1 Probing the oldest stars in the Milky Way

The first, so-called Population III stars are believed to have been formed from gas unpolluted by heavy elements, after which all subsequent generations of stars contained increasing fractions of metals. This process has continued during the entire lifetime of the universe. Hence the most metal-poor stars in the Milky Way and other galaxies are the oldest stars. In their atmospheres these old objects preserve details of the chemical composition of their birth gas cloud. These very old stars are hidden among a vast number of stars formed later in time. Once found, understanding the chemical composition of the oldest stars provides a direct probe of the initial conditions of star formation as well as the details of chemical evolution and nuclear astrophysics in the early universe.

In the spectra of the metal-poor stars, since the relevant absorption lines appear quite weak (Fig. 49), the necessary chemical composition studies require high spectral resolution ($R = \lambda/\delta\lambda \sim 50\,000$ or greater) and high S/N ($\sim$100 per spectral resolution element) observations. These requirements lead to extremely long integration times on the largest telescopes currently available. For example, an 18-hour integration with UVES on the VLT was obtained in an attempt to determine the oxygen abundance in HE1327–2326, the most extreme metal-poor turn-off star known ([Fe/H] ~ -5.5 dex, U $\sim$13.8, V $\sim$13.5), but even with such a long exposure, the UV-OH band was not

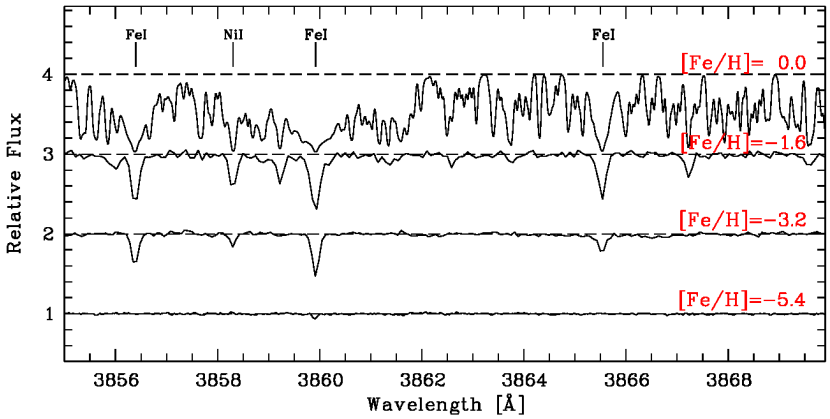

Fig. 49 Spectral comparison of stars in the main sequence turn-off region with different matellicities. Several atomic absorption lines are marked. The variations in line strength reflect the different matellicities. From top to bottom: Sun with [Fe/H] = 0.0, G66–30 with [Fe/H] = –1.6 (Norris et al. 1997), G64-12 with [Fe/H] = –3.2 (Aoki et al. 2006), and HE 1327–2326 with [Fe/H] = –5.4 (Source: Frebel 2010)

detected; its spectrum showed only very weak metal absorption lines with weak CH and NH bands detected was required to determine abundances for HE1327–2326, the most extreme metal-poor turn-off star ([Fe/H] ~ -5.5 dex); its spectrum shows only weak metal absorption lines (Frebel et al. 2006).

The number of stars accessible to TMT will be much larger; for the seeing-limited high-resolution spectrograph HROS, the total improvement relative to VLT/UVES or Keck/HIRES or Subaru/HDS is expected to be 15–20. For example, a 4-hour integration with HROS will enable $R = \lambda/\delta\lambda \sim 40\,000$ spectroscopy with S/N = 100 per spectral resolution element for stars as faint as $V \sim$21 in the visible.

7.4.2 Mass distribution of first generation of stars

Formation of massive and possibly very massive stars is predicted by the simulations of the structure formation in the very early universe. Recent discoveries of halo stars with [Fe/H] $<$ –5 and measurements of their chemical abundances suggest that the progenitors of such objects are massive stars with several tens of solar masses, which might be typical masses of the first stars in the universe. Detailed measurements of their chemical compositions require high quality, high resolution spectra which will become available with TMT/HROS. For instance, only an upper-limit of Fe abundance ([Fe/H] $<$ –7) is determined for the most Fe-deficient star discovered very recently (Keller et al. 2014). Candidates of such stars will be discovered in the surveys of metal-poor stars over the next several years and follow-up spectroscopy with TMT will play an essential role. Moreover, searches for evidence of very massive stars ($>$ 100 $M_{\odot}$) in the first generations of stars are important to examine the simulations of the formations of first stars (Aoki et al. 2014). Detailed measurements of chemical compositions for metal-poor stars with peculiar abundance ratios, that will require high quality spectra expected to be obtained with TMT/HROS, will provide useful constraints on the existence or fraction of such stars in the early universe.

7.5 The Structure of the Milky Way and Nearby Galaxies

7.5.1 Dissecting the Galactic halo: ages and metallicities of old, nearby low-mass stars and white dwarfs

Recent estimates suggest that close to 70% of the stars in the local Galactic field population are M dwarfs, and about 6% are WDs. The local population of old stars from the Galactic halo is expected to hold a larger fraction of M dwarfs and WDs. These stars however have low luminosities, and are not amenable to detailed spectroscopic analysis with current telescopes unless they lie within about 100–200 parsecs of the Sun.

Low-mass stars and WDs can be highly useful to map out the halo population for three reasons: (1) they are by far the dominant stellar population of the halo; they are the old population, holding the majority of the baryonic mass, (2) their 3-D velocity components can be determined to much higher accuracy, because of their large proper motions, (3) physical properties of low-mass stars, and in particular their metallicity, can be constrained using low to medium resolution spectroscopy, because their spectra are dominated by broad molecular bands, and with suitable spectral synthesis techniques, can now be modeled in detail.

Upcoming deep imaging surveys such as Pan-STARRS and LSST are expected to identify low-mass stars in huge numbers (millions) through proper motion analyses. These surveys will effectively provide a statistically complete census of the halo population out to several kiloparsecs from the Sun. Spectroscopic data are required to measure and constrain the temperature and metallicity of M dwarfs, and also to determine the mass and ages of WDs. As the photometric distances of M dwarfs and WDs are generally unreliable, spectroscopic data are needed to constrain their luminosities. Thus a better understanding of the spatial distribution and kinematics of these objects depends on spectroscopic follow-up observations.

The sensitivity of the TMT along with the multi-object capabilities provided by WFOS will make possible a large-scale spectroscopic follow-up of low-mass stars and WDs of the Galactic halo. These observations will enable:

- Spectral classification of the candidates to confirm their Galactic halo membership, and use the existing spectroscopic distance calibrations to determine their distances, which are required to calculate their transverse motions.
- Measurement of metallicity [Fe/H] and relative abundances of critical elements [α/Fe] from the relative intensity of molecular bandheads.
- Measurement of RVs to km/s precision to calculate the full 3-D motion of the stars.

Along with proper motion and photometric data from large imaging surveys, such as Gaia, the spectroscopic data from TMT will produce a detailed census of the nearby halo population, drawing their detailed distribution in velocity space. The combination of metallicity information from the M dwarfs and age information from the WDs will identify possible substructure in the velocity space distribution. This will provide additional constraints on the shape of the halo, and also on the possible existence of accretion events, that would show up as streams in the local volume.

7.5.2 Planetary nebulae as tracers of substructures in nearby galaxies

PNe are descendants of low- and intermediate-mass stars. Being bright and widely distributed, they are excellent tracers to study the chemistry, kinematics, and stellar contents of substructures in nearby galaxies. As the nearest large spiral system to the Milky Way, the Andromeda galaxy (M31) is an ideal laboratory to assess the theory of hierarchical cosmology. PNe are easily detectable at the distance of M31 (~ 780 kpc; McConnachie et al. 2005) and can be used to investigate the properties of the intriguing substructures such as the Northern Spur and the Giant Stream in the outskirt of

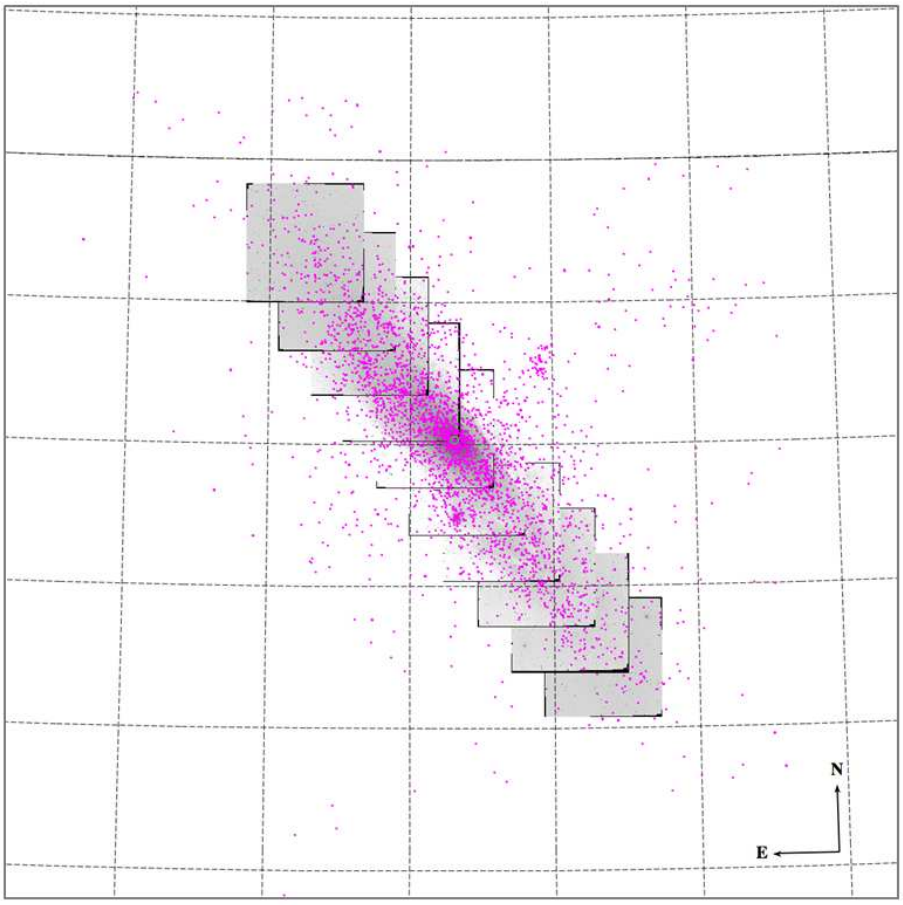

Fig. 50 Positions of PNe (the magenta dots) overlying on the ten mosaic fields of M31 that were targeted in the Local Group Survey by Massey et al. (2006). The mosaic images are in V band (on a logarithmic scale, inverted color) and each field is roughly $36' \times 36'$ in size. The PNe sample (in total $\sim$3000) includes those observed by Merrett et al. (2006) and LAMOST (Yuan et al. 2010, 2015). Horizontal divisions of the dashed grid are 0.75°, and vertical divisions are 1° (Source: Yuan et al. 2010).

M31, see Figure 50. High-quality spectra of PNe in these regions are still conspicuously lacking. It is proposed to create the first 2-D maps of nebular abundances and properties of the PN progenitors, which will allow the tracing of different substructures.

Out of nearly 3000 PNe in M31 revealed by a kinematic survey (Merrett et al. 2006), reliable elemental abundances have been derived for only a few dozen M31 PNe. Recently, the LAMOST telescope has discovered PNe in the outskirts of M31, including the most distant one, 3.6° from the center, see Figure 50 (Yuan et al. 2010). This PN is both spatially and kinematically related to the Giant Stream, and is the first one discovered in the outer streams of M31.

The α-element abundances of PNe reflect those in the ISM at the time when the progenitor stars formed. We can derive properties (luminosities, effective temperatures) of the central stars (CSPNe) based on the nebular spectrum using models (e.g., CLOUDY; Ferland et al. 1998), given that distance

of the PN is known. Using evolution models of the post-asymptotic giant branch star (Vassiliadis & Wood 1994) and the initial-final mass relationship of WDs (Catalán et al. 2008), one can estimate the masses and ages of the progenitors. If the substructures are the debris of dwarf galaxies of M31, the stellar populations therein could be different from those on the disk.

Spectroscopy of PNe has seldom been used to study the substructures in M31. In order to investigate the origin of substructures, deep spectroscopy of PNe in the substructures is required, covering 0.3–0.6 μm and 0.55–1.0 μm in the blue and red channels of the proposed WFOS instrument respectively. At a resolution $R \sim 5000$, 15 target PNe can be observed simultaneously for a full wavelength coverage. The instrument setup will enable detection of the [O II] $\lambda\lambda$3726, 3729 doublet and [S II] $\lambda\lambda$6716, 6731 lines, which are the traditional electron density diagnostics. The temperature-sensitive [O III] λ4363 and [N II] λ5755 auroral lines will also be efficiently detected and lines such as [O II] $\lambda\lambda$7320, 7330 and [S III] λ6312 will also be observed, enabling determination of electron temperatures for different excitations and consequently accurate elemental abundances for N, O, Ne, S, and Ar. Given the excellent observing condition at Mauna Kea, the 30 m aperture of TMT will achieve an optical spectrum with a S/N ratio of about 10 for a faint ($m5007 \sim 22$) PN in M31 with only a 15 min exposure. With a 30 min exposure for each observing field of WFOS (~ 15 PNe targeted simultaneously), one can cover about 12–14 fields, or ∼200 PNe, in a single night. Thus, a one-week survey will produce more than 1000 high-quality spectra for the M31 PNe in a homogeneous manner. These spectra, together with the accurate luminosity information of the PNe (given that distances of all PNe are known), could be used as inputs for the nebular code CLOUDY, which has been modified and will be used to determine the luminosities and effective temperatures of the CSPNe. The masses and ages of the progenitor stars can then be estimated using stellar evolution models. The elemental abundances and the properties of PN progenitors in the substructures will be compared with those on the disk to investigate the origin of substructures. The survey will allow a determination of properties of a significant number of PNe (>1000) across M31 and creation of the very first 2-D maps of nebular abundances and the ages and masses of progenitor stars. These maps will allow the tracing of different substructures.

7.5.3 Chemical tagging of individual stars and Galactic substructures

A systematic study of stellar motions and composition is essential to reveal the origin and evolution of the Galaxy and its present structure. The Galaxy is broadly composed of three major structural components: the disk, the bulge, and the halo. Stars can be grouped into these components based on their kinematic properties, and their chemical composition (Eggen et al. 1962). In addition to the above three components, the Milky Way Galaxy is found to have substructures which are in agreement with the theoretical predictions for a hierarchical formation of the Galaxy via mergers. Understanding the different structures of the Milky Way - their origins, and dynamics, is one of the fundamental issues in astronomy. This clearly requires decomposing the components of the Galaxy based on the age, kinematics, and chemical composition of the stars.

For a decomposition of the Milky Way, measuring accurate astrometry (parallaxes, proper motions) and hence the kinematic motion for a large number of stars is essential. The Hipparcos Space Mission in 1998 provided accurate astrometry for around one hundred thousand stars in the solar neighborhood ($d \sim 200$ pc). Combining the ground based high resolution spectroscopy and the Hipparcos astrometry, the Galactic disk is decomposed into thin and thick disks (Reddy et al. 2003). Stars in the thick disk are old ($\sim 8 - 10$ Gyrs), metal-poor ([Fe/H] ~ -0.6) and have distinct kinematic motions and chemical composition from that of the thin disk population. Abundances of elements with different nucleosynthesis history suggest that the thick disk stars formed mainly from SN II ejecta, the formation of the thick disk was rapid (<2 Gyrs) and there is no current star formation. The thick disk population is believed to be the result of a major merger of a metal-poor dwarf galaxy when the Milky Way was just 1–2 Gyr old. There are many unanswered questions regarding

the thick disk and the composition of the Milky Way galaxy: Is the thick disk really a frozen entity? What is the metal-poor end of the thick disk? Are there any smaller components in the disk? What is the structure of the bulge and the halo?

To answer these questions one needs to measure astrometry for a large number of stars beyond the solar neighborhood and obtain high resolution spectra for chemical tagging of individual stars. The space observatory Gaia will measure astrometry for one billion stars up to mv$\sim$20. Gaia will also measure RVs for a large number of stars. Together with astrometry and RV, it would be possible to construct a 3-D view of our Galaxy and identify the distinct components based on kinematic motion. Chemical tagging of individual stars of different kinematic groups would help in better understanding the evolution of the Galaxy in a chronological order, its merger history, etc., due to the expanding scope of faint and old stars that can be observed with the TMT.

7.6 Kinematics and Dynamics of the Milky Way and Nearby Galaxies

7.6.1 Kinematics of the Local Group

The Local Group has been the benchmark for testing and calibrating many aspects of cosmology and galaxy formation, hence a clear understanding of the internal kinematics of the Local Group as well as the nearby groups is necessary. The formation and evolution of the Local Group of galaxies in the Local Volume is not clearly understood, as we do not have reliable estimates of the space velocities of the galaxies. The major hindrance in the estimation of space velocity is the difficulty in measuring the very small proper motion of the distant galaxies.

Recent estimations found that the Magellanic Clouds, which were once thought to orbit around the Milky Way are now found to be on the first passage. Sohn et al. (2013) found that for most plausible Milky Way masses, the observed velocity implies that Leo I is bound to the Milky Way, which is based on the proper motion estimates from the HST. Sohn et al. (2012) obtained the first ever proper motion measurement for M31. The proper motion is consistent with a head-on collision orbit for M31 toward the Milky Way (van der Marel & Guhathakurta 2008). The required accuracy to estimate the proper motion for the nearby galaxies is about 50 microarcsec/yr.

However, estimation of the proper motion of the galaxies near M31 is not possible with existing facilities; these estimates are necessary to reveal the orbits of individual galaxies within the Local Group and its eventual destiny.

Figure 51 shows the mean orbital history of Leo I (Sohn et al. 2013). Similar orbital history for all the galaxies in the Local Group is proposed. TMT with at least one order better resolution in astrometry (50 microarcsecond accuracy) combined with deeper photometry can be used to estimate the proper motion of all the galaxies in the Local Volume. We expect to achieve orbital calculations of all members, which then will let us understand the kinematical history of interactions in this volume and predict the destiny of this group. These in combination with the proposed studies of chemical composition and star formation history will be able to decipher the formation, evolution and future of the Local Group.

7.6.2 Internal dynamics of dwarf-spheroidal galaxies: density profiles of dark matter halo

High-resolution spectroscopy of resolved member stars in dwarf-spheroidal galaxies (dSphs) has revealed that the measured LOS velocities show much larger velocity dispersions, $\sigma_{\rm los}$, than expected from the stellar system alone. Indeed, dynamical analysis of $\sigma_{\rm los}$ and its spatial dependence inside dSphs has provided density profiles of dominant dark matter halos in dSphs, which can be compared with the predictions of ΛCDM theory (see Sect. 3.1.1 for a detailed discussion).

Previous studies of $\sigma_{\rm los}$ in dSphs have revealed several discrepancies with ΛCDM theory, which include:

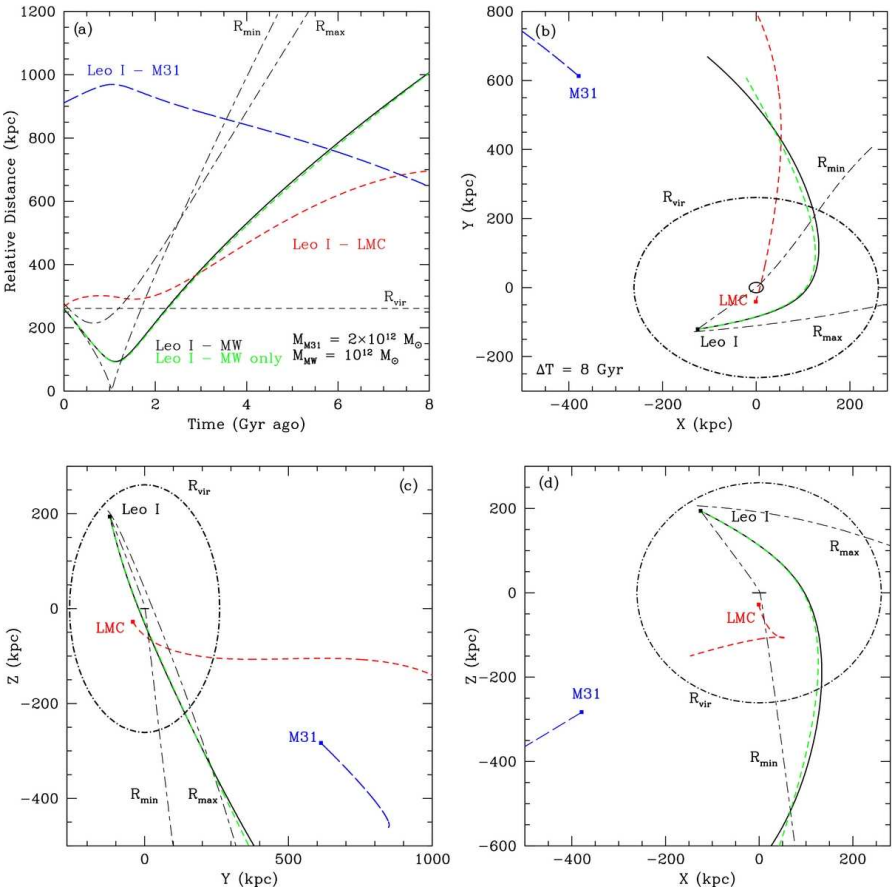

Fig. 51 The mean orbital history of Leo I from Sohn et al. (2013).

– Dark halos in some dSphs show cored central densities in contrast to cuspy ones as suggested from so-called NFW density profiles,
– Average densities of dark halos in bright dSphs are systematically small compared with those of mostly massive subhalos in Milky Way-sized halos.

These results are based on the analysis of $\sigma_{\rm los}$ alone, where specific assumption for anisotropy of velocity dispersions of stars is usually made, such as a constant isotropy/anisotropy along the projected distance from the galaxy center. However detailed information for velocity anisotropy and its spatial dependence for stars over the 2-D projected area of dSphs is actually required to obtain tighter and thus more realistic limits on the density profiles and global shapes of their dark halos (e.g., Hayashi & Chiba 2012).

It is proposed to measure proper motions of member stars and their spatial distribution in the Milky Way dSphs using TMT/IRIS. Provided typical internal velocities of stars are $\sim$10 km s^{-1}, one can expect proper motions of $\sim$0.03 mas yr^{-1} in dSphs at a distance of 70 kpc from the Sun, which can be achievable with TMT astrometry over a few years of coordinated observations of stellar positions. The available information of velocity dispersions perpendicular to the LOS will allow researchers to construct more realistic mass models of dSphs and to set important constraints on the density profiles of dark matter halos in comparison with ΛCDM theory.

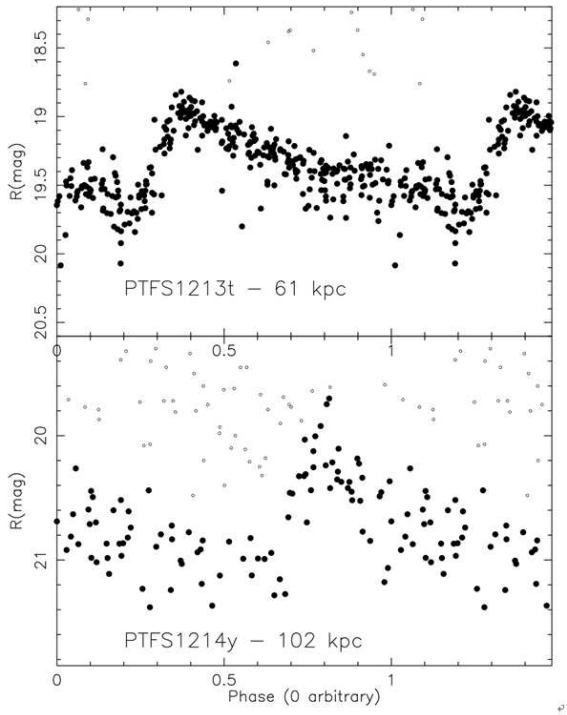

Fig. 52 Examples of PTF RR Lyr light curves. *Top*: An RR Lyr at a distance of 61 kpc whose field has 340 PTF images, with 312 detections (upper limits are indicated by small open circles). *Bottom*: A RR Lyr at a distance of 10^2 kpc with 149 PTF epochs, 61 detections and 88 upper limits (Source: Judy Cohen).

7.6.3 The mass of the Milky Way

In spite of several efforts we still do not know the Milky Way total mass to within a factor of two due to the lack of understanding of the dark matter dominated halo, the issue of the isotropy of the orbits and the shape of the potential (spherical or not) in the outer halo. The total mass of the Galaxy is usually determined through the motion of tracers (stars, dwarf galaxies, etc.) in the outer part of the galaxy beyond 50 kpc. These are combined with assumptions regarding the isotropy of orbits and the radial density distribution of the tracers to determine the total mass of the Milky Way.

In an effort to determine the total mass of the Milky Way, Deason et al. (2014) considered Blue Horizontal Branch (BHB) stars beyond 80 kpc as tracers of the outer halos. However this sample which was selected from the SDSS database (stripe 82 region) was found to contain mostly Blue Stragglers and a few QSOs, with distance uncertainties exceeding 30% in many cases. The sample contained only a few outer halo Galactic satellite dSph galaxies with reliable distances. This study reported that the number density of their outer halo stars falls very rapidly ($\rho \sim r^{-6}$ at $r > 50$ kpc) and that the RV dispersion of their sample is quite cold ($\sigma(v_{\rm r})50 - 60$ km s^{-1}) in the outer halo for ($100 < r < 150$ kpc); the estimated total mass for the Milky Way is rather small, $\sim 5 \times 10^{11}\ M_{\odot}$.

Cohen and Sesar (priv. comm.) explored the outer halo of the Milky Way considering RR Lyrae variables found by the PTF. They have selected 1257 RR Lyrae variables at distances beyond 50 kpc in the Milky Way halo, specifically to probe the density distribution as well as the total mass of our

Galaxy. The distance of this sample could be determined to an accuracy of 5%, and the contamination by QSOs is expected to be minimal. From a detailed analysis they found a density law, $\rho \sim r^{-3.4}$, between 50 and 85 kpc, which is close to the results found by Watkins et al. (2009) and Sesar (2010) for the inner Milky Way halo.

For stars to be used as tracers of the outer halo, one needs to know their RVs and the proper motions. With TMT it will be possible not only to measure the RVs of PTF RR Lyr stars out to 100 kpc but also the RVs of the RR Lyr stars to be found with LSST out to a distance of 200 kpc and beyond leading to an improved understanding of the total mass of the Milky Way. Figure 52 shows examples of PTF RR Lyr light curves.

7.6.4 Luminosity-metallicity and mass-metallicity relations for dwarf galaxies beyond the Local Group

The average metal content of a galaxy correlates with its mass. More massive galaxies are more metal-rich than less massive galaxies. The relation can be explained by the retention of metals in the galaxies' gravitational potential wells (Dekel & Silk 1986). High-mass galaxies have deep potential wells that can resist some of the expulsion of gas and metals by supernova winds, stellar winds, and galaxy-scale feedback. Low-mass galaxies lack the gravity to resist these feedback mechanisms.

Kirby et al. (2013a) compiled the metallicity of individual stars in seven gas-rich dwarf irregular galaxies (dIrrs) and dwarf spheroidal galaxies in the Local Group and produced a stellar mass-metallicity relation for the Local Group dwarf galaxies (Fig. 53). Further, they have combined this with the mass-metallicity relation for more massive galaxies (Fig. 54) observed in the SDSS (Gallazzi et al. 2005). This relation can be used to estimate the mass of the merging satellites. The mass-metallicity relation of Kirby et al. (2013a) depends on the mean metallicity of a dwarf galaxy. They do not consider the full range of metallicities within each dwarf galaxy, which could provide additional information about the mass distribution and star formation history of the satellite. Using TMT it would be possible to derive metallicity on an individual stellar spectrum for the resolved stellar population (without having to use coadded spectra for metallicity determination, as was done for DEIMOS M31 satellite spectra in Kirby et al. (2013a). Improved metallicity estimates will lead to tighter relations and with TMT it will also be possible to check the universality of such relations extending to much fainter limits and beyond the Local Group.

7.6.5 Milky Way satellites and dark matter distribution

The presence of low-mass galaxies swarming around the Milky Way had long been predicted. The inability to detect them was a major issue till the discovery of Segue 2 in the SEGUE survey (an extension of the SDSS) by Belokurov et al. (2009) (Fig. 55; also called the Aries ultra-faint dwarf). Undoubtedly, many more such galaxies are orbiting the Milky Way that are currently beyond our ability to detect.

Segue 2 is the least massive galaxy in the known universe consisting of about 1000 stars with dark matter holding them together. Keck/DEIMOS spectroscopy of 25 members of Segue 2 (Kirby et al. 2013b) revealed that the stars' [α/Fe] ratios decline with increasing [Fe/H], indicating that Segue 2 retained SNe Ia ejecta despite its presently small mass and that star formation lasted at least for 100 Myr. The mean metallicity ([Fe/H] ~ -2) was found to be higher than expected from the luminosity- metallicity relation defined by more luminous dwarf galaxy satellites of the Milky Way. The dynamical and chemical characteristics of Segue 2 are suggestive of two possible scenarios for its formation: Segue 2 may be the barest remnant of a tidally stripped, Ursa Minor-sized galaxy that came to be ultra-faint through tidal stripping. Gravitational interaction with the Milky Way's gravitational potential removed nearly all of its stars and dark matter halo, leaving only the dense center of the galaxy. Further studies and simulations are needed to test whether tidal stripping of a

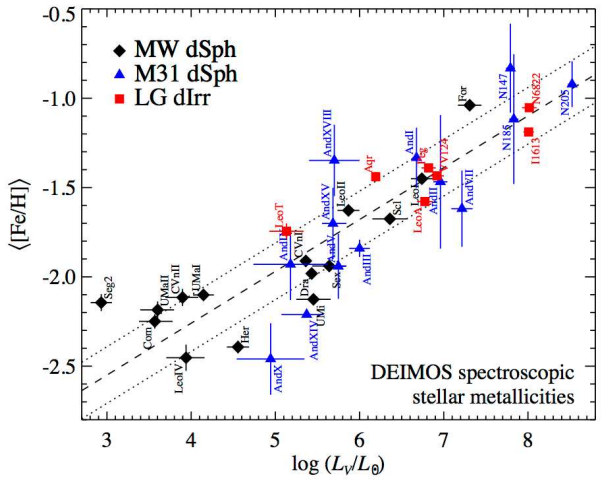

Fig. 53 Luminosity-stellar metallicity relation for Local Group dwarf galaxies. The black diamonds (Milky Way dSphs) and red squares (dIrrs) are the average stellar iron abundances from spectroscopy of individual stars. The blue triangles (M31 dSphs) are the average stellar iron abundances from coadded spectroscopy of groups of similar stars within each dwarf galaxy. The dashed line shows the least squares fit, excluding the M31 data points and Segue 2. The dotted lines show RMS about the best fit. (Kirby et al. 2013a).

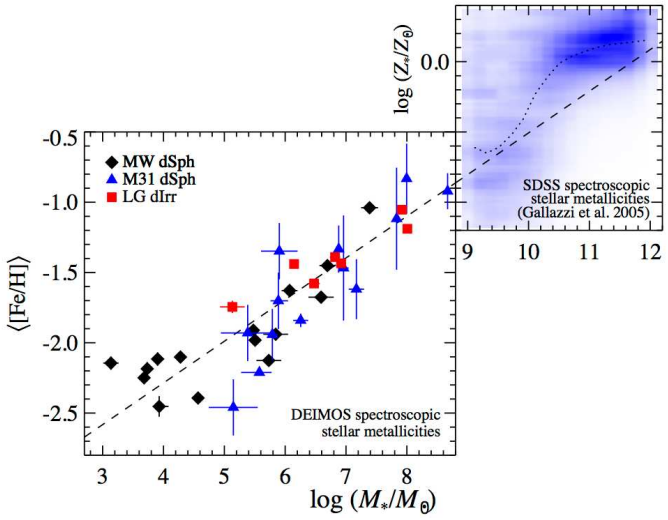

Fig. 54 Stellar mass-stellar metallicity relation for Local Group dwarf galaxies (*left*) and more massive SDSS galaxies. The Local Group metallicities ($\langle$[Fe/H]$\rangle$) were measured from iron lines, and the SDSS metallicities ($\log Z_\star$) were measured from a combination of absorption lines, mostly Mg and Fe. The conversion between $\langle$[Fe/H]$\rangle$ and $\log Z_\star$ depends on [Mg/Fe]. The Local Group data are the same as those in Figure 53, but they are plotted here vs. stellar mass rather than luminosity. The dashed line is the least-squares fit to the Local Group galaxies, and the dotted line in the right panel is the moving median for the SDSS galaxies. Although the techniques at measuring both mass and metallicity differ between the two studies, the mass-metallicity relation is roughly continuous over nine orders of magnitude in stellar mass. (Kirby et al. 2013a)

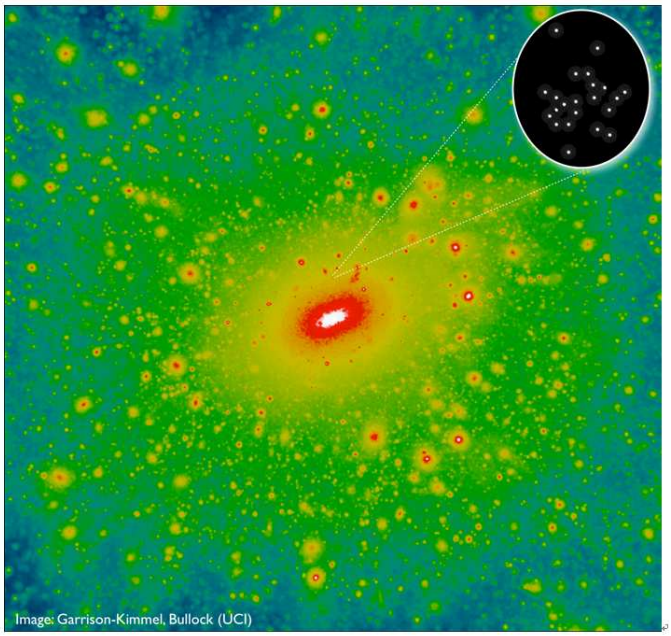

Fig. 55 The image shows a standard prediction for the dark matter distribution within about 1 million light years of the Milky Way Galaxy, which is expected to be swarming with thousands of small dark matter clumps called 'halos'. The scale of the image is such that the disk of the Milky Way would reside within the white region at the center. Untill now, there was no observational evidence that dark matter actually clumps this way, raising concerns that our understanding of the cosmos was flawed in a fundamental way. Observations of the UFD galaxy Segue 2 (zoomed image) have revealed that it must reside within such a tiny dark matter halo, providing possibly the first observational evidence that dark matter is as clumpy as long predicted (Source: Garrison-Kimmel, Bullock (UCI)).

dSph with the stellar mass of Ursa Minor could produce Segue 2. Alternatively, Segue 2 could have been born in a very low mass dark matter subhalo.

Reliable estimates of RVs could not be measured for many of the spectroscopic targets used in the Kirby et al. study of Segue 2 due to the low S/N of their Deimos data. Accurate RV estimates are required to measure the dynamical mass. The velocity dispersion of Segue 2 is very small, so resolving the dispersion would require higher resolution spectroscopy. High resolution spectrographs like Kech/HIRES and Subaru/HDS could possibly measure the velocity distribution of ~ 10 stars in Segue 2 over three to four nights. The Dark Energy Survey Collaboration recently reported (The DES Collaboration 2015) the discovery of eight new Milky Way satellites from the first year of the DES survey data (see also Koposov et al. 2015, ApJ, submitted). Discovery of additional new dwarf satellites can be expected in the near future from the Skymapper survey and from future data releases by the DES. In the longer time frame, LSST will find even fainter satellites. Some of these may have velocity dispersions too small to be resolved with medium-resolution, multiobject spectrographs (MOSs). The TMT equipped with a high resolution spectrograph will provide the essential combination of light collecting area and spectral resolution required for measurements of the velocities of the fainter, more common stars in Segue 2, as well as in yet undiscovered galaxies like it, and measure their dynamical masses.

7.6.6 Velocity anisotropy of distant Milky Way halo: evidence of accretion event

The oldest and most metal-poor stars in our Galaxy reside in the stellar halo, a diffuse envelope of stars extending out to a distance of ∼100 kpc from the GC. The orbital timescales of these halo stars are very long compared to the age of the Galaxy, thus the phase-space structure of the stellar halo is intimately linked to its accretion history. The extreme radial extent of halo stars, well beyond the baryonic center of the Galaxy, makes them excellent tracers of the dark matter halo.

Based on long baseline (5–7 years) multi-epoch HST/ACS photometry, Deason et al. (2013) have measured proper motions of 13 main sequence Milky Way halo stars at an average distance of ~ 24 kpc from the GC with a root-mean-square (RMS) spread of 6 kpc and median proper motion accuracy of ~ 5 km s^{-1} at this distance. These observations point to a fairly complex velocity anisotropy profile at large distances which is likely affected by substructure in the stellar halo. Their results suggest that the stellar halo velocity anisotropy out to a distance of ∼30 kpc is less radially biased than solar neighborhood measurements. This is opposite to what is expected from violent relaxation, and may indicate the presence of a shell-type structure at a distance of ∼24 kpc (Fig. 56). Rather than a constant or continuous decline, the velocity anisotropy is found to have a 'dip' at 20 kpc. The location of this 'dip' is coincident with a break in the stellar halo density. Although the origin of the break radius is still uncertain, Deason et al suggest that the break radius in the Milky Way may be due to a shell-type structure built up from the aggregation of accreted stars at the apocenter.

An independent measure of velocity anisotropy is vital to derive the mass profile of our Galaxy. A measure of the tangential motion of the distant halo stars will allow astronomers to address whether or not this cold RV dispersion is due to a shift in pressure from radial to tangential components. Currently, using multi-epoch HST images seems to be the only way to measure velocity anisotropy at these large distances. The Gaia mission will measure proper motions for an unprecedented number of halo stars with $V < 20$, and will likely revolutionize our understanding of the inner stellar halo. However, even with bright halo tracers (e.g. BHB or carbon stars), the proper motion accuracy of Gaia, ∼0.3 mas/year, will be unable to accurately constrain the tangential motion of very distant halo stars.

In the ideal case, one would like to directly measure the tangential motion of the halo stars. At large distances in the halo, 10–100 kpc, a tangential velocity of 100 km s^{-1} would correspond to a proper motion on the sky of 2–0.2 mas yr^{-1}. This requires an astrometric accuracy that is unfeasible for current proper motion surveys. TMT is likely to enable such studies with desired accuracy.

7.6.7 The Milky Way halo streams and the Galaxy's gravitational potential

Stellar tidal streams are believed to be the remnants of accreted Milky Way satellites that were disrupted by tidal forces and stretched into filaments as they orbited in the Galaxy's potential. The orbits of stars in these streams are sensitive to the properties of the potential and thus allow us to constrain the potential over the range of distances spanned by the streams. Thus they provide important tools to determine the Galaxy's gravitational potential, knowledge of which is required in the study of the dynamics or evolution of the Galaxy.

Stellar streams, such as the GD-I stream (Grillmair & Dionatos 2006), the Sagittarius tidal streams (Majewski et al. 2003), and the Orphan stream (Grillmair 2006) have been used to constrain the circular velocity at the Sun's radius (Koposov et al. 2010), the total mass within 60 kpc (Newberg et al. 2010), and the shape of the dark matter halo potential.

The metallicity and spatial extent of the Orphan stream is studied in Sesar et al. (2013), based on 30 RRab stars. These stars in the Orphan stream have a wide range of metallicity from –1.5 to –2.7 dex. The average metallicity, ~ -2.1 dex, is similar to that found for BHB stars by Newberg et al. There exists a metallicity gradient along the stream length, and the distant parts (40–50 kpc from

the Sun) are about 0.3 dex more metal-poor than the parts within ∼30 kpc. Comparing the distances of Orphan stream RRab stars with the best fit orbits of Newberg et al. (2010), Sesar et al. found that the best fit to distances of Orphan stream RRab stars and to the local circular velocity is provided by potentials where the total mass of the Galaxy within 60 kpc is $\sim 2.7 \times 10^{11}\ M_{\odot}$.

Many more streams likely to be found by deep imaging with Pan-STARRS and LSST will be accessible with TMT. Detailed studies of the resolved stellar populations in these streams with improved precision of stellar distances would provide great insight into the total mass of the Galaxy and the Galaxy's gravitational potential.

7.6.8 The Galactic halo formation: is the Milky Way halo formed by disrupting accreted dwarf galaxies?

Whether the Milky Way halo is formed by disrupting accreted dwarf galaxies (Searle & Zinn 1978) still remains an open question. Three formation scenarios have been proposed till now for the stellar halos that surround galaxies. Evidence for this mechanism exists in the form of debris structures in space and velocity around the Galaxy (Majewski et al. 2003; Belokurov et al. 2006; Schlaufman et al. 2009). However, attempts to find the chemically primitive stellar populations in the relatively luminous ($L > 10^5 L_{\odot}$) classical dwarf galaxies suggested a statistically significant absence of extremely metal-poor stars with [Fe/H] < –3; based on which, Helmi et al. (2006) claimed that the Galactic building blocks must have been different from the surviving dwarfs. Later studies by Kirby et al. (2009) based on medium resolution spectroscopy found an extremely iron-poor star, S1020549, in the Sculptor dwarf spheroidal galaxy. Follow-up high-resolution spectral analysis of this object by Frebel et al. (2010) confirmed its Sculptor membership and determined a metallicity ([Fe/H] = –3.81) for this object. Derived chemical abundances obtained for other elements suggest that the elemental abundance ratios of this star have a chemical pattern nearly identical to that of similarly metal-poor halo stars (Fig. 57). The agreement of the abundance ratios of S1020549 with those of the halo suggests that the classical dwarf spheroidal galaxies experienced very similar chemical enrichment in the earliest phases to the Milky Way halo and UFDs.

As discussed by Frebel et al. (2010), this result provides evidence that the early chemical evolution of galaxies spanning a factor of more than 1 million in luminosity is dominated by the same type of stars, and possibly the same mass function, namely massive core-collapse SNe as indicated by the alpha-element enhancement found in all of the most metal-poor stars. This universality would also characterize any dwarf galaxies that were accreted at early times to build the Milky Way and its stellar halo. Those accreted systems are therefore unlikely to have been significantly different from the progenitors of the surviving dwarfs. In that case, the oldest, most metal-poor stars observed in present-day dwarf galaxies should be representative of the stars found in the Galactic building blocks before their destruction. The latest observational results thus support the idea that mergers and accretion of small, generally metal-poor systems, as predicted by ΛCDM models, can in principle explain the metal-poor stellar content of the Galactic halo.

The picture that is now emerging from the agreement in terms of abundance suggests that the old, low-metallicity tail of the outer halo could have been populated with metal-poor stars deposited by small dwarf galaxies that were destroyed long ago. The question remains, whether enough dwarf galaxies accreted to account for all of the metal-poor halo stars. The surviving UFDs are the least luminous and most dark matter-dominated galaxies (Simon et al. 2007) and they possess very few stars despite containing some extremely metal-poor stars. It is thus unclear whether the accretion of even large numbers of analogs to such systems can provide enough stellar mass to account for the entire population of low-metallicity field stars.

The presence of S1020549 in a relatively modest survey indicates that future searches are likely to discover more such objects in Sculptor and other dwarf galaxies. Acquiring high resolution spectra for such distant faint member stars in any of the dwarf Milky Way satellites with the existing 8–10 m

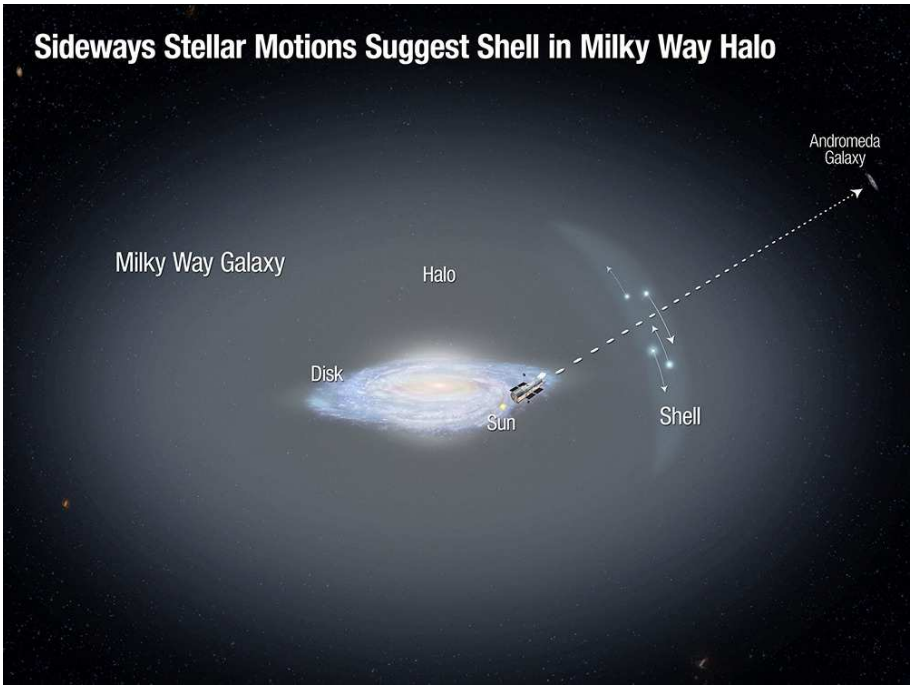

Fig. 56 The figure shows the disk of our Milky Way Galaxy, surrounded by a faint, extended halo of old stars. Deason et al. (2013) using the HST to observe Andromeda galaxy serendipitously identified a dozen foreground stars in the Milky Way halo. They measured the first sideways motions (represented by the arrows) for such distant halo stars. The motions indicate the possible presence of a shell in the halo, which may have formed from the accretion of a dwarf galaxy. This observation supports the view that the Milky Way has undergone continuing growth and evolution over its lifetime by consuming smaller galaxies (Credit: NASA, ESA, and A. Field (STScI)).

telescopes will be quite challenging. TMT, once equipped with a high-resolution spectrograph, will open up a new window for thoroughly studying early galaxy assembly through stellar chemistry, providing great insight into the Galactic halo formation history.

Although the Tri And stellar clouds were originally viewed as the remnants of an accreted and now disrupted satellite galaxy, the recent suggestion by Price-Whelan et al. (2015) that these stellar clouds may be a population that was kicked out of the Galactic disk is very intriguing. They carried out a critical examination of the possible mode of formation of this system in the halo ($R \sim 30$ kpc, $Z \sim -10$ kpc), by comparing the ratio of RR Lyraes to M giants with other structures in the Galaxy. They found that unlike any of the known satellites of the Milky Way, this ratio for Tri And gives a value more like the population of stars born in the much deeper potential well inhibited by the Galactic disk. N-body simulations of a Milky Way like galaxy perturbed by an impact of a dwarf galaxy demonstrate that, in the right circumstances, concentric rings propagating outwards from that of the Galactic disk can plausibly produce similar overdensities. These results provide support for the recent proposal by Xu et al. (2015) that, rather than stars accreted from other galaxies, the Tri And clouds represent stars kicked out from the Galactic disk. This represents the first population of disk stars to be found in the Galactic halo.

Yet another formation scenario suggests that stars might form in situ from gas located in the halo itself (Eggen et al. 1962). While such populations have been seen in hydrodynamic simulations of

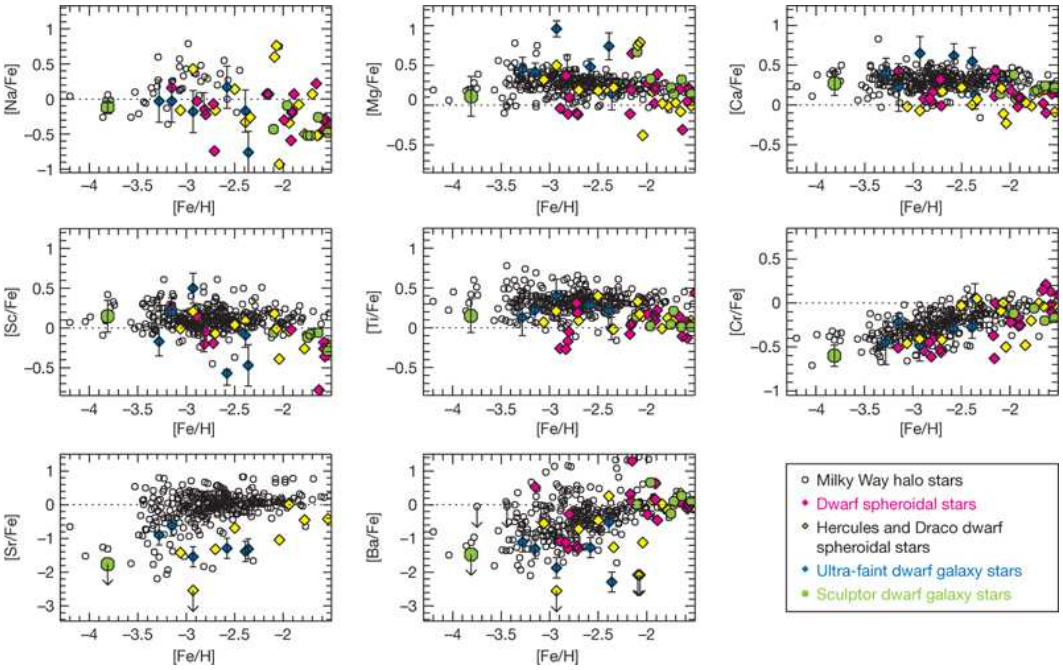

Fig. 57 Abundance ratios as a function of iron abundance in S1020549 and other metal-poor stars from the literature. In eight elements, S1020549 (*big green filled circles*, at [Fe/H] = –3.8) is compared with halo stars (*black circles*), UFD galaxy stars (*blue diamond*) and the brighter dwarf galaxy stars (*pink and yellow diamond*). Smaller green circles indicate higher metallicity Sculptor targets (Frebel et al. 2010). Elemental abundance ratios show that this star has a chemical pattern nearly identical to that of similarly metal-poor halo stars.

galaxy formation (Abadi et al. 2006; Tissera et al. 2014), the observational evidence for the existence of this population remains controversial (Carollo et al. 2008).

The above studies indicate that the Galactic halo is rather complex, with at least more than one population, each of different origins. The outer halo, beyond 15–20 kpc from the GC, has an average metallicity a factor of four lower than that of the inner halo (Carollo et al. 2007). More observations of dwarf galaxies are needed clarify this situation, and TMT/HROS is expected to play a significant role in unraveling the Galactic halo formation history.

7.7 Cosmic Chemistry

7.7.1 Nucleosynthesis in stars

Big Bang nucleosynthesis in the first 20 minutes of the universe is believed to have created deuterium, the two isotopes of He (3He and 4He) and a very small amount of lithium as well as 1H. Almost all other elements in the periodic table are synthesized in the stellar interiors and envelopes during hydrostatic and explosive burning.

Each stellar nucleosynthetic path has a different timescale and produces characteristic elemental abundance patterns. Interpretation of the observed abundance ratios and abundance patterns in the framework of a proper galactic chemical evolution model allows researchers to trace back the nucle-

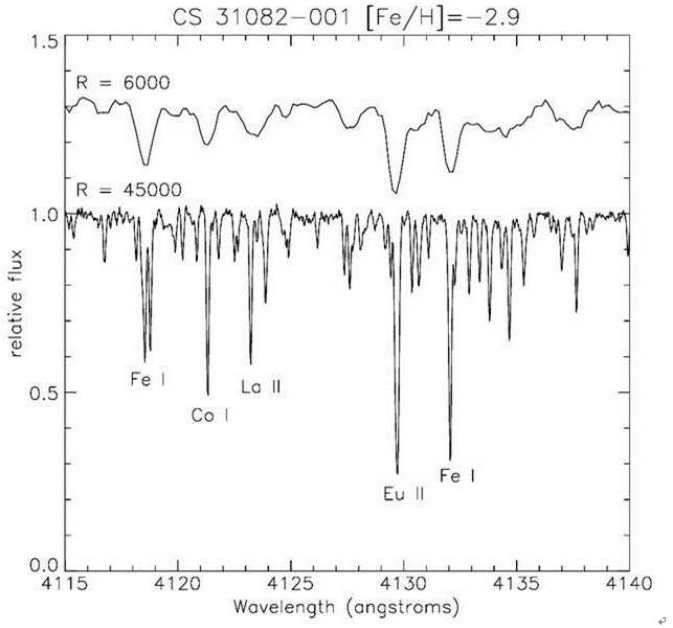

Fig. 58 Comparison of a moderate vs. high-resolution stellar spectrum. Comparison of spectra taken at moderate resolution (*upper curve*) and high resolution (*lower curve*) of a metal-poor star. At higher resolution, many important absorption lines become available for study (Credit: R. Guhathakurta, UCSC).

osynthetic origin and the prevailing astrophysical conditions. Chemical evolution in differing stellar populations traces the star formation history and age and provides insight into the chemical evolution of galaxies and their interstellar matter. For accurate abundance measurements high spectral resolution ($R > 20\,000$) with a good S/N (>50) ratio are required, especially to detect and analyze faint spectral features. As compared to low and moderate resolution, at higher resolution many important absorption lines become available for study (Fig. 58). At resolution $R > 90\,000$ (S/N ∼200) estimates of isotope abundances become possible. TMT equipped with a high resolution spectrograph will have a dramatic impact in nucleosynthesis studies as it will aid detection of faint spectral features and also open up hitherto unreachable classes of stars for study.

While elements are formed inside stars, some light elements such as D, Li and Be are also destroyed inside stars under certain conditions. The detection and abundance estimate of these elements is important to understand the stellar structure, evolution and mixing process in stars and the amount of stellar processing. We discuss a few outstanding questions related to stellar nucleosynthesis, answers to which can be sought from TMT observations.

7.7.2 Li and Big Bang Nucleosynthesis

WMAP determination of the cosmic baryon density, combined with the Big Bang nucleosynthesis theory, tightly predicts a Li abundance value that differs from the value of 'Spite Plateau' (Spite & Spite 1982) by a factor of two or more. Several possible solutions, such as stellar destruction and astration, nuclear uncertainties and new physics, atomic diffusion etc. have been proposed to

explain this discrepancy. The Li abundances observed in hyper metal-poor stars that are still in the main sequence turn-off phases (Aoki et al. 2006; Caffau et al. 2011) might provide a clue to this problem. High resolution and high sensitivity of TMT/HROS are required for measurements of low Li abundance and Li isotope ratios in hyper metal-poor stars as well as in extreme metal-poor stars. An understanding of the Li problem and depletion processes inside stars may be achieved better from a detailed study of metal poor globular clusters. Estimating the Li abundance in the faint main sequence stars is very challenging with existing 8 to 10m telescopes but will be relatively easy with TMT. Correlating the Li abundance with other heavy elements will help understand the discrepancy between the observed Li abundance compared to WMAP results.

7.7.3 C, N, O elements and the Be puzzle

C, N and O are produced in all types of stars during hydrogen and helium burning. These elements play an important role in star formation by cooling the clouds through several fine structure lines. The observations of the increase of C with decrease in the metallicity may possibly be evidence of a gradual change in the characteristic mass of the IMF, which is likely to be mediated by CMB temperatures acting as a minimum temperature (Tumlinson 2007). With the TMT it will be possible to look for such correlations in the local dwarf Galaxies and test the theoretical prediction.

Be abundances in the Galaxy and satellites of the Milky Way provide constraints on the pre-Galactic cosmic ray fluxes and cosmic magnetic fields. If Be and B are produced as secondary elements, one would expect the Be abundance to decrease quadratically with respect to metallicity. However, the observation of a small sample of metal-poor stars shows that there is a linear decrease with metallicity (Primas et al. 2000), indicating a primary production of C, N, O and Be from the same mechanism. The TMT will enable such studies to fainter limits, extending the sample beyond the Milky Way to the Local Group dwarfs.

7.7.4 Isotopic abundance ratios and the origin of heavy elements

Very metal-poor stars (–3<[Fe/H]<–2) show large star-to-star scatter in abundances of elements heavier than Fe; a large fraction of them show large enhancements of heavy elements (e.g. [Ba/Fe], [Eu/Fe]) caused by the r- or s-process. In contrast, abundances of heavy elements are generally very low, (i.e., [Sr,Ba/Fe] ~ -1.5) particularly in stars with [Fe/H] $<$ –3.5, suggesting that r- and s-processes contributed little to stars formed in the very early Galaxy. The heavy elements Sr and Ba are however detected in almost all stars with such low metallicity, even though the abundances are quite low ([Sr,Ba/Fe] ~ -1.5). Detailed measurements for heavy elements in extreme metal-poor stars will provide a new constraint on the origins of heavy elements in the Galaxy.

Any neutron-capture element with multiple isotopes that are produced in different amounts by the s- and r-processes can be used to assess the relative s- and r-process contributions to the stellar composition. So, the isotopic abundances of these elements are more fundamental indicators of neutron-capture nucleosynthesis and can be directly compared to r-process and s-process predictions without the smearing effect of multiple isotopes (Mashonkina et al. 2003; Mashonkina & Zhao 2006). The combination of Ba, Nd, Sm and Eu isotopic fractions can provide more complete knowledge of the neutron-capture nucleosynthesis, constrain the conditions (e.g., temperature, neutron density, etc.) that are required to produce the r-process elements, and determine the actual r-process path by identifying the individual isotopes that participate in this process (Roederer et al. 2008). To reconstruct the evolutionary history of neutron-rich elements in the Galaxy it is thus important to extend our study to the isotopic level. Along lines of sight with low interstellar reddening, HROS will enable high-precision measurements of the isotopic ratios of Li, C, Mg, Ba, and Eu throughout the Milky Way, its globular cluster system, and its halo.

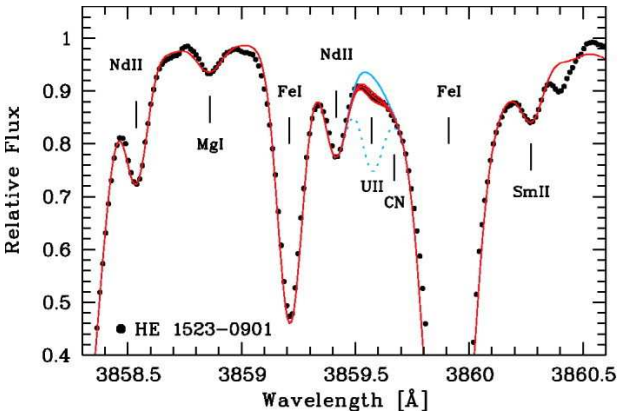

Fig. 59 Spectral region around the U II line in HE 1523–0901 (*filled dots*). Overplotted are synthetic spectra with different U abundances. The dotted line corresponds to a scaled solar r-process U abundance present in the star if U were stable did not decay (Source: Frebel et al. 2007).

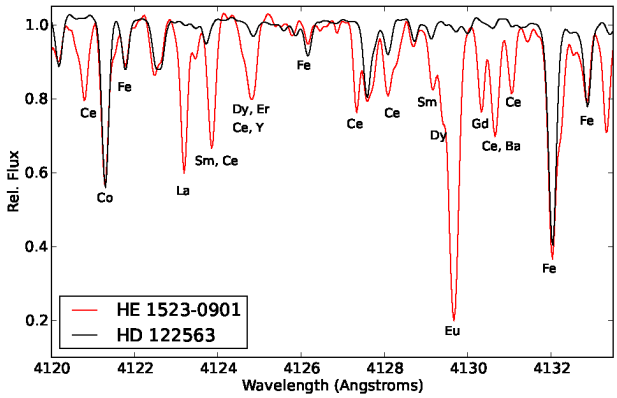

Fig. 60 The spectra of the r-process element rich HE 1523-0901 (*red*) and the r-process element deficient star HD 122563 (*black*). These two stars have similar [Fe/H] values and atmospheric parameters (Source: Jacobson & Frebel 2014).

7.7.5 Cosmo-chronometry

The r-process elements thorium and uranium are radioactive and have long-lived isotopes, 232Th and 238U, with half-lives of 14 Gyr and 4.5 Gyr respectively. The spectral region around a U II feature is shown in Figure 59. The half-lives of 232Th and 238U cover cosmic timescales which make these elements suitable for age measurements.

Chronometers such as Th/Eu, U/Os, U/Eu, U/Th, etc. can be used to measure stellar ages. Knowing abundances of Th, U and Pb provides a self-consistency test for r-process calculations. These three abundances are intimately coupled to the conditions and environment of the r-process. Hence constraints on the different models yielding different abundance distributions can be obtained by explaining the stellar triumvirate of the Th, U and Pb abundances. Such constraints lead to a

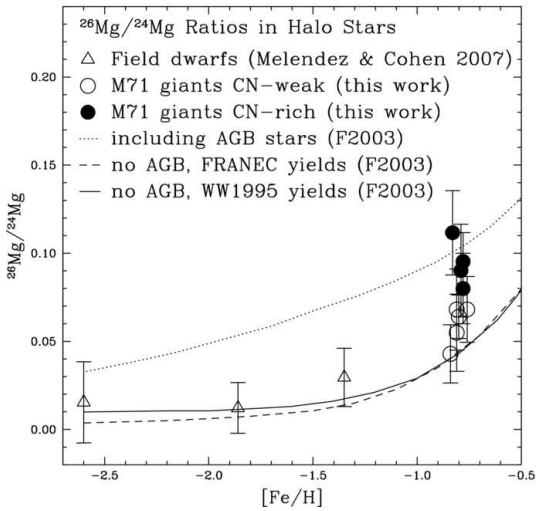

Fig. 61 ^{26}Mg/^{24}Mg ratios in both field dwarfs (*triangles*; Meléndez & Cohen 2007) and M71 giants (*circles*) as a function of [Fe/H]. Chemical evolution models by Fenner et al. (2003) including (*dotted lines*) and excluding (*solid and dashed lines*) AGB stars are shown. At the metallicity of M71 ([Fe/H] = –0.8 dex) the isotopic ratios in the CN-weak stars (*open circles*) are explained by massive stars, but the CN-strong stars (*filled circles*) may have been polluted by intermediate-mass AGB stars. (Source: Meléndez & Cohen 2009).

better understanding of how and where r-process nucleosynthesis can occur. Improved r-abundance calculations are crucial for reliably predicting the initial production ratios of Th/r, U/r and Th/U, which are implicitly necessary for more accurate age dating of r-process enhanced stars. Based on seven chronometer abundance ratios, the age of HE 1523-001, the metal-poor star with the strongest enhancement in neutron-capture elements associated with the r-process that has been found thus far (Fig. 60), was found to be $\sim$ 13 Gyr (Frebel 2010). The lead abundance is usually measured using the Pb I line at 4057.81 Å. High resolution > 90 K is required to separate the Pb I 4057.81 Å line from a CH line lying less than 0.1 Å blueward. For a number of r-process metal-poor stars stellar ages have been derived using the Th/Eu chronometer (Sneden et al. 1996). These age estimates range from $\sim$ 11 to 14 billion years and provide a lower limit to the age of the galaxy. With the TMT, lines due to these elements could be measured more easily in fainter old stars than can be done with existing 8–10 m telescopes, thus reducing the uncertainties in the age estimate.

7.8 Chemical Evolution: The Milky Way, Local Group and Nearby Galaxies

7.8.1 Probing the onset of contribution from AGB stars to the Galactic chemical enrichment using isotopic ratios of Mg

Measurement of isotopic ratios provides a completely new window into nucleosynthesis, galactic chemical evolution, mixing within stars and stellar evolution. Such data, when available, significantly improve our understanding of nuclear processes in various astrophysical sites. However, as the isotopic shift is very small at optical wavelengths, very high spectral resolution and S/N ($R \sim 90\,000$, S/N $\sim$200) are required to measure isotopic ratios in stellar spectra.

There are three stable isotopes of Mg. 24Mg is produced via routine burning of carbon in the interior of massive stars during their normal evolution as a primary element, and is subsequently

injected into the ISM by SNII. The two heavier isotopes, 25Mg and 26Mg are secondary isotopes, believed to be produced primarily in intermediate mass AGB stars. In the young Galaxy, there was not enough time for AGB stars to contribute, while core collapse SN started exploding quickly after massive stars first formed. One can thus use the ratios among the Mg isotopes to explore when the AGB stars began to contribute to the Galactic chemical inventory (Goswami & Prantzos 2000). For example, from an analysis of high resolution ($R \sim 100\,000$), high S/N Keck I spectra of M71 giants, Meléndez & Cohen (2009) have demonstrated that M71 has two populations, one having weak C and N, normal O, Na, Mg and Al, and a low ratio of 26Mg/Mg ($\sim 4\%$) consistent with models of galactic chemical evolution with no contribution from AGB stars. The Galactic halo could have been formed from the dissolution of globular clusters prior to their intermediate-mass stars reaching AGB. The second population has enhanced Na and Al accompanied by lower O and higher 26Mg/Mg ($\sim 8\%$), consistent with models that incorporate ejecta from AGB stars via normal stellar winds (Fig. 61; Fenner et al. 2003). Such studies can be significantly extended due to the expanding set of faint and old stars that can be observed with TMT/HROS leading to an improved understanding of the contribution of the first AGBs to the Galactic chemical enrichment.

7.8.2 Probing chemical evolution in Local Group dwarf galaxies

CDM simulations of the growth of galaxy structure suggest that halos of the galaxies like the Milky Way have accreted (and subsequently destroyed) 10s to 100s of small, dwarf galaxies in the past 10 Gyr. However, detailed stellar atmosphere analyses of individual RGB stars in current day Local Group dwarf galaxies show very little in common with the chemistry of stars in the Milky Way halo, disk, bulge, and moving groups (Venn et al. 2004; Navarro et al. 2004). Furthermore, the number of surviving dwarf galaxies in the immediate neighborhood of the Milky Way is far lower than predicted.

To resolve these questions it is necessary to investigate environmental differences between the various dwarf galaxies, and perform a detailed examination of the kinematics, metallicities, and abundance ratios of stars in dwarf galaxies beyond the Milky Way halo. With TMT/HROS, it will be possible to carry out detailed abundance analyses of stars at or just above the tip of the RGB throughout the Local Group. For example, current generation high-resolution spectrographs on 8–10 m telescopes have been able to study tens of stars in Local Group dwarf spheroidal galaxies at V = 17–18 with exposure times up to 14 hours. Those systems lie as far away as 250 kpc. TMT/HROS will be able to obtain similar results for stars at V ~ 20 in more distant ($\sim 400 - 500$ kpc) and hence more isolated systems. These optical measurements can be supported by K band measurements – TMT/NIRES can easily reach below the tip of the RGB throughout the Local Group (see Table 3). Such K band measurements will be invaluable for CNO abundance measurements.

With such data, the chemistry of the old stellar population in dwarf irregular galaxies (which tend to be more distant and more isolated satellites of the Milky Way) can be compared directly to the old populations of the dwarf spheroidals and Magellanic Clouds. These latter systems are within the dark matter halo of the Milky Way and are thought to have been interacting with the Galaxy

Table 3 Estimated Limiting Distances for Spectroscopic Observations of Point Sources

	MV (mag)	WFOS (Mpc)	HROS (Mpc)	NIRES (Mpc)
Blue supergiant	–6.7	10.0	7.0	2.5
Red supergiant	–5.9	7.0	3.5	8.0
RGB Tip	–2.7	1.5	0.5	3.8

Notes: assumes 4 hour integrations at $\lambda/\Delta\lambda = 5000$, 50 000, and 25 000 for WFOS, HROS, and NIRES, respectively. The corresponding central wavelengths are 0.5 μm, 0.5 μm, and 1.2 μm. The final S/N per spectral resolution element are 100, 100, and 60, respectively. Courtesy: J. Cohen (CIT).

over most of their lifetimes, likely affecting star formation histories and chemical evolutions. A comparison with cleaner, more isolated dwarf irregulars will allow us to establish and characterize, for the first time, the effects of environment on chemical evolution through the chemical similarities and differences in old populations. To compare dwarf irregular galaxies to the Galactic halo and other Local Group dwarf galaxies, and test their impact on merging hypotheses of galaxy formation, detailed chemical analyses of their old RGB stars are required.

Analysis of spectra of young giant stars in nearby active star forming galaxies in the Local Group has become possible in the past decade due to a combination of observational data from 8–10 m telescopes and advances in model atmosphere techniques. The latter include the development of non-local thermodynamic equilibrium (LTE) hydrodynamic 3-D extended stellar atmospheres, necessary to understand absorption features influenced by supersonic outflowing stellar winds. As shown in Table 3, observations with TMT will extend these studies to very large distances allowing the investigation of a variety of star formation environments and galaxy morphologies.

Sophisticated models of galactic chemical evolution are based on nucleosynthetic yields of various elements from each of the possible sources together with the amount of mass ejected from each of these sources, all as a function of stellar initial mass (and to a lesser extent stellar initial metal content). These are folded in with assumptions regarding gas flows within the galaxy and possible accretion of primordial material. Formation rates and an IMF for stars, both as a function of time, must be adopted as well. Prediction of trends of abundance ratios within the galaxy as a function of location require knowledge of any dependencies of all of these inputs on position as well as an assumption regarding migration of stars within the galaxy.

Figure 62 shows the trend based on detailed abundance analyses of large samples of stars in the disk and halo of the Milky Way for the alpha-element Ca. Figure 63 shows the same for the iron-peak element Co. The solid lines are predictions for Galactic chemical evolution by Prantzos (2006) and Prantzos (2014, private communication). The gentle rise towards lower Fe-metallicity is generally ascribed to the difference in characteristic timescale for SNII, the major production site for the alpha-elements, as compared to SNIa, where most Fe is produced. The former is much shorter than the latter, which may be as long as ~ 1 Gyr after the initiation of star formation.

Although creating a model of galactic chemical evolution requires many assumptions, it does work most of the time. In other words, such models can fairly closely reproduce most observed trends in abundance ratios with time since the formation of the Milky Way with reasonable input data. Such models, with different inputs justified by observational data, also appear to work for the nearby galaxies. However, our knowledge of extragalactic stellar populations and their chemical inventory is much more limited than is that of our own galaxy. TMT will make a major contribution to improve our knowledge of the chemical evolution of nearby galaxies. In the TMT era, high dispersion spectroscopy using HROS and NIRES will enable detailed abundance analyses with high accuracy for individual stars in the outer parts of the nearest groups of galaxies, including the M81 group, and for the brightest globular clusters well beyond the Virgo Cluster. We will then finally obtain a full picture of the chemical evolution of the nearest galaxy groups out to the Virgo Cluster, and be able to compare it to that of the Milky Way.

7.8.3 Abundance anomalies in Ultra-Faint Dwarf galaxies

TMT has the potential to revolutionize study of the chemical evolution of Local Group systems, including the unique cases of the UFDs in our own galaxy, and the halo and dwarf galaxies of M31/M33.

The handful of members of the UFDs in the Milky Way subjected to high dispersion abundance analysis shows striking anomalous enhancements in individual elements; they are often referred as "chemical oddballs" (Fig. 64). TMT has the potential to obtain spectra of stars with $r = 20 - 21$ at S/N$\sim$50 and $R = 15\,000$ or greater (once HROS is implemented). WFOS will have multislit

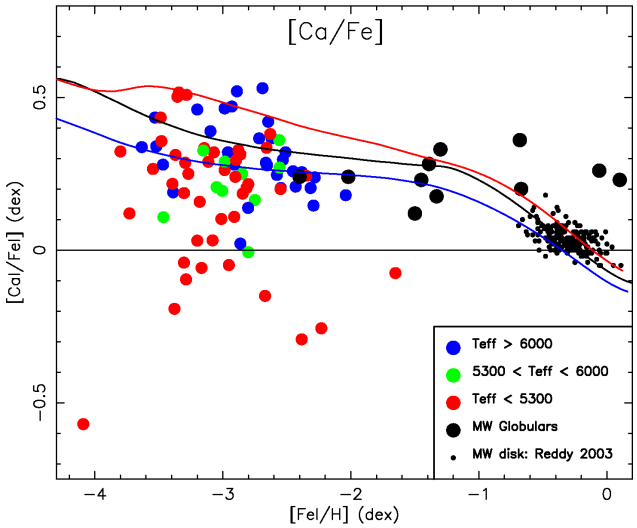

Fig. 62 The element ratio [Ca/Fe] as a function of [Fe/H] for a large sample of C-normal extremely-metal-poor halo stars (Cohen et al. 2013); colors of the filled points indicates the Teff of the star. The disk stars from Reddy et al. (2003) are indicated as small black dots concentrated near solar metallicity, and large black dots indicate ratios for samples of stars within selected Milky Way globular clusters. The curves denote the predictions for Galactic chemical evolution by Prantzos (2006) and Prantzos (2014, private communication) adopting nucleosynthesis yields from various sources including Nomoto et al. (2006) or Woosley & Weaver (1995) for massive stars, Karakas (2010) for low mass stars, and Greggio (2005) for SNIa. (Source: J. Cohen).

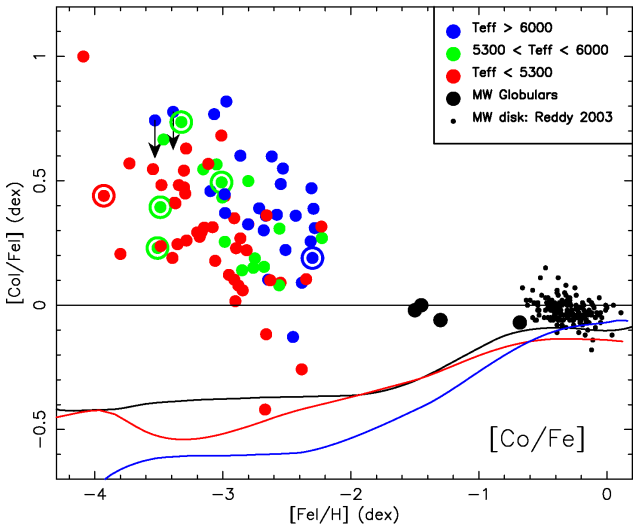

Fig. 63 The same as Figure 62 but for cobalt. Note that in this case all the predicted models fail to reproduce the trends seen among Milky Way halo stars. There must be a problem either in the nuclear yields or in the stellar abundance analysis (Source: J. Cohen).

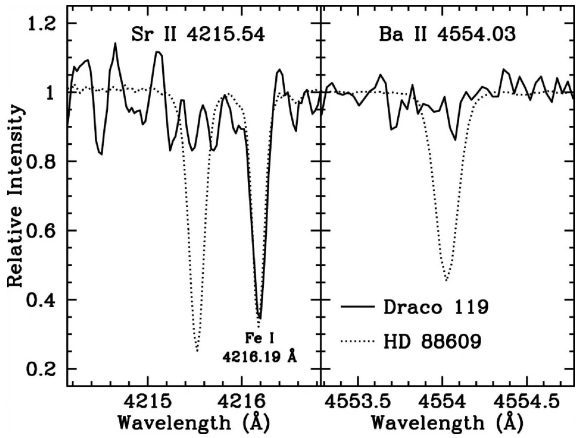

Fig. 64 Neutron-capture elements are deficient in a red giant (D119) in the Draco Dwarf Spheroidal galaxy (Fe/H = –2.95); comparison with HD 88609, which has similar metallicity (Fulbright et al. 2004). The Hercules dwarf spheroidal galaxy shows similar striking deficiencies (Koch et al. 2013). The proposed WFOS instrument on TMT would be capable of making measurements on giants similar to these even as distant as the Andromeda galaxy. Recently, a metal-poor giant has been found in a binary system in Hercules (Koch et al. 2014).

spectroscopy of a field of order $3' \times 3'$ or greater, sufficient to cover the size of UFDs in the Milky Way, or dwarf galaxies in M31. For the TMT, the Andromeda/M33 system becomes available for study in much the same way that the Magellanic Clouds have been unveiled for 8 m class telescopes.

One of the striking accomplishments of our current era of 6.5–10 m class telescopes is that moderate to high resolution spectroscopy of stars as faint as $V = 18.5$ has become routine. The multi-object fiber-fed *FLAMES* at VLT has made high resolution investigation of hundreds of stars in the bulge and globular clusters a routine program. Keck with HIRES and MIKE at Magellan have delivered high dispersion spectra of metal poor stars in the halo and dwarf spheroidals. Experiments that push the limits of high dispersion spectroscopy are underway to get spectra of thousands of giants in dwarfs and also to derive composition from the integrated light spectra of globular clusters in M31 and beyond. This study will include all populations in M31, including the bulge.

The TMT with high resolution spectrographs places us on the threshold of investigating chemical evolution throughout the Local Group and by using globular cluster integrated light, throughout the Local Volume. Such work can address the cause for the multiple subclasses of metal poor stars (e.g. carbon enhanced) and *chemically oddball* stars, and one can ask whether the picture of chemical evolution seen in our Milky Way halo extends to the Local Group, see Figure 64.

Some cherished ideas are under challenge. Is the "knee" in the [α/Fe] vs [Fe/H] trend where elemental trends move toward solar scaled composition, due to the onset of iron produced in SNe Ia? Or is the knee arising from the natural metallicity dependent yields of massive star SNe? Is our now roughly 40 year old depiction of chemical evolution therefore in need of major restatement? What is the full range of primordial chemical enhancements that are observable in various stellar systems? Although the broad brush description of chemical evolution and nucleosynthesis is well known, it is clear that many aspects of nucleosynthesis are poorly understood and our best hope for pushing theoretical work is new observations. Large improvements in our modeling of stellar atmospheres are expected soon as non-LTE 3-D models will become available in large grids within the next few years.

7.8.4 Resolved stellar populations as tracers of galaxy evolution

Ground-based resolved stellar population studies of galaxies necessarily target galaxies within the Local Group and its immediate vicinity. While a range of morphological types are present, the statistics are poor and some notable galactic types are entirely absent (in particular massive elliptical galaxies). The resolving power of the HST pushes such studies out to distances of several megaparsecs, improving statistics and sampling a broader range of galaxy type. But even here such studies are limited, and importantly the galaxies still sample the rather benign environment of our local cosmic neighborhood. Only with the collecting power and exquisite spatial resolution of TMT can resolved stellar population studies come of age and reveal the evolutionary histories of galaxies at all luminosities and morphologies, spanning a complete range of environment, from isolated systems, through loose groups, to groups and clusters.

Studies of the integrated light of galaxies necessarily rely on stellar population synthesis to reproduce the broadband spectral energy distribution of the galaxy. The galaxy's light represents the sum-total of the baryonic evolution of the system over cosmic time, and is contributed to by stars of varying mass and of varying age, the proportions of which depend upon the star formation history specific to that galaxy. In this respect, the star formation history is one of the most significant uncertainties in these studies.

By sampling the resolved stellar populations of a galaxy and decomposing the CMD into its constituent stellar types, we can obtain temporally-resolved information on the history of star formation, with additional information such as metallicity available for certain stellar types and/or under certain assumptions, e.g., using the red clump or RGB color. Figure 65 illustrates how the stellar CMD of a complex stellar population can encode essential physical information (see Gallart et al. 2005 and Tolstoy et al. 2009, for reviews).

Figure 66 shows cumulative star formation histories of individual galaxies for various morphological types. Such analyses can be conducted for any subset of galaxies split by any physical parameter, and it is here that TMT can enable a revolution.

7.8.5 Reconstructing the star formation histories of nearby galaxies

Reconstructing the star formation history for a given stellar system by analyzing its CMD is a fundamental tool for understanding its age and chemical composition that has been calibrated by decades of observational and theoretical work. However, progress with obtaining good CMDs within more massive galaxies (or their denser sub-components) has been limited by stellar crowding. Recently, higher spatial resolution observations have become possible using NIR AO systems on ground-based 8–10 m class telescopes. By scaling up to 30 m and implementing AO systems with improved performance, TMT will enable another giant step forward.

Figure 67 shows a comparison of the crowding limits for $\Sigma_{\rm K} = 19$ mag arcsec^{-2} observed with NIR AO-corrected 8 m and 30 m telescopes, as well as HST working in the optical at $\Sigma_{\rm V} = 22$ mag arcsec^{-2}. The calculations demonstrate that TMT will be able to resolve individual stars in regions with $\Sigma_{\rm K} = 19$ mag arcsec^{-2} in galaxies as far away as 15 Mpc. Of course, as distance increases, the required photometric accuracy becomes more difficult and only feasible for the intrinsically brightest stars.

A long sought goal is to construct a deep CMD for a normal elliptical galaxy. Several candidate targets lie within 10–15 Mpc, including (e.g.) NGC 3379 ($d \sim 11$ Mpc). Table 4 provides crowding limits at three galactocentric radii for NGC 3379. The crowding limit is defined to be the magnitude at which photometric errors due to crowding reach 20%, corresponding to 50% completeness. At 1 $R_{\rm e}$, only the brightest RGB and AGB stars will be accessible before the crowding limit is reached. However, at 3 $R_{\rm e}$ (perhaps the lowest practical surface brightness given required exposure times) it will be possible to reach the horizontal branch before reaching the crowding limit. This can be

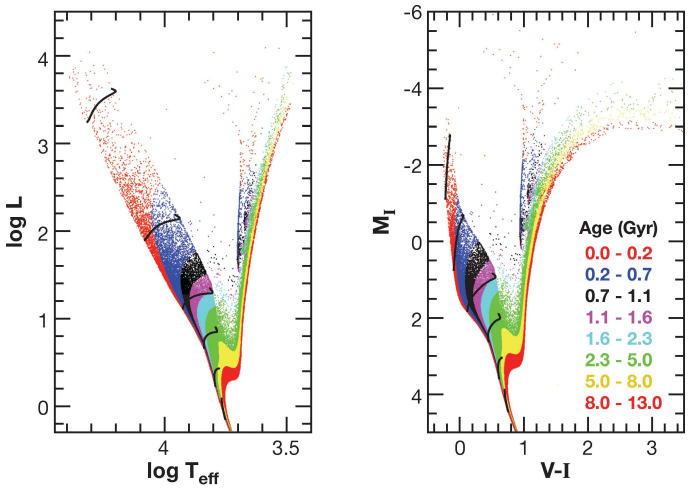

Fig. 65 Figure from Gallart et al. (2005), Hertzsprung-Russell diagram (*left*) and CMD (*right*) of a synthetic complex stellar population, illustrating how different regions of the CMD are occupied by different ages of stars, the precise distribution of which allows a (partial) reconstruction of the overall star formation history of the system.

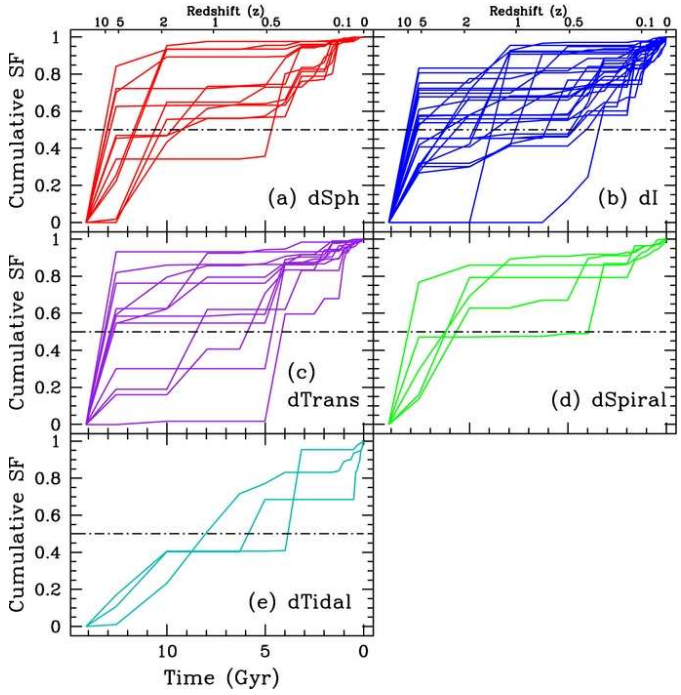

Fig. 66 Cumulative star formation histories of 60 dwarf galaxies, split by morphological types, as derived by Weisz et al. (2011). Statistical comparison of the star formation histories for each type reveals the similarities and key differences, and the epochs at which they occur.

Table 4 Crowding Limits for NGC 3379

Name	r (arcsec)	$\Sigma_{\rm K}$ (mag arcsec^{-2})	$K_{\rm lim}$	Time (s)
$R_{\rm e}$	30	17.0	25.7	282
$3R_{\rm e}$	90	19.3	28.5	47200
$R_{\rm tot}$	190	22.5	31.6	∞
K (1 hour)	—	—	27.9	3600

Notes: the second column (r) is galactocentric distance, the third ($\Sigma_{\rm K}$) is assumed surface brightness at that distance, the fourth ($K_{\rm lim}$) is the point source magnitude at the crowding limit (as defined in the text), and the last column (t) is the exposure time to reach these limits. For reference, the last row shows the point source limiting magnitude for $\tau = 3600$ s in the absence of crowding.

compared to actual HST/NICMOS observations at 3 $R_{\rm e}$ that only reach ~ 1 mag below the tip of the RGB significant crowding limits photometric accuracy (Gregg et al. 2002).

7.8.6 Time-resolved history of the galaxies in the Local Volume: the TMT era

Figure 68 shows the spatial locations of all the known galaxies out to a distance of ~ 11 Mpc, of which there are nearly 900.

Every known galaxy type at $z \sim 0$ is now accessible for color-magnitude analysis, and nearly every type of environment is accessible (isolated, loose group, group or cluster), most with good statistics. The wealth of questions that can be probed is diverse, and addresses some of the key topics in galaxy formation and evolution today. There is a well described strongly bimodal, double Gaussian distribution among the rest-frame colors of galaxies out to redshifts of $z \sim 1$, separating galaxies into a 'red sequence' with a small spread in colors and a 'blue cloud', with a broad spread of colors, see Section 5.1.3. There is a lack of galaxies with colors between the two peaks, often referred to as the 'green valley' which represents a probable transition region.

By conducting analyses of populations of galaxies we can ask questions such as:

- What are the key differences in the star formation histories of galaxies in the blue cloud, green valley and red sequence, at a fixed stellar mass, and at what epoch do these differences set-in?
- When did the galaxies in the red sequence become red, and does the green valley population actually distinguish itself in any meaningful way from either of its two better-defined counterparts?
- What are the key differences in the star formation histories of galaxies at a fixed stellar mass as a function of environment, and at what epoch do these differences set in?
- For galaxies that are quenched, at what epoch did quenching set in? Is the timing of the onset of quenching correlated with any key physical property, such as cluster-centric distance or total stellar mass?

Such questions cannot be answered with the limited range of galaxies accessible on HST or from the ground using 10 m class facilities, but they can be tackled with the D4 advantage provided by TMT.

7.8.7 Probing LSB and BCD galaxies: star formation, chemical evolution, dark matter

The class of Blue Compact Dwarf (BCD) galaxies exhibit recent star formation in the current epoch, and appear to have survived merging or some other perturbation that would have led to an active past star-formation history. They appear to have produced stars intermittently over the Hubble time. The BCD population is somewhat diverse and so is their evolution. The amount of dark matter in BCD galaxies is of interest in testing various hypotheses regarding the stability of these HI-rich

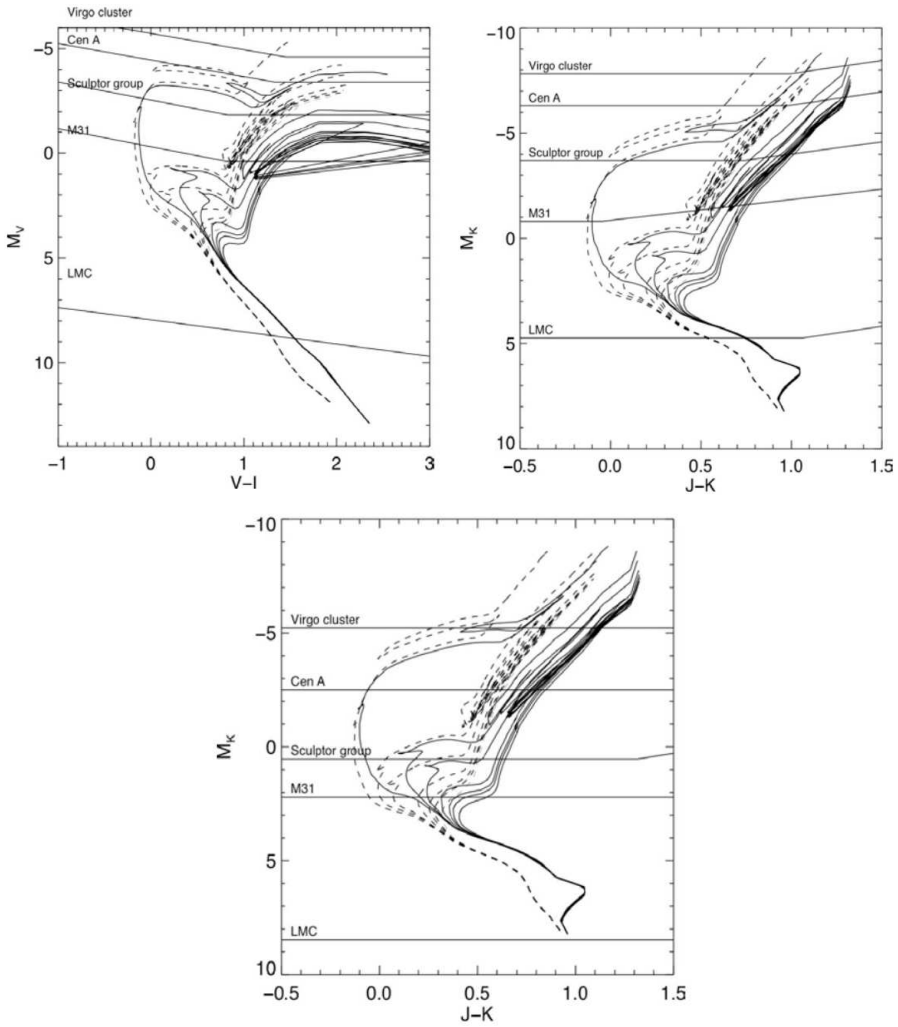

Fig. 67 Magnitudes at which crowding limits photometry to 10% accuracy in regions with $\Sigma_{\rm K} = 19$ and $\Sigma_{\rm V} = 22$ mag arcsec^{-2} at the distances indicated are shown as horizontal lines on top of Girardi et al. (2000) isochrones of various ages and metallicities. *Top left*: HST in the optical. *Top right*: Gemini North + NIRI/Altair. *Bottom*: TMT in the NIR. These crowding limits were calculated analytically by comparing the contribution of surface brightness fluctuations on the scale of a telescope resolution element to that of a star of a given magnitude (Olsen et al. 2003). The ratio depends on the distance, surface brightness, and luminosity function of the stellar population as well as the photometric accuracy required for a given magnitude of star.

systems against perturbations that can trigger star formation. Studying the dynamics of BCD galaxies through high spatial resolution spectroscopy of individual stars and HII regions will be invaluable in this context. Since BCDs by definition are compact objects (scale lengths < 4 kpc in most cases), the high spatial resolution offered by AO is crucial to derive their velocity fields.

The LSB galaxies are a related class of galaxies having gaseous disks that are very stable against perturbations, and show very sparse star formation at the current epoch. It appears that some of them

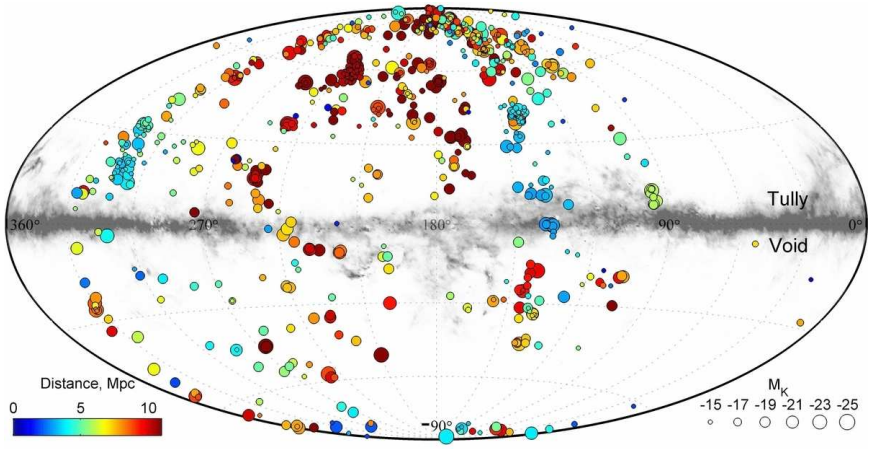

Fig. 68 Aitoff projection in Galactic coordinates of the locations of $\sim$ 900 galaxies within 11Mpc. The resolved stellar populations of all of these, and more distant systems, are accessible with TMT and E-ELT. Figure from Karachentsev et al. (2013).

could be BCD galaxies in their quiescent phase, but others are comparable to normal galaxies in size and mass. More detailed study of LSBs and BCDs is required to place them in proper perspective in the picture of galaxy evolution.

Some of the most metal poor galaxies that we know are dwarf or irregular LSB galaxies. The low metal content of these systems suggests that they are ideal targets to search for traces of population II stars. However, LSB disks are very faint and to do single stellar population (SSP) analysis of their disks requires high S/N spectra not possible to obtain with current facilities. The high resolution of TMT will help us observe, model and understand the chemical evolution of these low luminosity disks. Also, TMT IRMOS-IFU integral field spectroscopy would be able to map SFR to a much higher level of resolution than current Hα imaging (where, again, resolution is sacrificed for S/N). Although LSB galaxies are gas rich their dark halos lead to low SFRs and hence overall lower luminosities. The low luminosity and low stellar surface density makes the disks difficult to study, especially the galaxies at larger distances and beyond our local universe. The high sensitivity of the TMT will enable the detection of the disks of LSB galaxies and determine their population density and properties.

7.8.8 Resolving extreme star formation environments in Luminous Infrared Galaxies at low redshift

Luminous Infrared Galaxies (LIRGs; LIR $> 10^{11}\ L_{\odot}$) and Ultra Luminous Infrared Galaxies (ULIRGs; LIR $> 10^{12}\ L_{\odot}$) are some of the most important targets for revealing the star formation history in the universe. They dominated the SFR density (e.g., Magnelli et al. 2013) at $1 < z < 3$, when most galaxy growth took place in dusty environments. The spatial extent of star formation in high-z (U)LIRGs more resembles local LIRGs than local ULIRGs. With diffraction limited resolution (λ/D = 0.008″ at 1.2 μm), TMT/IRIS will reveal the morphology and gas conditions in low-z LIRGs with a physical scale of $\sim$15 pc at 1.2 μm at the luminosity distance ($d_{\rm L}$) of $\sim$400 Mpc (or $z = 0.088$, the largest distance for IRAS Revised Bright Galaxy Sample; Sanders et al. 2003). This scale is near the minimum size of typical HII regions measured in nearby galaxies with Paα emission (Liu et al. 2013a). We will be able to resolve individual sites of current star formation, re-

veal gas properties associated with the star formation (ionization, metallicity), and explore feedback processes (outflow velocity, outflow rates) that affect conditions of the ISM. Taking advantage of the high spectral resolution observations of TMT to investigate the properties of individual HII regions in each galaxy lets us explore the building blocks of recent massive star formation, to better understand star formation in extreme environments. In addition, where an AGN exists, the high resolving power of TMT will be able to distinguish the emission from the AGN and nuclear star formation. With a planned spectral resolution of $R = 4000$ (potentially $R = 8000$) for IRIS, we will be able to resolve diagnostic emission lines, and together with a spatial resolution that is better than HST, we will be able to disentangle heating from young stars, shocks and AGNs in hundreds of starburst galaxies.

High resolution TMT observations of molecular hydrogen, H_2, together with atomic hydrogen emission lines will provide new insights into the molecular gas temperature and density structure of photo-dissociation regions (PDRs), the primary heating and cooling processes, and the mechanism of H_2 formation (e.g., Sugai et al. 1997) on a scale of each individual HII regions in the local universe. In addition, with a 30 m telescope, ground-based MIR observations will provide synergy with space-based infrared observatories. One of the TMT first decade instruments, MICHI (Mid-Infrared High-dispersion and IFU Spectrograph), yields 15 times higher sensitivity ($\sim$0.1 mJy with 5σ detection in a 1 hour integration in the 10 μm (N band) imaging) and 4.5 times better spatial resolution (0.07″ at 10 μm, corresponding to 33 pc at $d_{\rm L} = 100$ Mpc) than the current ground-based 8-m class telescopes. Although the sensitivity is not as high as that of JWST, the 4.5 times better spatial resolution of TMT/MICHI will allow us to investigate physical processes in deeply dust embedded nuclei of low-z LIRGs. Using the 7–25 μm wavelength coverage of MICHI, a suite of MIR features can be accessed to diagnose the physical and chemical conditions of the gas and dust in galaxies. From the ground, we expect to readily detect at least the Ar^{+2}, S^{+3}, Ne^{+}, and S^{+2} atomic fine structure emission lines, the H_2 molecular emission lines from molecular gas with a few hundred K, the polycyclic aromatic hydrocarbon (PAH) emission bands, and the 9.7 μm silicate features for local objects. Although all of these emission lines were and will be accessible from Spitzer/IRS, JWST/MIRI, and SPICA/MCS, in the local universe, the 0.07″ spatial resolution at 10 μm of TMT/MICHI will resolve the obscured dense clouds in the innermost regions of nuclei and star-forming regions where star formation is most intensive.

Spatially resolved line emission obtained via MICHI will provide the detailed gas properties on each of the dusty star-forming sites. The line flux ratios of [SIV]10.51 μm/[SIII]18.71 μm and [SIV]10.51 μm/[ArIII]8.99 μm are powerful at setting constraints on the hardness of the ionizing radiation, and the [SIII]18.71 μm/[NeII]12.81 μm ratio is sensitive to the electron density (Snijders et al. 2007). Because the hardness of the radiation field is sensitive to the stellar population of galaxies, we will be able to determine the obscured stellar population in dusty galaxies. A combination of two sets of emission line ratios can be an even more powerful tool for diagnosing galaxy properties (e.g., Groves et al. 2008; Hao et al. 2009; Inami et al. 2013). With the emission lines that can be observed from the ground, comparisons of the emission line ratio diagram [SIV]10.51 μm/[ArIII]8.99 μm vs. [SIII]18.71 μm/[NeII]12.81 μm to those predicted from models can constrain age, metallicity, density, and ionization parameter with model assumptions of star formation history, IMF, stellar atmosphere models, and stellar evolutionary tracks (see figures 11 and 15 of Snijders et al. 2007). MICHI with TMT will elicit different views of the physical properties and mechanisms of star formation in regions deeply embedded in dust, which we have not yet been been able to examine with optical and NIR facilities due to the very high extinction.

8 THE BIRTH AND EARLY LIVES OF STARS AND PLANETS

Formation of stars is the principal driver of galaxy evolution and chemical enrichment in the universe, which in turn affects the process of star birth. On the other hand, it also provides the sites

of planet formation and development of life. Therefore, understanding *how stars and planets form* has long been one of the central problems in astrophysics. In fact, significant progress has been seen especially in the last decades, but the detailed processes are still quite elusive. ALMA, JWST, and next generation instruments on ground-based telescopes will yield further scientific advances prior to the TMT's first light. However, we definitely need TMT to have unprecedented angular resolution with very high sensitivity in the near- to MIR, which is critical for this science topic. TMT, with the great complementarity with those telescopes and instruments, will provide a big step forward to more complete understanding of star and planet formation as outlined in this chapter.

8.1 Star Formation

Star formation is a fundamental astrophysical process; and yet we still lack a quantitative and predictive theory for how stars and clusters form (Krumholz 2014). Among the key ingredients for building such a theory are observations of young star clusters over a wide range of environments that can be used as benchmarks to test star formation models. Young clusters serve as laboratories with controlled conditions (same age, metallicity, distance, initial conditions) and many stars to sample the distributions of stellar masses, kinematics, and multiplicities that arise during the star formation process. The requisite range of initial conditions in metallicity, external pressure, cloud mass/density, and environment can only be found outside of our own Galaxy where studying clusters in detail has been extremely challenging. Fortunately, TMT's spatial resolution and sensitivity will allow individual young stars to be spatially resolved, even in the largest star clusters, within a wide range of environments throughout the Local Group galaxies and beyond. TMT observations of young clusters, which are the output of the star formation process, will complement ALMA studies of the gas clumps and cores that are the input to the star formation process.

In the section below, we highlight TMT science cases for measuring the IMF, internal kinematics, and multiplicity in young clusters, followed by the sections focusing on high- and low-mass ends of the IMF. These observations will help constrain star formation theories such that reliable predictions can be incorporated into models of planet formation, stellar evolution, galaxy formation and evolution, and cosmology.

8.2 Developing a Predictive Theory of Star Formation

8.2.1 IMF vs. environment

The relationship between the ISM and the resulting stars is, arguably, the most fundamental objective in star-formation research. The Kennicutt-Schmidt (K-S) law establishes a correlation between the integrated rate of star formation and the surface density of dense gas (Schmidt 1959; Kennicutt 1998) in extragalactic sources. Heiderman et al. (2010), among others, investigated this relationship for clouds in the Milky Way and found significant (by a factor ~ 2) discrepancies for the K-S slope compared to external galaxies. Other smaller-scale ($\lesssim$100 pc) measurements also tend to show the deviation from the K-S law or the larger scatter, which may be plausible since high angular resolution distinguishes local, inhomogeneous distributions of dense gas and stars. The problem is that the current spatial resolution is not enough small to explore the cause of the observed behavior. One way to tackle this issue is going to finer scales to have a more comprehensive understanding of the IMF by resolving stellar populations (providing a more accurate yield of star formation), and to know the *local* star-forming environment (e.g, metallicity, radiation field, cluster density, gas density distribution). Such an approach, if applied under various environments, can lead to an understanding of the origin of the K-S law, and ultimately, how physical processes in the ISM control star formation.

The TMT's combination of high spatial resolution and sensitivity will offer unprecedented capabilities for studying the IMF in distant star-forming regions not limited to our Galaxy but also in the

Local Group galaxies (see also Sect. 7). This is the area where a 30 m class telescope, with AO, has a real niche in the field of star-formation; HST and its successors including JWST are less competitive due to their significantly smaller mirror diameters.

Diffraction-limited TMT observations of rich, dense clusters in the distant Milky Way and local universe in NIR will enable determination of the shape of the IMF over the entire range of masses, from $\sim$ 100 $M_{\odot}$ to below 1 $M_{\odot}$. TMT will allow us to probe the brown dwarf, and even the planetary-mass regime in young clusters at distances of several kpc. It will also enable investigations of the low-mass ($\lesssim$1 $M_{\odot}$) stellar regime in a representative slice of the universe, including the nearest large spiral galaxies (M31 and M33) (Table 5) and the very low-metallicity environments provided by Local Group galaxies such as NGC 6822 and IC 10. Preliminary results for the low-mass IMF in the Magellanic Clouds suggests that metallicity-related differences affecting the shape of the stellar mass distribution require significantly lower metallicities to become apparent (e.g., Da Rio et al. 2009). The stellar density in a given cluster, which is another environmental parameter, can be retrieved from such resolved observations, enabling us to establish the relationship with emerging stellar mass.

Table 5 Limiting K band Magnitudes and Corresponding Lower Mass Limits in Arches-like Clusters

	Limiting K Magnitude		Limiting Mass ($M_{\odot}$)	
Radius (Re)	M33	M82	M33	M82
0.5	17	< 19.8	...	...
1.0	18.9	< 19.8	65	...
2.0	22.3	20	3	...
5.0	27.5	23.9	1.1	32

Notes: for illustrative purposes, photometric crowding and photon statistic limits have been computed for target environments in the M33 and M82 using the radial profiles of the Arches and R136 clusters, coupled with the crowding limit algorithm given by Olsen et al. (2003). The K band magnitudes are for crowding limited photometry to 10% accuracy. The input luminosity function used for these calculations is a hybrid based on measurements in the Arches cluster (Blum et al. 2001) for the high-mass stars ($\geqslant 2M_{\odot}$) and measurements in the Trapezium by Hillenbrand & Carpenter (2000) for the low-mass stars ($\leqslant 3\ M_{\odot}$). The Arches radial profile is a re-fit to HST data by Blum et al. (2001).

Based on the expected performance of the IRIS IFU, it will also be possible to obtain spectra of stars with masses significantly smaller than 1 $M_{\odot}$ at the GC, while the mass limit lies at $\sim 10\ M_{\odot}$ with current 10 m class telescopes (Lu et al. 2013). With TMT, a similar detection limit as currently obtained in the center of the Milky Way can be achieved in the Local Group (Fig. 69).

ALMA, on the other hand, will provide superb spatial resolution at complementary, dust-penetrating (sub-)millimeter wavelengths. This is a fortunate situation, as it will allow us to probe right into the core of the most active, dust-enshrouded star-forming regions, covering the entire useful wavelength range from the infrared to millimeter waves. This will potentially help solve the key outstanding issue of how star formation occurs, proceeds, and is triggered, as well as the importance of the interaction between the newly-born stars and their environments. We will be able to study the early evolution and the transformation from the youngest star-forming cluster-like regions to more mature, partially virialized systems.

8.2.2 Kinematic evolution

Young stars within a star-forming region interact with each other in complex ways. Simulations of star cluster evolution generally assume that the stars are initially smoothly distributed and in dynamical equilibrium. However, both observations and theories tell us that this may not be how clusters

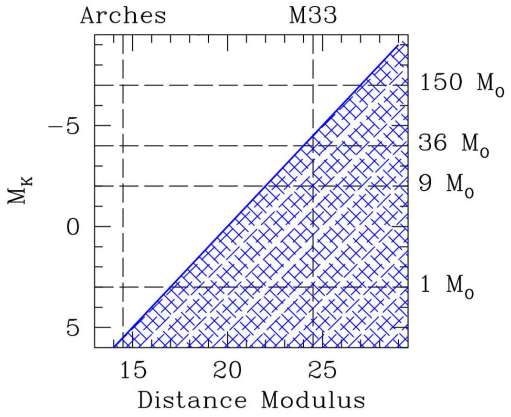

Fig. 69 M_K limits for S/N = 50 at $R = 4000$ with IRIS in IFU mode during a 3 hour total exposure time. These numbers are valid for the uncrowded outer regions of clusters. At a given distance modulus, stars within the blue area are either not observable or only with lower S/N.

form. Emerging evidence suggests that star formation in molecular cloud cores follows a spatial distribution imprinted by the properties of the prevailing turbulence, which can be conveniently approximated by a fractal (clumpy) distribution (e.g., Bastian et al. 2009); numerical simulations of such initial stellar distributions suggest rapid subsequent formation of dense cluster cores by the collapse of protoclusters, given the expected cool (subvirial) dynamical conditions in such environments (e.g., Allison et al. 2009). Dynamical mass segregation is predicted for stellar masses down to a few $M_\odot$ on timescales of a few Myr during the collapse.

To answer the question of the nature of early dynamical mass segregation, precise mass, position and velocity measurements are required. It is also critical to systematically study the most likely initial conditions for cluster formation which lead to the observed configurations. The radial density profiles of young and embedded clusters can shed light on the structure of those clusters. Colors can help classify types of young stellar objects to trace the progress of star formation and help distinguish between different star formation models. Analytical techniques like the nearest neighbor method for infrared-excess stars can be used to identify structures in star-forming regions. Those data can show if clusters are expanding or contracting. The TMT instruments, IRIS, WFOS, NIRES, and in particular MICHI will play a very important role in this subject with the very high angular resolution ($\sim$ 10 AU at 140 pc at 10 μm) and the capability of high-dispersion ($R \sim 100\,000$) spectroscopy.

8.2.3 Multiplicity

The multiplicity properties of young stars offer a powerful diagnostic of the star formation process. The binary fraction has been shown to be a function of primary mass, with nearly 100% of the highest mass stars having companions, down to a mere $\sim 20\%$ for BDs (e.g., Raghavan et al. 2010). The multiplicity fraction also seems to be a function of stellar age and environment, with younger stars exhibiting a generally higher multiplicity fraction (e.g., Duchêne 1999). It has also been demonstrated that the mass ratio distribution is roughly constant except among the lowest mass objects (e.g., Duchêne & Kraus 2013). These multiplicity statistics inform our understanding of the

overall star formation process, as different formation theories often make different predictions for the multiplicity fraction as a function of mass and environment (e.g., Bate 2012).

Although recent technological advances allowed for the charting of new realms of parameter space, significant uncertainties still exist in the distribution of all types of binaries at all separations. In particular, the range of period/separation space typically left unprobed by current spatially resolved imaging or RV monitoring is log(P) $\geqslant 3$ and/or $\rho \leqslant 0.05''$ (Duchêne & Kraus 2013). This regime is easily observable with any diffraction-limited imager on TMT, such as IRIS. Furthermore, TMT's unparalleled spatial resolution will allow us to resolve known spectroscopic binaries, a niche previously only available to long baseline interferometry. The combination of astrometry and spectroscopic orbital monitoring provides a means of measuring component masses, which are essential for calibrating theoretical evolutionary models (e.g., Hillenbrand & White 2004). In addition, instruments such as PFI and/or SEIT will discover high contrast ratio binaries, such as BDs around O or B type stars, at separations unachievable with current generation high contrast imagers. This will fill in currently unknown regions of mass ratio parameter space.

There is tantalizing evidence of differing multiplicity fractions for stellar types as a function of environment. It has been suggested that the density of a star-forming environment will ultimately drive the final multiplicity fractions. Dense, high mass environments may trigger dynamical interactions that ionize binaries (e.g., Bonnell et al. 2003) or disrupt disks before they have a chance to collapse and form low mass companions (e.g., Zinnecker & Yorke 2007). The resolution and sensitivity of TMT will also allow us to push multiplicity surveys to more distant, and often more massive, star-forming regions such that the statistics match those of nearby regions such as Taurus and Upper Scorpius (~ 150 pc, e.g., Kraus et al. 2011). Current AO-fed instruments on 8–10 m class telescopes can achieve physical separation limits of ~ 7 AU for these regions. With TMT, the equivalent will be achievable for star-forming regions as distant as ~ 2 kpc, encompassing clusters such as M8, M16, and M20. Furthermore, instruments such as HROS and NIRES will vastly improve our identification of spectroscopic binaries in star forming regions, particularly for the lowest mass objects that are too faint to target with current instrumentation. By achieving new statistics on more star forming regions, TMT with IRIS, PFI/SEIT, HROS, and NIRES will offer a new window into the complicated dynamical processes during star formation that ultimately drives the multiplicity fraction we observe among field objects.

An additional niche provided by TMT will be its ability to probe the multiplicity of Class I protostars with high resolution using instruments like MICHI. Catching binaries shortly after formation has the potential to revolutionize our understanding of the binary formation process. Thus far, the multiplicity statistics of this class of objects are poorly constrained over a limited set of regions and separations ($\sim 50 - 2000$ AU, e.g., Connelley et al. 2008, 2009). Probing closer separations has thus far been limited in spatial resolution or spectral sensitivity. With MICHI, binaries with separations $<$20 AU will be resolvable visually in nearby star forming regions. With the high-resolution spectroscopy mode of MICHI and the sensitivity of TMT, RV variables will also be identifiable, providing important statistics on the tight binary frequency in this regime. For this science case, TMT offers a unique complement to JWST and ALMA. TMT will have superior spatial resolution for visual binary identification. ALMA will achieve similar statistics for even more embedded Class 0 protostars, providing an important comparison sample for Class I objects.

8.3 Star Formation at the Extreme Ends of the Mass Function

8.3.1 Formation of high-mass stars

Massive stars impact many astrophysical systems, including forming galaxies, their interstellar media, young star clusters and protoplanetary disks therein. Several theories for massive star formation are being debated: core accretion, competitive accretion, and stellar collisions (Tan et al. 2014).

These vary in their assumptions about how material is accreted to the protostar and thus make different predictions for the structure of the gas envelope, the accretion disk, outflows, and possibly binary properties and (low-mass) protostellar crowding around the forming massive protostar.

TMT can make several important contributions to our understanding of massive protostellar environments. First, high resolution NIR and MIR imaging will reveal the structures of heated dust around massive protostars, which can arise from the accretion envelope, accretion disk (including spiral structure and binary companions forming in the disk), outflow cavities and other protostellar companions forming as part of a fragmenting protocluster. Typical Galactic massive protostars are at ~ 3 kpc (the closest is in Orion KL at ~ 400 pc), so structures on ~ 1000 AU scales, e.g. approximately corresponding to disk diameters, extend over $\sim 0.3''$. IRIS and MICHI will enable dramatic improvements over current observations of NIR (e.g., Preibisch et al. 2011) and MIR (e.g., de Wit et al. 2009) dust continuum from massive protostars, first by having a factor of three better angular resolution compared with current 8–10 m class telescopes and second by being sensitive to fainter emission features (coronographic capabilities will be useful to block compact emission from the target protostar to help reveal disk, envelope and outflow structures). These images will constrain radiative transfer simulations of massive protostars (e.g., Zhang et al. 2014). Galactic massive protostars are bright, so it will be necessary to check that saturation is not a problem. In addition, imaging at wavelengths of 24 μm or longer may be feasible (potentially differentiating TMT from other ELTs), increasing the wavelength range over which radiative transfer models can be constrained. Galactic massive star-forming regions often have relatively extended MIR morphologies, requiring relatively large chop throw angles of $\gtrsim 30''$.

Spectroscopy opens up new windows on composition and kinematics. Some probes are common to those used in studies of low-mass star formation, including H_2(1–0) S(1) (e.g., Martín-Hernández et al. 2008), CO(2–0) bandhead emission/absorption (e.g., Testi et al. 2010, who used $R \sim$9000 observations to measure velocity dispersions of ~ 30 km s^{-1} from the ∼3000 K emitting region of a massive protostellar disk) and the shape of the 10 and 18 μm silicate absorption features. The Brγ (2.17 μm), He I (2.06 μm) recombination lines and [Ne II] line at 12.8 μm are especially relevant for massive protostars that are beginning to ionize their surroundings, with expected line widths at least ~ 10 km s^{-1} and typically much greater. Bik et al. (2006) observed Brγ emission from 20 young massive stars ($R \sim$10 000), finding EWs from about 1 to over 100 Å and line widths of $100 - 200$ km s^{-1}. Zhu et al. (2008) studied [Ne II] emission from ultracompact HII regions: the small thermal width of the [Ne II] line helps reveal intrinsic kinematic structure having velocities < 10 km s^{-1}.

IRIS IFU and/or MIR studies of Galactic ultra-compact HII regions have the potential to reveal their kinematic structure in unprecedented detail, and this can help to discriminate between different formation and feedback models: e.g., Is the ionized gas associated with outflows, accretion flows or both? How ordered/symmetric are the accretion and outflow structures around massive protostars? Such questions could begin to be addressed by a survey of the nearest ∼30 massive protostars that sample a range of luminosities/masses and star-forming environments, ideally with a velocity resolution reaching or exceeding ~ 10 km s^{-1} (i.e. $R \sim$30 000).

8.3.2 Formation of brown dwarfs and planetary-mass objects

Stellar objects with masses less than ~ 75 Jupiter mass ($M_{\rm Jup}$) are unable to sustain nuclear fusion in their cores and thus represent a separate category referred to as BDs, bridging the mass gap between the planets and stars. While the distinction between stars and BDs is clear enough by regarding the hydrogen-burning limit as the boundary, the mass boundary with planets is still vague. Various works have adopted the criterion that free-floating objects are above the deuterium-burning limit ($\sim 13\ M_{\rm Jup}$) to distinguish BDs from planets, though the discovery of free-floating planets seems to have further muddied the water. While there is an overall consensus on the formation of

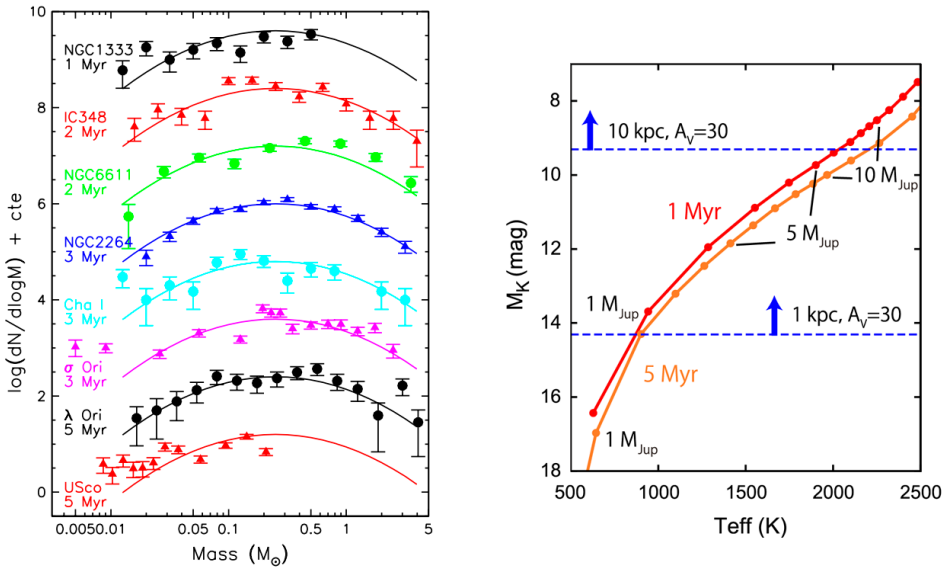

Fig. 70 *Left*: IMFs for eight star-forming regions (Offner et al. 2014 and references therein). The solid lines show the log-normal distribution by Chabrier (2005) with the normalization to roughly match the data. *Right*: M_K for young (1 and 5 million year) Jupiter-mass ($1\,M_{\rm Jup} = 10^{-3}\,M_\odot$) objects predicted in the evolutionary model by Baraffe et al. (2003). IRIS photometry can detect $\sim 1\,M_{\rm Jup}$ objects at 1 kpc with $A_V = 30$, at S/N=5 with a total exposure time of 30 minutes.

stars (molecular cloud collapse) and planets orbiting parent stars (accretion of planetesimals in the circumstellar disk), the formation mechanisms of BDs and free-floating planets are still puzzling. The main sticking point of the BD formation appears to be the fact that a much larger molecular gas density than observed is required for the low Jeans mass of BDs. Explanation for this has necessitated invocation of scenarios such as dense core ejection and turbulent fragmentation. Free-floating, planetary-mass objects may represent an extension of BDs sharing the same formation process, but it is also possible to attribute them to dynamical ejection from planetary systems forming around stars via mutual gravitational interaction between multiple planets.

Direct, high sensitivity (spatial resolution) observations of nearby stellar clusters will help in reaching up to much lower mass limits (Fig. 70). For comparison, Peña Ramírez et al. (2012) have reached the lowest mass of 6 $M_{\rm Jup}$ with a 4m telescope, thus TMT will enable us to study sources with the completeness going down to or lower than the Jupiter mass in nearer clusters. We can hence obtain statistically significant samples of candidate BDs and giant planets, then examine and compare a number of properties (such as SED slopes) to distinguish between BDs, free-floating planets, and bound planets (see also Section 10). This could help in solving the long standing confusion over whether a source is to be considered a BD or a giant planet.

The bottom of the IMF has long been a significant topic of analysis. Though there is wider consensus on the high mass end, the sub-stellar end still needs significant observations and proper analysis (Fig. 70). Spectroscopy is important to better constrain the IMF as it provides a more reliable estimate of temperature, and thus mass and age, compared to using photometric color information. Alves de Oliveira et al. (2012, 2013) have carried out such a study in the ρ Ophiuchi and the IC 348 regions. They have achieved the detection limit of the order of $\sim 10\,M_{\rm Jup}$ using various telescopes.

Much deeper samples can certainly be obtained with TMT, especially in close-by stellar clusters (e.g. Scholz et al. 2012). It should also be noted that constraining the multiplicity could play a key role in IMF determinations (Sect. 8.2.3).

In addition, spectroscopy of BD candidates enables us to detect signatures from accretion disks/jets/outflows as well as chemical properties, and thus help in understanding if they form in any manner similar to stars. Thus far, it has been difficult to do this on a statistically significant basis due to the lack of BD candidates. With TMT, BDs of ~ 1 Myr with 13 $M_{\rm Jup}$ at a distance of a few kpc can be observed in NIR spectroscopy, depending on the amount of visual extinction, which will greatly enlarge the current BD sample.

8.4 Young Planet-forming Disks

Protoplanetary disks are flattened rotating structures of gas and dust, formed as a natural outcome of star formation process. They are the birth places of planets, and hence provide the initial condition of planet building including density and temperature distributions of disk material which are the ingredients for planets and possibly life. Disks also interact with newly-born planets, resulting in re-distribution of gas and dust or orbital migration of planets. After most gas dissipates, evolution of a planetary system is expected to further proceed, such as with violent orbital re-configuration and growth of rocky bodies in debris disks around young main sequence stars (see Sect. 10.2). Therefore, observational understanding of young disks is essential to address the questions of when, where, and how planets form and evolve?

What is most critical for disk observations is high angular resolution. It is required to spatially resolve the local physical and chemical conditions in a disk to finally constrain planet formation theories. In this respect, there is no doubt that TMT will play a major role in this science field, providing a resolution of $\sim$1 AU at 1 μm for disks in the nearest star-forming regions at 140 pc. The high sensitivity of TMT allows us to significantly increase the sample size for resolved observations and to discuss any dependence in planet formation as a function of stellar properties. The list of disk-bearing objects has been growing thanks to Spitzer, AKARI, Hershel, and WISE (e.g., Evans et al. 2009), thus it is not hard at all to extract hundreds of targets for TMT.

The inner ($\lesssim$10 AU) regions of protoplanetary disks are particularly interesting. Given the abundance of exoplanets, we know that protoplanets must be common in the 0.5–10 AU range (Cassan et al. 2012), while current direct detection surveys show that they are rare beyond $\sim$30 AU (e.g., Chauvin et al. 2010). These inner regions also intersect the habitable zone of their parent stars. Such inner disks can be resolved either directly, or kinematically where the (nearly) Keplerian rotation of disks can be used to separate disk regions in velocity (and hence radius). Spectro-astrometry is another advanced, promising technique to probe spatial scales much smaller than the nominal spatial resolution. Given the expected temperatures of these disks, atomic and molecular lines of interest will lie between 1 and 25 μm. The classical infrared "finger-print" region contains transitions from many molecular species, including important bulk tracers, such as water, CO and CO_2, as well as a potentially long list of organic species (HCN, C_2H_2, CH_4, etc.) (Fig. 71).

Disk observations, including detection of footprints of planets, can be extensively done from the early phase of TMT without coronagraphy. As high contrast second generation instruments become available on TMT, lots of detections of exoplanets will be expected. This may be the most compelling and exciting period since the connection between disks and planets can be established, which represents substantial progress toward the ultimate goal of understanding planet formation.

TMT will be highly complementary to JWST and ALMA. TMT and JWST will probe the inner disk region while ALMA more typically traces the outer disk (Fig. 71). Because of its higher spatial and spectral resolution, TMT will be much superior to JWST in constraining the spatial origin of disk emission features and their dynamics.

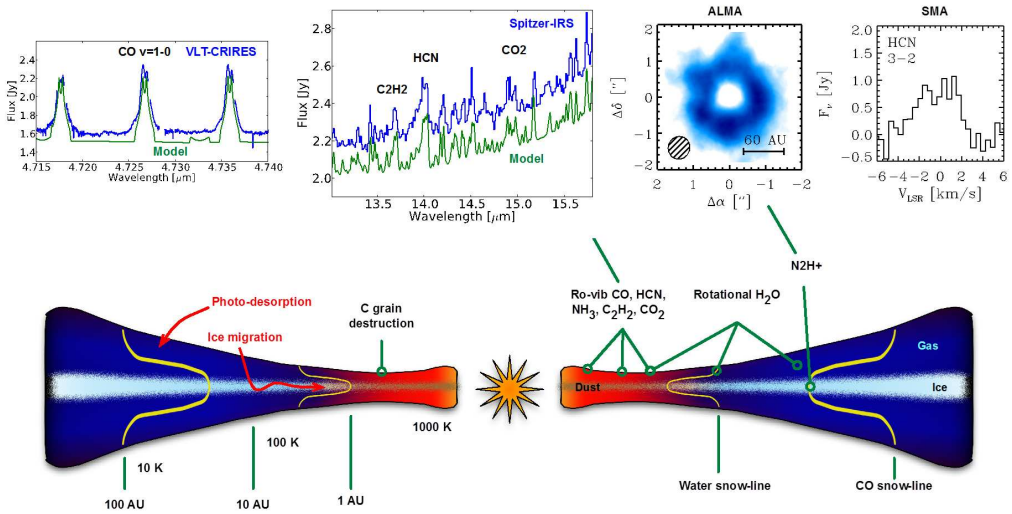

Fig. 71 Sketch of different probes of molecules in disks. The MIR predominantly traces the inner few AU, corresponding to the terrestrial planet-forming region.

In the following, we describe some intriguing science topics where a 30 m class telescope can uniquely contribute; conditions of planet formation, disk-planet dynamical interaction including growth of gaseous planets and circumplanetary disks, and distribution of ice, water, and organic material in young plant-forming disks.

8.5 Conditions for Planet Formation

8.5.1 Planet formation vs. host star properties

The diversity of exoplanets and circumstellar disks seen thus far is, in many cases, related to properties of the stellar hosts. Metallicity is strongly correlated with the presence of giant planets but not necessarily small planets. Warm debris disks, indicative of collisions between planetesimals near the star in asteroid-like belts, are much more common (by a factor of ten or more) around intermediate mass stars than solar mass stars (e.g., Su et al. 2006). Debris disks are also surprisingly frequent for binary star systems (Trilling et al. 2007), and the Kepler survey confirms that planets around and within multiple star systems are present, although the statistics are not yet robust (Armstrong et al. 2014). All of these observations indicate that properties of the host star strongly influence protoplanetary disks and their evolutionary paths toward new planetary systems.

With an inner working angle of approximately 70 mas using high contrast coronagraphy, TMT will be able to detect young planets in K and *L* bands within disks found by Spitzer, WISE, and Herschel in nearby star-forming regions and young associations out to the distance of Orion, greatly expanding the range of stellar properties that can be directly related to characteristics of disks and planets. In some cases these planets may be detectable spectroscopically with TMT, so atmospheric composition of the planet may be compared with the abundances of the host star. Although TMT may not have the MIR power of JWST or cryogenic space surveys for detecting disks, with high quality AO correction it can resolve the sources of near- and mid-infrared excess emission from young stars in crowded fields and tight multiples. TMT will also have the ability to resolve sharp structures within disks and will be especially powerful for study of the gaps in transitional disks. For

distant star-forming regions, TMT will obtain metallicities and spectral types for stars with disks, as well as resolving their multiplicity.

8.5.2 Gas dissipation timescale of protoplanetary disks

The gaseous component of protoplanetary disks is expected to dissipate by processes such as accretion onto the star, photo-evaporation (by stellar or external radiation), and giant planet formation. The timescale for gas dissipation provides a valuable upper limit on the timescale for giant planet formation, as giant planets must accrete their gaseous envelopes on a shorter timescale than this. The dissipation of the gaseous disk also limits the time available to circularize terrestrial planet orbits through interactions with the gas disk. For example, if the late stages of terrestrial planet formation occur during an epoch when the disk has a surface density $\sim 0.01\% - 0.1\%$ that of the minimum mass solar nebula, planets with the masses and eccentricities of Earth, Venus, Mars, and Mercury can be produced (Kominami & Ida 2002).

While stellar accretion rates, which are known to decline with age (e.g., Fig. 2 of Sicilia-Aguilar et al. 2010), measure the amount of disk gas that reaches the star, it is difficult to be certain how much gas remains in the disk without an understanding of the mechanisms that drive disk accretion. Hence what is needed is *in situ* measurements of the gaseous reservoir. As one example diagnostic, the 12.8 μm [Ne II] line is appealing because Ne is expected to remain in the gas phase; [Ne II] is expected to be ionized and heated by stellar X-rays, which are long lived compared to the expected gas dissipation timescale, and the 12.8 μm line is expected to robustly probe small column densities of gas ($N_{\rm H} \sim 10^{19}$–10^{20} cm^{-2}; Glassgold et al. 2007).

The 4.7 μm CO fundamental rovibrational lines are also attractive diagnostics of the gaseous disk at larger column densities. The high abundance of CO in disks and the modest A-values of the fundamental transitions have made them a reliable and often used tracer of the inner regions of disks surrounding T Tauri stars and Herbig Ae/Be stars. A versatile diagnostic, the formation of CO, is robust in disks even in the absence of grains (Glassgold et al. 2004; Bruderer 2013), and the transitions can be excited into emission by UV fluorescence (e.g., Brittain et al. 2009), IR pumping (Pontoppidan & Lockwood 2015, in preparation), as well as thermally.

In addition to measuring the gas dissipation timescale, these diagnostics may also probe the dissipation process itself. Theoretical arguments (Ercolano & Owen 2010) and blueshifted line profiles suggest that photo-evaporative winds can be probed by [Ne II]. The CO rovibrational lines can also show line profiles indicative of a wind origin, suggesting its potential role in studying the gas dissipation process (Pontoppidan et al. 2011).

The measurement of line profiles as well as spectro-astrometric signatures of these diagnostics can be used to determine where the emitting gas arises (disk or wind, and at what radii) and to constrain the gas reservoir in the disk as a function of stellar age. When combined with theoretical model predictions, these measurements could also be used to measure the rate of gas removal from the disk (e.g., the disk photo-evaporation rate).

Giant planet formation itself is another disk dissipation pathway and locating CO emission within a disk can be used to look for radial gaps created by planets (see next section). Constraints from the lack of UV fluoresced emission are particularly useful in showing that there are gaps in the gas (e.g., Brittain et al. 2013).

8.6 Planet-disk Interaction

8.6.1 Disk structure by planets

Planets can dynamically interact with their parent disk, leaving footprints which in most cases are more readily detected than planets themselves. In a gaseous protoplanetary disk, the simplest form

of the footprints is a radial gap along the orbit of a giant planet. Once formed, the gap can excite instabilities due to the pressure gradient at its outer edge, resulting in dust traps which can be favorable locations of planetesimal formation and growth, providing the formation site of additional members of a young planetary system (e.g., Lyra et al. 2009). Dynamical processes can also excite small-scale structures such as spiral waves either in association with instabilities or companions even for those insufficiently massive to carve a gap. In fact, via direct imaging with 8–10 m class telescopes, gaps have been uncovered in transitional disks of T Tauri and Herbig Fe/Ae/Be stars, while spirals were detected preferentially toward warmer disks around earlier type stars in scattered light (e.g., Muto et al. 2012). Yet, with the current instruments, the primary focus is still onto the disk regions of several tens of AU. New high-contrast instruments are now being delivered, but if their extreme AO systems are not equipped with laser guide stars, most T Tauri stars, which are relatively faint at optical wavelengths, will not be observable.

Higher angular resolution and contrast, afforded by a 30 m class telescope with an advanced AO system, are the key to detect planetary signatures in the inner disk region and to resolve smaller-scale structures. For instance, the typical requirement for the detection of spirals is to resolve the spatial scale comparable to the disk vertical thickness. In the case of nearby star-forming regions at 140 pc, the resolution of about $0.01''$ is needed to distinguish tightly-wound spirals at 30 AU in a colder T Tauri disk than Herbig systems, with the aspect ratio (the ratio of the scale height to the radius) of $\sim$0.1. This can be confirmed in the simulations of disk scattered light (Fig. 72) which demonstrate that TMT has an ability to reveal signatures of an embedded planet of $\lesssim$0.1 $M_{\rm Jup}$ at $\lesssim$10 AU from the central star at 140 pc. A gap and spirals by a planet at 10 AU can be detected in the mode of direct imaging, preferably with polarimetry. Structures within 10 AU can be studied with the smaller inner working angle provided by PFI or SEIT. Furthermore, the innermost region lying beneath the coronagraphic mask or the bright stellar halo in NIR can be explored in thermal emission in MIR. The diffraction-limited resolution in N band is $\sim 0.07''$ for TMT, which allows us to study distributions of warm dust with a spatial scale of about $0.02''$, corresponding to 3 AU at 140 pc.

It is worth noting that multi-epoch observations are quite useful to put a strong constraint on planet location through disk dynamics. A spiral arm caused by a planet in a disk is expected to co-rotate with the planet, resulting in the pattern rotation velocity slightly different from the local Keplerian velocity. With the spatial resolution of TMT, the rotation of the spiral can be detected by observations several years apart if a planet is orbiting at 30 AU around a solar-mass star.

Near- and mid-infrared observations are sensitive to the distribution of small, micron-sized grains at the surface of an optically thick protoplanetary disk, while (sub)mm observations probe large, mm-sized grains in the midplane in the continuum as well as the gaseous component at various heights through line emission. The synergy of ALMA with TMT is thus of great importance to understand the 3-D distribution of different components that make up the disk. Needless to say, such comprehensive understanding has a strong impact on theory of planet formation, and is critical to understanding the origin of the observed structures like a dust trap (Birnstiel et al. 2013) or a planet (Zhu et al. 2014).

8.7 Growth of Planets

Giant planets form during the gas-rich protoplanetary disk phase within the first few million years after the formation of the central star. Beyond a certain mass, the forming protoplanet will interact with its natal disk in multiple ways that may lead to direct or indirect detections of the planet itself. A giant planet may open a gap in the gas disk, inducing local non-Keplerian velocity fields with characteristic structure and time variability. This has been proposed to create observable spectroscopic signatures in the 4.7 μm rovibrational CO lines (e.g., Regály et al. 2014). The planet may host a relatively massive, moon-forming, circumplanetary disk (Lubow et al. 1999; Machida et al. 2008;

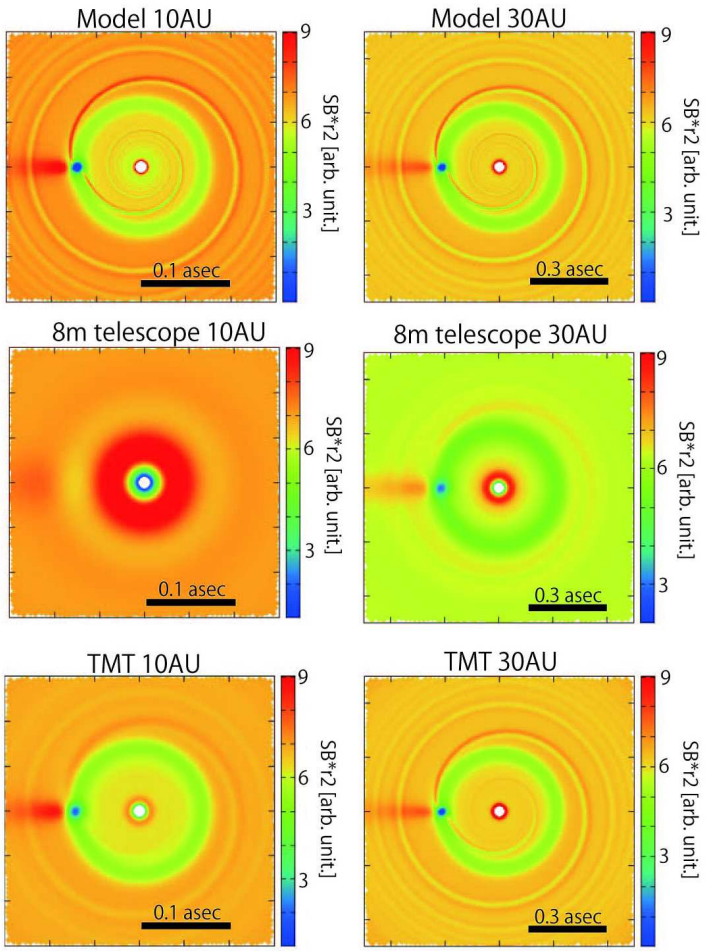

Fig. 72 Model images in H band for gaps and spirals in a disk caused by a 0.1 $M_{\rm Jup}$ planet around a solar-mass star, obtained with 2-D hydro-dynamical simulations. Disk aspect ratio of 0.05, and local isothermal, hydrostatic balance was assumed for the vertical structure. The color scale denotes surface brightness multiplied by r^2 (r is distance from central star). *Top*: The models at the raw resolution with a planet at $r = 10$ AU (*left*) and $r = 30$ AU (*right*). *Middle*: Images expected with an 8 m telescope. *Bottom*: Images expected with TMT, where models were convolved with Gaussian functions of diffraction-limited FWHMs assuming a distance of 140 pc. Dark spots are "planet shadows", indicating the location of the planet (Jang-Condell 2009). Note: 3-D thermal balance calculations are necessary to predict planet shadows; the sizes of dark spots are tentative in these images.

Brittain et al. 2013), and it may even produce strong emission lines from accretion flows (Zhou et al. 2014). All of these tracers will be accessible to TMT. Indeed, they are already being pursued with existing 8–10 m class telescopes as well as with ALMA, and initial results are promising.

Therefore, while TMT may detect protoplanets through broadband imaging of their thermal continuum emission, there is also the prospect of using kinematic gas tracers to detect the *growth* of giant protoplanets. TMT is able to detect gas tracers in the optical and infrared at very high spatial

resolution; 40 mas for the four main CO isotopologues around 4.7 μm that trace the velocity field of the protoplanetary material, as well as a host of tracers of accretion onto the planet itself, including hydrogen recombination lines such as Brγ (2.16 μm).

It should be emphasized that the detection of a gap-opening accreting planet, will have a strong impact on the theory of planet formation and migration. Measurements of the gas accretion rate onto a planet along with the depth and width of the gap are critical to know the angular momentum transfer rate through the gap and therefore the final mass and type-II migration of the planet (Tanaka et al. 2002; Crida et al. 2006; Fung et al. 2014).

Planet and/or moon formation in action can be caught even after the gas dissipation (see also Sect. 10.2.3). There have been recent detections of warm dust belts in a number of debris disks (e.g., Morales et al. 2011). This is the dust originating in the inner region at ∼1–10 AU where the habitable zone resides, and can be interpreted to be evidence for ongoing, oligarchic growth of terrestrial bodies. The high spatial resolution of TMT will be critical in characterizing this terrestrial material to gain new unique insight into the building blocks and mechanisms of terrestrial planet formation. In nearby debris disks, imaging from K to N band will be capable of resolving the 1 AU region. The precise structure such as azimuthal asymmetries and sharp boundaries of the disk edges can inform us of the presence of planets and help establish the connection between the dust belt and planet formation/evolution activity.

8.8 Mapping the Prebiotic Landscape in Protoplanetary Disks

8.8.1 Snow line and beyond

The snow line is a condensation/sublimation front of (water) ice in a protoplanetary disk; water is present in the form of vapor (gas) within the snow line and as ice (solid) beyond it. The formation of giant planet cores is believed to be enhanced because the solid surface density increases and the inward radial drift of solids may be slowed-down across the snow line (Brauer et al. 2008). It helps to explain why Jupiter-like gas giants are not the closest to the Sun in our solar system. While the snow line is located at a radial distance of ∼3 AU in the current solar system, it may have been as close as ∼0.7 AU in the early, optically thick phase (Garaud & Lin 2007), and therefore abundant water ice may have been present in the terrestrial planet region. Thus understanding the location of the snow line, at various evolutionary stages, is important given its relation to both planet formation and the origin of the water in terrestrial planets.

The snow line in protoplanetary disks can be predicted through observations of water vapor. Water emission lines in NIR and MIR can be used to determine the radial extent of water vapor in the warm disk atmosphere (e.g., Pontoppidan et al. 2010a). For instance, this approach was was successful at showing the snow line location at ∼4 AU in the disk surrounding the nearby (54 pc) young star TW Hya (Zhang et al. 2013). With the high-spectral resolution (R ∼100 000) of MICHI and NIRES, the number of sources studied in this way can dramatically increase, (see Figure 73) enabling us to investigate the evolution of the snow line as a function of stellar age and mass.

The distribution of water ice can also be traced via spatially resolved spectroscopy of disk scattered light (Fig. 73). Water ice has a strong absorption band at ∼3.1 μm which should be imprinted in the scattered light spectra (Honda et al. 2009). Disk models predict that the surface snow line in protoplanetary disks around intermediate-mass young stars ($L_\star = 10L_\odot$) is located at ∼20 AU (Oka et al. 2012), which corresponds to $\sim 0.14''$ at 140 pc. This is expected to be within reach of TMT without coronagraphy (IRIS, NIRES), and the observations will surely be feasible with PFI, owing to its much better inner working angle.

The outer region, well beyond the snow line, can be the formation site of icy planets. Comets can also form in such a cold region and could be ingredients of icy planets. Although comets are known to contain pristine frozen material, they also contain incompatible, high-temperature products such

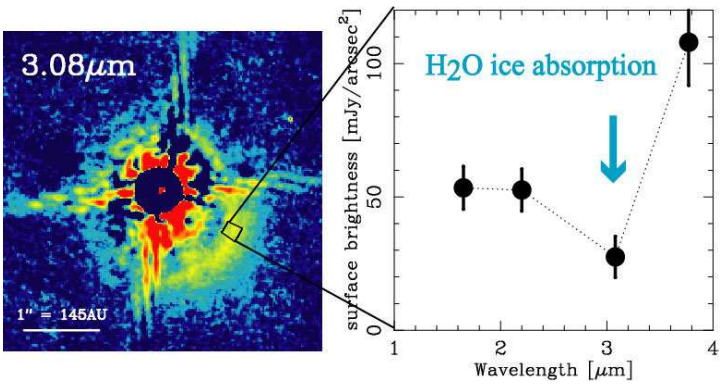

Fig. 73 Scattered light image of the dispk around the Herbig Fe star HD 142527 at 3.08 μm (*left*) and the scattered light spectra (*right*). The $\sim$ 3.1 μm absorption feature, probably due to the scattering by water ice grains, is clearly seen in the spectra. As we go closer to the central star inside of the snow line, this absorption band will disappear due to the absence of water ice, which will directly show the snow line location at the disk surface.

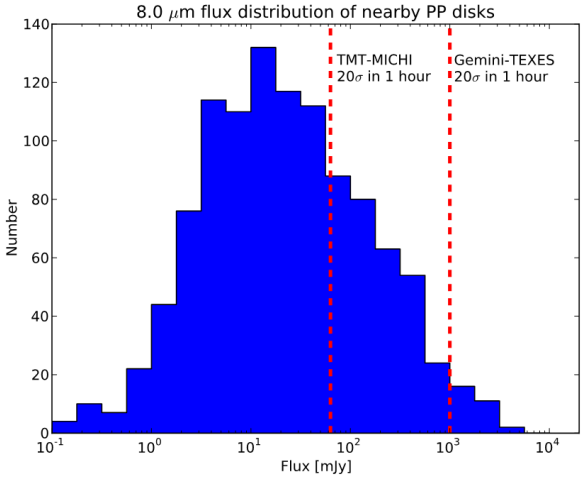

Fig. 74 The 8 μm brightness distribution of protoplanetary disks and young stars in nearby star-forming clouds, as observed with the Spitzer Cores to Planet-Forming Disks legacy survey (Evans et al. 2009). It shows how many more protoplanetary disks can be reached with the TMT relative to current high-resolution MIR spectrometers.

as crystallized silicate grains, which indicates dynamical mixing between the hot inner and the cold outer regions. It is still a matter of debate how the mixing occurs and how the high-temperature material is incorporated into comets. A key to understanding such a process is obtaining the spatial distribution of various kinds of grains in young planet-forming disks. With the high-spatial resolution of TMT, MICHI will offer a unique opportunity to uncover both mineralogical evolution of solids and transport of material within a disk by spatially-resolved MIR spectroscopy (e.g., Okamoto et al. 2004).

8.8.2 Formation and evolution of prebiotic molecules

Planets in the habitable zone are generally expected to be depleted in the elements required to support life as we know it; carbon, hydrogen, oxygen, nitrogen, phosphorous and sulfur (CHONPS). However, some amounts of these elements and the molecules that carry them do end up on terrestrial planetary surfaces, and the processes that deliver them are intimately linked to protoplanetary disks (see reviews by Pontoppidan et al. 2014; van Dishoeck et al. 2014). The amount and molecular form of CHONPS molecules delivered to potentially habitable planets ultimately provide the basis for the formation and evolution of terrestrial atmospheres. Complex organic species may also be synthesized in the warm irradiated environments of disks. Indeed, the warm, energetic environments of disks within a few AU of the central star are thought to be highly chemically rich, with short timescales for the formation of a wide range of organic species (e.g., Henning & Semenov 2013).

Spitzer demonstrated that strong emission from gas-phase species is from disks around solar-mass young stars (e.g., Carr & Najita 2008, 2011; Pontoppidan et al. 2010b). Favorable geometries can also lead to deep absorption lines from disks (Lahuis et al. 2006), which at high dispersion are sensitive to much rarer species (Knez et al. 2009). We now know that planet-forming regions are chemically rich, highly heterogeneous objects, with strong chemical differences between demographical groups. Herbig stars have relatively simple surfaces, dominated by harsh, destructive UV fields (e.g., Fedele et al. 2011), while inner disks around solar-mass stars are rich in both oxygen and carbon-dominated species (Salyk et al. 2011), and inner disks around low-mass stars are dominated by organics (Pascucci et al. 2013). Critically, it was also demonstrated that many of these lines are accessible to ground-based facilities (e.g., Pontoppidan et al. 2010a; Mandell et al. 2012).

There are several aspects of prebiotic chemistry that can be uniquely explored using molecular emission lines from warm gas. (1) The warm gas represents the most volatile reservoir that is lost to planetesimal and terrestrial planet formation. Observations of it therefore test whether the CHONPS depletions observed in the Earth and the inner solar system are universal. For instance, the Earth's carbon is orders of magnitude more depleted than what would be expected, given the relatively large fraction of refractory organic carbon in the ISM and in comets (Lee et al. 2010). Observations of volatile carbon carriers with the TMT can constrain models for carbon grain destruction. (2) Icy bodies in protoplanetary disks are generally affected by aerodynamics. In particular, they migrate against pressure gradients, leading to a net flow of ice inwards, across the snow line (Ciesla & Cuzzi 2006). Thus, the observed warm molecular gas may be recently sublimated, comet-like material, and the infrared lines trace chemical and photo-chemical processing of prebiotic material. The action of such a process has been suggested as an explanation for the observed oxygen isotopic fractionation in solar system meteorites (Lyons & Young 2005). It may also affect the local carbon/oxygen ratio, thereby producing a sharp transition from an oxygen to a carbon-dominated chemistry, with potentially profound consequences for prebiotic chemistry (Najita et al. 2013). Finally, observations of some exoplanetary atmospheres have compositions that suggest the influence of a large-scale elemental re-distribution in their natal disks (Öberg et al. 2011). *Observations of planet-forming CHONPS molecules with the TMT will therefore provide observable links to the growing population of exoplanets.*

Medium ($R \sim 10\,000$ for maximizing the line-to-continuum ratio) and/or high-resolution spectroscopy ($R \sim 100\,000$, for kinematic information) in the thermal infrared (3–14 μm) on the TMT is poised to deliver transformative data on this subject. The increase in sensitivity over the previous generation of MIR spectrometers on 8–10 m class telescopes, both due to the larger aperture and improvements in detector technology, leads to a tremendous increase in the numbers and types of protoplanetary disks for which molecular lines can be observed. Specifically, while ground-based high resolution N band spectroscopy can only reach the few brightest protoplanetary disks, the TMT can select targets from a reservoir of 100–1000 protoplanetary disks across the stellar mass range (see Fig. 74). The JWST will be more sensitive, but has too low of a spectral resolution to resolve

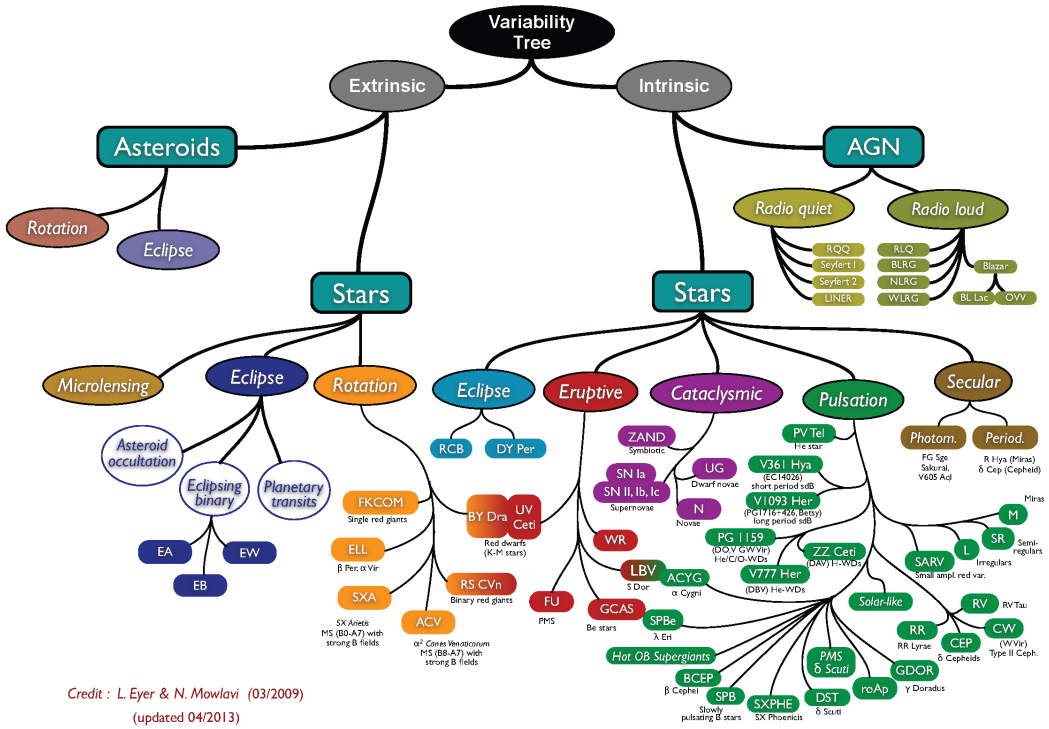

Fig. 75 Variability tree summarizing different kinds of variable objects. In this chapter we describe a subset of examples that have high scientific impact and require more stringent observing capabilities and operational modes.

lines or to separate weak lines of rare species from the forest of bright water lines that is typical for protoplanetary disks.

9 TIME-DOMAIN SCIENCE

Time domain astronomy as discussed here is the study of transient and variable sources, see Figure 75. Transients are usually the result of some kind of explosion or collision that leads to a change in the physical character of the source (e.g. SNe, GRBs, NS mergers), or a result of accretion of matter (nova outbursts, TDEs, AGN flares). These events are unpredictable, show a temporal evolution of the physical conditions, and often fall below the detection threshold when faint. Such ToO transient events generally require a rapid response to a trigger of observations. Variability in sources can be intrinsic; caused by either a change in the physical conditions (e.g. Cepheid variables and stellar flares), or accretion induced (e.g. cataclysmic variables (CVs), AGNs), or extrinsic; as a result of geometry (e.g. binaries, lensed objects and transiting planets). Variability observations can be time dependent, or time critical requiring observations that are time-resolved.

Time-domain astronomy will be an exciting area of research in the TMT era, in part thanks to the synergy with various surveys from up-coming facilities such as the LSST, WFIRST, and Euclid, and the search for GW sources, see Section 9.5. In this section, we discuss a few interesting time-

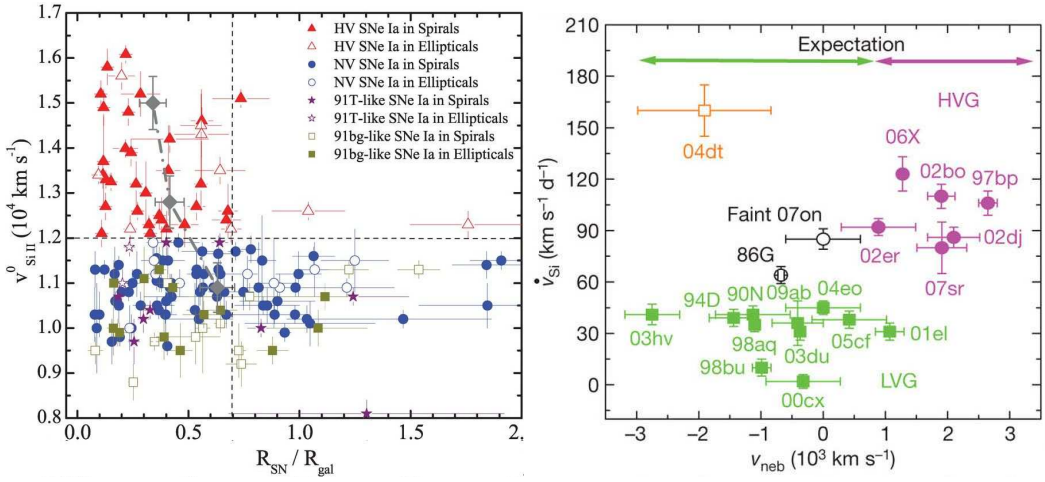

Fig. 76 Observational indications of the origin of diversity in SNe Ia. *Left*: HV SNe Ia are more concentrated in the inner and brighter regions of their host galaxies than NV SNe Ia (Figure from Wang et al. 2013). *Right*: HV (*magenta*) and NV (*green*) SNe Ia have systematically different velocity shift in the nebular emission lines (Figure from Maeda et al. 2010).

domain science cases that benefit from the unique capabilities of TMT. Important science areas that are not discussed in this section but that could definitely benefit from the observing capabilities of the TMT include, among other things, follow-up of microlensing events (Sects. 3.2 and 10.4), young stellar object variability, exoplanet transit and eclipse (Sect. 10.3), various processes on solar system objects (Sects. 11.2.2 and 11.3.2) and astrometric studies of stellar motions (Sect. 6.1.3). The observing requirements of science programs discussed in detail here are summarized in Figure 85, Figure 86 and Table 6.

9.1 Understanding the Nature of Type Ia Supernovae

Over the past decades, SNe Ia have been used as one of the best distance indicators to measure extragalactic distances. Observations of such events at higher redshifts directly led to the discovery of the accelerating universe (Riess et al. 1998; Perlmutter et al. 1999). Among the existing methods to measure the dark energy EOS parameter w, the distances to SNe Ia provide the best single constraint up to date. This recently inspired many wide-field SN surveys such as the PTF, the La-Silla Quest Supernova Survey (LQSS), and the Dark Energy Survey (DES) that discovered thousands of SNe Ia that exploded in the local and distant universe. This number is expected to increase dramatically, especially at high redshifts with the planned future wide field surveys.

An increased sample of SNe Ia will reduce the allowed ranges of various cosmological parameters due to improved statistics (Pandey 2013). However, accurate determination of the dark energy EOS parameter still relies on a better control of the systematic effects in determining the distance to each SNe Ia. The larger systematic uncertainties include dust absorption, environmental dependencies of the observables, and possible evolution with redshift (e.g., Howell 2011; Wang et al. 2013). Because of the huge light collecting area, IR capability, and the powerful AO system, TMT will make important contributions to unveil the nature of SNe Ia and improve their applications in precision cosmology.

9.1.1 Characterizing high-z Type Ia supernovae: towards a better standard candle

Recent reports suggest that SNe Ia with high-velocity (HV) ejecta velocities (e.g., V(SiII) $>$12 000 km s^{-1}) tend to inhabit larger and more-luminous hosts and are substantially more concentrated in the inner and brighter regions of their host galaxies than the normal-velocity (NV) sample (V(Si II) $\sim$10 000 km s^{-1}), see Figure 76 left. The HV and NV populations have different colors around maximum brightness (Wang et al. 2009). These results suggest that HV SNe Ia most likely originate from more metal-rich progenitors than NV SNe Ia, and are restricted to galaxies with substantial chemical evolution. As an alternative to the probable distinction between the HV and NV SNe Ia as different populations, Maeda et al. (2010), based on the ejecta kinematics in the deepest layer as seen in the optically thin, late-phases, suggest the viewing direction is another function to produce the HV and NV appearance, see Figure 76 right. The dependence of SN Ia ejecta velocity on progenitor environment could be relevant when using SNe Ia as cosmological yardsticks, as this may lead to a change in the ratio of the HV and NV population with redshift. The observed relative fraction of the HV to NV population might become smaller at great distances due to a real decrease in the HV SN Ia rate in low-metallicity environments and/or the increased difficulty of observationally spectroscopically classifying SNe in the central regions of distant galaxies. Observationally testing for evolution in the low-z and high-z samples is important for precision cosmology but can be only tested with future high-redshift SN Ia samples having better spectroscopic classification, as the spectral quality and wavelength coverage of current high-z samples are not good enough for this kind of analysis.

Since the LSST will discover thousands of high-redshift SNe Ia ($z \sim 1.0$) within 1 to 2 days of explosion, one would need spectroscopic follow up for these SNe, beginning within a few hours of target discovery, with repeat observations starting with 1 day cadence to understand the progenitor and explosion mechanism. NIR space missions such as Euclid and WFIRST can discover SNe Ia at higher redshifts ($z >$1.0). In addition, gravitationally lensed SNe can be discovered even at higher redshift ($z >$1.0, Amanullah et al. 2011), and surveys looking for SNe behind a massive galaxy cluster are ongoing with 8 m class telescopes and HST, trying to go beyond a redshift of 2, see Section 3.1.6. Moreover, SNe can also be strongly lensed by a relatively faint galaxy, as seen by (Quimby et al. 2013, 2014; Kelly et al. 2015, see Fig. 77), and discovery of such a system could be accelerated by new selection techniques. Present ground-based facilities cannot obtain high-quality spectra for SNe Ia beyond $z = 1.5$. The IRIS and/or IRMS on TMT can easily obtain spectra of SNe up to $z = 4$ with better wavelength coverage, enabling accurate spectroscopic classification for future samples of high-z SNe Ia and IRIS will provide important information on the host galaxy such as the SFR. Combined with the low-z SNe Ia, the high-quality spectra obtained with TMT for the high-z SNe Ia identified with LSST, WFIRST or Euclid could investigate possible evolution of the SN Ia population with redshift. It will become possible to use a specific subclass of SNe Ia that are more uniform to constrain the nature of the dark energy EOS parameter and its dynamic behavior.

9.1.2 Unveiling the explosion mechanism of Type Ia supernovae

The explosion mechanism of SNe Ia is yet to be clarified. The explosion mechanism can be dependent on the progenitor systems, e.g., single degenerate (SD) vs. double degenerate (DD), but also there are variants within the same progenitor model. Since the explosion mechanism sets the ejecta structure and ^{56}Ni yields, which determine the optical luminosity and light curve, understanding the explosion mechanism is a key toward developing precision SN Ia cosmology. An understanding of the physical causes of the peculiar SNe Ia, such as SN 2005hk (Sahu et al. 2008, Foley et al. 2013) and 2005gj (Hughes et al. 2007; Prieto et al. 2007), has the promise to constrain models for normal SNe Ia and illuminate the underlying reason for the diversity of normal SNe Ia.

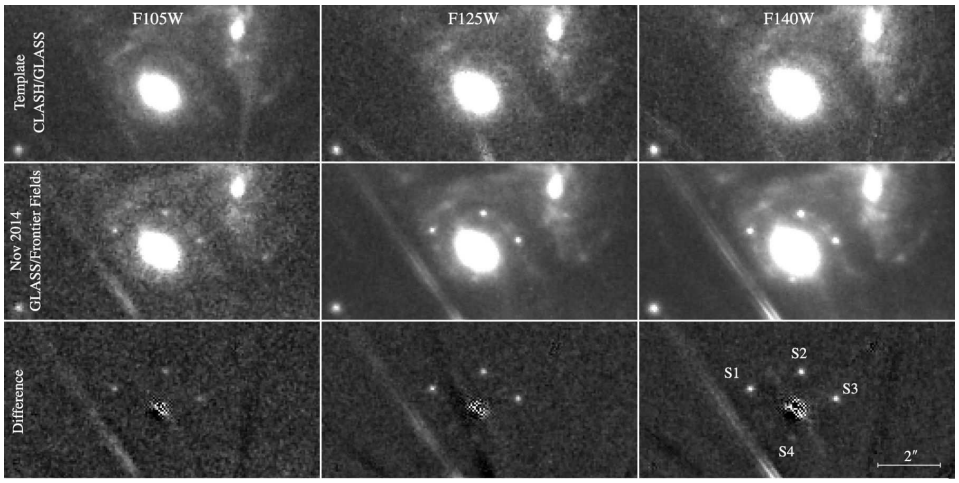

Fig. 77 HST WFC3 images of an SN gravitationally lensed by an early type galaxy cluster (Kelly et al. 2015).

Very early spectroscopic follow-up is still rare for SNe Ia, and so far is restricted only to the local universe. The early-phase spectra reveal the outermost ejecta composition, which is highly dependent on the mode of the explosion. Especially, carbon abundance is quite sensitive to the progenitor evolution and thermonuclear flame propagation mode. Recent results suggest that unburned carbon frequently remains in the outermost layer of SNe Ia, more commonly for the NV SNe (Parrent et al. 2011; Folatelli et al. 2012). Given the environmental/explosion difference between the HV and NV SNe, investigating the carbon signature in the high-z sample is an important step. In the NIR, the magnesium feature is expected in addition to carbon (Marion et al. 2009), and this oxygen-burning product is a key to diagnose the extent of the thermonuclear burning. An early response follow-up of a series of observations with a few minute cadence for a few hours within 2 days of the start of explosion with IRIS, IRMS or WFOS, of a large sample of SNe Ia, including those at high redshift, will make an important contribution.

On the other extreme, very late-time spectroscopy is a strong diagnostic of the ejecta kinematics and thermonuclear products at the explosion trigger, thus being a direct method to constrain the explosion mechanism (Maeda et al. 2010). The high spectroscopic sensitivity of IRIS, IRMS, and WFOS of TMT will open up a new window to study the explosion mechanism: (1) NIR spectroscopy at $\sim$ 1 year and (2) a very late-time (at $>$ 1 year after the explosion) optical spectroscopy. Due to sensitivity limits with 8 m/10 m class telescopes such study is limited in the optical to $\leq$ 1 year after the explosion. As for NIR, there are only a few examples so far taken by 8 m class telescopes, showing that NIR spectra provide qualitatively different diagnostics on the explosion mechanism than in optical (Motohara et al. 2006). As for the very late-time spectroscopy, it is an almost unexplored area due to the faintness of the SNe at such late phases. At such late phases, the dominant energy source is no longer γ-rays, but positrons from the ^{56}Co decay and other minor radioactive species (Seitenzahl et al. 2013).

9.2 Identifying the Shock Breakout of Core-Collapse Supernovae

Massive stars end their lives as core-collapse SNe. As a result of core-collapse, a shock wave is formed in the star, which propagates its stellar mantle outward. When the shock wave emerges from

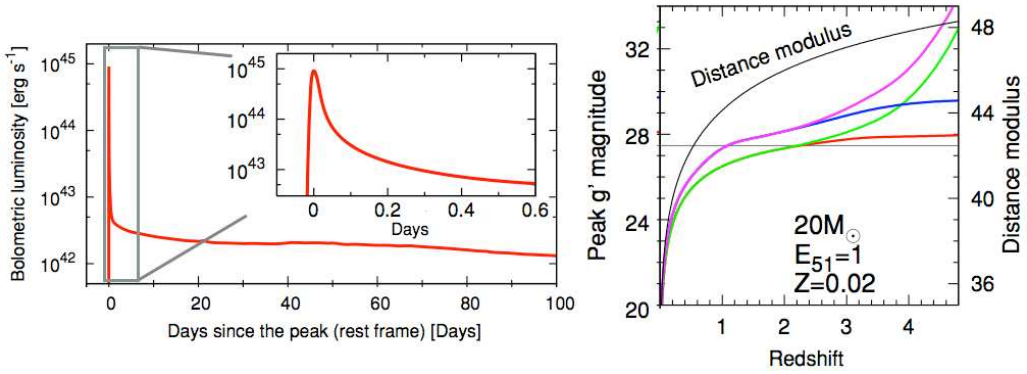

Fig. 78 *Left*: Light curve of SN shock breakout. *Right*: Expected peak magnitude of SN shock breakout as a function of redshift. Different colors show models with different assumptions for the reddening (from Tominaga et al. 2011).

the stellar surface, a fireball suddenly appears. This is the brightest radiative phenomenon in an SN, called "shock breakout", see Figure 78. Its observational properties, e.g., duration and color, strongly depend on the pre-SN radius; the shock breakout of a star with a larger pre-SN radius has a longer duration and redder color. Therefore, detection of shock breakout will provide a direct link between SNe and their progenitor stars. The typical duration and peak wavelength are several seconds to 1 day and soft X-ray to UV, respectively. Since the shock breakout can be detected even $z > 1$, it can be used to probe the SFR at high redshifts (e.g., Chugai et al. 2000). However, the short duration and soft X-ray/UV-peaked spectra make the detection of shock breakout difficult. There are only serendipitous detections in the rising phase of a Type Ib SN (at 27 Mpc, Soderberg et al. 2008), Type II plateau SN ($z = 0.185$, Schawinski et al. 2008; Gezari et al. 2008), and SN II-P ($z = 0.324$, Gezari et al. 2008).

In spite of the soft X-ray/UV-peaked spectra, it is shown that the shock breakouts will be most effectively detected by optical facilities, such as Subaru/Hyper Suprime-Cam (HSC) and LSST, with deep and wide-field capability (Tominaga et al. 2011). The redshift range of the detection extends to $z \geq 2.5$ with the limiting magnitude in g' band of 27.5 mag, see Figure 78. According to theoretical predictions, the typical decline rate of the shock breakout is 0.1 mag/hr at $z = 2$ and a quasi-blackbody spectrum characterizing the shock breakout is more clearly identified at earlier phases (Gezari et al. 2008). The first role of TMT for studies of shock breakouts is a spectroscopic identification. This is achieved only with a rapid (< 1 night) ToO observation. Since the shock breakout is blue and has smooth spectra, the most suitable instrument is WFOS with $R \leq 500$. Spectroscopic data taken with 1–2 hr sampling would give unique information of the temperature evolution on the first day of SNe. The second role is a continuous ($\sim 2-3$ days) observation following the first ToO observation to reveal the spectral evolution of SNe during the very early epochs, see Figure 78, in which metal lines gradually become prominent. The evolution will provide clues to properties of shock breakouts and SNe, e.g., pre-SN radius, CSM structure, and mass loss at the last stage of the evolution.

9.3 Tracing the High-z universe with Supernovae

Core-collapse SNe are the fates of massive stars with short life times and thus can be used to trace the star formation history of the universe. Although such a study has been difficult at high redshift due

to their faintness, a combination of planned transient surveys with 8–10 m class telescopes and spectroscopic identification by TMT will dramatically change this situation. Since SNe are detectable even in diffuse galaxies, the derived cosmic star formation history is independent/complementary to that derived from galaxy studies.

Very bright subclasses of SNe are one of the most promising targets. With optical surveys using 8–10 m class telescopes, bright Type IIn SNe (SNe with narrow emission lines) and "superluminous" SNe can be detectable even at $z > 6$. Spectroscopic observations with TMT will be critical to firmly identify such high-z events, as current 8–10 m telescopes do not have spectral sensitivity to identify SNe at $z > 3$. These classes of SNe tend to show a blue spectrum, thus TMT/WFOS will be the best to obtain the rest-frame far-UV emission. A response time of ~ 10 days is enough as these classes of SNe show relatively long-lived light curves. An interesting application of identification of high-z SNe is probing the IMF in the early universe. At high redshifts, we may also be able to detect pair instability SNe (PISNe, e.g., Scannapieco et al. 2005). Since superluminous SNe and PISNe are thought to arise from very massive progenitors, a number ratio of these types of SNe and normal SNe will provide unique information about the IMF.

To study the high-z universe with SNe, a better understanding of SN rate in the low-z universe is also critical. Currently, the SN search and follow-up in the most active star-forming regions are rather limited, while such regions can provide a large fraction of the star formation in the local universe and even a dominant fraction toward high redshifts, interstellar extinction is one of the major limiting factors (Mattila et al. 2012). The main problem is that the spectroscopic follow-up is currently nearly impossible, thus even the SN typing has not been secured – at $z = 0.03$, a typical SN would have a peak magnitude of $J \sim 22 - 23$ if J band extinction toward the SNe is ~ 5 mag. TMT will make the spectroscopic follow-up for these obscured SNe possible, clarifying for the first time the SN populations and stellar evolution in the active star forming galaxies.

9.4 Characterizing the Circumstellar Environment around Supernovae - Clues to the Identity of the Progenitor Systems

Detection of circumstellar material (CSM) around SNe could provide an alternative way of discriminating different evolution scenarios. If SNe Ia arise from single WDs in binary systems, one generally expects that there should also be considerable H-rich (or possibly He-rich) CSM within tens of AU around the progenitor system. Claims for detection of such CSM around a few nearby SNe Ia have been made in recent years, based on the discovery of time-variable Na I absorptions in several cases (Patat et al. 2007; Simon et al. 2009; Dilday et al. 2012), see Figure 79. On the other hand, there is also evidence for nondetections of variable Na I lines in SNe Ia (Simon et al. 2007; Patat et al. 2013). Such a dichotomy might be related to differences in the progenitor environments, as suggested by the correlation of the ejecta velocity $V_{\rm SiII}$ with the location in their host galaxies (see Sect. 9.1.1). Nevertheless, the origin of the absorbing clouds is still controversial, as such absorptions may also arise in a DD scenario or ISM (Chugai 2008; Shen et al. 2013). To address this issue, one needs a larger sample of SNe Ia with multi-epoch, high-resolution spectra.

At the distance of the Virgo Cluster (~ 16 Mpc), for a SN Ia discovered within 1 day after explosion, the typical R band magnitude is about 19.0–20.0, well before the maximum brightness 10 to 20 days after. TMT/WFOS can provide the highest spectral sensitivity with complete wavelength coverage (0.33–1.0 μm) in a slit-viewing target acquisition mode. A resolution of $R \sim 7500$ enables measurements of the overall evolution of Na I and Ca II absorption, allowing important parameters of the absorbing material that may be associated with the progenitor system to be determined. This includes the distance to the absorbing material, recombination timescale of Na ions, and outflow velocity, parameters important for understanding the origin of the absorbing cloud and hence the nature of the companion stars.

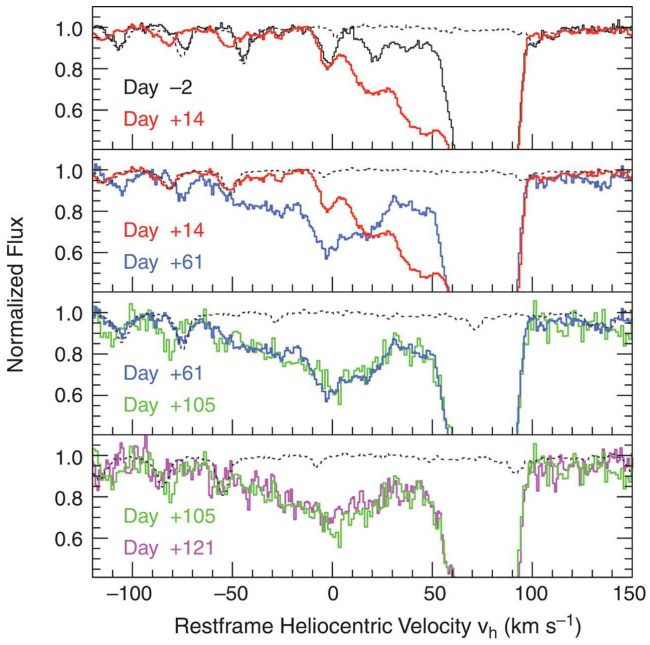

Fig. 79 Time series of high-resolution spectra of SNe Ia (Patat et al. 2007). Time variability of Na I absorption indicates that absorbing material is located in CSM around SN Ia.

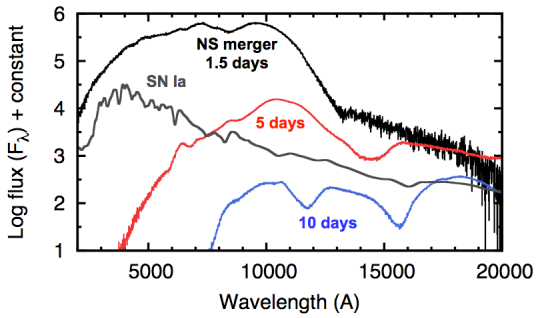

Fig. 80 Expected spectra of radioactively powered emission from NS merger (Tanaka & Hotokezaka 2013). The spectra are expected to be extremely red and featureless. Optical-NIR spectroscopy with TMT will be important to classify a detected transient as a GW source.

9.5 Identification and Investigation of Gravitational Wave Sources

The second generation GW detectors, such as advanced LIGO, advanced Virgo, INDIGO and KAGRA, are planned to start operation in the TMT era. They are expected to directly detect GWs from NS mergers at a distance within about 200 Mpc. The number of GW detections will be in a range of 0.4–400 per year (e.g., Abadie et al. 2010). With the GW detection alone, the position of the sources can only be moderately determined with a localization of about 10–100 deg^2 (e.g., LIGO

Scientific Collaboration & Virgo Collaboration 2012; Nissanke et al. 2013). Therefore, to fully understand the nature of the GW sources, electromagnetic observations should pin down the position of the sources and identify the host galaxy and environment. Among possible electromagnetic emissions from the NS merger, optical and NIR emission powered by radioactive decay energy, so called kilonova (see Sect. 9.6), are of great interest (Li & Paczyński 1998; Kulkarni 2005; Metzger et al. 2010) because of the isotropic nature of the emission and the relatively short rise time of $\sim$1 day after the merger (i.e., the detection of GWs).

Detailed numerical simulations of the EM counterparts of NS mergers (Kasen et al. 2013; Barnes & Kasen 2013; Tanaka & Hotokezaka 2013; Tanaka et al. 2014) show that the expected emission peaks at the red edge of optical or NIR wavelengths, see Figure 80. At 200 Mpc, the expected brightness is 22–25 mag in i or z bands and 21–24 mag in NIR JHK bands (in AB magnitude). Transient search observations with wide-field 8 m class telescopes in optical and wide-field space telescopes in NIR (e.g., WFIRST) are crucial to detect the electromagnetic counterpart of GW sources. Deep transient surveys using 8 m class telescopes will discover an overwhelming number of SNe within the GW localization area ($\sim$50 SNe/deg^2/yr with 24 mag depth, Lien & Fields 2009). Therefore, rapid ToO response follow-up spectroscopy ($R \sim 500$) within 1 day with either TMT WFOS or IRIS will be critical to identify the detected transient as a true GW source, by finding the expected red, featureless spectrum. Similar observations daily over the following 14 days will allow tests of models of the evolution of the ejecta.

The source of certain r-process (i.e. heavy) elements is controversial, theoretical studies favor creation in NS mergers over SNe. Observations of the evolving GW source EM spectrum as described above will allow the characterization of the expected r-process elements and settle the controversy (Kasen et al. 2015).

9.6 Understanding Progenitors of Gamma-ray Bursts: Connection to Supernovae and Kilonovae

GRBs are observed through the whole electromagnetic spectrum, from GHz radio waves to 10 MeV gamma-rays. Although each is unique, the bursts fall into two rough categories. Bursts lasting less than two seconds are classified as short, and those that last longer, the observed majority, as long. All of the confirmed long GRB host galaxies are actively forming stars. The total stellar mass in these host galaxies is low and their colors are bluer than present-day spiral galaxies. The ages implied for the progenitors of long GRBs are estimated to be < 0.2 Gyr which is significantly younger than the minimum ages derived for the early-type galaxies found to be associated with short GRBs. These results suggest that (1) long GRBs arise from young massive stars (e.g., Woosley & Bloom 2006), and (2) short GRBs are results of NS mergers (e.g., Berger 2014).

Observations of long GRBs at low redshifts clearly show that SNe arise from the GRBs themselves. However, clear spectroscopic confirmation of SNe is limited to low-redshift GRBs because at $z > 0.5 - 1.0$, the SN component is too faint and most of the important features are redshifted to NIR wavelengths. TMT/IRIS will enable spectroscopic identification of SNe in long GRBs at $z = 0.5 - 1.0$. For this purpose, continuous spectroscopic monitoring from $\sim$1 day to 30 days after the GRB is important. Even at low redshifts, for some GRBs, no SN component was discovered down to a flux limit at least hundreds of times fainter than the expected SN flux (Gehrels et al. 2006; Della Valle et al. 2006; Gal-Yam et al. 2006). Spectroscopy with TMT/WFOS will be important to search for the SN component in low-redshift GRBs if GRBs are possibly associated with faint SNe.

In contrast to long GRBs, any SN-like event accompanying short GRBs is currently limited by observation to being over 50 times fainter than normal SNe Ia or Type Ic hypernovae (Kann et al. 2011). Recently, a NIR excess associated with a short GRB (Tanvir et al. 2013; Berger et al. 2013) was broadly consistent with the expectation of an r-process powered kilonova (Barnes & Kasen 2013; Tanaka & Hotokezaka 2013) (see Sect. 9.5). However, current observational data are only one

NIR photometric point with HST, and the source is too faint for spectroscopy. To fully understand the progenitor of short GRBs, TMT/IRIS will be the ideal instrument to perform ToO NIR spectroscopic observations of kilonova event associated with short GRBs, at a timescale of $\lesssim 1$ day.

9.7 Probing The High-z universe with Gamma-ray Bursts

While interesting on their own, long GRBs are rapidly becoming powerful tools to study the high-redshift universe and galaxy evolution due to their apparent association with massive star formation and brilliant luminosities (Pandey 2013). There are three basic ways of investigating the evolution of luminous matter and gas in the universe: (1) direct detection of host galaxies in emission (in the UV/optical/NIR for the un-obscured components, in the FIR/sub-mm/radio for the obscured component), (2) the detection of galaxies selected in absorption along the lines of sight to luminous background sources, traditionally QSOs, (3) diffuse extragalactic backgrounds. Studies of GRB hosts and afterglows can contribute to all three of these methodological approaches, bringing in new, independent constraints for models of galaxy evolution and of the history of star formation in the universe.

Absorption spectroscopy of GRB afterglows is now becoming a powerful new probe of the ISM in evolving galaxies, complementary to traditional studies of background-quasar absorption line systems. The key point is that the GRBs probe lines of sight in the dense, central regions of their host galaxies. In contrast, the background-quasar absorption systems are selected by the gas cross section, and favor large impact parameters, mostly probing the gaseous halos of intervening or foreground field galaxies, where the physical conditions are very different to the dense central regions where GRBs occur. The growing body of data on GRB absorption systems shows exceptionally high column densities of gas, when compared to the typical quasar absorption systems. This opens the interesting prospect of using GRB absorbers as a new probe of the chemical enrichment history in galaxies in a more direct manner than with the quasar absorbers, where there may be very complex dynamics of gas ejection, infall, and mixing at play.

Possibly the most interesting use of GRBs in cosmology is as probes of the early phases of star and galaxy formation (e.g., Robertson & Ellis 2012), and the resulting re-ionization of the universe. GRBs are bright enough to be detectable, in principle, out to much larger distances than those of the most luminous quasars or galaxies detected at present. Within the first minutes to hours after the burst, the optical light from afterglows is known to have a range of visual magnitudes far brighter than quasars, albeit for a short time. To identify GRBs to be high-z events, prompt NIR spectroscopic observations of high-z GRBs are essential. Required response time is $\sim$5 minutes from the discovery (discovery is essentially instantaneous) and brightness changes of up to a factor 10 per minute can occur.

9.8 Studying Tidal Disruption Events and Supermassive Black Holes

The nuclei of some galaxies undergo violent activity, with quasars being the most extreme instances of this phenomenon. Such activity is short-lived compared to galactic lifetimes, and was more prevalent when the universe was only about one-fifth of its present age (Kormendy & Richstone 1995). Dead quasars – massive BHs now starved of fuel, and therefore quiescent – should be more common than active quasars and are now being discovered in nearby galaxies (Ho 2008). The presence of these BHs is not surprising – we expect to find a BH in most galaxies on the basis of the number density of quasars and their typical lifetimes (Soltan 1982; Chokshi & Turner 1992). But we must ask a further question: can a BH lurk in these quiescent galaxies without showing other evidence for its presence? So could a BH be so completely starved of fuel that it does not reveal its presence? The search for switched off, dim or dead engines – starving BHs – has therefore become one of the hottest topics in extragalactic astronomy.

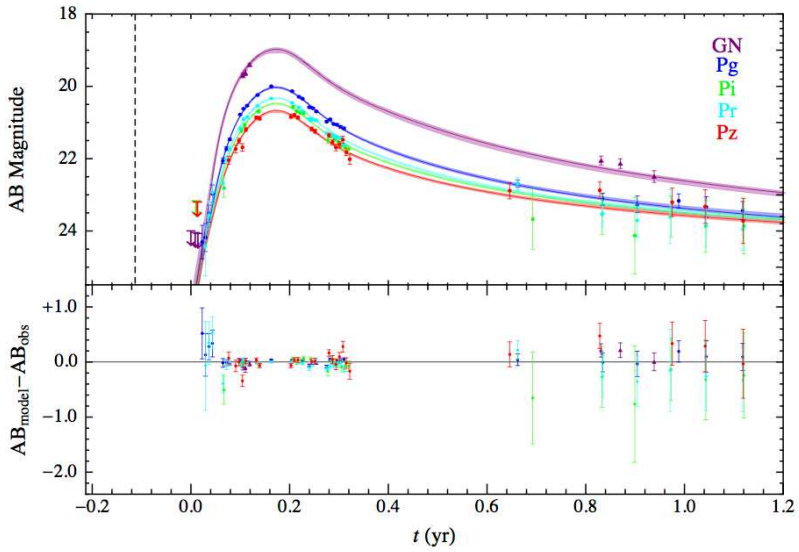

Fig. 81 Observed and modeled light curves of TDE PS1-10jh (Guillochon et al. 2014).

Each star near a massive BH traces out a complicated orbit under the combined influence of all other stars and the BH itself. Due to the cumulative effect of encounters with other stars the orbits gradually diffuse. If a star wanders too close to the BH it is violently ripped apart by the black hole's tidal field – a TDE (Rees 1988). About half of the debris of tidal disruption eventually falls back and accretes onto the BH. This accretion powers a flare, which is a definitive sign of the presence of an otherwise quiescent SMBH and a powerful diagnostic of its properties, see also Section 6.5.

Only two claimed TDEs capture the rise, peak and decay of the flare (Gezari et al. 2012 and Chornock et al. 2014), see Figure 81. Capturing all three phases photometrically and with additional spectroscopic information, these impressive data sets have already shown several interesting behaviors indicating that TDEs are not as simple as one might first guess. The light curve is consistent with the bolometric luminosity closely following the rate of mass fallback (Guillochon et al. 2014, see Figure 81), suggesting that the accretion disk viscous time is significantly shorter than the fallback time, and that the returning material must circularize by the first epoch of observation. The spectra resemble a single blackbody, with a temperature that evolves weakly in time, and a radius 10 times larger than the tidal disruption radius. As the light from the accretion disk itself should appear as a superposition of hotter blackbodies, this hints at the presence of a spatially extended reprocessing region surrounding the disk. The fact that broad HeII emission lines are seen, but hydrogen lines are missing suggests that material may be highly ionized, and outflowing at velocities $\sim$10 000 km s^{-1}, reminiscent of the BLRs found around some steadily-accreting AGNs.

Ongoing and future transient surveys and future radio surveys are predicted to discover 10–100 such events per year (van Velzen et al. 2011). Depending on the BH mass, these events are expected to last for a few days to a few months. Imaging with TMT's IRIS would precisely establish the position of the source. Optical spectroscopic follow-up observations provide diagnostics which help elucidate the demography of massive BHs in the local universe. Data should be taken in the rise, peak, and decay phases with frequent cadence. Each of these phases of a TDE contains vital information about the disruption, and can be used to constrain the properties of the host BH and the object that was disrupted.

The modeling of tidal disruption will also be significantly improved once a large sample of TDEs has been collected. Tidal disruptions offer a unique opportunity to study a single BH under a

set of conditions that change over a range of timescales. TDEs offer the firmest hope of studying the evolution of their accretion disks for a wide range of mass accretion rates and feeding timescales. For a disruption with a well-resolved light curve, models permit a significant reduction of the number of potential combinations of star and BH properties, enabling a better characterization of the massive BH and the dense stellar clusters that surround them The TMT will allow the detection and study of TDEs up to much higher redshifts than previously possible. Because of the "negative" K-correction (TDEs emitting primarily in the restframe UV with a characteristic 10^5 K blackbody) TDEs will be visible by TMT to redshifts of 6 or larger, enabling constraints on SMBH properties and evolution over a vast range of cosmic time.

9.9 Time Domain Studies of AGNs and Blazar Variability

Blazars, the most extreme variety of AGNs and the most luminous long-lived individual objects in the universe, are powered by accretion of gas onto SMBHs ($\sim 10^{8\pm2} M_{\odot}$). A pair of oppositely directed jets of magnetized, high-energy plasma continuously flow outward at speeds up to $\sim 0.998c$, presumably along the rotational poles of the BH system. Since the radiation observed from blazars is non-thermal and the luminosities are so high yet extremely time-variable, electrons (including any positrons) in the jet must be accelerated with high efficiency to energies exceeding $\sim 10^4$ to $10^5 mc^2$ as blazars are seen to emit TeV gamma-rays. Shock waves, turbulence, and magnetic reconnections have all been proposed as the main means of particle acceleration, and all three might be operating inside relativistic jets. The efficiency of particle acceleration by these processes is strongly dependent on the magnetic field geometry. In the case of shocks, charged particles follow the magnetic field lines back and forth across the shock front. The efficiency of acceleration depends on the angle that the magnetic field subtends to the shock. In MHD turbulence, the energization occurs statistically as particles bounce off randomly moving regions of stronger-than-average magnetic fields. In reconnections, particles become trapped in shrinking magnetic flux tubes or in converging, oppositely directed field lines created by current sheets. Each of these processes has a different signature of time-variable linear polarization: in shocks, a favored polarization direction parallel to the shock front during peaks in flux; in turbulence, low, rapidly fluctuating polarization vectors with higher amplitudes of variations on longer timescales; and in reconnections, polarization in a direction that remains stable during a flare but changes from one flare to the next. Discerning among these possibilities requires precise spectropolarimetric monitoring on timescales as short as a few minutes with the TMT in order to measure fluctuations in polarization and flux on. This will determine the power spectrum of the fluctuations down to small size scales, testing emerging models of particle acceleration and blazar variability (e.g., Sironi & Spitkovsky 2014; Marscher 2014). It will be particularly important to follow with the TMT the changes in optical/NIR polarization during the night of a blazar being observed by the future Cherenkov Telescope Array in order to relate acceleration of the highest-energy electrons to the magnetic field direction.

Variability of AGNs in the optical is typically about 10% over all timescales from less than an hour to years. There is a wide range of stochastic behavior between different AGNs. Fully characterizing the stochastic properties of spectro-photometric measurements is vital to refining the model for the emission process and discerning between the possible AGN emission mechanisms.

Figure 82 shows light curves collected with Kepler of two AGNs. The power spectra show that neither light curve is consistent with the simple stochastic random walk model for variations (Mushotzky et al. 2011; Carini & Ryle 2012; Kasliwal et al. 2015). The lack of faster sampled spectro-photometric measurements constrains further understanding. The Kepler data are insufficient to study AGN variability data as a function of radial position within the accretion disk of the AGN.

The TMT will provide new capabilities for studying the structure of AGNs. Moderate resolution optical and MIR spectra will make it possible to observe rapid changes in the spectral features of nearby AGNs on timescales as short as $\sim$1 hour, sampling every few minutes, allowing us to map

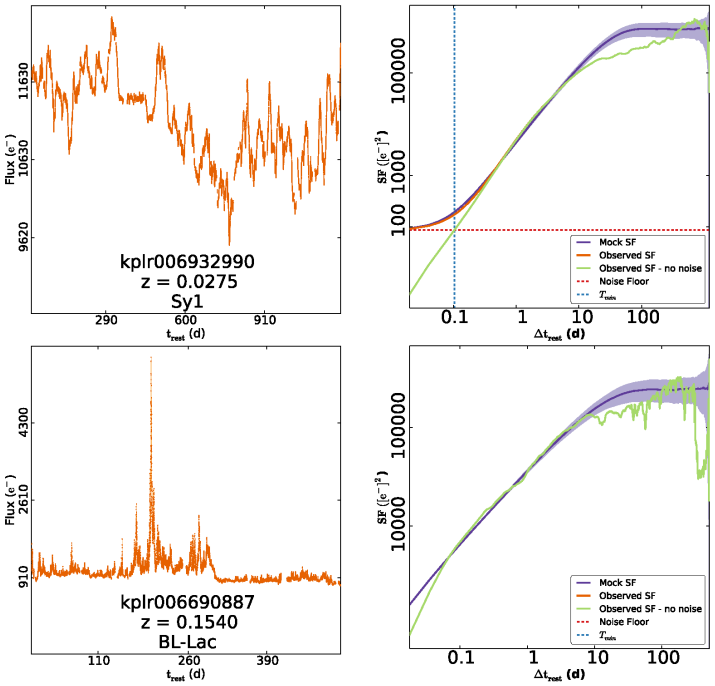

Fig. 82 *Top left*: Kepler light curve of Seyfert Zw 229-15 and, *Right*: The power spectrum indicating that the fastest variations are on a timescale of ∼2 hr. *Bottom left*: The Kepler light curve of BL Lac kplr006690887 showing fast flares and, *Right*: The power spectrum indicating that the fastest variations are faster than the 26 min rest frame probed by Kepler.

out the structure of the accretion disk and BLRs with great accuracy and providing new insights into the structure of the jet region. TMT's instruments will also be able to probe the structure of the accretion disk region by performing rapid optical and MIR observations ($t_{\rm samp}$ ∼10 mins) to carry out reverberation mapping. Observational evidence (Bhatta et al. 2013) has led to the development of a model for micro-variability that predicts variations on timescales of less than 30 seconds, these predictions are supported by Webb et al. (2013) but the full investigation is severely limited by the need for high S/N optical and NIR low resolution wide wavelength coverage spectro-photometry with $t_{\rm samp}$ ∼1s to 3s.

9.10 Cataclysmic Variables

CVs are interacting binary systems with an accreting WD primary and a main sequence mass losing M star secondary. The binary orbital periods in these systems typically range from tens of minutes to a few days. CVs display a wide range of variability, be it accretion disk related phenomena or nova outbursts due to thermonuclear runaway in the accreted hydrogen-rich material.

9.10.1 Investigating the dissipative process in cataclysmic variable accretion disks and disk evolution during outburst cycles

Accretion is a very common process in astrophysical systems but is very poorly understood. CV accretion diss are a very convenient laboratory for studying the angular momentum dissipation

mechanism and the relation between dissipation and disk density, temperature, magnetic field and RV profile. CVs display rapid variability related to the accretion process that has timescales from sub-second to hours due to a number of reasons; interactions of the disk and mass transfer stream, processes in the accretion disk itself (as modeled by Ribeiro & Diaz 2008) and accretion onto the compact primary, which may be influenced by magnetic fields. The location of the source of the variability can be isolated by studying the temporal variations in the velocity of the emission and in some systems by eclipse mapping. Combining the velocity and temporal information from time resolved spectroscopy with the method of eclipse mapping and monitoring disk changes on a weekly basis will transform our understanding of the processes occurring within CV accretion disks, particularly in systems whose disks display changes in state or have regular outbursts on timescales of months.

For example, in rapid (72 ms) spectroscopic observations of a bright ($M_v \sim 11$) dwarf nova short (2 to 3 minute) flares were found whose temporal and spectroscopic behavior were consistent with arising in the accretion disk (see Fig. 83) and could be described with a Fireball model (Pearson et al. 2005). From broadband photometry Baptista & Bortoletto (2008) and Baptista et al. (2011) respectively derived the spatial distribution of flickering in the disks of the nova-like UU Aqr and the systematic changes in the flickering distribution across the disk through an outburst of the dwarf nova HT Cas when the disk collapsed.

Time resolved optical spectrometry with WFOS with $R = 4000$, duration about 20 minutes centered on mid-eclipse and $t_{\rm samp} = 50$ ms will give S/N$\sim$1000 in each resolution element for $M_v \sim 15$ (calculated with TMT-J ETC). At this magnitude there are an order of 100 eclipsing CVs (*http://www.mpa-garching.mpg.de/RKcat/cbcat*) that show a range of different accretion disk behaviors, allowing the development of a comprehensive understanding of accretion disk physics that is impossible to obtain with existing facilities.

9.10.2 Revealing the geometry and populations of classical novae

Nova systems serve as valuable astrophysical laboratories in the studies of physics of accretion onto compact, evolved objects, thermonuclear runaways on semi-degenerate surfaces that give insight into nuclear reaction networks, and line formation and transfer processes in moving atmospheres. Nova outbursts are seen in all wavelengths from γ-ray to radio and can reach $M_v = -10$ mag, placing them among the brightest transient sources known. The outburst intervals range from decades (recurrent novae) to thousands (classical novae) of years. Novae can rise in luminosity by $>$6 mags in a day, with a rise time of about 1 to 2 days in the very fast novae, while the slowest novae have a rise time of the order 10s of days. The outbursts generally cause the systems to increase in brightness by about 10 mags at the peak. The decline rates can be between $\sim$1 mag/day to $\sim$0.03 mag/day, depending on the speed class of the nova. The nova outburst characteristics are particularly sensitive to the mass of the accreting WD (e.g., Starrfield et al. 2012). The high luminosities, coupled with a rate of $\sim$ 35/yr in a galaxy like our own (Shafter 1997), make novae ideal for probing the properties of close binary stars in varied (extragalactic) stellar populations.

The geometry of novae is important for understanding the explosive process on the surface of the compact star. Nova shells have revealed polar-blob, equatorial-ring geometry and/or multiple blob-like condensations in the shell. There is also increasing evidence that nova phenomenology is best explained by non-spherical ejecta, see Figure 84 (e.g., Woudt et al. 2009; Ribeiro et al. 2011). One leading scenario to explain such observations as well as spectrophotometric development of novae is bipolar (although not jet-like) mass ejection (Shore 2013). Alternatively, the ejecta may consists of blobs of very high density gas that expand to create within each clump a wide range of emitting density, ionization, and velocity, while the circumbinary envelope is more homogeneous (Williams 2013).

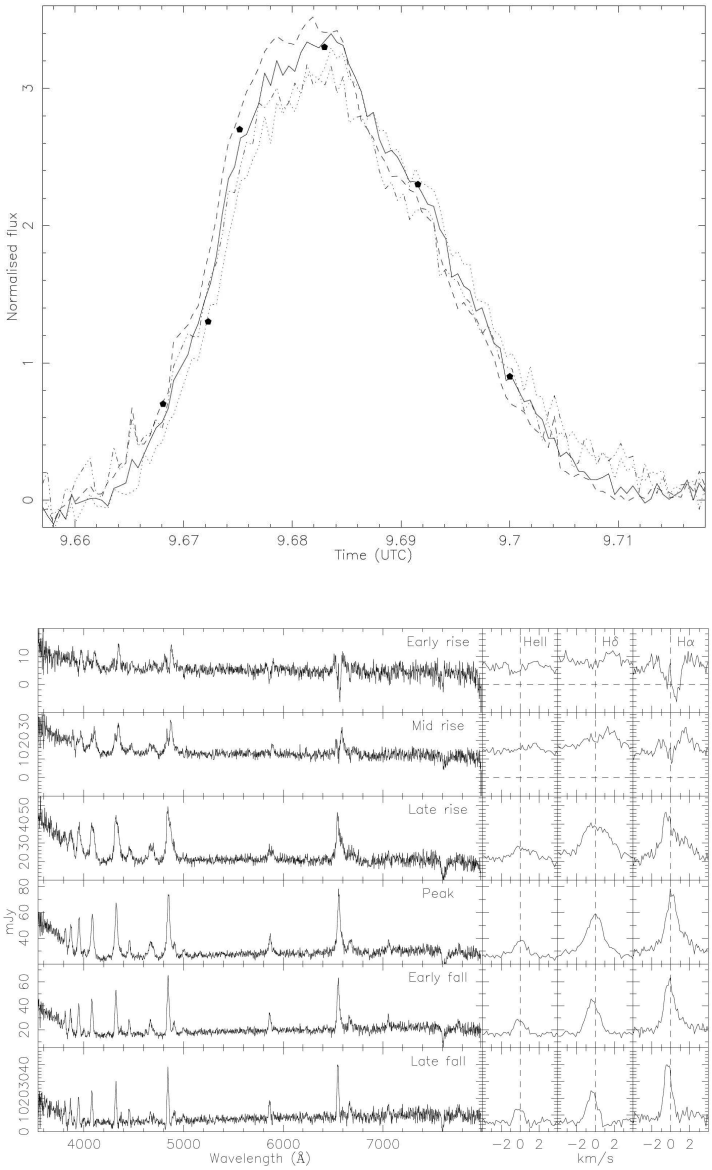

Fig. 83 *Top*: Continuum light curves of a small flare seen in the Dwarf Nova SS Cyg. Observations were made with Keck/LRIS. Light curves are 3615A (*dot-dashed*), 4225A (*dashed*), 5500A (*solid*) and 7320A (*dotted*). *Bottom*: Spectra at times (*dots in top panel*) throughout the flare (Skidmore et al. 2004).

The geometry of the postoutburst structure of novae will be further constrained by coordinated spectroscopic follow up of novae over all wavelength regimes. Since important aspects of the ejecta activity occur at the time of outburst, spectral studies are best conducted as early as possible. The timely discovery of outbursts before maximum light occurs by the large surveys, such as LSST, will enable early observations. Spectrophotometry and spectropolarimetry ($R \sim 5000-30\,000$) would be

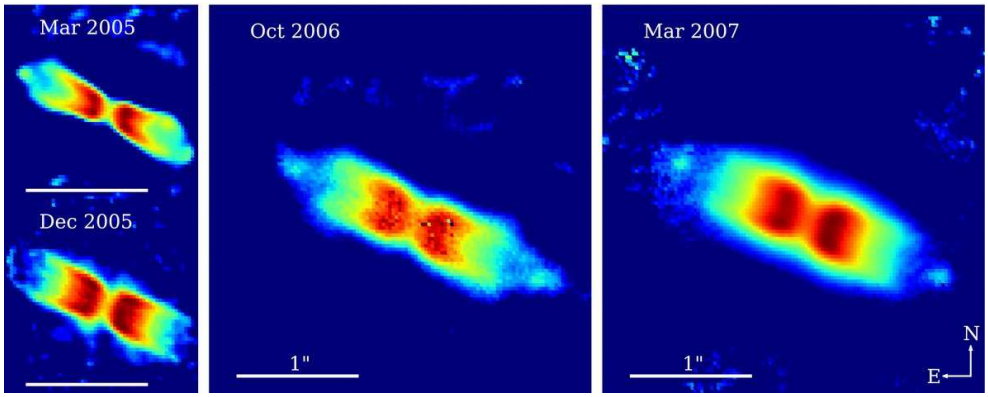

Fig. 84 Expanding bi-polar shell of the helium nova V445 Pup (2000) imaged in the NIR K_s band using the NAOS/CONICA AO system on the *VLT* (Woudt et al. 2009).

required to establish the presence of the two distinct components and blobs, and the evolution of the spectrum as the fireball progresses. Spectropolarimetry, in particular, holds the key as polarimetric measurements will help quantify the degree of non-spherical symmetry in the early expanding nova shell.

The geometry of the expanding fireball can also be studied by direct imaging. A nova at 5 kpc (novae have been observed at distances 1–10 kpc) which is ejecting mass at 1000 km s^{-1} (ejection velocity ranges from 300 km s^{-1} for slow novae to 10 000 km s^{-1} for the very fast novae), as seen from the Earth, will have an ejected shell of size 10 mas (0.01″) in around 87 days. For a very fast nova, the time taken would be around 9 days. [10 mas is chosen because it is $\sim 2\times$ pixel sampling of IRIS]. If the nova is at 1 kpc and ejecting mass at 1000 km s^{-1}, it will have a size of 10 mas in 17.4 days. Thus, outbursting novae can be observed as extended objects after the first week of outburst. A nova situated even 10 kpc away would be very bright (e.g. $M = -9 => m = 11$ even with 5 magnitudes of extinction) for the TMT. A solution to this would be to use AO combined with coronographic techniques. For studying the early fireball phase of novae, the occulting mask needs to be 10 mas or slightly bigger[3]. The geometry and evolution of the expanding fireball have in recent years been studied using NIR interferometric imaging (e.g. Chesneau & Banerjee 2012; Schaefer et al. 2014) but studies are limited to the very rare cases where the system rises to $M_{\rm app} < 6$. Direct imaging with TMT+AO will open up several orders of magnitude more targets to studies with IFU type instruments.

In addition to Galactic novae, novae have been observed in more than a dozen galaxies, some as distant as the Coma Cluster (Shafter et al. 2011, 2014). Photometric and spectroscopic observations of novae in the Local Group suggest that galaxies dominated by a younger stellar population (M33 and the LMC) generally tend to host novae with a faster photometric evolution. The question that arises is; are there really two distinct populations of novae that are dependent on the metallicity and star formation history of its host galaxy? Observing the evolution of the spectrum of an increased number of extragalactic novae would provide an answer. So far, 8–10 m class telescopes have been efficiently used to photometrically detect novae in the Fornax cluster of galaxies at 20 Mpc, but spectroscopic observations have been difficult. With the TMT, one could easily do optical spectroscopy of novae at this distance.

[3] A 10 milli-arc second occulting mask translates to 22 microns at the TMT focal plane.

9.11 Improving the Hubble Constant and Measuring Extragalactic Distances

Cepheid variables are the primary distance indicator for galaxies with recent star formation. They are very luminous at NIR wavelengths, with $M_{\rm abs}$ from -6 to -8.5 for periods of 20 and 100 days, respectively. The intrinsic dispersion of the NIR Period-Luminosity relation is 0.1 mag (Persson et al. 2004), making it possible to obtain Cepheid-based distances with statistical uncertainties of a few percent for modest sample sizes. In the absence of recent star formation, RR Lyrae variables provide a suitable alternative, although their range is much more limited given their considerably fainter luminosities ($M_{\rm k} = -0.55$ at $P = 0.5$ d, Benedict et al. 2011).

By 2018, Gaia will measure parallaxes for ∼5000 Milky Way Cepheids (Windmark et al. 2011), resulting in an absolute calibration of the Period-Luminosity relation with sub-percent systematic uncertainty. Similarly, Gaia will deliver an excellent calibration of the more plentiful RR Lyraes. We can readily envision two applications of TMT for extragalactic variables, both relying on diffraction-limited imaging with IRIS: (1) improving the determination of the Hubble constant ($\rm H_0$) and (2) measuring extragalactic distances to the Coma Cluster ($D < 100$ Mpc).

Reducing the uncertainty of the Hubble constant below 1% would play a critical role in the determination of cosmological parameters (Weinberg et al. 2013). By providing largely orthogonal constraints with other cosmological probes (e.g. high-redshift SNe, CMB anisotropies and BAO), a precise determination of $\rm H_0$ would serve to critically test the need for "new Physics" beyond the ΛCDM model, such as a time-dependent component in the dark energy EOS or additional neutrino species.

A potential key program could be to use TMT to greatly improve the NIR photometry of Cepheids already discovered with HST in a dozen nearby hosts of SNe Ia ($D < 50$ Mpc Riess et al. 2011). Current studies are limited by crowding due to HST's angular resolution and coarse sampling of WFC3/IR, yielding Period-Luminosity relations with dispersions $3\times$ larger than the intrinsic width. Diffraction-limited images with TMT/IRIS will give a $> 10\times$ increase in angular resolution and $25\times$ finer pixel scale, removing biases due to crowding, yielding a $3\times$ improvement in distance uncertainty. S/N = 50 photometry can be obtained in less than 120s (Japan TMT ETC) for any object of interest (the faintest being a 20-day Cepheid at 50 Mpc, with $K = 26.8$ mag). Several neighboring fields (within $2'$ of each other) containing Cepheids of the same host galaxy could be observed in quick succession.

Once the JWST mission is complete, and in the absence of any comparable space-based assets, TMT will play a unique role in Extragalactic Distance Scale work. Precise extragalactic distances have many other useful applications; e.g. the accurate calibration of the bulge luminosity and BH mass relation, which cannot be performed using samples in the Hubble flow. NIR AO imaging with TMT/IRIS will set xtragalactic distances beyond 10 Mpc, using either RR Lyrae ($P_{\rm cyc}$ ∼0.5 day) out to $D \sim 1$ Mpc (requiring ten ∼1hr exposures) or Cepheids out to the Coma Cluster ($D = 100$ Mpc, requiring 1.5 hours of telescope time per integration and 10 observations over several months) for late-type systems.

9.12 Summary of Requirements

Table 6 summarizes requirements for the telescope and instruments to realize the science cases described in this chapter. In order to maximize scientific outcome from time-domain astronomy, response time for ToO observations and sampling time for time-resolved observations are especially important, these requirements are summarized in Figures 85 and 86.

10 EXOPLANETS

In the past two decades, our inventory of known planets has grown from just the eight in our solar system to over one thousand *extrasolar* planets detected around nearby stars through a variety of

Table 6 Summary of Requirements for Time-Domain Science. Capabilities which are not planned for the first-generation instruments are written in Italic font. The absolute accuracy on the timestamp depends on the particular science program but a general rule of thumb is $t_{\rm error} < 0.1 t_{\rm int}$ where $t_{\rm error}$ is the uncertainty on the mid-point of the time when photons are actually hitting the detector.

Science Case	Response time	Sampling time[1]	Cadence	Brightness (mag)	Observing mode	Notes
SNe Ia evolution (9.1.1)	3–10 days	–	3–10 days	24 (NIR)	$R = 500$ NIR spectroscopy	Synergy with surveys
SNe Ia explosion mechanism (9.1.2)	1 hr - 1 day	–	Initially 1hr After 30 days weekly for 2 years	26 (opt.) 23 (NIR)	$R = 500 - 3000$ opt./NIR spectroscopy	Synergy with surveys Need spectropolarimetry
CCSNe shock breakout (9.2)	1 hr	–	1hr for 3 days	26 (optical)	$R = 500$ opt. spectroscopy	Synergy with surveys
Luminous high-z SNe (9.3)	10 days	–	10 days	26 (opt., NIR)	$R = 500$ opt./NIR spectroscopy	Synergy with surveys
NIR search Low-z SNe (9.3)	3 days	–	10 days	25 (NIR)	$R = 500$ NIR spectroscopy	
SNe CSM (9.4)	1 day	–	1 day	19–20 (optical)	$R \sim 30000$ opt. spectroscopy	
ID of GW sources (9.5)	1 day	–	1 day	26 (opt) 24 (NIR)	$R = 500$ opt./NIR spectroscopy	Synergy with GW astronomy
GRB-SN/ kilonova (9.6)	1 day[2]	1 hr (For short GRBs)	1 day	28 (opt) 26 (NIR)	Opt/ NIR spectroscopy ($R = 500$)	Synergy with X-ray/γ-ray surveys
High-z GRBs (9.7)[3]	$<$ 1 hr	1 min initially	1hr - 1 day after 1$^{\rm st}$ 2 hours	> 22	*NIR high-resolution spectroscopy*	Synergy with X-ray/γ-ray surveys
TDEs (9.8)	1 day	–	1–10 day	> 22	Optical/ NIR spectroscopy	Synergy with surveys
Accretion disk in CVs (9.10.1)	$<$ 1 hr from discovery with LSST	50 ms for up to a few hours	daily to weekly	15 (opt)	Time resolved spectroscopy ($R = 4000$)	*Spectropolarimetry for magnetic CVs*
Classical novae - Early evolution (9.10.2)	1hr -1 day	–	1 hr	10–25	*R ∼30 000 Opt./ NIR spectroscopy / spectropolarimetry*	*Synergy with wide field surveys*
Classical novae - geometry (9.10.2)	$\sim$ 10 days	–	None	10–19	NIR AO imaging with occulting mask	
Extragalactic distance (9.11)	–	–	3–5 days Cepheids, 1h RR Lyr	27 (NIR)	NIR imaging	Synergy with LSST, HST, and JWST
AGN reverb mapping (9.9)	–	$>$ 10 mins for a few hours	–	17 to 22	$R =$ 1k to 4k Opt./ NIR spectroscopy	
Blazar jet $\mu-$variability (9.9)	–	1s to 3s	–	17 to 22	$R = 500 - 3000$ Opt./ NIR spectroscopy	
Blazar jet Polarimetry (9.9)	–	$\sim$ 30s to 2 minutes	–	17 to 22	*R=500–3000 Opt./ NIR spectropolarimetry*	

[1] Sampling time relates to the integration and deadtime of individual exposures in sequences of time resolved observations that require fast detector readout schemes. If single observations that are repeated on longer timescales then this is captured in the Cadence and nothing is reported in the Sampling time.

[2] Prompt observations with response time of $>$10 minutes, sampling cadence of $\sim$ 1 s, spectral resolution of $\sim$100 in the optical and NIR are needed to study the GRB fireball.

[3] Some ideas for observations of High-z GRBs require faster sampling and lower spectral resolution.

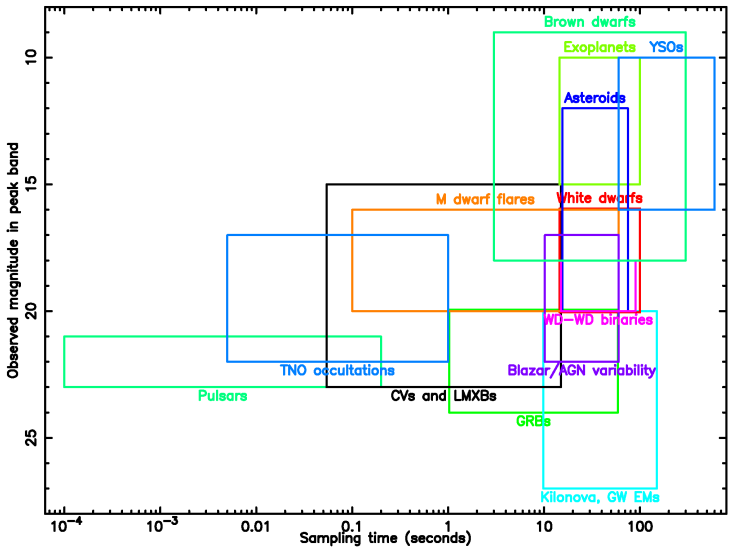

Fig. 85 The ranges of sampling times required for observations of variable objects. In some cases the objects are continuously variable, observations can be scheduled at any time, in other cases rapid observations are needed to follow a transient object after a rapid response ToO program is initiated (see Fig. 86).

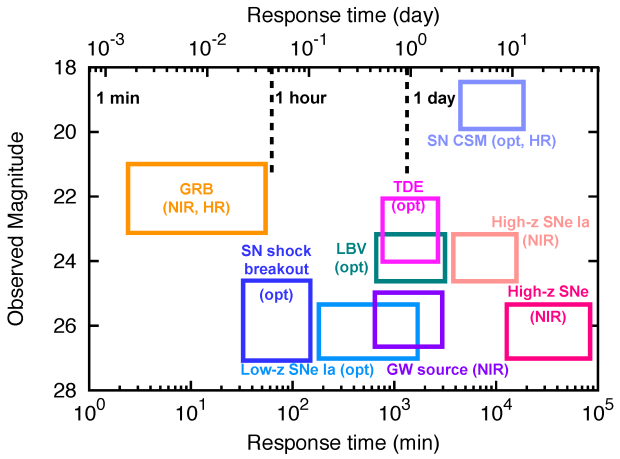

Fig. 86 Required ToO response time for different science cases.

techniques (e.g. Mayor & Queloz 1995; Charbonneau et al. 2000; Marois et al. 2008). Extrasolar planets have been found orbiting the youngest stars to post-main sequence stars and around subsolar to intermediate-mass stars (Kraus & Ireland 2012; Currie et al. 2014b; Sato et al. 2003; Johnson et al. 2010). Statistical studies of exoplanets suggest that planet formation is common, occurring around about half of nearby Sun-like stars (e.g. Howard 2013 and references therein).

Extrasolar planets are a diverse population, spanning a wide range in mass and orbital separation. Some exoplanets have similar properties (i.e. mass, orbital separation) to those in our own solar system. However, nearby exoplanets detected by two main methods – Doppler radial velocimetry and transit photometry, and distant exoplanets discovered by microlensing and direct detection, have revealed entirely new classes of planets such as hot Jupiters, super-Earths, and wide-separation super-jovian planets.

Although extrasolar planets discovered thus far have provided important clues about the context within which the Earth and other solar system planets fit, our knowledge of the overall census remains highly incomplete. We have good constraints on the (high) frequency of planets larger than the Earth with orbital periods less than 100 days and on (the dearth of) the widest-separation, most massive planets (e.g. Howard et al. 2012; Nielsen et al. 2013). However, other classes of planetary systems are almost entirely unexplored – e.g. massive planets beyond a few AU, or planets with radii smaller than Earth. Furthermore, our knowledge about the physical properties of exoplanets (e.g. density, atmospheric/bulk composition) is much weaker, and is restricted to a handful of favorable cases. While we have detected both rocky planets and planets located on Earth-like orbits (e.g. Howard et al. 2013), we have yet to conclusively identify a true (potentially habitable) Earth twin around a Sun-like star, let alone determine their frequency.

The TMT will provide an enormous advance in our ability to identify and characterize extrasolar planets. New technological advances – e.g. high-precision Doppler measurements, high-precision space-based photometry, and advanced AO – have driven a large number of exoplanet discoveries. The TMT's instrumentation will generate an incredible number of additional discoveries, will drastically expand the kinds of planets we can detect, will provide a rich understanding of these planets' physical properties, and will potentially yield the first detections of habitable rocky planets.

10.1 Doppler Detection of Planetary Systems

With echelle spectrometers approaching the 0.1 m s^{-1} RV measurement precision threshold needed to detect habitable Earth mass planets around Sun-like stars, the continuation of Doppler surveys on state-of-the-art telescopes is imperative. Such surveys, conducted with the optical and infrared echelle spectrometers being built for the TMT, have the potential to complete the census of Earth-mass planets in our stellar neighborhood. The collection of such systems will provide a valuable sample for follow-up programs to characterize their atmospheres through direct imaging.

Prior to the launch of the Kepler telescope in 2009, RV surveys were the dominant method for discovering new exoplanetary systems, with over 400 systems discovered between 1995 and 2009 (*http://exoplanets.eu*). During the first decade and a half of the planet discovery era, Doppler surveys expanded their reach and progressed steadily from measurement precisions of 3–10 m s^{-1} to 1 m s^{-1} as a consequence of improvements in instrument stability and data analysis methods.

The RV method originally focused on finding exoplanets around main sequence FGK stars. These targets are ideal, both due to their similarity to our Sun, and due to the abundance of atomic lines in their spectra. The gravitational velocity perturbation exhibited by the host star is directly related to the mass of the planet and is inversely related to its orbital distance. Hence, the RV detection method is most sensitive to massive, close-in planets. This ease of detection led to a substantial number of early discoveries of 'hot Jupiters', but as observing temporal baselines grew longer and as measurement sensitivities improved, the Doppler searches gradually expanded into more of the exoplanet phase space. As more planets were discovered, key physical trends began to emerge. Notable examples include a correlation between planet occurrence and stellar metallicity (Fischer & Valenti 2005; Johnson et al. 2010), a peak in the distribution of planets with orbits of 3 days (Cumming et al. 2008), and a gradual increase in the number of planets with increasing period and decreasing mass (Cumming et al. 2008). RV surveys have also lead to the discovery of complex planetary systems like HD 69830, which has three Neptune-mass planets and an asteroid belt (Lovis et al. 2006; Beichman

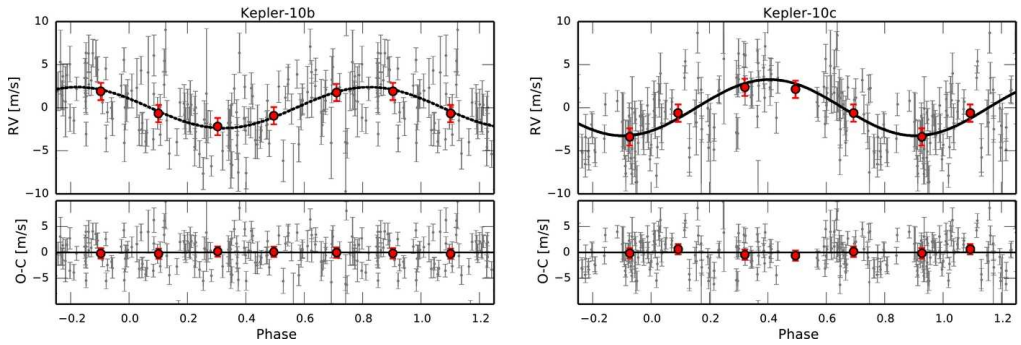

Fig. 87 HARPS measurements of RVs for the system Kepler 10 showing the separate phased components for Kepler 10b and Kepler 10c (Dumusque et al. 2014). For this faint Kepler star, TMT observations would be significantly more precise.

et al. 2005), the multiple-planet system orbiting the M dwarf, GJ 581 (Mayor et al. 2009) and the planet around the nearby young dusty star ε Eridani (Hatzes et al. 2000; Benedict et al. 2006). RV planet detection programs are naturally limited to planets with periods that are shorter than the length of the survey, which currently amounts to somewhat more than 5 AU for the longest-running projects (Jupiter, for example has a 11.86 year orbital period and induces a 12 m s^{-1} RV half amplitude). In recent years, a major focus has been on RV observations for characterization of transiting systems, particularly those discovered by the Kepler mission; the joint detection of a planet via radial velocimetry and transit photometry is exceptionally powerful, allowing measurements of planetary densities (Fig. 87).

With multiple ongoing RV surveys focused on nearby stars, and improvements in both the hardware and RV data analysis techniques, imminent technical goals include pushing the RV precision beneath the $\sim$ 1 m s^{-1} state-of-the-art threshold. Optical RV measurement precisions have advanced to the point where 1–2 m s^{-1} observations are routine with high temporal stability using high-resolution instruments such as Keck/HIRES Lick/APF, and Magellan/PFS (all using iodine cells) and ESO/HARPS and HARPS-N (using fiber scrambling and ThAr calibration). Under ideal circumstances, observers have reached 70 cm s^{-1} single measurement precision (Lovis et al. 2008). RV measurments have reached the point where they are confronted by limitations such as the intrinsic RV noise of F and G stars, and to where further advancement requires new technology for calibration sources (Lovis et al. 2006; Udry & Mayor 2008; Osterman et al. 2007; Li et al. 2008).

An RV precision goal of 0.1 m s^{-1} has been set for the ESPRESSO (Echelle SPectrograph for Rocky Exoplanet- and Stable Spectroscopic Observations, on-sky 2016) optical echelle spectrograph that will be deployed on the VLT (Pepe et al. 2013). Doppler precision measured in mere centimeters per second will only be accomplished with instruments that have very high spectral resolution ($R > 100\,000$) and fiber-scrambling capabilities to aid with spectral stabilization. Achieving this precision, of course, also requires very high S/N and hence a bright star with long exposures. Probing a large sample of stars at this precision will require a telescope such as TMT.

The past decade has also shown the exceptional power of RV techniques in synergy with transit observations. Only for planets with both transit radius measurements and RV mass measurements can we determine density, and by extension, clues to the physical composition of the planets. With Kepler's demonstration that small (1–4 $R_{\rm E}$) planets are common, the next step in understanding the frequency of earthlike planets is to determine the density of a significant number of these planets, especially those at large semi-major axes. The time needed for these RV observations are a significant bottleneck in completing Kepler's scientific legacy. The TESS mission will have a similar need for

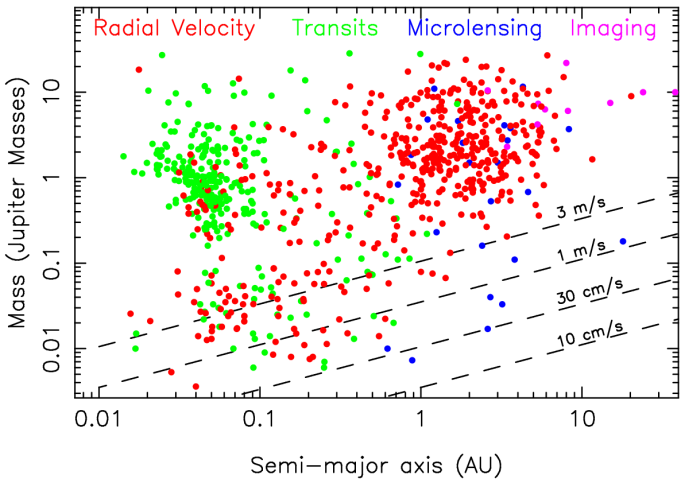

Fig. 88 Known extrasolar planets and Doppler sensitivity. Dashed lines show the typical detectable mass for a given level of Doppler precision, assuming edge-on circular orbits around a solar-type star.

RV follow-up (albeit around brighter stars, but needing even higher levels of precision.) A high-precision RV capability, particularly optimized for late-type stars, on TMT, would be a powerful component of an integrated exoplanet roadmap, and would forge a near-complete understanding of nearby planetary systems.

10.1.1 TMT's role in Doppler studies of exoplanets

The TMT's primary advantage for both optical and infrared RV studies will be an increased sensitivity due to its larger collecting area as well as the suite of state-of-the-art echelle spectrometers that will be designed with RV exoplanet detection in mind. The two echelle instruments contemplated for the first decade of the TMT science program include the High Resolution Optical Spectrometer (HROS) and the Near-InfraRed Echelle Spectrometer (NIRES). Both will have similar spectral resolutions to the current echelle spectrometers responsible for hundreds of RV discovered planets. (MIR high-resolution spectrographs such as MIRES and the MICHI concept may also play a role in the Doppler detection of planetary atmospheres, see below). With current optical RV surveys limited to stars with $V \sim 14$ or brighter, the larger collection area of the TMT will allow us to be able to complete an RV survey of all FGK stars within 25 parsecs. The advantage of such a large aperture can only be realized with an echelle tailored for precision RV measurements. Such an spectrometer might also include external wavelength stabilization, image slicers, or a fiber-feed spectrograph similar to the designs set forward for the HROS and hence reach significantly better instrumental precision than Keck HIRES.

In the infrared, we will be able to significantly increase the number of M dwarfs that can be surveyed for habitable planets. The benefits of this investment would be substantial, and could extend those surveys being completed with SPIRou, CARMENES and the Habitable Zone Planet Finder (Amado et al. 2013; Delfosse et al. 2013; Mahadevan et al. 2012) to cover sub-Earth-mass planets across the entire range of the habitable zones for the more massive M3-M4 dwarfs that are the most common star in the solar neighborhood. The larger aperture will also extend our ability to detect planets around the latest M dwarf spectral types that are too faint to be efficiently surveyed down to the RV precision necessary to detect habitable Earth-mass planets. By combining the results from

both the optical and infrared surveys, the TMT will we will enable the definitive census of habitable planets around our nearest neighbors.

RV surveys of young stars have yet to produce a sufficient sample of planetary systems from which we can search for changes in the architecture of planetary systems with age. Such trends would provide insight into planet formation and evolution models. At distances of a hundred parsecs and more, only the most massive stars in nearby star formation regions like Taurus, the Hyades, Orion and Sco Cen are bright enough for RV planet search programs (i.e. Paulson et al. 2004; Quinn et al. 2014). The TMT will be able to push detection limits to solar-mass stars and below as well as allow for thorough surveys of hundreds of stars in much less time than what is currently possible with 10 m class telescopes. Direct imaging techniques (Sect. 10.2) will also favor young stars; the combination of Doppler monitoring and ExAO direct imaging could completely sample the giant planets around nearby young stars. Section 10.1.3 discusses how we might overcome the photospheric noise inherent to young stars.

Although a precision Doppler capability for TMT would be powerful, the exact scientific optimization is complicated. Targets for most programs are relatively bright, and although high S/N is needed for 10 cm s^{-1} precision, achieving that also requires multiple exposures to average over stellar oscillations. Instrumental and stellar noise sources may well set a floor that lies substantially above the photon noise floor of a 30 m telescope. Indeed, the development of Doppler capability on TMT would augment, rather than replace, large-scale programs on 6–10 m telescopes for mass determination of TESS transiting planets, coronagraphic planet discoveries, and blind searches for earth-mass planets. TMT could be exceptionally important for follow-up of fainter stars hosting highly unusual or interesting planet candidates (e.g. Kepler and PLAnetary Transits and Oscillations of stars (PLATO) discoveries or low-mass stars imaged with direct techniques), high cadence observations (e.g. Rossiter-McLaughlin effect), and of course for the characterization of the transiting planets' themselves (see Sect. 10.3).

10.1.2 Landscape in 2022

In addition to completing the survey of nearby habitable planets, the TMT will provide follow-up observations for numerous space-based NASA missions set to launch near TMT first light. Both HROS and NIRES will measure the masses of small transiting planets discovered by TESS (Ricker et al. 2014), K2 (Howell et al. 2014), and PLATO (Rauer et al. 2014) in specific high-value cases where it is imperative to obtain spectra with the highest possible resolution and S/N. TMT will also be able to collect supporting observations of the stars hosting planets detected with JWST, Gaia and AFTA-WFIRST. By the time TMT will be on-sky, some of these planets will have been known for many years, however the S/N needed to reach the RV precisions for planet confirmation will not be reasonably achievable without the TMT. If the TMT can deliver sufficient precision, its observations will determine whether the planetary mass-radius diagram for large terrestrial-mass planets differs for M dwarfs as compared to more massive solar type stars. This will directly probe the differences in planet formation, evolution, and migration as a function of stellar mass. Given the expected plethora of newly discovered and potentially complex planetary systems from these missions, the shorter total on-sky time needed to collect a statistically robust sample of RV measurements at RV precisions of < 1 m s^{-1} will be key to the efficient characterization of exoplanetary systems.

10.1.3 Limits to Doppler studies due to stellar activity

Even if the newest spectrographs are able to reach instrument precisions of $\sim$0.1 m s^{-1}, it is still not clear whether we will be able to reach this precision for all nearby stars due to their intrinsic photospheric RV noise due to starspots, granulation and p-modes. Such stellar "jitter" has lead to the mis-identification of a few extrasolar planets including the one around the young star TW Hydra

(Setiawan et al. 2008) which was quickly shown to be a false-alarm (Huélamo et al. 2008) produced by starspot activity. On the other hand, the recent discovery of Alpha Cen Bb with an RV semi-amplitude of only 51 cm s^{-1} in Dumusque et al. (2012) demonstrates that high cadence observations can partially overcome the limitations of stellar jitter. (Even the Alpha Cen Bb result, however, comes with a note of caution, see Hatzes 2013). Future RV surveys of young stars are being designed to collect measurements at both optical and at infrared wavelengths where the starspots produce a reduced RV perturbation (i.e. Crockett et al. 2012). Similarly, the combination of RV measurements from the TMTs optical and NIR echelle spectrometers could be used to discern between low-mass planets and stellar activity which plagues both M dwarfs and young stars.

Recent efforts comparing the photometric and RV variability of Kepler targets (Bastien et al. 2014) show a correlation between RV jitter and a value called the "flicker" which is the RMS of the photometry on an 8-hour timescale. It is currently unclear as to whether making similar measurements of nearby stars in an attempt to predict their RV jitter is feasible. If our goal is to survey all nearby stars for the presence of terrestrial planets, the M dwarfs - which constitute the majority of nearby stars - with typical rotational velocities and starspot populations will require hundreds of individual measurements (Barnes et al. 2011). With all this in mind, future RV programs can and will be able to detect rocky planets around nearby stars with improved instrumentation, photometric target vetting and high cadence observations.

10.2 Direct Detection and Characterization of Exoplanets

Direct imaging enables study of planets at wider separations and younger ages than are accessible to transit and radial-velocity methods. Observations obtained in the past 7 years on the largest ground-based telescopes equipped with AO have yielded the first images of planetary companions (Fig. 89). The planets imaged thus far only trace the extremes of the population, typically orbiting at $\sim$30–150 AU around stars more massive than the Sun and having masses of $\sim$5–10 $M_{\rm Jup}$. The vast majority of planets imaged to date have been detected from their thermal emission, with only one planet (or its surrounding disk) detected in reflected light (Fomalhaut b; Kalas et al. 2008) and one multi-planet system imaged (HR 8799; Marois et al. 2008) so far. Imaged planets are mostly young ($\sim 1-100$ Myr), where the planet-to-star contrasts are most favorable. Thus our current knowledge represents only a mere glimpse of the full range of planet demographics across stellar hosts, planet masses, orbital separations, and compositions.

Direct imaging discoveries thus far have sparked intensive follow-up efforts and, despite their limited number, illustrate the potential advances from comparative studies of exoplanets. These include the first insights into the atmospheric properties of young gas-giant planets (Fig. 90). NIR photometry indicates that young planets are dustier/cloudier than their older, field BD counterparts at similar effective temperatures (e.g., Bowler et al. 2010a; Currie et al. 2011). NIR spectra clearly show the empirical hallmarks of reduced surface gravity, as expected given the young ages (e.g., Barman et al. 2011; Currie et al. 2014a; Bowler et al. 2014). Such low gravities lead to thicker condensate clouds and enhanced non-equilibrium carbon chemistry in the young planetary photospheres compared to field BDs (e.g. Marley et al. 2012; Skemer et al. 2012, 2014). High-spectral-resolution data of imaged extrasolar planets have provided clues to planetary formation histories, by quantifying the relative abundances of carbon and oxygen in HR 8799c (Konopacky et al. 2013), yielding the rotation period of β Pic b (Snellen et al. 2014), and highlighting ongoing accretion in the circumplanetary disk around GSC 06214-00210 (Bowler et al. 2011). Spectra and photometry also show evidence for non-equilibrium chemistry. However, obtaining similar data for larger samples of gas-giant planets, as well as extending such work to lower-mass planets, is currently well out of reach.

Many more discoveries are expected from new planet-hunting instruments on 8–10 m telescopes such as the Gemini Planet Imager (GPI; Macintosh et al. 2014), the SpectroPolarimetric High-

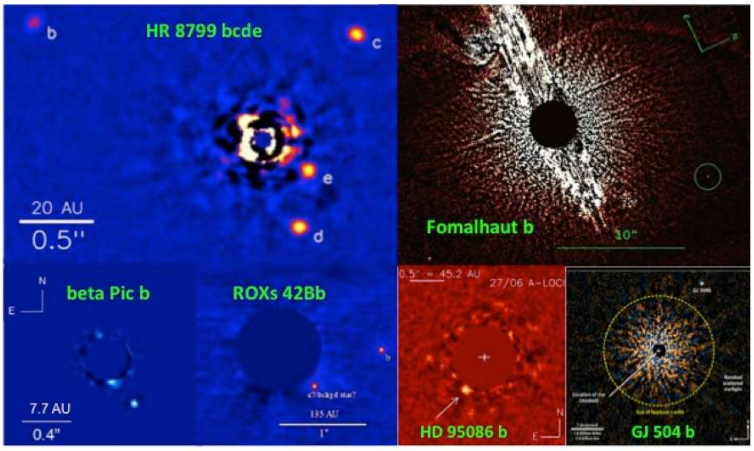

Fig. 89 A gallery of directly-imaged planets: (clockwise from the top-left) HR 8799 bcde (Marois et al. 2008, 2010b), Fomalhaut b (Kalas et al. 2008), GJ 504 b (Kuzuhara et al. 2013), HD 95086 b (Rameau et al. 2013), ROXs 42Bb (Currie et al. 2014b), and β Pic b (Lagrange et al. 2010). Other companions with masses below/near the deuterium-burning limit ($\sim$13 $M_{\rm Jup}$) have also been imaged, many of them at wider separations (e.g., Chauvin et al. 2005; Goldman et al. 2010; Ireland et al. 2011; Luhman et al. 2011; Bowler et al. 2013; Delorme et al. 2013; Kraus et al. 2014; Bailey et al. 2014; Naud et al. 2014).

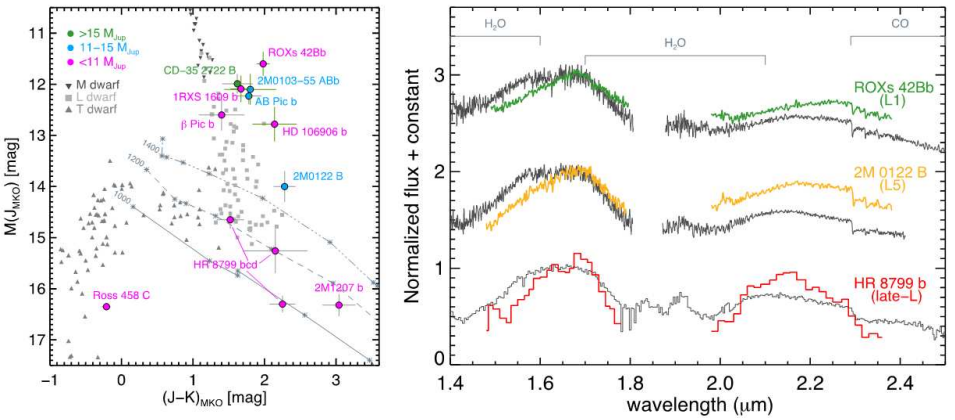

Fig. 90 Atmospheres of directly imaged planets. *Left*: NIR CMD comparing field BDs (*grey symbols*) and young substellar companions (*circles*, based on Liu et al. 2013b and references therein). The young objects form a distinct sequence in the diagram from the field objects, most of them being redder and some extending to fainter J band magnitudes. Diagonal grey lines show models from Barman et al. (2011) of constant temperature with cloud thickness increasing from left to right. Thicker clouds alter the spectral energy distributions of young planets, leading to suppressed emission in the NIR (1–2 μm region) and higher fluxes in the thermal IR (3–4 μm). *Right*: NIR spectra of the young companions ROXs 42Bb ($\sim$9 $M_{\rm Jup}$, $\sim$3 Myr, Currie et al. 2014b; spectra are from Bowler et al. 2014), 2MASS 0122–24B ($\sim$13 $M_{\rm Jup}$, 125 Myr; Bowler et al. 2013), and HR 8799b ($\sim$5 $M_{\rm Jup}$, 30 Myr; Barman et al. 2011), arranged from the hottest object at the top to the coolest object at the bottom. For each companion, a field object of comparable spectral type is also plotted, normalized to the peak H band flux. The differing colors and continuum shapes reflect the lower surface gravities (i.e. younger ages) of the companions.

contrast Exoplanet REsearch (SPHERE; Beuzit et al. 2008), and the Subaru Coronagraphic Extreme Adaptive Optics project (SCExAO; Martinache & Guyon 2009). Large AO imaging surveys so far have shown that Jovian planets at large (tens of AU) separations are relatively rare (e.g. Vigan et al. 2012; Nielsen et al. 2013). On the other hand, radial-velocity data for 1.5–2 $M_{\odot}$ stars show that Jovian planets increase in frequency with orbital separation out to several AU (e.g. Bowler et al. 2010b). Near-future AO surveys with these planet-hunting instruments should reveal much of the gas-giant population at intermediate separations. One of the most significant steps in the study of extrasolar planets in the years leading up to TMT will be direct imaging and spectroscopy of a large sample of young self-luminous exoplanets.

Direct imaging with the TMT will deepen our understanding of exoplanet properties and formation. Here we provide a brief list and in subsequent sections we expand upon these ideas:

– First-light NFIRAOS+IRIS observations will provide unique and powerful follow-up observation of gas-giant planets found by GPI, SPHERE, and SCExAO. High spectral-resolution spectroscopy will establish chemical abundances and rotation speeds, thereby shedding light on planetary origins. High-precision astrometry will enable monitoring of planetary orbits, providing a unique window into the dynamical history. Potential upgrades to IRIS for thermal-IR (L' band) imaging and low-resolution NIR imaging would also boost its ability to directly detect self-luminous planets and characterize their ultracool atmospheres.
– NFIRAOS+IRIS will also be a unique instrument for extending direct imaging studies to new domains, by targeting optically faint stars that are inaccessible to current AO systems. (1) Low-mass stars (M dwarfs) may be the most common type of planetary host, and NFIRAOS+IRIS will be able to detect sub-Jupiter mass planets around these stars. (2) Similarly, high-contrast imaging of dust-extincted young stars in the nearest star-forming regions will observe planet formation in action during the critical $\sim 1-10$ Myr epoch when gas-giant planets are assembling.
– TMT's proposed extreme-AO (ExAO) imaging platforms, Planetary Systems Imager (PSI; originally referred to as the Planetary Formation Imager) and Second Earth Imager on TMT (SEIT), will achieve deeper contrast at much ($> 4\times$) closer separations than GPI and SCExAO. These instruments will probe orbital separations previously only accessible to long temporal baseline Doppler monitoring. Resolving Doppler-detected planets will allow direct dynamical mass measurements, thereby testing planetary evolutionary models (e.g. Crepp et al. 2012).
– TMT ExAO imaging will radically increase the variety of planets we can image from the ground, including numerous infant planets in the nearest Myr-old star-forming regions and lower mass self-luminous planets. TMT will also be able to image mature giant planets in reflected light. The phase space of imageable planets with TMT ExAO will complement planned high-contrast imaging observations from space.
– TMT ExAO could be capable of imaging a large rocky planet in reflected light in the habitable zone around the nearest subsolar-mass stars, before such capabilities are reached from space-borne instruments targeting Sun-like stars.
– Around young nearby stars where the final assembly phases of terrestrial planet formation is underway, TMT ExAO will be sensitive to molten rocky planets and could identify signposts of active planet assembly, providing a unique window into the early history of the solar system's terrestrial planets.

10.2.1 Landscape in the 2020s

Direct imaging with the TMT will build upon current and upcoming exoplanet imaging facilities, in many cases built by TMT partner institutions. Additionally, TMT's exoplanet imaging capabilities will complement upcoming space missions. Figure 91 displays a timeline for the development of

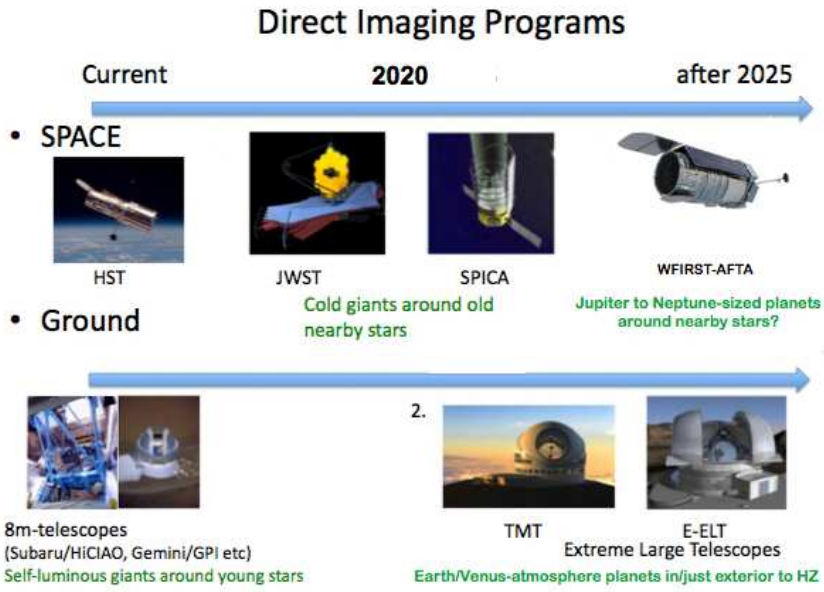

Fig. 91 Timeline of direct imaging-capable space-borne missions and ground-based facilities from the present (2014) to TMT first light in the early 2020s and their unique phase space.

these capabilities, summarizing TMT's unique science focus and the other platforms that will be contemporaneous with TMT.

The new generation of dedicated exoplanet imaging instruments (e.g. Gemini-South/GPI, VLT/SPHERE, and Subaru/SCExAO) are taking steps toward achieving prime science goals of direct imaging. At first-light in November 2013, GPI achieved a Strehl ratio of $\sim$89% and $\sim 10^{-6}$ contrast at $0.6''$ (Macintosh et al. 2014). SCExAO is undergoing commissioning and should achieve similar contrasts down to $\approx 0.1''$. Both GPI and SCExAO will allow us to detect and characterize Jovian planets that are much lower mass and closer to their stars (e.g., 2 $M_{\rm Jup}$ at 5–15 AU around an A-type star at 30 pc) than can currently be done with conventional AO systems (e.g. Subaru/AO-188 and Keck/NIRC2). Adaptive secondary systems on LBT and Magellan telescopes are also showing the power of high-contrast imaging in the 3–5 μm region where giant exoplanets are exceptionally bright.

The startlingly-advanced capabilities of these upcoming instruments stem from new science modules and wavefront control architectures, which will serve as important technical milestones on the road to exoplanet imaging by TMT. (1) The GPI and SCExAO integral field spectrographs (IFS) yield low-resolution spectra that are amenable to the development of post-processing algorithms to boost planet detection capability (Marois et al. 2010a; Currie et al. 2012; Marois et al. 2014). (2) SCExAO and the LBT/Magellan instruments employ advanced wavefront sensors that outperform traditional Shack-Hartmann systems, and the extensive on-sky experience obtained during the next 5–10 years will spur advances in wavefront control architectures for high-contrast imaging. (3) GPI and SCExAO are commissioning novel coronagraphs and other speckle removal techniques to suppress the stellar halo. GPI uses an apodized-pupil Lyot coronagraph to improve contrast for planet detection. SCExAO is deploying a suite of technologies, such as the Phase Induced Amplitude Apodization coronagraph and employs "speckle nulling", a form of coherence differential imaging,

to better suppress static speckles near the diffraction limit and observe at very small inner working angles (Martinache et al. 2014). Overall, the technical advances emerging from upcoming instruments on 8–10 m telescopes will boost the scientific gains to be garnered from TMT's much larger aperture, far beyond what could be imagined during the initial round of TMT instrument studies (Macintosh et al. 2006).

Finally, direct imaging with the TMT will complement upcoming space-borne missions such as the JWST and the proposed SPICA and WFIRST-AFTA missions. SPICA and JWST are MIR optimized 3.5 and 6.5m telescopes, respectively, with superb sensitivity to mature, wide separation planets. While such planets are probably not detectable at the shorter wavelengths probed by TMT, JWST and SPICA have far poorer planet detection capabilities at the $\sim 0.2'' - 0.6''$ separations probed by 8–10 m telescopes and no capabilities at the much smaller separations ($\sim 0.02'' - 0.1''$) that TMT can probe.

TMT's discovery space likewise is complementary to the proposed coronagraph component of WFIRST-AFTA. The coronagraph architectures being considered for WFIRST-AFTA focus on exoplanet imaging at $0.15'' - 0.6''$ separations. Smaller separations will remain the exclusive domain of TMT. For some nearby stars, WFIRST and TMT could both search for and characterize planets in different regions: Neptune to Jupiter-sized planets near the ice line for WFIRST and super-Earths to Neptune-sized planets at smaller separations for TMT. While WFIRST may be able to target large habitable zone planets around Sun-like stars or those slightly more massive, TMT would allow us to search for planets in the habitable zones of the nearest sub-solar mass stars.

Working in concert, TMT and space-borne missions will transform our knowledge of the diversity of nearby exoplanetary systems and take significant steps toward being able to image and characterize a habitable Earth-like planet.

10.2.2 Exoplanet imaging at first-light with NFIRAOS and IRIS of young gas giants

TMT's NIR integral field spectrograph (IRIS) coupled with the facility AO system (NFIRAOS) will provide a powerful exoplanet imaging capability at TMT's first light. The raw planet detection capability for NFIRAOS/IRIS is unlikely to exceed the current/upcoming ExAO systems targeting the bright stars. However, NFIRAOS/IRIS will vastly expand the range of systems around which we can image planets and also will yield significant gains in studying the atmospheres and dynamics of GPI/SCExAO/SPHERE-discovered exoplanets.

One unique and powerful capability offered by TMT will be laser guide star (LGS) AO imaging of a variety of potential planet host stars, thanks to the far greater angular resolution and sensitivity than currently possible. Many nearby stars are too faint for ExAO systems on current telescopes (which are limited to I = 8–9 mag) but are highly desired as science targets in order to reveal the diversity of planetary systems. Low-mass stars ($< 0.5\ M_{\odot}$) are the most common types of stars in the stellar neighborhood and thus represent the most common hosts of planetary systems. Since these stars are much less luminous, NFIRAOS+IRIS imaging using ADI and SDI will be able to detect sub-Jupiter planetary companions. Determining the frequency and properties of gas-giant planets as a function of stellar host mass is a necessary step toward understanding the planet formation process. Extending this concept, deep imaging of BDs in the solar neighborhood (both young and old) can detect companions at colder temperatures than those previously found. We know that at the youngest ages ($\sim 1 - 10$ Myr), BDs can possibly harbor planetary-mass companions, e.g. the $\sim 5\ M_{\rm Jup}$ companion to the $\sim 25\ M_{\rm Jup}$ object 2MASS 1207–39 (Chauvin et al. 2004). TMT will be able to identify the evolved (cooler, fainter) counterparts to these BD companions around older BDs and obtain detailed spectra for objects as cold as ~ 250 K. Imaging planets around low-mass stars in nearby open clusters (e.g. the Pleiades and Hyades) and young moving groups (e.g. TW Hya Association) will provide strong benchmarks for testing thermal evolution models. These stellar associations have well-calibrated ages based on stellar isochrones and metallicities based

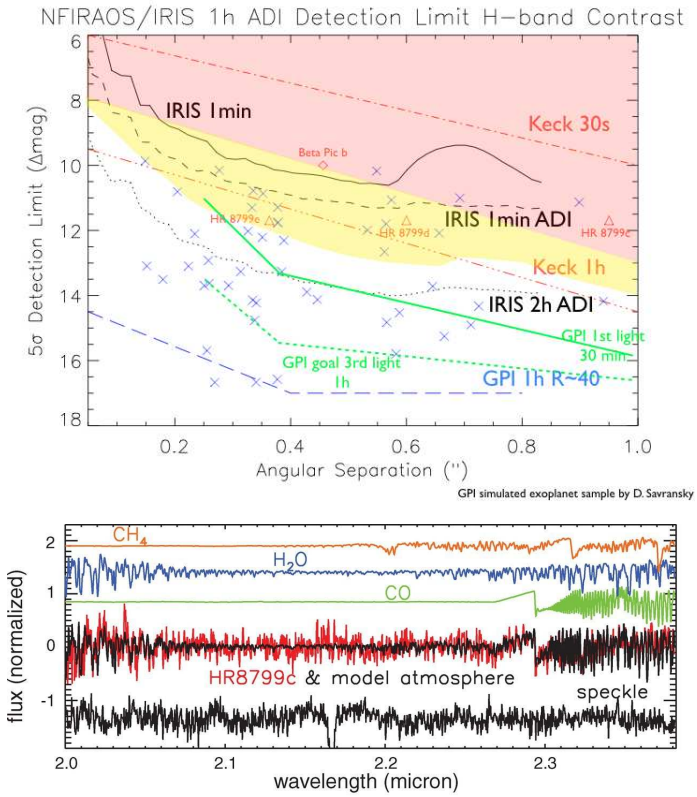

Fig. 92 Exoplanet imaging science with TMT/IRIS. *Top*: Predicted contrast of TMT/IRIS using angular differential imaging (ADI) compared to contrasts for Gemini/GPI and Keck/NIRC2 and a simulated population of 50 super-Jovian exoplanets imaged around a sample of 600 stars (crosses; Marois et al. 2012). Further gains in IRIS contrast will be possible with spectral differential imaging (SDI). Many/most of the GPI-detected exoplanets can be followed up with TMT/IRIS. *Bottom*: High-resolution Keck/OSIRIS spectrum of HR 8799 c from Konopacky et al. (2013) showing multiple water and CO lines but little evidence for methane. Atmospheric modeling of HR 8799 c's spectrum indicates an enhanced C/O ratio, suggesting that the planet formed by core accretion. IRIS will allow us to obtain similar quality spectra for many more exoplanets spanning a broad temperature range discovered by GPI/SPHERE/SCExAO.

on spectroscopic analyses, thereby providing a sample of benchmark planets with well-established physical properties.

Similarly, NFIRAOS+IRIS will open new regimes for identifying and characterizing exoplanets, around stars at larger distances from Earth than what is possible with current ground or space-based telescopes. LGS imaging will enable studies of faint companions around the young ($\lesssim$10 Myr) stars in the Taurus, Sco-Cen, and ρ Ophiuchus regions ($\sim$ 150 pc). According to the core-accretion model, direct imaging at such young ages would discover these planets as they are in the act of forming (e.g. Kraus & Ireland 2012). The relevant physical scales correspond to angular separations of $\sim 0.5''$ or less. NFIRAOS+IRIS would be sensitive to the most luminous, wide separation objects, and then future TMT ExAO systems (see Sect. 10.2.3 below) will probe lower masses and smaller separations. Colors and spectra of these young planets will provide their temperatures, surface gravity and accretion activity, all of which are highly uncertain in present theoretical models.

Building on pre-TMT planet discoveries, one of IRIS's major advances will come through follow-up spectroscopy and high-precision astrometry (Fig. 92). Only a fraction of the directly-imaged exoplanets have been amenable for spectroscopic observations given their contrast. Upcoming instruments such as GPI will only provide low-resolution ($R \sim 50$) spectra. An illuminating example of the gains possible from TMT comes from the high spectral resolution ($R \sim 4000$) study of the HR 8799 c planet (Konopacky et al. 2013), where such data provide a wealth of information about the planet's atmospheric composition and chemistry inaccessible from photometry or low resolution spectroscopy.

TMT's continued astrometric monitoring of known directly imaged planets will open a unique window into additional planetary properties such as mass and orbital eccentricity. The GPI, SPHERE, and SCExAO surveys are expected to directly image tens of young Jovian planets in orbits larger than 5–10 AU. Because the orbital periods of these planets will be tens to hundreds of years, the orbital coverage from by GPI/SPHERE/SCExAO during their lifetime and the expected astrometric accuracy (~ 3 mas, S/N-dependent) will leave large uncertainties in the orbital parameters. While IRIS will deliver lower raw S/N than the original discovery instruments, the $3\times$ smaller angular resolution of TMT will result in comparable or better astrometric precision. Precise multi-epoch astrometry of soon-to-be imaged exoplanets will constrain their orbital properties and (for multi-planet systems) may even produce mass limits from dynamical stability considerations (e.g. Fabrycky & Murray-Clay 2010; Marois et al. 2010b; Currie et al. 2011).

10.2.3 Exoplanet imaging with TMT ExAO: rocky planets and planetesimals

A dedicated exoplanet imager for TMT using ExAO will enhance TMT's planet imaging capabilities well beyond those available at first light with NFIRAOS+IRIS. The PSI is the 'baseline' TMT extreme AO system, designed early in the project and configured for a flexible range of exoplanet science emphasizing a moderately high contrast (10^{-7}), a small inner working angle ($0.03''$) for studies of giant planets, and the ability to work with guide stars as faint as H=14 (Macintosh et al. 2006). SEIT would be a more sophisticated instrument – either standalone or as an add-on to PSI - aggressively optimized for high performance at very small inner working angles (perhaps as small as 10 mas), the regime in which rocky planets may be detectable. On the order of ten sub-Neptune-sized planets are expected to be detectable around nearby stars, a few of which will be rocky bodies (Crossfield 2013). TMT's new capability will allow us to image those planets which are inaccessible by any previous facilities, either from the ground or space.

Detecting Habitable Planets Around Low-Mass Stars – Liquid water on a planetary surface may be critical for the development of life. The ability to directly image planets at the narrow range of separations where liquid water can exist (a.k.a. the habitable zone) is therefore required to identify a habitable extrasolar planet. Detecting habitable-zone Earth-sized planets around Sun-like stars requires contrasts better than 10^{-10}, which are only achievable from space. Habitable-zone (super-) Earths around subsolar-mass stars have much more favorable planet-star contrasts ($\sim 10^{-7} - 10^{-9}$), which are potentially achievable from the ground. However, these planets are located at small angular separations (e.g. tens of milliarcseconds) inaccessible by 8–10 m class ground-based telescopes or planned space missions. Around the nearest M stars, TMT's large aperture will allow imaging of habitable-zone super-Earths (Fig. 93).

TMT is well-poised to identify biomarkers in the spectra of the habitable-zone super-Earths that it directly images. If it imaged the Earth itself from the vantage of a very nearby star, it would be sensitive to diatomic oxygen produced by photosynthesis due to plant life (Owen 1980; Angel et al. 1986; Leger et al. 1993; Léger et al. 2011; Selsis 2002; Kaltenegger et al. 2010). If the AO system and coronagraph can suitably suppress the starlight, simulations indicate that a five-hour TMT observation can detect the 1.27 μm oxygen line in the spectrum of a super-Earth that possesses an Earth-like oxygen abundance.

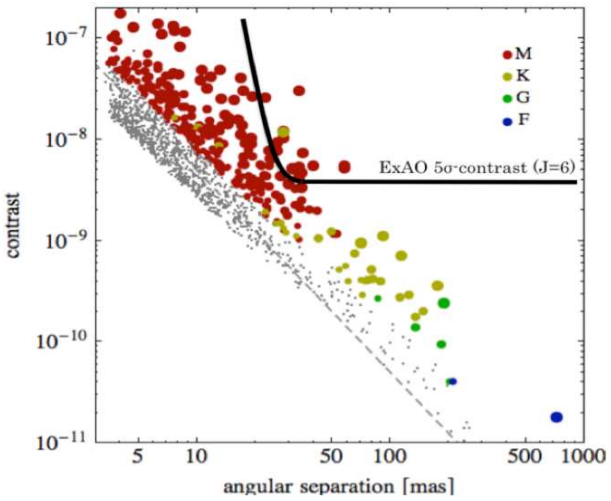

Fig. 93 Contrasts for the reflected light from Earth-radius planets at the inner edge of the habitable zone around a sample of nearby stars. Host stars are drawn from real catalog of the solar neighborhood. The black solid line shows a theoretical best-case 5σ detection limits when observing a star with an apparent J band magnitude of 6 and assuming photon-limited performance. About 10 stars fall above this solid black line.

Witnessing Rocky Planet Assembly – In addition to detecting fully-formed rocky planets, the TMT will provide crucial information about their formation history. During the terrestrial planet formation process, a typical rocky world like the Earth will likely experience on the order of 10 giant impact-type events with Mars-sized bodies. These events impart an immense amount of energy, melting and vaporizing its surface. As the energy from impact-heating fades over 10^5 years, the planet is significantly brighter. A dedicated TMT ExAO instrument may be capable of imaging molten terrestrial planets (Fig. 95).

For Sun-like stars, Melis et al. (2010) show observationally that giant impact-type events related to terrestrial planet formation are only observed when the host star is between 10–100 Myr of age, consistent with expectations from solar system formation simulations. Lupu et al. (2014) estimate that a survey of 15–40 stars in this age range would yield one post-impact planet. Such young stars are numerous in the solar neighborhood, but the expected orbital semi-major axis of these terrestrial worlds combined with the inner working angle of TMT ExAO instruments sets a tight distance constraint. For a nominal inner working angle of 50 mas for PSI to achieve 10^{-8} contrast, we would need stars within 50 pc to probe separations of 2.5 AU or closer (corresponding to separations within the snow line where terrestrial planets are thought to form). Stars in the β Pictoris (10–20 Myr), AB Doradus ($\sim$ 100 Myr old), and Argus ($\sim$40 Myr old) moving groups are at the right distance. In addition the Gaia mission should greatly expand the sample of such stars. SEIT would relax the target distance constraints considerably with its planned contrast inner working angle of 10 mas. Such an instrument would be sensitive to the terrestrial planets around those stars around which giant impact-type collisions have recently occurred (e.g., HD 15407; Melis et al. 2010).

Mapping Planetary Debris Systems – Planetesimal belts are more than just signposts for larger planets. They are crucial components of a complete planetary system, capable of influencing the final configuration of the matured planets. Dynamical friction between these small rocky bodies and planets can drive orbital migration of the planets and circularize planet orbits. In our solar system, such processes are envisioned to have occurred through interaction with the Kuiper Belt which drove

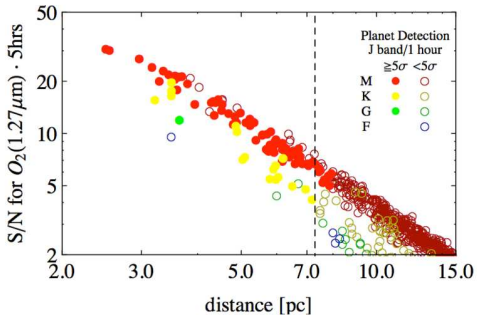

Fig. 94 Detectability of the 1.27 μm band from a super-Earth with an Earth-like atmosphere at the inner habitable edge with a 5-hour TMT exposure, assuming perfect suppression of residual starlight. Filled circles indicate the candidates that will be detected with S/N $>$ 5 in 5-hour photon-noise limited observation on TMT and with an angular separation of $>$20 mas. The vertical line is the approximate detection limit of the photon-noise limited detector for 1-hour exposure.

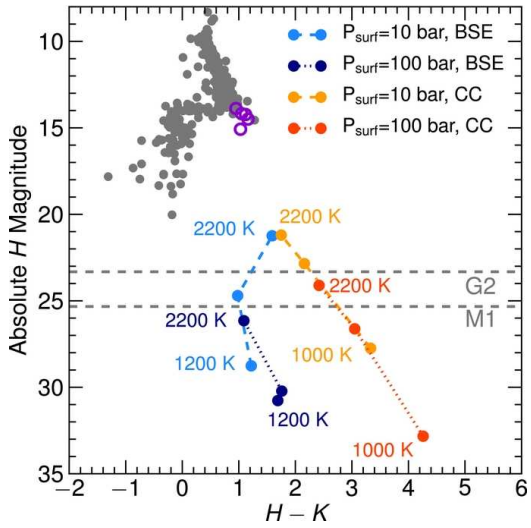

Fig. 95 Detecting post giant-impact emission from forming terrestrial planets, from Lupu et al. (2014). The figure shows the CMD of worlds that recently experienced an energetic impact with a planetary embryo as a function of composition (BSE = bulk silicate Earth, CC = continental crust), atmospheric pressure, and surface temperature. For comparison, observed BDs are shown as gray circles and directly imaged planets (four HR 8799 planets and 2M1207b) are shown as purple open circles. The dashed horizontal lines show detection limits for a TMT ExAO instrument assuming a contrast of 10^{-8} and a Sun-like (G2) or low-mass (M1) star.

the giant planets into new orbits (the so-called Nice model). Thus, to have a complete understanding of any planetary system and its current configuration (and hence develop robust formation and evolution models) it is necessary to characterize any belts of planetesimals that may also be orbiting the same host star.

TMT NIR ExAO instruments and the Mid-Infrared Camera, High-Disperser, and IFU spectrograph (MICHI) will be capable of detecting and characterizing planetesimal belts through the ther-

mal emission from small dust grains that are generated during collision events. NIR ExAO imaging will detect light scattered and polarized by small dust grains, while MICHI will resolve thermal emission from such debris (see Sect. 8.6.1). According to the models of Roberge et al. (2012), debris-producing planetesimals located at 1 AU from their host stars could be identified out to 10 pc, while asteroid belt-like separations could be detected around stars out to 30 pc. If these planetesimal belts are in a steady-state collisional cascade, then around Sun-like stars we could detect collections of small rocky bodies with total mass of roughly ten times the mass of our own asteroid belt and roughly a tenth of the mass of our Kuiper Belt.

10.3 Transiting Exoplanets

A planet whose orbit intersects our LOS to its host star repeatedly transits the stellar disk, producing a small and (in general) extremely-periodic attenuation of the light. Transiting planetary systems can usually be better characterized than systems detected by other methods because the radius of the planet and the inclination of the orbit are established. Observations during transit also probe a planet's atmospheric composition, therefore, one of TMT's most compelling science cases is the potential for detection of O_2 or other biosignature gases via transmission spectroscopy.

10.3.1 Landscape in 2022

With its unprecedented aperture and its access to three-quarters of the sky from Mauna Kea, TMT will be well poised to carry out verification and follow-observations of transiting systems detected by other observatories. TMT's observations of transiting planetary systems will involve either spectroscopy or spectrophotometry to obtain more information about the properties of the planet or its host star, or high-spatial resolution imaging to identify stellar companions to stars or unassociated background objects. The observational modes will be dictated by the brightness of the target and the required cadence of the observations, e.g. at least several exposures per hour for monitoring during a planetary transit. Fainter stars or short cadence observations demand compensatory trade-off, i.e. with spectral resolution or resorting to spectrophotometry. This suggests that future instrumentation and configurations for TMT studies of transiting planets can be organized along three science goals: (1) characterization of faint host stars of transiting (candidate) planets using high-resolution spectroscopy and high angular-resolution imaging; (2) photometric and low-dispersion transit spectroscopy of the brightest systems observed by Kepler and K2, and many of the fainter systems discovered by TESS, (3) high-resolution transit spectroscopy of the brightest transiting systems discovered by TESS and eventually PLATO.

The NASA Kepler mission (2009–2013) dramatically expanded the scope of transit studies to Earth-size (and smaller) planets and to populations of thousands of planets on which robust statistical methods can be applied. However, Kepler surveyed only $\sim$1/400th of the sky and the host stars of most Kepler systems are relatively distant ($\sim$1 kpc) and faint ($V\sim$14, $K\sim$12), making follow-up observations such as Doppler RV measurements of mass or transit spectroscopy difficult or impossible even with 10 m class telescopes. For example, many Kepler host stars at $\sim$1 kpc are probably unresolved binaries and it is often important to establish which star the planet transits to accurately determine its mass and rule out the possibility of a "false positive" (see Sect. 10.3.4): the K band diffraction limit of a 10 m telescope is 55 AU and spectroscopic detection of single-line systems with separations of tens of AU requires high-S/N, high-resolution spectra that are difficult to obtain for these faint stars.

The next decade will welcome new space-based telescopes that will survey more of the sky and include many more brighter and nearby and hence observationally accessible host stars for transiting planets. The Kepler-2 or "K2" mission is surveying $\sim$10 000 targets per field in 80-day campaigns (Howell et al. 2014; Prša et al. 2015). TESS will survey most of the sky (excepting the ecliptic

plane) with durations of 27-351 d (Ricker et al. 2014). Both of these missions, especially TESS, will discover transiting planets around bright stars, including a small number of Earth- to super-Earth-size planets around the brightest M dwarfs (see Fig. 96). ESA's PLATO mission will launch in 2024, and is expected to discover hundreds of Earth- and super-Earth-size planets (as well as thousands of larger ones) around 4th–11th magnitude stars. PLATO will also discover numerous transiting planets in the habitable zones of solar-type stars (Rauer et al. 2014). Stars in this magnitude range offer the opportunity for high-cadence, high-spectral resolution observations of transits to search for emission associated with the planet, transit signals from other planets in the system, or physical properties of the stellar disk.

Thus TMT will have access to a census of thousands of comparatively poorly-studied Earth- and super-Earth-size Kepler and K2 planets and similar numbers of large and hotter planets around brighter and more accessible nearby stars, discovered by TESS and PLATO.

10.3.2 Transit photometry and low-dispersion spectroscopy

Precise ground-based transit photometry or low-dispersion spectroscopy require simultaneous observation of multiple stars: one star exhibits a transit or eclipse, while the others serve as reference sources to reject common-mode temporal variations from telluric or instrumental sources. Such observations attempt to serve two masters: brighter stars provide more photons and higher precision, but comparison stars of comparable brightness are only found at increasing wider angular separations on the sky. At first light, IRMS will likely be the instrument of choice for infrared work because it will obtain integral field spectra that do not suffer from slit loss effects: however, the relatively narrow FOV ($2' \times 2'$) will prevent IRMS from observing all but a few of the systems being studied today (2014). At visible wavelengths, WFOS has a wider FOV (40 sq. arcminutes) therefore it could be use to observe some of the faintest Kepler transiting systems where the density of comparative stars is sufficiently high.

Considering only statistical noise, TMT should measure transit-derived quantities 3–4$\times$ more precisely than what is possible with 8–10 m telescopes. Observations with these telescopes already show hints of a systematic photometric noise floor in the infrared, with observations coming within factors of 2–3$\times$ of the Poisson limit (e.g., Croll et al. 2010; Bean et al. 2011). The current source of this noise remains unknown. One approach to mitigation is to employ very narrow, customized filters that exploit the light-collecting area of TMT while avoiding telluric absorption or emission features.

10.3.3 High-dispersion spectroscopy

Transit observations at high spectral resolution can measure the orbital alignment of planetary orbits (see Sect. 10.1.1 – Rossiter McLaughlin effect), determine the atmospheric composition and structure of both transiting and non-transiting planets (Brogi et al. 2012), measure atmospheric wind speeds and circulation patterns (Showman et al. 2013), and potentially detect molecular oxygen or other biosignature gases (Webb & Wormleaton 2001; Snellen et al. 2013; Rodler & López-Morales 2014). These observations do not require simultaneous reference stars, and regularly reach the photon noise limit at high spectral resolution (Brogi et al. 2014). Thus, TMT transit observations at high spectral resolution are very promising. Although no first-light instruments offer high spectral resolution, several "first decade" instruments do (HROS, NIRES, and MICHI).

In the infrared, NIRES and MICHI spectroscopy of planets with H_2-dominated atmospheres will extend current detections of CO and H_2O to more exotic hydrocarbons such as such as HCN and C_2H_2 (see Fig. 97) which have not yet been observed in exoplanet atmospheres (de Kok et al. 2014). For the hottest planets, wind speeds of up to 1–2 km s^{-1} will be directly measured via the mean Doppler shift of the planet's absorption spectrum (Kempton & Rauscher 2012). Molecular

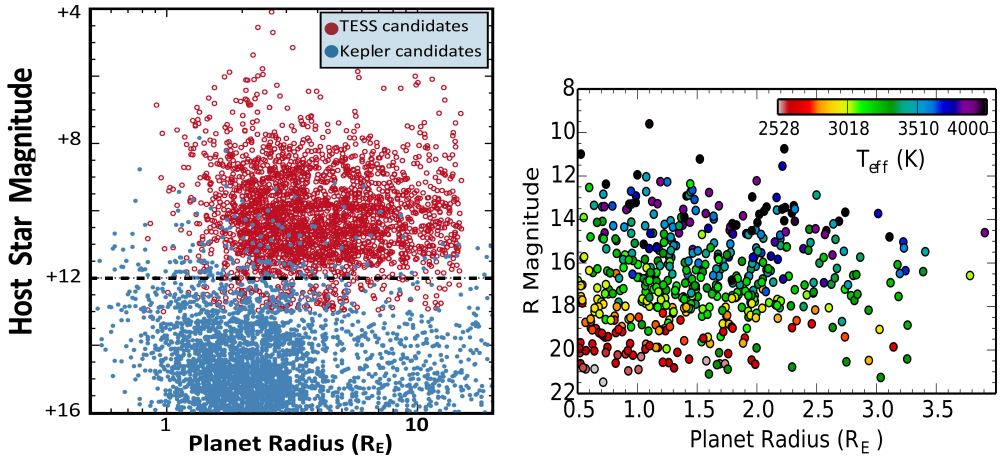

Fig. 96 Predicted planet yields from TESS (*left*; Ricker et al. 2014) and K2 (*right*). Both these surveys will be complete when TMT operations begin. TESS will find many planets around bright stars, while K2 will find larger numbers of planets around cooler stars.

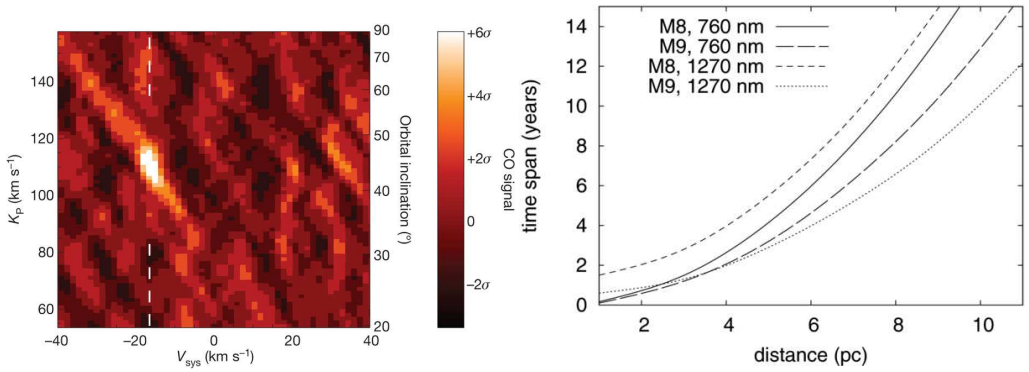

Fig. 97 Studies of exoplanet atmospheres at high dispersion. At left, the detection of CO and exclusion of any stratosphere in the hot Jupiter tau Boo b (Brogi et al. 2012); TMT will measure longitudinally-resolved atmospheric chemistry and structure for such systems. At right, the time required to detect O_2 in the atmosphere of an Earth analog transiting a nearby M dwarf using a TMT-like facility (Rodler & López-Morales 2014).

detections and measurements of thermal structure will be measured as a function of rotational phase for a large sample of both transiting and non-transiting hot Jupiters and hot Neptunes, perhaps finally answering the question of why – or whether – some close-in planets show thermal inversions in their upper atmospheres (Fortney et al. 2008; de Kok et al. 2014).

The most exciting possibility is the ability to search for biosignature gases in the atmospheres of nearby planets. The most well-studied spectral feature is from the molecular oxygen band head at 765 nm, which could be detected with a set of dedicated HROS observations of a rocky planet transiting a late-type (>M3) star within ∼8 pc. The exoplanet's atmosphere would be distinguished from the Earth's oxygen via the Doppler shifts resulting from the two planets' relative orbital motions;

detection would come not in a single night but would require observations spread over many years (Rodler & López-Morales 2014, see Fig. 97). Although any detection would be challenging and O_2 is neither an unambiguous indicator of life (Tian et al. 2014) nor uniquely associated with life, the detection of free oxygen in a nearby rocky planet's atmosphere would be a landmark result for the study of planetary atmospheres, habitability, and astrobiology.

10.3.4 Characterization of transit planet hosts

A number of effects can mimic the periodic dip in the light curve of a transiting planet system, thus stars with transit-like signals remain candidate systems until the possibility of a "false positive" (e.g. grazing transit, or diluted eclipsing binary) can be rule out to an acceptable level. Moreover, the presence of unresolved stellar companions can make interpretation of the signal ambiguous (it is necessary to know which star is being transited) as well as requiring correction for the fact that the transit signal is being diluted by the star that is not being transited. Finally, planet occurrence rates and the properties around single vs. multiple stellar systems provide tests of theories of planet formation and evolution (Quintana et al. 2007).

Most Kepler and K2 systems are too faint and the planets too small to have detectable Doppler RV signals (c.f. Fig. 96). Ten-meter class telescopes can rule out large Doppler signals from stellar companions but these measurements are observationally expensive and not practical for the hundreds or even thousands of systems of interest, but TMT/NIRES could rapidly screen these systems with well-timed observations at quadrature points in the orbit of the candidate planet where the maximum change in RV is expected. High-resolution AO imaging using the PFI should also allow more rapid screening of binary systems, with detection at closer inner working angles than is possible with 10 m telescopes or AO systems on smaller telescopes (Law et al. 2014). Stellar companions of any sort will be detectable with PFI at angular separations of 30 mas, corresponding to 30 AU at 1 kpc.

10.4 Gravitational Microlensing

A gravitational microlensing event is due to the rare occurrence of extremely close alignment of two stars on the sky, within $\sim$1 mas for Galactic microlensing. Currently $\sim$2000 microlensing events are discovered per year by monitoring hundreds of millions of stars in the dense stellar fields toward the Galactic bulge (see, e.g. Gaudi 2012).

A planet accompanying the foreground "lens" star reveals its presence by producing a short-duration deviation on the otherwise smooth and symmetric amplification pattern of the background "source" star produced by the host star only (Mao & Paczynski 1991). The planet detection sensitivity of microlensing peaks at intermediate orbital separations ($\sim$1–10 AU) (e.g., Gould & Loeb 1992; Bennett & Rhie 1996; Dong et al. 2006), which bridge the close-in planet discoveries by RV/transit detection surveys and the wide-separation regime probed by direct imaging programs. Unlike all other planet detection methods, microlensing is sensitive to the mass of the host star and the planet rather than the light, so it is capable of discovering planets around stars across the stellar mass function, even "free-floating" planets unbound to stars (Sumi et al. 2011). Microlensing can detect planets in the Galactic disk as well as the faraway bulge planets all the way to the GC (e.g., Janczak et al. 2010). In the coming decade, microlensing is expected to enjoy orders-of-magnitude boosts in planet detections thanks to future wide-field ground-based and space-based microlensing surveys (Gaudi 2012).

It is important to stress that the science gains from microlensing planet discoveries can be seriously compromised without measuring the physical properties of the planet hosts. The high-resolution and deep follow-up observations enabled by TMT could potentially make detailed characterizations of planet hosts with unprecedented accuracy thus helping to complete and enhance the microlensing planet census.

10.4.1 Landscape in 2022

In the last decade, nearly 30 microlensing planet discoveries have been published, and most of them have been found by adopting the two-stage survey/follow-up strategy (Gould & Loeb 1992; Griest & Safizadeh 1998). In carrying out this strategy, follow-up groups make high-cadence, round-the-clock observations of a few microlensing events selected from those discovered by the survey groups with low-cadence monitoring. These discoveries have offered us some early glimpses into the distribution of planets more massive than $\sim$ few Earth mass near or beyond the so-called nebular "snow line" (Gould et al. 2006, 2010; Cassan et al. 2012).

In the coming decade, high-cadence, continuous, wide-field surveys without the aid of follow-ups are expected to dominate the landscape of microlensing planet detections (Gaudi 2012). Such a "pure" survey mode has already been started by the joint efforts of the OGLE-IV (Udalski 2009), MOA-II (Hearnshaw et al. 2006; Sako et al. 2008), and the "Wise" observatory's (Shvartzvald & Maoz 2012) microlensing survey programs. The most ambitious ground-based survey, KMTNet, will come online in 2015. It consists of three dedicated 1.6m, 4 deg^2 FOV telescopes completely covering the longitudes to observe the bulge continuously with $\sim$10-minute cadence. Their survey will have an order-of-magnitude leap in planet sensitivity, and in particular, it is expected to probe the low end of planet mass function by discovering $\sim$10 planets with 0.1 $M_{\rm Earth} < M < 5M_{\rm Earth}$ per year (Henderson et al. 2014). The planned launch of the wide-field IR survey space mission WFIRST(-AFTA) at the end of the decade would bring a further order-of-magnitude leap in planet detection sensitivity. The mission is sensitive to planets down to $\sim$2 lunar masses and is expected to detect $\sim$3000 bound planets in the range of $\sim$0.3–30 AU as well as probe the free-floating planet population down to Mars mass (Spergel et al. 2013).

10.4.2 TMT microlensing science

The high angular resolution of TMT IRIS AO imaging and IFU (Wright et al. 2010) could potentially play a significant role in characterizing the host stars for the ground-based microlensing planetary candidates in the next decade, and it would also aid space-based satellites such as WFIRST in studying the planet host stars.

For the majority of microlensing planet detections, even though the precise planet-to-star mass ratios and angular planet-to-star separation can be directly inferred, the masses and distances of planet host stars cannot be separately constrained from the microlensing light curves alone. The degeneracy can be broken when additional microlens parallax signals are measured, which can be accomplished for a small fraction of exceptional events (e.g., Dong et al. 2009; Muraki et al. 2011) or by using a dedicated satellite to survey many events from another vantage point at $d \sim$ AU separation from the Earth (Gould & Horne 2013; Dong et al. 2007).

An effective way to break the degeneracy is to directly measure the flux of the host star. For the ground-based observations, a microlensing target is typically blended with significant flux from unrelated stars due to crowding of the bulge field. High-resolution follow-up observations from HST or with AO systems on ground-based 10 m class telescopes have been performed to resolve the unrelated stars (e.g., Bennett et al. 2006; Dong et al. 2009; Janczak et al. 2010; Batista et al. 2014). The typical relative proper motion between the source and lens is $\sim$6 mas/yr for a lens in the disk and $\sim$4 mas/yr for a bulge lens, so it generally takes more than a decade for the lens to be separately resolved from the background star even with such high-resolution images (Han & Chang 2003). So far, the lens and source have been separately resolved for only two non-planetary microlensing events (Alcock et al. 2001; Kozłowski et al. 2007). Only the combined flux of the source and lens have been measured for planetary microlensing events with HST or AO, and the lens flux is constrained by subtracting the source flux, which can be precisely extracted from the light curve. In practice, the measurement uncertainty is dominated by the accuracy in aligning the

high-resolution and microlensing light curve photometric systems, and the lenses have been robustly detected for source/lens contrast ratios up to factor of a few (Dong et al. 2009; Janczak et al. 2010).

With a 30 m telescope, the lens would be separated from the source by $\sim 2\lambda/D$ in H band in $\sim$5 years after the peak of the detection of the event. Therefore, at the time of commissioning, TMT/IRIS would be able to resolve most of the planet hosts collected by a few years of operation by the KMTNet survey (see, e.g Henderson et al. 2015). An average source would be at H $\sim$ 18, and for a typical $\sim 0.3\ M_{\odot}$ M dwarf lens at $\sim$4 kpc, the required contrast ratio is about 10:1, easily observable by IRIS LGS. At $\sim$2–3 λ/D, the achievable contrast ratio is $\sim$1000:1, capable of detecting the lens population down to the bottom of the stellar mass function for the majority of events except those with the brightest giant sources, which only comprise a few percent of all KMTNet detections (Henderson et al. 2015). For some nearby lens systems, it is also possible to image the BD planet hosts. In these cases, the lens identification is considerably more secure, as its separation from the source can be checked with the independent relative source-lens proper motion due to finite-source effects, which are well measured for most planetary microlensing events. The lens flux measurements would offer a mass-distance relation for the lens after including models of extinction and mass-luminosity relation. The relative lens-source proper motion and event timescale provide tight constraints on the angular Einstein radius, which offer another mass-distance relation for the lens. The mass and distance of the lens star can be constrained down to $\sim$10% by combining these constraints.

Once the lens is resolved, an exciting prospect for TMT is to obtain a medium resolution ($R \sim 4000$) spectrum of the star with the IRIS NIR IFU, which has the smallest plate scale of 9 mas. An exposure of approximately ten minutes on IRIS could obtain a spectrum of typical lens at reasonable S/N (≥ 10 per wavelength channel). The IRIS spectrum would enable identification of planet host's stellar type, metal abundance as well as kinematic constraints through RV measurements. It has been well established by RV surveys that the frequency of close-in Jovian planets increases as a function of host metallicity (Santos et al. 2004; Fischer & Valenti 2005). Recently, there is evidence from RV surveys and from the Kepler transiting planets that smaller planets at short-period orbits are distributed over a wide range of metallicity (Mayor et al. 2011; Buchhave et al. 2012). Spectroscopic characterization of microlensing hosts by TMT would open up a new window in studying whether the distribution of planets ranging from super Jupiters to sub-Earths at long periods depends on the environment of the star (metal rich vs. metal poor, bulge vs. disk).

During the operational span of a mission like WFIRST, the lens and source are typically not sufficiently separated to be completely resolved. However, thanks to a well-calibrated PSF, even when the lens and source are separated by a fraction of the PSF, it is possible to measure the lens flux from modeling the image elongation. It is expected that $\sim$10% mass measurement can be routinely done in this way (Bennett et al. 2007; Spergel et al. 2013). TMT can still contribute to studying the WFIRST planet discoveries by making spectroscopic measurements of the planetary hosts. These measurements will determine important stellar parameters such as metallicity and surface gravity as well as imaging some low-mass hosts that are challenging for WFIRST.

11 OUR SOLAR SYSTEM

The solar system is the closest and the best-studied planetary system. Observations of the planets, satellites, and small bodies in the solar system provide indispensable information about planet formation and evolution processes that remain unattainable for other planetary systems. The advent of TMT will enable us to tackle long-standing questions concerning the formation of the solar system, the origin of planetary volatiles, the physics of the ice and gas giants, and the unraveling of the complex dynamical history recorded in the Kuiper belt.

11.1 Primitive Bodies

11.1.1 Asteroids

Asteroids in the main belt between Mars and Jupiter are probably remnants of high temperature accretion in the inner solar system, perhaps with additions accreted from the outer solar system in an early phase of dynamical chaos. Their low total mass (3×10^{-4} Earth mass) reflects clearing of perhaps 0.5 Earth mass of material by dynamical processes that remain to be elucidated from the dynamical imprints. While nearly a million asteroids have been identified that are larger than 1 km in size, the physical properties remain relatively poorly known. However, as the source of meteorites, the main belt asteroids can, with care, be directly linked to samples in the laboratory, providing unique opportunities for hands-on, detailed isotopic and compositional measurements that are otherwise impossible.

11.1.2 Active asteroids

A recently discovered hybrid population also exists. The so-called "active asteroids" (also known as "main-belt comets") have the orbits of asteroids but lose mass, giving them the appearance of comets (Jewitt 2012). Some of these objects may contain water ice, trapped from beyond the snow line in the solar system. When exposed to the Sun by the removal of a protective layer of debris, this ice sublimates, producing the comet-like appearance. Active asteroids are potentially important because some are located in a region of the main belt from which the terrestrial planets are thought to have acquired their volatiles and some biogenic precursor molecules. Study of the active asteroids may help us to understand the origin of the oceans. TMT will be useful because most active asteroids are faint. TMT's large aperture will permit spectroscopic studies in search of volatiles released by outgassing.

11.1.3 Asteroid satellites

Over 200 asteroids known to have satellites and, at small scales, radar and photometric observations have shown that satellites are extremely common. Asteroidal satellites are thought to form via a variety of scenarios including collisions, capture through 3-body interaction, and/or disruption. Asteroids with satellites (e.g. Marchis et al. 2005) are the best study cases for understanding the dynamical history, impact process, and physical properties of the primary. Moons provide the most accurate way to measure the mass and the internal structure of the asteroids (Beauvalet et al. 2013). Density, which is directly related to the composition and internal structure of the asteroid, can be estimated if the shape of the primary is available. If the primary is associated with a young dynamical family, then the combination of the moon and the dynamical family provides strong constraints on the family-forming process. TMT's unprecedented angular resolution will allow it to resolve and directly image either tightly-bounded systems or systems that have high primary-to-secondary mass ratios.

11.1.4 Physical properties of the outer-belt asteroids

The origin of outer belt asteroids (namely Cybeles, Hildas and Trojans) is unclear. They may consist of materials that formed the cores of Jupiter and Saturn, or they may be objects formed at larger distances (perhaps in the Kuiper belt) and then scattered inwards to their present locations. The physical and dynamical properties of these objects enable key tests of the competing scenarios for the evolution of the early solar system. Composition of an asteroid can be best determined through moderate resolution ($R \sim 1000$) spectroscopy in the NIR (1 – 2.5 μm; NIR), where most important ices and organic materials show diagnostic features. It is expected that hundreds (if not thousands) of km-size

Fig. 98 Artist's representation of an icy KBO showing the faint Sun in the upper right. Courtesy ESO.

Cybeles, Hildas and Trojans will be observable spectroscopically by IRIS on TMT. Investigating the outer-belt objects, especially the small ones, with TMT may provide answers to the outstanding issues, such as: What are the cores of the giant planets made from? Where and how did the Trojans form? What is the dynamical history of the solar system?

11.1.5 Kuiper belt objects

Beyond Neptune, a much larger population of small bodies exists in the Kuiper belt (Fig. 98), Kuiper belt objects (KBOs) outnumber asteroids by 1000:1. These objects result from low temperature accretion in the outer regions and they are thought to be ice-rich. About 1500 KBOs are known but physical properties have been established for only a 100 or less. TMT will provide dramatic improvement for optical detection of these bodies. Study of collisional processes there will have impact on the interpretation of the much more distant (but numerous) main sequence debris disks, about which much less is known.

Density is a fundamental property for the understanding of their composition and internal structure. The mean density of distant planetesimals is expected to be markedly different from that of native main-belt asteroids. The most promising method to estimate the shape, and subsequently infer the density, is via analyzing light curves of binary systems. For ground-based measurements, the precision on the diameter is the limiting factor of the most accurate density estimates. Giving the advantage of its high-angular resolving power ($\sim$ 7 mas), TMT will be able to resolve a dozen large Trans-Neptunian objects and $\sim$50–100 Trojan asteroids, providing a good estimate of their size. If a moon is detected, TMT will also derive high-precision densities of these objects. This study will greatly improve the number and quality of density measurements of the outer-belt asteroids, to a degree not possible before TMT.

Because of the vast distance (30–50 AU) of this region from the Sun and the Earth, even with the largest telescopes currently available, only the largest KBOs ($>$ several hundred km) are observable. The Kuiper Belt is therefore the region about which we know the least in the solar system. On the other hand, due to the low temperature and the relatively slow dynamical evolution, the Kuiper belt can be considered a "debris disk" of our planetary system, comparable to the counterparts of other stars (e.g., Kalas et al. 2006; Trilling et al. 2008). The belt contains essential information about the planetary formation processes, including both the "cold disk" that harbors the objects that are thought to formed in situ with the whole planetary system, and the "hot/scattered disk" that is the refuge of objects that are dynamically scattered into it during the dynamical evolution of the inner solar system. Comparisons of the Kuiper belt with the debris disks around other stars provide important indications about both the Kuiper belt itself and the planetary environment around other stars. TMT allows the characterization of more small KBOs by providing greater sensitivity. Compositional data will also greatly aid the study of dynamically families, which are generally formed during collisions of the parent bodies. Finally, spectroscopic analysis may also reveal evidence of evolutionary processes on KBOs, such cryovolcanism, volatile loss and surface gardening. The large aperture of TMT allows for the collection of the spectra of relatively smaller KBOs, vastly increase the number of samples for which we can study surface compositions.

11.1.6 Centaurs

Centaurs are recently (within 10 Myr) escaped KBOs on their way to becoming Jupiter family comets. They are relatively nearby (5–30 AU), compared to the belt, making them relatively easier to observe using the high resolution capability of TMT. They also remain pristine, enabling us to determine the composition of the solar nebula. The IRIS instrument with its diffraction limited imaging and spectroscopic capabilities make it ideal to study the actual shapes and composition of these objects, resolving complex structure such as the rings around Chariklo (Braga-Ribas et al. 2014) that have a diameter of $\sim 0.1''$. The increase in sensitivity will enable us to characterize several new centaurs as small as 20 km in size at a distance of 10 AU and larger ones further away.

11.1.7 Comets

Comets represent the icy planetesimals that are left over building blocks from the collapse of the solar nebula (Fig. 99). A majority have been stored at temperatures ranging from 10 K to 40 K in one of two reservoirs: the Kuiper belt that extends from Neptune's orbit at 30 AU to at least several thousand AU and the Oort cloud, a spherical assemblage that reaches 50 000 to 100 000 AU from the Sun. These reservoirs contain, respectively, 1 billion and 100 billion comets larger than about 1 km in scale. Comets are important as carriers of the most primitive material in the solar system. Their study allows us to probe the chemical make-up of the system at its origins.

The 2.9–5.0 μm region (3450–2000 cm^{-1}) is the single most important region for spectroscopy of simple molecules (up to 8 atoms). Virtually all simple gases have at least one vibrational fundamental band in this spectral region, which spans $\sim$1450 cm^{-1}. For emission spectra, resolving powers to 10 000 (even 300 000) are preferred in order to discriminate densely packed and blended lines. Some important work can be done in the 1–2.5 μm region - mainly on absorption spectra of combination bands, which are weaker than fundamental bands by large factors (typically 100 or more). With NIRES it will be possible to measure emission lines from the dominant primary volatile (H_2O) at 2.0 μm in (active) distant comets. It may be possible to measure hot bands of CO_2, the CO overtone (2.4 μm), and various other species as well. And ices can be investigated, through their solid-state absorption bands, in a variety of objects - from active comets to satellites and trans-Neptunian objects.

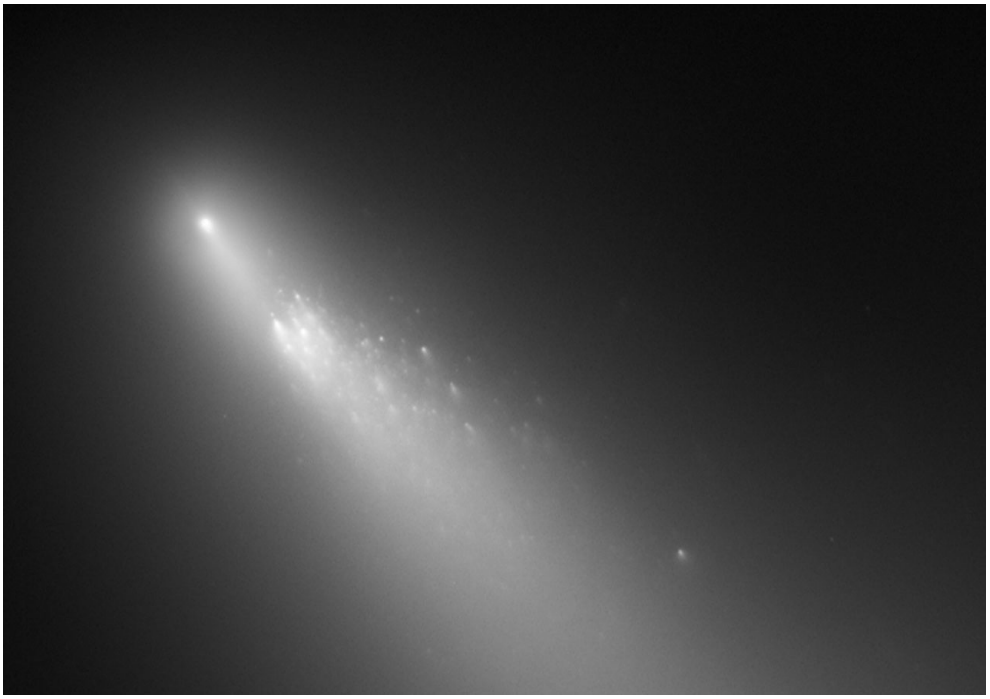

Fig. 99 Comet Schwassmann-Wachmann 3 disintegrating. Properties of the cometary nuclei will be highly susceptible to physical investigation with TMT (Courtesy STSCI – NASA/ESA).

At optical wavelengths, high resolution spectroscopy can be used to determine nuclear spin temperatures in NH_3 and H_2O through emission lines of their dissociation products NH_2 and H_2O+. The nuclear spin temperature is believed to be preserved indefinitely after the formation of a molecule, and hence gives an estimate of the temperature prevailing at the time of the last condensation of the ice. Extending these measurements to fainter objects and to a larger sample will allow us to examine temperature differences that might correlate with formation location in the protoplanetary disk.

11.1.8 Source of planetary volatiles

Comets are likely carriers of part (but not all) of Earth's water. With TMT, a large number of comets, especially short-period comets, will have their D/H ratios measured. A larger contribution is expected from outer-belt asteroids, which also contain water. Since 2005, a new class of comets has been identified residing in the main asteroid belt, these are known as main belt comets (MBCs). At least two MBCs have shown recurrent dust production near their perihelia, suggesting that their activity is driven by water sublimation result from increased surface temperature near perihelion. These discoveries might blur the distinction between comets and asteroids, causing a paradigm change. MBCs are considered as a promising reservoir of terrestrial water and yet direct evidence of water sublimation has not yet been detected even with the largest existing telescopes. The lack of gas detection is likely due to their very low level of sublimation. TMT is expected to be superb in detecting low-level sublimation, which will enable identification orders of magnitude more MBCs and likely direct detection of volatiles in MBCs.

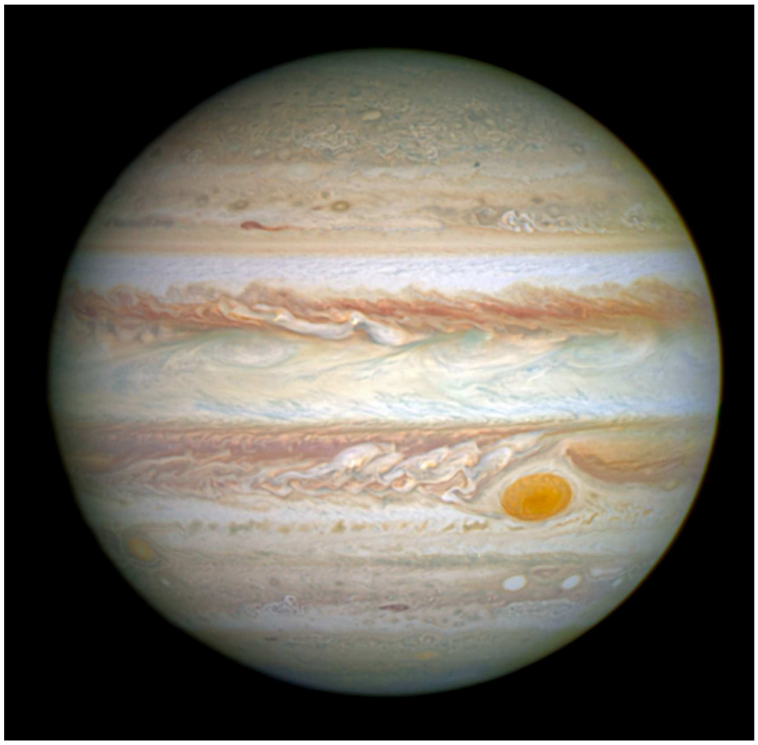

Fig. 100 Cloud decks of Jupiter, showing the Great Red Spot and other circulation systems that will be probed with TMT.

11.2 Giant Planets

11.2.1 Introduction

The giant planets of the solar system offer unique opportunities for study that will enhance our understanding of planets everywhere. The relative proximity of the solar system planets permits investigations that may never be possible on the much more remote planets of other stars. Key areas that can be addressed include:

(1) Temporal evolution of giant planet atmospheres to study fundamental dynamics, meteorology, chemistry and global circulation.
(2) Vertical structure analyses to see how the 'visible atmosphere' responds to energy, momentum and material fluxes from (a) below the clouds and (b) the upper atmosphere.
(3) The measurement of the bulk composition (elemental abundances, isotopic ratios) both as a window on the composition of the proto-solar nebula and to test models for the growth of the planets.

11.2.2 Vortices and thermal waves

Jupiter's red spot and other cloud features (Fig. 100) are large-scale coherent vortices whose physics is still unclear. TMT observations of large-scale will enable time-resolved high resolution spec-

troscopy and imaging of these structures and provide important information about the coupling of chemistry and dynamics in the vortices. Similar structures are observed on Saturn.

Thermal waves are ubiquitous in giant planet atmospheres. The characteristics of the thermal waves (phase speed, propagation direction, and wave number) provide important clues in understanding the generation mechanism of these waves and the formation of jets in giant planet atmospheres (Li et al. 2004). However, due to the long integration time of the low-resolution telescopes, many characteristics of these waves, such as the phase speed and propagation direction, have not been measured directly. TMT observations with short integration time will be able to map thermal waves in giant planet atmospheres in much enhanced details and reveal the characteristics of thermal waves on different giant planets.

Interestingly Io's calderas can be used as occultation sources to study waves propagating through Jupiter's atmosphere and the vertical structure of Jupiter by targeting volcanic calderas on Io as Io goes into eclipse. The volcanic calderas have temperatures of $\sim$1300 K (Spencer et al. 2007) with spatial extents of 10–50 km^2. These bright emission sources are just below the spatial resolution of TMT at all wavelengths so they could serve as point like emission sources to be observed while going in and out of eclipse. With an orbital period of 42 hours about Jupiter, this would afford repeated ingress and egress observation possibilities every 4 Jovian rotations. There are often several volcanoes active on Io simultaneously. Using an integrated field unit one could imagine observing all of Io's disk simultaneously, gathering possibly as many as 5–10 occultation light curves nearly simultaneous, yet slightly offset both in time and spatially.

11.2.3 Planetary seismology from impacts on giant planets

The internal structures of giant planets are much less well known than those of main sequence stars because of uncertainties in the EOS of degenerate gas, the composition (typically non-solar), the interaction with the magnetic field and, in the upper layers, the relative magnitudes of internal heat and energy deposited from the Sun. Giant planet interiors are inaccessible to direct study from above, but oscillations excited by asteroid and comet impact can generate waves that are potentially observable. Such waves will propagate through the planetary interiors, allowing giant planet seismology to constrain internal structure in much the same way as done for our planet using earthquakes. The model is the impact of comet Shoemaker-Levy 9 on Jupiter in 1994, although the state of technology then did not permit the detection of planet-wide waves. Asteroid impacts, especially the large ones, can excite atmospheric waves capable of revealing information about the internal structures of the planets that probably cannot be obtained in any other way. TMT would be able to measure the propagation direction, propagation speed, as well as the energy containing wave number of the atmospheric waves. Such measurements will probe the atmospheric structure and composition, providing unique information useful not just in the solar system but also in the study of Jupiter-like exoplanets, where no comparable data will be available for the foreseeable future.

11.2.4 Source of internal heat in Uranus and Neptune

Ice giants Uranus and Neptune have only been visited once (by Voyager 2). They remain the least understood and most mysterious planets in the solar system and yet Kepler has already shown that planets of similar mass (in between that of Earth and Jupiter) are widespread outside the solar system. Thus, TMT observations will play a very important role in understanding these ice giants. High angular and high spectral resolution observations by TMT will be used to constrain the bulk composition and the mean vertical distribution of temperatures and gas abundances, to shed light on how planetary atmospheres form and evolve as a function of distance from their host stars.

TMT observations can also determine the different spatial variability of temperature and gaseous abundance on Uranus and Neptune. The spatial variability is strongly connected to the atmospheric

dynamics, such as the vertical propagation of waves from the troposphere to the stratosphere. TMT can observe these waves by taking direct optical images of the planets. In combinations with numerical simulations, these observations can help constrain the properties of the waves, as well as the background states for wave propagation, for instance, the atmospheric stratification. Thus, they are crucial for investigating the different atmospheric conditions on Uranus and Neptune.

11.3 Rocky Planets and Moons

11.3.1 Titan

Titan maintains a high pressure ($>$ 1 bar) nitrogen atmosphere and an active hydrological cycle driven not by water, as on Earth, but by hydrocarbons. Its atmosphere is often compared to that of the young Earth, albeit cooled too much lower temperatures ($<$90 K) than ever found on our planet. It offers a valuable opportunity to study a high mass atmosphere on a solid-surface planetary body, and so to advance models of atmospheric circulation, precipitation and seasonal response. Current observations suggest that Titan has lakes mainly in the northern polar region and has tropospheric clouds mainly in the southern middle latitudes and polar region. Recent numerical simulations suggested the lake formation is due to the cold-trapped methane accumulated in the polar region, and predicted prominent clouds will form within about two (Earth) years while lake levels will rise over the next fifteen years due to the seasonally varying solar radiation on Titan. TMT will be a powerful telescope with which to observe and monitor exciting climate change on Titan. In particular, the high spatial and spectral resolution offered by TMT will reveal the spatial distribution and temporal variation of methane clouds, and separate the high clouds generated by deep convection from the low clouds formed over the surface methane reservoirs. When combined with General Circulation Models, such observations would be essential in understanding the hydrological cycle and seasonal variation on Titan.

11.3.2 Planetary atmospheres

The TMT with its high spatial resolution brings to the ground based observer a unique observing technique long held as only possible from spacecraft that undertake planetary limb sounding. The limb sounding method offers an observer the ability to probe a planetary atmosphere at distinct tangent points giving remarkable vertical resolution. These types of observations can be used to look for vertical variations of the chemical constituents and temperature structure. Many of the planetary scale atmospheric waves are expressed as thermal variations on the background atmosphere. These waves would be easily observable with the TMT in this limb sounding geometry. As an example, Mars orbits the Sun at a mean orbital distance of 1.52 AU and thus can be observed as close as $\sim$0.5 AU from the Earth. Looking at shows that the spatial resolution afforded by the TMT in the NIR ($\sim$1–5 μm) is more than adequate to resolve the 11 km scale height of the Martian atmosphere. At 8 microns, when mapping of the deuterium isotope of hydrogen (HDO) and H_2O_2 abundance, the TMT would offer 20 km spatial resolution to sample the vertical extent of the Martian atmosphere, $>$ 100 km.

Atmospheric features of the planets change on a range of timescales that can be probed using TMT. For example, Mars experiences global dust storms in addition to its annual cycles of atmospheric freeze-out at the poles. The cloud decks of the giant planets evolve in dramatic and unpredictable ways, as recently shown by the emergence of a super-storm on Saturn (Sayanagi et al. 2014). Multi-wavelength imaging and spectroscopy with TMT will bring capabilities for high-resolution observations of sudden atmospheric changes that cannot be matched by telescopes in space.

Table 7 Spatial resolution achieved by diffraction limited performance of the TMT with the use of AO. For unresolved objects the integration time to achieve a given S/N scales as the square of the ratio of the telescope apertures. For resolved objects, the integration for a given S/N is the same for all telescopes with apertures large enough to resolve the source. However, the spatial resolution scales as the ratio of the telescope apertures.

Spatial Resolution (mas)	7	14	34	55	83	138	193
Wavelength (μm)	1	2	5	8	12	20	28
Source Radius (km) Distance (AU)	Spatial Resolution (km)						
Mars (3390) ∼ 0.5	2.5	5	12.5	20	30	50	70
Venus (6052) ∼ 1.0	5	10	25	40	60	100	140
Io (1830) ∼ 4	20	40	100	160	240	400	560
Titan (2575) ∼ 9.5	47	95	240	380	570	950	1330
Uranus (25 559) ∼ 19.2	95	190	380	770	1150	1920	2680
Neptune (24 764) ∼ 30	150	300	750	1200	1800	3000	4200
Pluto (1151) ∼ 39.5	200	400	990	1600	2400	3900	5500

11.3.3 Volcanism (Io)

Io is the most active volcanic world in our solar system. Spacecraft imaging shows a world littered with volcanic eruptions (Fig. 101 and Fig. 102). Current research has shown that the atmosphere of Io is supported both by SO_2 frost sublimation as well as SO_2 and other gasses erupting from the volcanoes found there. However, the relative dominance of the frost or volcanic input is still a subject of controversy. SO_2 has molecular bands at 7, 8 and 19 μm. At these wavelengths Io can just barely be resolved by an 8m telescope without AO (the case for TEXES on Gemini North). However, with the TMT Io will be resolved by 26 and 10 spatial resolution elements across its disk at 7 and 20 μm, respectively. This will transform the way we study Io.

Eclipse observations, where Jupiter eclipses Io for a few hours approximately every two days, also offer another way of testing atmospheric support. Eclipse events inhibit solar heating required for frost sublimation. Observing the atmosphere during eclipses will help to see if and how much the atmosphere condenses onto the cold surface. This process has never been observed for the primary atmosphere due to the lack of telescope light collecting power. Ultimately, MICHI on the TMT will be able to measure the spatial variation of SO_2 on Io both meridionally (with latitude) and zonally (with longitude), but critically as a function of local time and during Jupiter eclipses that are both strong functions of frost sublimation, and will allow us to determination of how much of Io's atmosphere is supported purely by sublimation and how much by volcanic activity.

Additionally, we can expect that individual plumes will be recognizable using MICHI as well. During the New Horizons flyby of Jupiter the volcano Tvashtar was imaged with a plume height varying between roughly 320 and 360 km and a full width of about 1100 km, consistent with the diameter of the pyroclastic deposits. With spatial resolutions ranging from 100 km at 5 μm, 240 km at 12 μm and 400 km at 20 μm, we should expect to be able to directly measure the composition of volcanoes with TMT and MICHI.

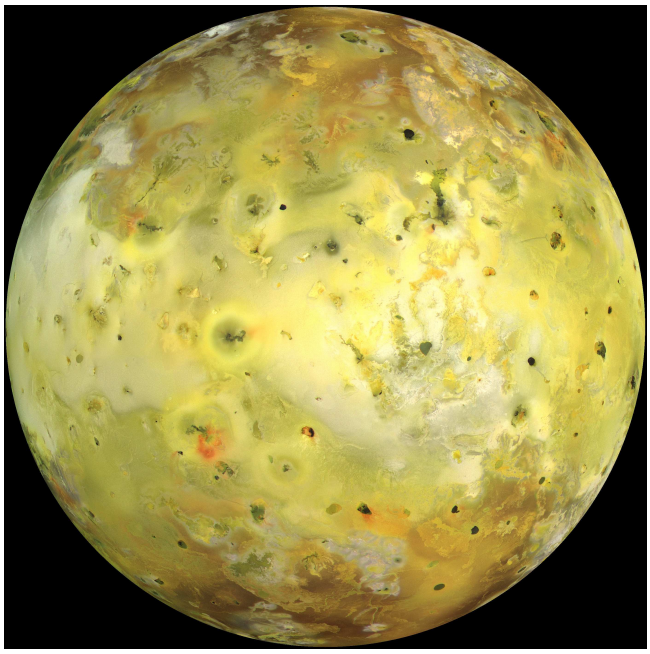

Fig. 101 Sulphur-covered surface of Jupiter's satellite Io. Circular features are regions of fallback of ejecta from active volcanos. No impact craters are visible owing to the extreme youth of the surface. Io will fill ∼600 TMT pixels at 0.7 μm, enabling real-time monitoring of activity on this body. The heat source is thought to be tidal flexing by the finite eccentricity of the orbit, itself a result of a Laplace resonance between the Galilean satellites.

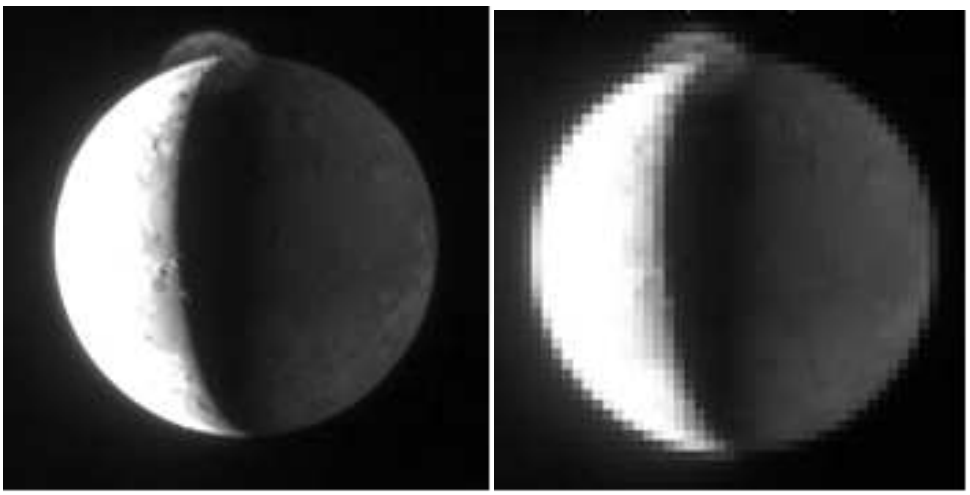

Fig. 102 *Left*: Visible image of Io and the Tvashtar volcano observed by New Horizons during the Jupiter flyby in 2007 (Spencer et al. 2007). *Right*: The same image, but convolved to the spatial resolution MICHI will have on the TMT at 5 μm.

Appendix A: ABBREVIATIONS AND ACRONYMS

ACS	Advanced Camera for Surveys (HST instrument)
ADI	Angular Differential Imaging
AGB	Asymptotic Giant Branch
AGN	Active Galactic Nucleus
ALMA	Atacama Large Millimeter/submillimeter Array
AO	Adaptive Optics
AU	Astronomical Unit
BCD	Blue Compact Dwarf galaxies
BCG	Brightest Cluster Galaxy
BH	Black Hole
BLR	Broad Line Region
CARMENES	Calar Alto high-Resolution search for M dwarfs with Exoearths with Near-infrared and optical Échelle Spectrographs
CMB	Cosmic Microwave Background
CMD	Color-Magnitude Diagram
CRIRES	Cryogenic Infrared Echelle Spectrometer (VLT)
CSPNe	Central Star of Planetary Nebula
dSphs	dwarf Spheroidal galaxies
DCC	Document Control Center
DE	Dark Energy
DEIMOS	Deep Imaging Multi-object Spectrograph (Keck)
DSC	Detailed Science Case
ELT	Extremely Large Telescope
ESO	European Southern Observatory
ESPRESSO	Echelle SPectrograph for Rocky Exoplanet Stable Spectroscopic Observations
FOV	Field Of View
GPI	Gemini Planet Imager
GRB	Gamma Ray Burst
HIA	Herzberg Institute of Astrophysics
HIRES	High Resolution Echelle Spectrometer (Keck)
HROS	High-Resolution Optical Spectrometer
HST	Hubble Space Telescope
IFU	Integral Field Unit
IGM	Inter-Galactic Medium
IMBH	Intermediate Mass Black Hole
IMF	Initial Mass Function
IR	Infrared
IRIS	InfraRed Imaging Spectrometer
IRMOS	InfraRed Multi-Object Spectrometer
IRMS	InfraRed Multislit Spectrometer
ISM	Inter-Stellar Medium
ISDT	International Science Development Team
JWST	James Webb Space Telescope
KBO	Kuiper-Belt Object
KMTNet	Korea Microlensing Telescope Network
LINER	Low-Ionization Nuclear Emission-line Region active galactic nuclei
LMC	Large Magellanic Cloud
LOS	Line Of Sight
LSB	Low Surface Brightness galaxies

MBCs	Main Belt Comets
MBH	Massive Black Hole
MCAO	Multi-Conjugate Adaptive Optics
MIR	Mid-Infrared
MIRES	Mid-Infrared Echelle Spectrometer
MOAO	Multi-Object Adaptive Optics
MOSFIRE	Multi-Object Spectrometer for Infra-Red Exploration (Keck)
NASA	National Aeronautics and Space Administration
NFW	Navarro, Frenk & White (dark matter density profile)
NIRES	NearInfraRed Echelle Spectrometer
NIR	Near Infrared
NIRSPEC	Near Infrared (echelle) Spectrograph (Keck)
NFIRAOS	Narrow Field Infrared Adaptive Optics System
NOAO	National Optical Astronomy Observatory
NRC	NAS National Research Council (USA) or National Research Council of Canada
NSF	National Science Foundation
NS	Neutron Star
PFI	Planet Formation Instrument
PNe	Planetary Nebulae
PSF	Point Spread Function
QSO	Quasi-Stellar Object (AGN)
RGB	Red Giant Branch
RV	Radial Velocity
SAC	Science Advisory Committee
SCExAO	Subaru Coronagraphic Extreme Adaptive Optics
SDI	Spectral Differential Imaging
SDSS	Sloan Digital Sky Survey
SFR	Star Formation Rate
SKA	Square Kilometre Array
SMBH	Supermassive Black Hole
SNe	Supernovae
S/N	Signal-to-Noise Ratio
SPIRou	SpectroPolarimètre Infra-Rouge
SPHERE	Spectro-Polarimetric High-contrast Exoplanet Research (VLT)
STScI	Space Telescope Science Institute
TDE	Tidal Disruption Event
TEXES	Texas Echelon Cross Echelle Spectrograph
TMT	Thirty Meter Telescope
UCI	University of California at Irvine
UCLA	University of California at Los Angeles
UCSC	University of California at Santa Cruz
UKIDSS	United Kingdom Infrared Deep Sky Survey
ULIRG	Ultra Luminous Infrared Galaxy
URL	Universal Resource Locator
UV	UltraViolet
UVES	Ultraviolet and Visible Echelle Spectrograph (VLT)
VLT	Very Large Telescope
WD	White Dwarf
WFC3	Wide Field Camera 3 (HST instrument)
WFOS	Wide-Field Optical Spectrometer
WMAP	Wilkinson Microwave Anisotropy Probe
YSO	Young Stellar Object
YMC	Young Massive Cluster

Appendix B: CONTRIBUTORS

B.1. Editing Team

Warren Skidmore (Thirty Meter Telescope Project Office, US) (Editor in-chief)
Ian Dell'Antonio (Brown University, US)
Misato Fukagawa (Osaka University, Japan)
Aruna Goswami (IIA, India)
Lei Hao (Shanghai Astronomical Observatory, China)
Paul Hickson (University of British Columbia, Canada)
David Jewitt (University of California Los Angeles, US)
Greg Laughlin (University of California Observatory Lick, US)
Luc Simard (NRC Herzberg, Canada)
Matthias Schöck (Thirty Meter Telescope Project, NRC Herzberg, Canada) (editorial support)
Charles Steidel (California Institute of Technology, US)
Tommaso Treu, UC Los Angeles (editorial support, ISDT coordinator)

The editors thank Judy Cohen (Caltech) for suggestions, comments and information that greatly strengthened this document.

B.2. TMT Science Advisory Committee (July 2014)

Masayuki Akiyama, Tohoku University
Michael Bolte, UC Santa Cruz
Ray Carlberg, University of Toronto
Judith Cohen, Caltech
Timothy Davidge, NRC/HIA
Ian Dell'Antonio, Brown University
Mark Dickinson, NOAO
Taotao Fang, Xiamen University
Paul Hickson, University of British Columbia
Jiangsheng Huang, Harvard-CfA
Garth Illingworth, UC Santa Cruz
Masanori Iye, NAOJ
Nobunari Kashikawa, NAOJ
Shri Kulkarni, Caltech
Xiaowei Liu, KIAA-PKU
Jennifer Lotz, STScI
Lori Lubin, UC Davis
Shude Mao, NAOC
Chris Martin, Caltech
Jerry Nelson, UC Santa Cruz (Project Scientist)
Shashi Bhushan Pandey, ARIES
C. Pilachowski, Indiana University
A.N Ramapraksh, IUCAA
B. E. Reddy, IIA
D. Silva, NOAO
A. Subramaniam, IIA
Charles Steidel, Caltech
Tommaso Treu, UC Los Angeles
Tomonori Usuda, NAOJ
Suijian Xue, NAOC

B.3. TMT International Science Development Teams and Other Contributors

Many scientists from across the TMT collaboration and also outside in the broader international astronomical community contributed to this document. These scientists are all members of the TMT ISDTs (except where noted below) and each chapter was developed by members of a particular ISDT and led by the ISDT conveners. Additional input from was sought from non-ISDT experts by ISDT conveners or DSC editors where needed. All contributing authors for each chapter are listed below, chapter editors that are mentioned below have also contributed content. Tommaso Treu, Todd Boroson and Mark Dickinson masterminded the establishment of the ISDTs and oversaw ISDT activities during the time leading up to and including the update of the DSC.

Fundamental Physics and Cosmology:
Marusa Bradac (UC Davis)
James Bullock (UCI)
Ray Carlberg (University of Toronto) (**Convener**)
Masashi Chiba (Tohoku University)
Ian Dell'Antonio (Brown University) (**Chapter editor**)
Jarah Evslin (IHEP)
Christopher Fassnacht (UC Davis)
Philip Lubin (UCSB)
Julio Navarro (University of Victoria)
Masamune Oguri (University of Tokyo)
Joel Primack (UCSC)
Anjan Ananda Sen (Jamia Millia Islamia Central University)
Tommaso Treu (UC Santa Barbara/Los Angeles) (**Convener**)
David Tytler (UCSD)
Gillian Wilson (UC Riverside)
Renxin Xu (Peking University)
Hongsheng Zhao (University of St. Andrews)
Gongbo Zhao (NAOC)

The Early Universe:
Marusa Bradac (UC Davis)
Scott Chapman (Dalhousie University)
Ranga-Ram Chary (IPAC)
Asantha Cooray (UC Irvine)
Mark Dickinson (NOAO) (**Convener**)
Masanori Iye (NAOJ/TMT-J)
Nobunari Kashikawa (NAOJ)
Masami Ouchi (University of Tokyo)
Toru Yamada (Tohoku University)

Galaxy Formation and the Inter-Galactic Medium:
Michael Cooper (UCI)
Taotao Fang (Xiamen University)
Roy Gal (University of Hawaii)
Mauro Giavalisco (University of Massachusetts)
Tadayuki Kodama (NAOJ) (**Convener**)
Jennifer Lotz (STSCI)
Crystal Martin (UC Santa Barbara)
Michael Pierce (University of Wyoming)
Jason X. Prochaska (UC Santa Cruz)
Naveen Reddy (UC Riverside)
Kartik Sheth (NRAO)
R. Srianand (IUCAA)

C.S. Steidel (Caltech) (**Chapter editor**) (non-ISDT)
Masayuki Tanaka (NAOJ)
Vivian U (UC Riverside)
Shelley Wright (University of Toronto)

Understanding Supermassive Black Holes With TMT:
Masayuki Akiyama (Tohoku University)
Aaron Barth (UC Irvine)
G.C. Dewangan (IUCAA)
Tuan Do (Dunlap Institute)
Andrea Ghez (UC Los Angeles)
Lei Hao (Shanghai Astronomical Observatory) (**Chapter editor**)
Fiona Harrison (Caltech) (**Convener**)
Luis Ho (KIAA Peking)
Masa Imanishi (NAOJ)
Enrique Lopez-Rodriguez (UT San Antonio)
Matt Malkan (UC Los Angeles) (**Convener**)
Claire Max (UC Santa Cruz)
Leo Meyer (UC Los Angeles)
Tohru Nagao (Kyoto University)
Chris Packham (UT San Antonio)
Yiping Wang (NAOC)
Mansi Kasliwal (Caltech) (non-ISDT)
Swara Ravindranath (STSCI) (non-ISDT)

Exploration of the Milky Way and Nearby Galaxies:
Wako Aoki (NAOJ)
Masashi Chiba(Tohoko)
Mousumi Das (IIA)
Richard de Grijs (KIAA)
Xuan Fang (Instituto de Astrofisica de Andalucia)
Rupjyoti Gogoi (Tezpur University)
Aruna Goswami (IIA) (**Chapter editor**)
Puragra Guhathakurta (UCSC, UC)
Hanae Inami (NOAO)
Jason Kalirai (STSCI)
Lucas Macri (Texas A&M)
Shude Mao (NAOC) (**Convener**)
Alan McConnachie (NRC Herzberg)
Stacy McGough (Case Western Reserve University)
Shalima Puthiyaveettil (Indian Institute of Astrophysics)
Catherine Pilachowski (Indiana University)
Michael Rich (UCLA)
James Schombert (University of Oregon)
Sebastien Lepine (Georgia State University/AMNH)
Jianrong Shi (NAOC)
Annapurni Subramaniam (IIA) (**Convener**)
Judy Cohen (Caltech) (non-ISDT)
Evan Kirby (Caltech) (non-ISDT)

The Birth and Early Lives of Stars and Planets:
Babar Ali (IPAC)
Adam J. Burgasser (UCSD)
Richard de Grijs (KIAA Peking University)

Misato Fukagawa (Osaka University)(**Chapter editor and convener**)
Carol, A. Grady (Eureka Scientific, NASA GSFC)
Priya Hasan (Maulana Azad National Urdu University)
Gregory J. Herczeg (KIAA Peking University)
Mitsuhiko Honda (Kanagawa University)
Quinn M. Konopacky (Dunlap Institute)
Di Li (NAOC)
Jessica R. Lu (University of Hawaii IfA) (**Convener**)
Takayuki Muto (Kogakuin University)
Joan R. Najita (NOAO)
Devendra K. Ojha (TIFR)
Yoshiko K. Okamoto (Ibaraki University)
Deborah L. Padgett (NASA GSFC)
Klaus M. Pontoppidan (STScI)
Matthew J. Richter (UC Davis)
Jonathan C. Tan (University of Florida)

Time Domain Science:
G.C. Anupama (IIA) (**Convener**)
Manjari Bagchi (Tata Institute of Fundamental Research)
Varun Bhalerao (IUCAA)
U.S. Kamath (IIA)
Enrique Lopez-Rodriguez (UT San Antonio)
Lucas Macri (Texas A&M)
Keiichi Maeda (Kyoto University)
Shashi Bhushan Pandey (ARIES)
Enrico Ramirez-Ruiz (UCSC)
Warren Skidmore (TMT) (**Chapter editor**)
Masaomi Tanaka (NAOJ) (**Convener**)
Nozomu Tominaga (Konan University)
Lingzhi Wang (NAOC)
Xiaofeng Wang (Tsinghua)
Chao Wu (NAOC)
Xufeng Wu (Purple Mountain Observatory)
Alan Marscher (Boston University) (non-ISDT)
Vishal Kasliwal (Drexel University) (non-ISDT)

Exoplanets:
Ian Crossfield (University of Arizona)
Thayne Currie (University of Toronto)
Michael C. Liu (University of Hawaii)
Bruce Macintosh (Stanford University) (**Convener**)
Norio Narita (NAOJ) (**Convener**)
Angelle Tanner (Mississippi State University)
Subo Dong (KIAA)
Eric Gaidos (University of Hawaii)
Christian Marois (NRC Herzberg)
Taro Matsuo (Kyoto University)
Carl Melis (UC San Diego)
Stephen Kane (SFSU), with input taken from the IRIS science case (TMT.INS.JOU.09.004.DRF01)

Our Solar System:
Thomas Greathouse (SWRI)
David Jewitt (UCLA) (**Chapter editor**)

Jianyang Li (PSI)
Junjun Liu (Caltech)
Franck Marchis (SETI Institute)
Angel Otarola (TMT)
Shalima Puthiyaveettil (IIA)
Tomohiko Sekiguchi (Hokkaido University of Education) (**Convener**)
Feng Tian (Tsinghua University) (**Convener**)
Bin Yang (University of Hawaii)
Michael A'Hearn (University of Maryland) (non-ISDT)
Leigh Fletcher (University of Oxford) (non-ISDT)
Michael Mumma (NASA GSFC) (non-ISDT)
Glenn Orton (NASA JPL) (non-ISDT)

Thank you to Amanda Cueto-Moll (TMT) for ensuring document compliance with TMT standards.

2007 TMT Detailed Science Case: Contributors to the original 2007 science case are listed within that document. The document is available at; *http://www.tmt.org/sites/default/files/TMT-DSC-2007-R1.pdf*

The TMT Project gratefully acknowledges the support of the TMT collaborating institutions. They are the Association of Canadian Universities for Research in Astronomy (ACURA), the California Institute of Technology, the University of California, the National Astronomical Observatory of Japan, the National Astronomical Observatories, Chinese Academy of Sciences and their consortium partners, and the Department of Science and Technology of India and their supported institutes. This work was supported as well by the Gordon and Betty Moore Foundation, the Canada Foundation for Innovation, the Ontario Ministry of Research and Innovation, the National Research Council of Canada, the Natural Sciences and Engineering Research Council of Canada, the British Columbia Knowledge Development Fund, the Association of Universities for Research in Astronomy (AURA), the U.S. National Science Foundation and the National Institutes of Natural Sciences of Japan.

References

Abadi, M. G., Navarro, J. F., & Steinmetz, M. 2006, MNRAS, 365, 747
Abadie, J., Abbott, B. P., Abbott, R., et al. 2010, Classical and Quantum Gravity, 27, 173001
Abazajian, K. N., Arnold, K., Austermann, J., et al. 2015, Astroparticle Physics, 63, 66
Adelberger, K. L. 2004, ApJ, 612, 706
Adelberger, K. L., Steidel, C. C., Shapley, A. E., & Pettini, M. 2003, ApJ, 584, 45
Adelberger, K. L., Steidel, C. C., Kollmeier, J. A., & Reddy, N. A. 2006, ApJ, 637, 74
Aitken, D. K., Briggs, G., Bailey, J. A., Roche, P. F., & Hough, J. H. 1984, Nature, 310, 660
Aitken, D. K., Hough, J. H., Roche, P. F., Smith, C. H., & Wright, C. M. 2004, MNRAS, 348, 279
Alcock, C., Allsman, R. A., Alves, D. R., et al. 2001, Nature, 414, 617
Allison, R. J., Goodwin, S. P., Parker, R. J., et al. 2009, ApJ, 700, L99
Aloisi, A., van der Marel, R. P., Mack, J., et al. 2005, ApJ, 631, L45
Alves de Oliveira, C., Moraux, E., Bouvier, J., & Bouy, H. 2012, A&A, 539, A151
Alves de Oliveira, C., Moraux, E., Bouvier, J., et al. 2013, A&A, 549, A123
Amado, P. J., Quirrenbach, A., Caballero, J. A., et al. 2013, in Highlights of Spanish Astrophysics VII, eds. J. C. Guirado, L. M. Lara, V. Quilis, & J. Gorgas, 842
Amanullah, R., Goobar, A., Clément, B., et al. 2011, ApJ, 742, L7
Amendola, L., & Tsujikawa, S. 2010, Dark Energy: Theory and Observations (Cambridge Univ. Press)

Anders, P., Bissantz, N., Fritze-v. Alvensleben, U., & de Grijs, R. 2004, MNRAS, 347, 196
Angel, R., Cheng, A., & Woolf, N. 1986, Nature, 324, 518
Angélil, R., & Saha, P. 2011, ApJ, 734, L19
Antoniadis, J., Freire, P. C. C., Wex, N., et al. 2013, Science, 340, 448
Aoki, W., Frebel, A., Christlieb, N., et al. 2006, ApJ, 639, 897
Aoki, W., Tominaga, N., Beers, T. C., Honda, S., & Lee, Y. S. 2014, Science, 345, 912
Arcavi, I., Gal-Yam, A., Sullivan, M., et al. 2014, ApJ, 793, 38
Armstrong, D. J., Osborn, H. P., Brown, D. J. A., et al. 2014, MNRAS, 444, 1873
Asmus, D., Gandhi, P., Smette, A., Hönig, S. F., & Duschl, W. J. 2011, A&A, 536, A36
Bañados, E., Venemans, B. P., Morganson, E., et al. 2014, AJ, 148, 14
Bagdonaite, J., Daprà, M., Jansen, P., et al. 2013a, Physical Review Letters, 111, 231101
Bagdonaite, J., Jansen, P., Henkel, C., et al. 2013b, Science, 339, 46
Bagdonaite, J., Ubachs, W., Murphy, M. T., & Whitmore, J. B. 2014, ApJ, 782, 10
Bailey, J., Axon, D. J., Hough, J. H., et al. 1988, MNRAS, 234, 899
Bailey, V., Meshkat, T., Reiter, M., et al. 2014, ApJ, 780, L4
Balogh, M. L., & Morris, S. L. 2000, MNRAS, 318, 703
Baptista, R., & Bortoletto, A. 2008, ApJ, 676, 1240
Baptista, R., Borges, B., Kolokotronis, V., Giannakis, O., & Papadimitriou, C. J. 2011, in Proc. of The Physics of Accreting Compact Binaries (Universal Academic Press, arXiv:1105.1382)
Baraffe, I., Chabrier, G., Barman, T. S., Allard, F., & Hauschildt, P. H. 2003, A&A, 402, 701
Barman, T. S., Macintosh, B., Konopacky, Q. M., & Marois, C. 2011, ApJ, 733, 65
Barnes, J. E., & Hernquist, L. 1992, ARA&A, 30, 705
Barnes, J., & Kasen, D. 2013, ApJ, 775, 18
Barnes, J. R., Jeffers, S. V., & Jones, H. R. A. 2011, MNRAS, 412, 1599
Bastian, N., Gieles, M., Ercolano, B., & Gutermuth, R. 2009, MNRAS, 392, 868
Bastien, F. A., Stassun, K. G., Pepper, J., et al. 2014, AJ, 147, 29
Bate, M. R. 2012, MNRAS, 419, 3115
Batista, V., Beaulieu, J.-P., Gould, A., et al. 2014, ApJ, 780, 54
Bean, J. L., Désert, J.-M., Kabath, P., et al. 2011, ApJ, 743, 92
Beauvalet, L., Marchis, F., & Ruffio, J. 2013, AGU Fall Meeting Abstracts, A1758
Becker, G. D., Rauch, M., & Sargent, W. L. W. 2009, ApJ, 698, 1010
Becker, G. D., Sargent, W. L. W., Rauch, M., & Calverley, A. P. 2011, ApJ, 735, 93
Beers, T. C., Preston, G. W., & Shectman, S. A. 1985, AJ, 90, 2089
Beers, T. C., Preston, G. W., & Shectman, S. A. 1992, AJ, 103, 1987
Begelman, M. C., Blandford, R. D., & Rees, M. J. 1980, Nature, 287, 307
Behroozi, P. S., Wechsler, R. H., & Conroy, C. 2013, ApJ, 770, 57
Beichman, C. A., Bryden, G., Gautier, T. N., et al. 2005, ApJ, 626, 1061
Bell, E. F., van der Wel, A., Papovich, C., et al. 2012, ApJ, 753, 167
Belli, S., Newman, A. B., Ellis, R. S., & Konidaris, N. P. 2014, ApJ, 788, L29
Belokurov, V., Zucker, D. B., Evans, N. W., et al. 2006, ApJ, 642, L137
Belokurov, V., Walker, M. G., Evans, N. W., et al. 2009, MNRAS, 397, 1748
Bender, R., Burstein, D., & Faber, S. M. 1992, ApJ, 399, 462
Benedict, G. F., McArthur, B. E., Gatewood, G., et al. 2006, AJ, 132, 2206
Benedict, G. F., McArthur, B. E., Feast, M. W., et al. 2011, AJ, 142, 187
Bennert, V. N., Auger, M. W., Treu, T., Woo, J.-H., & Malkan, M. A. 2011, ApJ, 742, 107
Bennett, D. P., & Rhie, S. H. 1996, ApJ, 472, 660
Bennett, D. P., Anderson, J., Bond, I. A., Udalski, A., & Gould, A. 2006, ApJ, 647, L171
Bennett, D. P., Anderson, J., & Gaudi, B. S. 2007, ApJ, 660, 781

Berger, E. 2014, ARA&A, 52, 43
Berger, E., Fong, W., & Chornock, R. 2013, ApJ, 774, L23
Bergeron, P., Saffer, R. A., & Liebert, J. 1992, ApJ, 394, 228
Berrier, J. C., Bullock, J. S., Barton, E. J., et al. 2006, ApJ, 652, 56
Bessell, M., Bloxham, G., Schmidt, B., et al. 2011, PASP, 123, 789
Best, P. N., Lehnert, M. D., Miley, G. K., Röttgering, H. J. A. 2003, MNRAS, 343, 1
Bhatta, G., Webb, J. R., Hollingsworth, H., et al. 2013, A&A, 558, A92
Beuzit, J.-L., Feldt, M., Dohlen, K., et al. 2008, in Society of Photo-Optical Instrumentation Engineers (SPIE) Conference Series, 7014, 18
Bik, A., Kaper, L., & Waters, L. B. F. M. 2006, A&A, 455, 561
Binney, J., & Tremaine, S. 1987, Galactic Dynamics (Princeton, NJ, Princeton University Press)
Birnstiel, T., Dullemond, C. P., & Pinilla, P. 2013, A&A, 550, L8
Blandford, R. D., & McKee, C. F. 1982, ApJ, 255, 419
Blandford, R. D., & Payne, D. G. 1982, MNRAS, 199, 883
Blanton, M. R., Eisenstein, D., Hogg, D. W., Schlegel, D. J., & Brinkmann, J. 2005, ApJ, 629, 143
Blum, R. D., Schaerer, D., Pasquali, A., et al. 2001, AJ, 122, 1875
Bolton, A. S., Schlegel, D. J., Aubourg, É., et al. 2012, AJ, 144, 144
Bonifacio, P., Pasquini, L., Molaro, P., et al. 2007, A&A, 470, 153
Bonnell, I. A., Bate, M. R., & Vine, S. G. 2003, MNRAS, 343, 413
Booth, C. M., & Schaye, J. 2010, MNRAS, 405, L1
Bouwens, R. J., Illingworth, G. D., Oesch, P. A., et al. 2015, ApJ, 803, 34
Bowler, B. P., Johnson, J. A., Marcy, G. W., et al. 2010a, ApJ, 709, 396
Bowler, B. P., Liu, M. C., Dupuy, T. J., & Cushing, M. C. 2010b, ApJ, 723, 850
Bowler, B. P., Liu, M. C., Kraus, A. L., Mann, A. W., & Ireland, M. J. 2011, ApJ, 743, 148
Bowler, B. P., Liu, M. C., Shkolnik, E. L., & Dupuy, T. J. 2013, ApJ, 774, 55
Bowler, B. P., Liu, M. C., Kraus, A. L., & Mann, A. W. 2014, ApJ, 784, 65
Boylan-Kolchin, M., Bullock, J. S., & Kaplinghat, M. 2011, MNRAS, 415, L40
Boylan-Kolchin, M., Bullock, J. S., & Kaplinghat, M. 2012, MNRAS, 422, 1203
Boylan-Kolchin, M., Bullock, J. S., & Garrison-Kimmel, S. 2014, MNRAS, 443, L44
Bradač, M., Allen, S. W., Treu, T., et al. 2008, ApJ, 687, 959
Bradač, M., Vanzella, E., Hall, N., et al. 2012, ApJ, 755, L7
Bradač, M., Ryan, R., Casertano, S., et al. 2014, ApJ, 785, 108
Braga-Ribas, F., Sicardy, B., Ortiz, J. L., et al. 2014, Nature, 508, 72
Brauer, F., Henning, T., & Dullemond, C. P. 2008, A&A, 487, L1
Brittain, S. D., Najita, J. R., & Carr, J. S. 2009, ApJ, 702, 85
Brittain, S. D., Najita, J. R., Carr, J. S., et al. 2013, ApJ, 767, 159
Brogi, M., Snellen, I. A. G., de Kok, R. J., et al. 2012, Nature, 486, 502
Brogi, M., de Kok, R. J., Birkby, J. L., Schwarz, H., & Snellen, I. A. G. 2014, A&A, 565, A124
Bromm, V., Kudritzki, R. P., & Loeb, A. 2001, ApJ, 552, 464
Bruderer, S. 2013, A&A, 559, A46
Buchhave, L. A., Latham, D. W., Johansen, A., et al. 2012, Nature, 486, 375
Busca, N. G., Delubac, T., Rich, J., et al. 2013, A&A, 552, A96
Butcher, H., & Oemler, Jr., A. 1984, ApJ, 285, 426
Caffau, E., Bonifacio, P., François, P., et al. 2011, Nature, 477, 67
Cameron, E., Carollo, C. M., Oesch, P., et al. 2010, MNRAS, 409, 346
Cano-Díaz, M., Maiolino, R., Marconi, A., et al. 2012, A&A, 537, L8
Cantalupo, S., Lilly, S. J., & Porciani, C. 2007, ApJ, 657, 135
Cantalupo, S., Arrigoni-Battaia, F., Prochaska, J. X., Hennawi, J. F., & Madau, P. 2014, Nature, 506, 63

Capak, P. L., Carilli, C., Jones, G., et al. 2015, Nature, 522, 455
Capetti, A., Axon, D. J., Macchetto, F., Sparks, W. B., & Boksenberg, A. 1995, ApJ, 446, 155
Carini, M. T., & Ryle, W. T. 2012, ApJ, 749, 70
Carollo, D., Beers, T. C., Lee, Y. S., et al. 2007, Nature, 450, 1020
Carollo, D., Beers, T. C., Lee, Y. S., et al. 2008, Nature, 451, 216
Carr, J. S., & Najita, J. R. 2008, Science, 319, 1504
Carr, J. S., & Najita, J. R. 2011, ApJ, 733, 102
Cassan, A., Kubas, D., Beaulieu, J.-P., et al. 2012, Nature, 481, 167
Cassata, P., Giavalisco, M., Guo, Y., et al. 2011, ApJ, 743, 96
Catalán, S., Isern, J., García-Berro, E., & Ribas, I. 2008, MNRAS, 387, 1693
Cen, R. 2012, ApJ, 755, 28
Chabrier, G. 2005, in Astrophysics and Space Science Library, 327, The Initial Mass Function 50 Years Later, eds. E. Corbelli, F. Palla, & H. Zinnecker, 41
Chand, H., Srianand, R., Petitjean, P., & Aracil, B. 2004, A&A, 417, 853
Charbonneau, D., Brown, T. M., Latham, D. W., & Mayor, M. 2000, ApJ, 529, L45
Chary, R., Berger, E., & Cowie, L. 2007, ApJ, 671, 272
Chauvin, G., Lagrange, A.-M., Dumas, C., et al. 2004, A&A, 425, L29
Chauvin, G., Lagrange, A.-M., Zuckerman, B., et al. 2005, A&A, 438, L29
Chauvin, G., Lagrange, A.-M., Bonavita, M., et al. 2010, A&A, 509, A52
Chesneau, O., & Banerjee, D. P. K. 2012, Bulletin of the Astronomical Society of India, 40, 267
Chevallier, M., & Polarski, D. 2001, International Journal of Modern Physics D, 10, 213
Chokshi, A., & Turner, E. L. 1992, MNRAS, 259, 421
Chornock, R., Berger, E., Gezari, S., et al. 2014, ApJ, 780, 44
Christlieb, N., Schörck, T., Frebel, A., et al. 2008, A&A, 484, 721
Chugai, N. N. 2008, Astronomy Letters, 34, 389
Chugai, N. N., Blinnikov, S. I., & Lundqvist, P. 2000, Mem. Soc. Astron. Italiana, 71, 383
Ciardi, B., Scannapieco, E., Stoehr, F., et al. 2006, MNRAS, 366, 689
Ciesla, F. J., & Cuzzi, J. N. 2006, Icarus, 181, 178
Cisternas, M., Jahnke, K., Bongiorno, A., et al. 2011, ApJ, 741, L11
Clowe, D., Bradač, M., Gonzalez, A. H., et al. 2006, ApJ, 648, L109
Coc, A., Descouvemont, P., Uzan, J.-P., & Vangioni, E. 2012, in Nuclei in the Cosmos (NIC XII), 73
Coe, D., Zitrin, A., Carrasco, M., et al. 2013, ApJ, 762, 32
Cohen, J. G., Christlieb, N., Thompson, I., et al. 2013, ApJ, 778, 56
Cole, S., Lacey, C. G., Baugh, C. M., & Frenk, C. S. 2000, MNRAS, 319, 168
Cole, S., Norberg, P., Baugh, C. M., et al. 2001, MNRAS, 326, 255
Comerford, J. M., Gerke, B. F., Newman, J. A., et al. 2009, ApJ, 698, 956
Connelley, M. S., Reipurth, B., & Tokunaga, A. T. 2008, AJ, 135, 2526
Connelley, M. S., Reipurth, B., & Tokunaga, A. T. 2009, AJ, 138, 1193
Conroy, C., Wechsler, R. H., & Kravtsov, A. V. 2006, ApJ, 647, 201
Cooke, R., Pettini, M., Steidel, C. C., Rudie, G. C., & Nissen, P. E. 2011, MNRAS, 417, 1534
Cooke, R., Pettini, M., Jorgenson, R. A., et al. 2013, MNRAS, 431, 1625
Cooke, R. J., Pettini, M., Jorgenson, R. A., Murphy, M. T., & Steidel, C. C. 2014, ApJ, 781, 31
Cooper, M. C., Newman, J. A., Croton, D. J., et al. 2006, MNRAS, 370, 198
Courteau, S., Andersen, D. R., Bershady, M. A., MacArthur, L. A., & Rix, H.-W. 2003, ApJ, 594, 208
Cowie, L. L., Songaila, A., Hu, E. M., & Cohen, J. G. 1996, AJ, 112, 839
Crepp, J. R., Johnson, J. A., Fischer, D. A., et al. 2012, ApJ, 751, 97
Crida, A., Morbidelli, A., & Masset, F. 2006, Icarus, 181, 587
Crockett, C. J., Mahmud, N. I., Prato, L., et al. 2012, ApJ, 761, 164

Croll, B., Jayawardhana, R., Fortney, J. J., Lafrenière, D., & Albert, L. 2010, ApJ, 718, 920
Crossfield, I. J. M. 2013, A&A, 551, A99
Croton, D. J., Springel, V., White, S. D. M., et al. 2006, MNRAS, 365, 11
Cumming, A., Butler, R. P., Marcy, G. W., et al. 2008, PASP, 120, 531
Currie, T., Burrows, A., Itoh, Y., et al. 2011, ApJ, 729, 128
Currie, T., Debes, J., Rodigas, T. J., et al. 2012, ApJ, 760, L32
Currie, T., Burrows, A., & Daemgen, S. 2014a, ApJ, 787, 104
Currie, T., Daemgen, S., Debes, J., et al. 2014b, ApJ, 780, L30
Da Rio, N., Gouliermis, D. A., & Henning, T. 2009, ApJ, 696, 528
Dai, S., Xu, R. X., & Esamdin, A. 2010, MNRAS, 405, 2754
Dalal, N., Holder, G., & Hennawi, J. F. 2004, ApJ, 609, 50
Davé, R., Oppenheimer, B. D., & Sivanandam, S. 2008, MNRAS, 391, 110
Davé, R., Finlator, K., & Oppenheimer, B. D. 2012, MNRAS, 421, 98
Davies, R. I., Thomas, J., Genzel, R., et al. 2006, ApJ, 646, 754
Davies, R. I., Maciejewski, W., Hicks, E. K. S., et al. 2014, ApJ, 792, 101
Davis, M., Faber, S. M., Newman, J., et al. 2003, in Society of Photo-Optical Instrumentation Engineers (SPIE) Conference Series, 4834, Discoveries and Research Prospects from 6- to 10-Meter-Class Telescopes II, ed. P. Guhathakurta, 161
Dawson, W. A., Wittman, D., Jee, M. J., et al. 2012, ApJ, 747, L42
de Felice, A., & Tsujikawa, S. 2010, Living Reviews in Relativity, 13, 3
de Grijs, R., Fritze-v. Alvensleben, U., Anders, P., et al. 2003, MNRAS, 342, 259
de Kok, R. J., Birkby, J., Brogi, M., et al. 2014, A&A, 561, A150
de Wit, W. J., Hoare, M. G., Fujiyoshi, T., et al. 2009, A&A, 494, 157
De Lucia, G., Poggianti, B. M., Aragón-Salamanca, A., et al. 2004, ApJ, 610, L77
Deason, A. J., Van der Marel, R. P., Guhathakurta, P., Sohn, S. T., & Brown, T. M. 2013, ApJ, 766, 24
Deason, A. J., Belokurov, V., Koposov, S. E., & Rockosi, C. M. 2014, ApJ, 787, 30
Dekel, A., & Silk, J. 1986, ApJ, 303, 39
Dekel, A., Birnboim, Y., Engel, G., et al. 2009, Nature, 457, 451
Delfosse, X., Donati, J.-F., Kouach, D., et al. 2013, in SF2A-2013: Proceedings of the Annual Meeting of the French Society of Astronomy and Astrophysics, ed. L. Cambresy, F. Martins, E. Nuss, & A. Palacios, 497
Della Valle, M., Chincarini, G., Panagia, N., et al. 2006, Nature, 444, 1050
Delorme, P., Gagné, J., Girard, J. H., et al. 2013, A&A, 553, L5
The DES Collaboration 2015, ApJ, 807, 50
Di Matteo, T., Springel, V., & Hernquist, L. 2005, Nature, 433, 604
Diamond-Stanic, A. M., Moustakas, J., Tremonti, C. A., et al. 2012, ApJ, 755, L26
Dilday, B., Howell, D. A., Cenko, S. B., et al. 2012, Science, 337, 942
Djorgovski, S., & Davis, M. 1987, ApJ, 313, 59
Do, T., Wright, S. A., Barth, A. J., et al. 2014, AJ, 147, 93
Dong, S., DePoy, D. L., Gaudi, B. S., et al. 2006, ApJ, 642, 842
Dong, S., Udalski, A., Gould, A., et al. 2007, ApJ, 664, 862
Dong, S., Gould, A., Udalski, A., et al. 2009, ApJ, 695, 970
Dressler, A. 1980, ApJ, 236, 351
Dressler, A., Faber, S. M., Burstein, D., et al. 1987, ApJ, 313, L37
Dressler, A., Oemler, Jr., A., Couch, W. J., et al. 1997, ApJ, 490, 577
Dressler, A., Oemler, Jr., A., Poggianti, B. M., et al. 2004, ApJ, 617, 867
Duchêne, G. 1999, A&A, 341, 547
Duchêne, G., & Kraus, A. 2013, ARA&A, 51, 269
Dumusque, X., Pepe, F., Lovis, C., et al. 2012, Nature, 491, 207

Dumusque, X., Bonomo, A. S., Haywood, R. D., et al. 2014, ApJ, 789, 154
Dvali, G., Gabadadze, G., & Porrati, M. 2000, Physics Letters B, 485, 208
Efstathiou, A., McCall, A., & Hough, J. H. 1997, MNRAS, 285, 102
Eggen, O. J., Lynden-Bell, D., & Sandage, A. R. 1962, ApJ, 136, 748
Eisenstein, D. J., Zehavi, I., Hogg, D. W., et al. 2005, ApJ, 633, 560
Eldridge, J. J., & Stanway, E. R. 2009, MNRAS, 400, 1019
Elitzur, M., & Shlosman, I. 2006, ApJ, 648, L101
Ellis, R. S., McLure, R. J., Dunlop, J. S., et al. 2013, ApJ, 763, L7
Emmering, R. T., Blandford, R. D., & Shlosman, I. 1992, ApJ, 385, 460
Ercolano, B., & Owen, J. E. 2010, MNRAS, 406, 1553
Eastman, J., Martini, P., Sivakoff, G., et al. 2007, ApJ, 664, L9
Evans, II, N. J., Dunham, M. M., Jørgensen, J. K., et al. 2009, ApJS, 181, 321
Evslin, J. 2015, MNRAS, 452, L41
Fabian, A. C. 2012, ARA&A, 50, 455
Fabrycky, D. C., & Murray-Clay, R. A. 2010, ApJ, 710, 1408
Fan, X., Strauss, M. A., Schneider, D. P., et al. 2000, AJ, 119, 1
Fan, X., Narayanan, V. K., Lupton, R. H., et al. 2001, AJ, 122, 2833
Fan, X., Strauss, M. A., Schneider, D. P., et al. 2003, AJ, 125, 1649
Fan, X., Hennawi, J. F., Richards, G. T., et al. 2004, AJ, 128, 515
Fan, X., Strauss, M. A., Becker, R. H., et al. 2006, AJ, 132, 117
Fedele, D., Pascucci, I., Brittain, S., et al. 2011, ApJ, 732, 106
Fenner, Y., Gibson, B. K., Lee, H.-c., et al. 2003, PASA, 20, 340
Ferland, G. J., Korista, K. T., Verner, D. A., et al. 1998, PASP, 110, 761
Ferrarese, L., & Merritt, D. 2000, ApJ, 539, L9
Filippenko, A. V., & Ho, L. C. 2003, ApJ, 588, L13
Finkelstein, S. L., Papovich, C., Ryan, R. E., et al. 2012, ApJ, 758, 93
Fischer, D. A., & Valenti, J. 2005, ApJ, 622, 1102
Folatelli, G., Phillips, M. M., Morrell, N., et al. 2012, ApJ, 745, 74
Foley, R. J., Challis, P. J., Chornock, R., et al. 2013, ApJ, 767, 57
Förster Schreiber, N. M., Genzel, R., Bouché, N., et al. 2009, ApJ, 706, 1364
Fortney, J. J., Lodders, K., Marley, M. S., & Freedman, R. S. 2008, ApJ, 678, 1419
Frebel, A. 2010, arXiv:1012.1323
Frebel, A., Christlieb, N., Norris, J. E., Aoki, W., & Asplund, M. 2006, ApJ, 638, L17
Frebel, A., Christlieb, N., Norris, J. E., et al. 2007, ApJ, 660, L117
Frebel, A., Kirby, E. N., & Simon, J. D. 2010, Nature, 464, 72
Freese, K., & Lewis, M. 2002, Physics Letters B, 540, 1
Freire, P. C. C., Wex, N., Esposito-Farèse, G., et al. 2012, MNRAS, 423, 3328
Fulbright, J. P., Rich, R. M., & Castro, S. 2004, ApJ, 612, 447
Fung, J., Shi, J.-M., & Chiang, E. 2014, ApJ, 782, 88
Gal-Yam, A., Fox, D. B., Price, P. A., et al. 2006, Nature, 444, 1053
Gallart, C., Zoccali, M., & Aparicio, A. 2005, ARA&A, 43, 387
Gallazzi, A., Charlot, S., Brinchmann, J., White, S. D. M., & Tremonti, C. A. 2005, MNRAS, 362, 41
Gallerani, S., Choudhury, T. R., & Ferrara, A. 2006, MNRAS, 370, 1401
Galli, S. 2013, Phys. Rev. D, 87, 123516
Garaud, P., & Lin, D. N. C. 2007, ApJ, 654, 606
Garrison-Kimmel, S., Rocha, M., Boylan-Kolchin, M., Bullock, J. S., & Lally, J. 2013, MNRAS, 433, 3539
Gaudi, B. S. 2012, ARA&A, 50, 411
Gebhardt, K., Kormendy, J., Ho, L. C., et al. 2000, ApJ, 543, L5

Gebhardt, K., Lauer, T. R., Kormendy, J., et al. 2001, AJ, 122, 2469
Gebhardt, K., Rich, R. M., & Ho, L. C. 2005, ApJ, 634, 1093
Gebhardt, K., Adams, J., Richstone, D., et al. 2011, ApJ, 729, 119
Gehrels, N., Norris, J. P., Barthelmy, S. D., et al. 2006, Nature, 444, 1044
Genzel, R., Tacconi, L. J., Eisenhauer, F., et al. 2006, Nature, 442, 786
Gezari, S., Dessart, L., Basa, S., et al. 2008, ApJ, 683, L131
Gezari, S., Chornock, R., Rest, A., et al. 2012, Nature, 485, 217
Girardi, L., Bressan, A., Bertelli, G., & Chiosi, C. 2000, A&AS, 141, 371
Glassgold, A. E., Najita, J., & Igea, J. 2004, ApJ, 615, 972
Glassgold, A. E., Najita, J. R., & Igea, J. 2007, ApJ, 656, 515
Gobat, R., Strazzullo, V., Daddi, E., et al. 2012, ApJ, 759, L44
Gobat, R., Strazzullo, V., Daddi, E., et al. 2013, ApJ, 776, 9
Goldman, B., Marsat, S., Henning, T., Clemens, C., & Greiner, J. 2010, MNRAS, 405, 1140
Golse, G., Kneib, J.-P., & Soucail, G. 2002, A&A, 387, 788
Goswami, A., & Prantzos, N. 2000, A&A, 359, 191
Goswami, A., Karinkuzhi, D., & Shantikumar, N. S. 2010, ApJ, 723, L238
Goswami, A., & Aoki, W. 2013, ApJ, 763, L37
Gould, A., & Loeb, A. 1992, ApJ, 396, 104
Gould, A., Udalski, A., An, D., et al. 2006, ApJ, 644, L37
Gould, A., Dong, S., Gaudi, B. S., et al. 2010, ApJ, 720, 1073
Gould, A., & Horne, K. 2013, ApJ, 779, L28
Governato, F., Brook, C., Mayer, L., et al. 2010, Nature, 463, 203
Greene, J. E., & Ho, L. C. 2007, ApJ, 667, 131
Greene, J. E., Peng, C. Y., Kim, M., et al. 2010, ApJ, 721, 26
Gregg, M. D., Lacy, M., White, R. L., et al. 2002, ApJ, 564, 133
Greggio, L. 2005, A&A, 441, 1055
Griest, K., & Safizadeh, N. 1998, ApJ, 500, 37
Grillmair, C. J. 2006, ApJ, 645, L37
Grillmair, C. J., & Dionatos, O. 2006, ApJ, 643, L17
Grogin, N. A., Kocevski, D. D., Faber, S. M., et al. 2011, ApJS, 197, 35
Groves, B., Nefs, B., & Brandl, B. 2008, MNRAS, 391, L113
Guillochon, J., Manukian, H., & Ramirez-Ruiz, E. 2014, ApJ, 783, 23
Gunn, J. E., & Gott, III, J. R. 1972, ApJ, 176, 1
Guo, Y., Giavalisco, M., Cassata, P., et al. 2012, ApJ, 749, 149
Han, C., & Chang, H.-Y. 2003, MNRAS, 338, 637
Hannestad, S., & Raffelt, G. 2004, J. Cosmol. Astropart. Phys., 4, 8
Hao, L., Wu, Y., Charmandaris, V., et al. 2009, ApJ, 704, 1159
Hatzes, A. P., Cochran, W. D., McArthur, B., et al. 2000, ApJ, 544, L145
Hatzes, A. P. 2013, ApJ, 770, 133
Hayashi, K., & Chiba, M. 2012, ApJ, 755, 145
Hazra, D. K., Majumdar, S., Pal, S., Panda, S., & Sen, A. A. 2015, Phys. Rev. D, 91, 083005
Hearnshaw, J. B., Abe, F., Bond, I. A., et al. 2006, in The 9th Asian-Pacific Regional IAU Meeting, eds. W. Sutantyo, P. W. Premadi, P. Mahasena, T. Hidayat, & S. Mineshige, 272
Heiderman, A., Evans, II, N. J., Allen, L. E., Huard, T., & Heyer, M. 2010, ApJ, 723, 1019
Helmi, A., Irwin, M. J., Tolstoy, E., et al. 2006, ApJ, 651, L121
Henderson, C. B., Gaudi, B. S., Han, C., et al. 2015, in American Astronomical Society Meeting Abstracts, 225, American Astronomical Society Meeting Abstracts, #202.03
Henderson, C. B., Gaudi, B. S., Han, C., et al. 2014, ApJ, 794, 52

Hennawi, J. F., & Prochaska, J. X. 2013, ApJ, 766, 58
Henning, T., & Semenov, D. 2013, Chemical Reviews, 113, 9016
Hicks, E. K. S., & Malkan, M. A. 2008, ApJS, 174, 31
Hicks, E. K. S., Davies, R. I., Malkan, M. A., et al. 2009, ApJ, 696, 448
Hicks, E. K. S., Davies, R. I., Maciejewski, W., et al. 2013, ApJ, 768, 107
Hillenbrand, L. A., & Carpenter, J. M. 2000, ApJ, 540, 236
Hillenbrand, L. A., & White, R. J. 2004, ApJ, 604, 741
Hirano, S., Hosokawa, T., Yoshida, N., et al. 2014, ApJ, 781, 60
Ho, L. C., & Filippenko, A. V. 1996, ApJ, 466, L83
Ho, L. C. W. 2004, Coevolution of Black Holes and Galaxies, 292
Ho, L. C. 2008, ARA&A, 46, 475
Honda, M., Inoue, A. K., Fukagawa, M., et al. 2009, ApJ, 690, L110
Hopkins, P. F., Hernquist, L., Cox, T. J., et al. 2006, ApJS, 163, 1
Hopkins, P. F., Hernquist, L., Cox, T. J., Dutta, S. N., & Rothberg, B. 2008, ApJ, 679, 156
Hopkins, P. F., Kereš, D., Murray, N., Quataert, E., & Hernquist, L. 2012, MNRAS, 427, 968
Howard, A. W., Marcy, G. W., Bryson, S. T., et al. 2012, ApJS, 201, 15
Howard, A. W. 2013, Science, 340, 572
Howard, A. W., Sanchis-Ojeda, R., Marcy, G. W., et al. 2013, Nature, 503, 381
Howell, D. A. 2011, Nature Communications, 2, 350
Howell, S. B., Sobeck, C., Haas, M., et al. 2014, PASP, 126, 398
Hu, W., Eisenstein, D. J., & Tegmark, M. 1998, Physical Review Letters, 80, 5255
Hu, W., & Sawicki, I. 2007, Phys. Rev. D, 76, 064004
Huélamo, N., Figueira, P., Bonfils, X., et al. 2008, A&A, 489, L9
Hughes, J. P., Chugai, N., Chevalier, R., Lundqvist, P., & Schlegel, E. 2007, ApJ, 670, 1260
Ichikawa, K., Ueda, Y., Terashima, Y., et al. 2012, ApJ, 754, 45
Imanishi, M., Imase, K., Oi, N., & Ichikawa, K. 2011, AJ, 141, 156
Inami, H., Armus, L., Charmandaris, V., et al. 2013, ApJ, 777, 156
Ireland, M. J., Kraus, A., Martinache, F., Law, N., & Hillenbrand, L. A. 2011, ApJ, 726, 113
Ishigaki, M., Kawamata, R., Ouchi, M., et al. 2015, ApJ, 799, 12
Jaacks, J., Thompson, R., & Nagamine, K. 2013, ApJ, 766, 94
Jacobson, H. R., & Frebel, A. 2014, Journal of Physics G Nuclear Physics, 41, 044001
Jaffe, W., Meisenheimer, K., Röttgering, H. J. A., et al. 2004, Nature, 429, 47
Jahnke, K., Bongiorno, A., Brusa, M., et al. 2009, ApJ, 706, L215
Jain, B., & Taylor, A. 2003, Physical Review Letters, 91, 141302
Jain, B., Joyce, A., Thompson, R., et al. 2013, arXiv:1309.5389
Janczak, J., Fukui, A., Dong, S., et al. 2010, ApJ, 711, 731
Jang-Condell, H. 2009, ApJ, 700, 820
Jauzac, M., Clément, B., Limousin, M., et al. 2014, MNRAS, 443, 1549
Jewitt, D. 2012, AJ, 143, 66
Johnson, J. A., Aller, K. M., Howard, A. W., & Crepp, J. R. 2010, PASP, 122, 905
Jones, T. A., Swinbank, A. M., Ellis, R. S., Richard, J., & Stark, D. P. 2010, MNRAS, 404, 1247
Jones, T., Stark, D. P., & Ellis, R. S. 2012, ApJ, 751, 51
Jones, T., Ellis, R. S., Richard, J., & Jullo, E. 2013, ApJ, 765, 48
Juarez, Y., Maiolino, R., Mujica, R., et al. 2009, A&A, 494, L25
Jullo, E., Natarajan, P., Kneib, J.-P., et al. 2010, Science, 329, 924
Kalas, P., Graham, J. R., Clampin, M. C., & Fitzgerald, M. P. 2006, ApJ, 637, L57
Kalas, P., Graham, J. R., Chiang, E., et al. 2008, Science, 322, 1345
Kaltenegger, L., Selsis, F., Fridlund, M., et al. 2010, Astrobiology, 10, 89

Kann, D. A., Klose, S., Zhang, B., et al. 2011, ApJ, 734, 96
Karachentsev, I. D., Makarov, D. I., & Kaisina, E. I. 2013, AJ, 145, 101
Karakas, A. I. 2010, MNRAS, 403, 1413
Kartaltepe, J. S., Sanders, D. B., Scoville, N. Z., et al. 2007, ApJS, 172, 320
Kartje, J. F., Königl, A., & Elitzur, M. 1999, ApJ, 513, 180
Kasen, D., Badnell, N. R., & Barnes, J. 2013, ApJ, 774, 25
Kasen, D., Fernández, R., & Metzger, B. D. 2015, MNRAS, 450, 1777
Kasliwal, V. P., Vogeley, M. S., & Richards, G. T. 2015, MNRAS, 451, 4328
Kassin, S. A., Weiner, B. J., Faber, S. M., et al. 2007, ApJ, 660, L35
Kauffmann, G., & Heckman, T. M. 2009, MNRAS, 397, 135
Keller, S. C., Bessell, M. S., Frebel, A., et al. 2014, Nature, 506, 463
Kelly, P. L., Rodney, S. A., Treu, T., et al. 2015, Science, 347, 1123
Kempton, M. E., & Rauscher, E. 2012, ApJ, 751, 117
Kennicutt, Jr., R. C. 1998, ApJ, 498, 541
Kereš, D., Katz, N., Weinberg, D. H., & Davé, R. 2005, MNRAS, 363, 2
Khoury, J., & Weltman, A. 2004, Phys. Rev. D, 69, 044026
Kimm, T., Somerville, R. S., Yi, S. K., et al. 2009, MNRAS, 394, 1131
Kirby, E. N., Guhathakurta, P., Bolte, M., Sneden, C., & Geha, M. C. 2009, ApJ, 705, 328
Kirby, E. N., Cohen, J. G., Guhathakurta, P., et al. 2013a, ApJ, 779, 102
Kirby, E. N., Boylan-Kolchin, M., Cohen, J. G., et al. 2013b, ApJ, 770, 16
Klypin, A., Kravtsov, A. V., Valenzuela, O., & Prada, F. 1999, ApJ, 522, 82
Knez, C., Lacy, J. H., Evans, II, N. J., van Dishoeck, E. F., & Richter, M. J. 2009, ApJ, 696, 471
Kocevski, D. D., Lubin, L. M., Lemaux, B. C., et al. 2009, ApJ, 703, L33
Kocevski, D. D., Faber, S. M., Mozena, M., et al. 2012, ApJ, 744, 148
Koch, A., Feltzing, S., Adén, D., & Matteucci, F. 2013, A&A, 554, A5
Koch, A., Hansen, T., Feltzing, S., & Wilkinson, M. I. 2014, ApJ, 780, 91
Koekemoer, A. M., Faber, S. M., Ferguson, H. C., et al. 2011, ApJS, 197, 36
Kollmeier, J. A., Gould, A., Rockosi, C., et al. 2010, ApJ, 723, 812
Kominami, J., & Ida, S. 2002, Icarus, 157, 43
Komossa, S., Burwitz, V., Hasinger, G., et al. 2003, ApJ, 582, L15
Konigl, A., & Kartje, J. F. 1994, ApJ, 434, 446
Konno, A., Ouchi, M., Ono, Y., et al. 2014, ApJ, 797, 16
Konopacky, Q. M., Barman, T. S., Macintosh, B. A., & Marois, C. 2013, Science, 339, 1398
Koopmans, L. V. E. 2005, MNRAS, 363, 1136
Koposov, S. E., Rix, H.-W., & Hogg, D. W. 2010, ApJ, 712, 260
Koposov, S. E., Belokurov, V., Torrealba, G., & Evans, N. W. 2015, ApJ, 805, 130
Kormendy, J., & Richstone, D. 1995, ARA&A, 33, 581
Kormendy, J., & Ho, L. C. 2013, ARA&A, 51, 511
Korn, A. J., Grundahl, F., Richard, O., et al. 2006, Nature, 442, 657
Koyama, Y., Kodama, T., Tanaka, M., Shimasaku, K., & Okamura, S. 2007, MNRAS, 382, 1719
Kozłowski, S., Woźniak, P. R., Mao, S., & Wood, A. 2007, ApJ, 671, 420
Krabbe, A., Böker, T., & Maiolino, R. 2001, ApJ, 557, 626
Kraljic, K., Bournaud, F., & Martig, M. 2012, ApJ, 757, 60
Kraus, A. L., Ireland, M. J., Martinache, F., & Hillenbrand, L. A. 2011, ApJ, 731, 8
Kraus, A. L., & Ireland, M. J. 2012, ApJ, 745, 5
Kraus, A. L., Ireland, M. J., Cieza, L. A., et al. 2014, ApJ, 781, 20
Krolik, J. H., & Begelman, M. C. 1988, ApJ, 329, 702
Krumholz, M. R. 2014, Phys. Rep., 539, 49

Kulkarni, S. R. 2005, arXiv: astro-ph/0510256
Kuo, C. Y., Braatz, J. A., Condon, J. J., et al. 2011, ApJ, 727, 20
Kurk, J. D., Walter, F., Fan, X., et al. 2007, ApJ, 669, 32
Kuzuhara, M., Tamura, M., Kudo, T., et al. 2013, ApJ, 774, 11
Lagrange, A.-M., Bonnefoy, M., Chauvin, G., et al. 2010, Science, 329, 57
Lahuis, F., van Dishoeck, E. F., Boogert, A. C. A., et al. 2006, ApJ, 636, L145
Laor, A., & Draine, B. T. 1993, ApJ, 402, 441
Larson, R. B., Tinsley, B. M., & Caldwell, C. N. 1980, ApJ, 237, 692
Larson, R. B. 1995, MNRAS, 272, 213
Law, D. R., Steidel, C. C., Erb, D. K., et al. 2007, ApJ, 669, 929
Law, D. R., Steidel, C. C., Erb, D. K., et al. 2009, ApJ, 697, 2057
Law, N. M., Morton, T., Baranec, C., et al. 2014, ApJ, 791, 35
Le Delliou, M., Lacey, C. G., Baugh, C. M., & Morris, S. L. 2006, MNRAS, 365, 712
Lee, J.-E., Bergin, E. A., & Nomura, H. 2010, ApJ, 710, L21
Lee, B., Giavalisco, M., Williams, C. C., et al. 2013a, ApJ, 774, 47
Lee, K.-G., Bailey, S., Bartsch, L. E., et al. 2013b, AJ, 145, 69
Lee, K.-G., Hennawi, J. F., White, M., Croft, R. A. C., & Ozbek, M. 2014, ApJ, 788, 49
Leger, A., Pirre, M., & Marceau, F. J. 1993, A&A, 277, 309
Léger, A., Fontecave, M., Labeyrie, A., et al. 2011, Astrobiology, 11, 335
Lemaux, B. C., Lubin, L. M., Shapley, A., et al. 2010, ApJ, 716, 970
Lemaux, B. C., Gal, R. R., Lubin, L. M., et al. 2012, ApJ, 745, 106
Li, L.-X., & Paczyński, B. 1998, ApJ, 507, L59
Li, L., Ingersoll, A. P., Vasavada, A. R., et al. 2004, Icarus, 172, 9
Li, C.-H., Benedick, A. J., Fendel, P., et al. 2008, Nature, 452, 610
Lien, A., & Fields, B. D. 2009, J. Cosmol. Astropart. Phys., 1, 47
LIGO Scientific Collaboration, & Virgo Collaboration 2012, A&A, 539, A124
Lilly, S. J., Le Fèvre, O., Renzini, A., et al. 2007, ApJS, 172, 70
Linder, E. V. 2003, Physical Review Letters, 90, 091301
Liu, G., Calzetti, D., Kennicutt, Jr., R. C., et al. 2013a, ApJ, 772, 27
Liu, M. C., Magnier, E. A., Deacon, N. R., et al. 2013b, ApJ, 777, L20
Lopez-Rodriguez, E., Packham, C., Young, S., et al. 2013, MNRAS, 431, 2723
Lopez-Rodriguez, E., Packham, C., Jones, T. J., et al. 2015, MNRAS, 452, 1902
Lotz, J. M., Davis, M., Faber, S. M., et al. 2008, ApJ, 672, 177
Lovis, C., Mayor, M., Pepe, F., et al. 2006, The Messenger, 124, 29
Lovis, C., Mayor, M., Pepe, F., Queloz, D., & Udry, S. 2008, in Astronomical Society of the Pacific Conference Series, 398, Extreme Solar Systems, eds. D. Fischer, F. A. Rasio, S. E. Thorsett, & A. Wolszczan, 455
Lu, J. R., Do, T., Ghez, A. M., et al. 2013, ApJ, 764, 155
Lubin, L. M., Oke, J. B., & Postman, M. 2002, AJ, 124, 1905
Lubin, L. M., Gal, R. R., Lemaux, B. C., Kocevski, D. D., & Squires, G. K. 2009, AJ, 137, 4867
Lubow, S. H., Seibert, M., & Artymowicz, P. 1999, ApJ, 526, 1001
Luhman, K. L., Burgasser, A. J., & Bochanski, J. J. 2011, ApJ, 730, L9
Lumsden, S. L., Moore, T. J. T., Smith, C., et al. 1999, MNRAS, 303, 209
Lupu, R. E., Zahnle, K., Marley, M. S., et al. 2014, ApJ, 784, 27
Lutz, D., Maiolino, R., Spoon, H. W. W., & Moorwood, A. F. M. 2004, A&A, 418, 465
Lyons, J. R., & Young, E. D. 2005, Nature, 435, 317
Lyra, W., Johansen, A., Klahr, H., & Piskunov, N. 2009, A&A, 493, 1125
Machida, M. N. 2008, ApJ, 682, L1
Machida, M. N., Kokubo, E., Inutsuka, S.-i., & Matsumoto, T. 2008, ApJ, 685, 1220

Macintosh, B., Troy, M., Doyon, R., et al. 2006, in Society of Photo-Optical Instrumentation Engineers (SPIE) Conference Series, 6272
Macintosh, B., Graham, J. R., Ingraham, P., et al. 2014, Proceedings of the National Academy of Science, 111, 12661
Madau, P., & Dickinson, M. 2014, ARA&A, 52, 415
Maeda, K., Benetti, S., Stritzinger, M., et al. 2010, Nature, 466, 82
Magnelli, B., Popesso, P., Berta, S., et al. 2013, A&A, 553, A132
Magorrian, J., Tremaine, S., Richstone, D., et al. 1998, AJ, 115, 2285
Mahadevan, S., Ramsey, L., Bender, C., et al. 2012, in Society of Photo-Optical Instrumentation Engineers (SPIE) Conference Series, 8446, 1
Majewski, S. R., Skrutskie, M. F., Weinberg, M. D., & Ostheimer, J. C. 2003, ApJ, 599, 1082
Mandell, A. M., Bast, J., van Dishoeck, E. F., et al. 2012, ApJ, 747, 92
Mao, S., & Paczynski, B. 1991, ApJ, 374, L37
Marchis, F., Descamps, P., Hestroffer, D., & Berthier, J. 2005, Nature, 436, 822
Marconi, A., & Hunt, L. K. 2003, ApJ, 589, L21
Marion, G. H., Höflich, P., Gerardy, C. L., et al. 2009, AJ, 138, 727
Marley, M. S., Saumon, D., Cushing, M., et al. 2012, ApJ, 754, 135
Marois, C., Macintosh, B., Barman, T., et al. 2008, Science, 322, 1348
Marois, C., Macintosh, B., & Véran, J.-P. 2010a, in Society of Photo-Optical Instrumentation Engineers (SPIE) Conference Series, 7736, 1
Marois, C., Zuckerman, B., Konopacky, Q. M., Macintosh, B., & Barman, T. 2010b, Nature, 468, 1080
Marois, C., Véran, J.-P., & Correia, C. 2012, in Society of Photo-Optical Instrumentation Engineers (SPIE) Conference Series, 8447, 26
Marois, C., Correia, C., Véran, J.-P., & Currie, T. 2014, in IAU Symposium, 299, eds. M. Booth, B. C. Matthews, & J. R. Graham, 48
Marscher, A. P. 2014, ApJ, 780, 87
Martin, C. L., & Bouché, N. 2009, ApJ, 703, 1394
Martín-Hernández, N. L., Bik, A., Puga, E., Nürnberger, D. E. A., & Bronfman, L. 2008, A&A, 489, 229
Martinache, F., & Guyon, O. 2009, in Society of Photo-Optical Instrumentation Engineers (SPIE) Conference Series, 7440, 0
Martinache, F., Guyon, O., Jovanovic, N., et al. 2014, PASP, 126, 565
Mashonkina, L., Gehren, T., Travaglio, C., & Borkova, T. 2003, A&A, 397, 275
Mashonkina, L., & Zhao, G. 2006, A&A, 456, 313
Mason, R. E., Geballe, T. R., Packham, C., et al. 2006, ApJ, 640, 612
Massey, P., Olsen, K. A. G., Hodge, P. W., et al. 2006, AJ, 131, 2478
Mattila, S., Dahlen, T., Efstathiou, A., et al. 2012, ApJ, 756, 111
Max, C. E., Canalizo, G., & de Vries, W. H. 2007, Science, 316, 1877
Mayor, M., & Queloz, D. 1995, Nature, 378, 355
Mayor, M., Bonfils, X., Forveille, T., et al. 2009, A&A, 507, 487
Mayor, M., Marmier, M., Lovis, C., et al. 2011, arXiv:1109.2497
McConnachie, A. W., Irwin, M. J., Ferguson, A. M. N., et al. 2005, MNRAS, 356, 979
McConnell, N. J., Ma, C.-P., Gebhardt, K., et al. 2011, Nature, 480, 215
McConnell, N. J., Ma, C.-P., Murphy, J. D., et al. 2012, ApJ, 756, 179
McConnell, N. J., & Ma, C.-P. 2013, ApJ, 764, 184
McDonald, P., Seljak, U., Burles, S., et al. 2006, ApJS, 163, 80
McDonald, M., Courteau, S., & Tully, R. B. 2009, MNRAS, 394, 2022
Medling, A. M., Ammons, S. M., Max, C. E., et al. 2011, ApJ, 743, 32
Medling, A. M., U, V., Guedes, J., et al. 2014, ApJ, 784, 70

Meléndez, J., & Cohen, J. G. 2007, ApJ, 659, L25
Meléndez, J., & Cohen, J. G. 2009, ApJ, 699, 2017
Meléndez, J., & Ramírez, I. 2004, ApJ, 615, L33
Melis, C., Zuckerman, B., Rhee, J. H., & Song, I. 2010, ApJ, 717, L57
Melvin, T., Masters, K., Lintott, C., et al. 2014, MNRAS, 438, 2882
Merrett, H. R., Merrifield, M. R., Douglas, N. G., et al. 2006, MNRAS, 369, 120
Merritt, D. 2006, ApJ, 648, 976
Merritt, D., Alexander, T., Mikkola, S., & Will, C. M. 2010, Phys. Rev. D, 81, 062002
Metzger, B. D., Martínez-Pinedo, G., Darbha, S., et al. 2010, MNRAS, 406, 2650
Meyer, L., Eckart, A., Schödel, R., et al. 2006, A&A, 460, 15
Meynet, G., Maeder, A., Hirschi, R., Ekström, S., & Chiappini, C. 2006, in Nuclei in the Cosmos IX, Proceedings of Science, IX, Nuclei in the Cosmos IX, Proceedings of Science, IX, see *http://pos.sissa.it /archive/conferences/028/015/NIC-IX_015.pdf*
Mieske, S., Frank, M. J., Baumgardt, H., et al. 2013, A&A, 558, A14
Mihos, J. C., & Hernquist, L. 1994, ApJ, 431, L9
Miller, S. H., Bundy, K., Sullivan, M., Ellis, R. S., & Treu, T. 2011, ApJ, 741, 115
Milosavljević, M., & Merritt, D. 2001, ApJ, 563, 34
Milosavljević, M., Merritt, D., Rest, A., & van den Bosch, F. C. 2002, MNRAS, 331, L51
Milosavljević, M., & Merritt, D. 2003, ApJ, 596, 860
Miralda-Escudé, J. 1998, ApJ, 501, 15
Miyoshi, M., Moran, J., Herrnstein, J., et al. 1995, Nature, 373, 127
Molaro, P., Centurión, M., Whitmore, J. B., et al. 2013, A&A, 555, A68
Moore, B., Ghigna, S., Governato, F., et al. 1999a, ApJ, 524, L19
Moore, B., Quinn, T., Governato, F., Stadel, J., & Lake, G. 1999b, MNRAS, 310, 1147
Morales, F. Y., Rieke, G. H., Werner, M. W., et al. 2011, ApJ, 730, L29
Mortlock, D. J., Warren, S. J., Venemans, B. P., et al. 2011, Nature, 474, 616
Moster, B. P., Naab, T., & White, S. D. M. 2013, MNRAS, 428, 3121
Motohara, K., Maeda, K., Gerardy, C. L., et al. 2006, ApJ, 652, L101
Moustakas, L. A., & Metcalf, R. B. 2003, MNRAS, 339, 607
Müller-Sánchez, F., Prieto, M. A., Hicks, E. K. S., et al. 2011, ApJ, 739, 69
Müller-Sánchez, F., Malkan, M., Hicks, E. K. S., & Davies, R. I. 2013a, in IAU Symposium, 292, eds. T. Wong, & J. Ott, 363
Müller-Sánchez, F., Prieto, M. A., Mezcua, M., et al. 2013b, ApJ, 763, L1
Muraki, Y., Han, C., Bennett, D. P., et al. 2011, ApJ, 741, 22
Murphy, M. T., Webb, J. K., & Flambaum, V. V. 2003, MNRAS, 345, 609
Murphy, M. T., Tzanavaris, P., Webb, J. K., & Lovis, C. 2007, MNRAS, 378, 221
Mushotzky, R. F., Edelson, R., Baumgartner, W., & Gandhi, P. 2011, ApJ, 743, L12
Muto, T., Grady, C. A., Hashimoto, J., et al. 2012, ApJ, 748, L22
Najita, J. R., Carr, J. S., Pontoppidan, K. M., et al. 2013, ApJ, 766, 134
Narayanan, V. K., Spergel, D. N., Davé, R., & Ma, C.-P. 2000, ApJ, 543, L103
Naud, M.-E., Artigau, É., Malo, L., et al. 2014, ApJ, 787, 5
Navarro, J. F., Frenk, C. S., & White, S. D. M. 1996, ApJ, 462, 563
Navarro, J. F., Helmi, A., & Freeman, K. C. 2004, ApJ, 601, L43
Nenkova, M., Ivezić, Ž., & Elitzur, M. 2002, ApJ, 570, L9
Newberg, H. J., Willett, B. A., Yanny, B., & Xu, Y. 2010, ApJ, 711, 32
Newman, J. A., Cooper, M. C., Davis, M., et al. 2013, ApJS, 208, 5
Nielsen, E. L., Liu, M. C., Wahhaj, Z., et al. 2013, ApJ, 776, 4
Nierenberg, A. M., Treu, T., Wright, S. A., Fassnacht, C. D., & Auger, M. W. 2014, MNRAS, 442, 2434

Nishiyama, S., Tamura, M., Hatano, H., et al. 2009, ApJ, 702, L56
Nissanke, S., Kasliwal, M., & Georgieva, A. 2013, ApJ, 767, 124
Noeske, K. G., Weiner, B. J., Faber, S. M., et al. 2007, ApJ, 660, L43
Nomoto, K., Tominaga, N., Umeda, H., Kobayashi, C., & Maeda, K. 2006, Nuclear Physics A, 777, 424
Norris, J. E., Ryan, S. G., Beers, T. C., & Deliyannis, C. P. 1997, ApJ, 485, 370
Norris, J. E., Yong, D., Bessell, M. S., et al. 2013, ApJ, 762, 28
Nowak, N., Saglia, R. P., Thomas, J., et al. 2008, MNRAS, 391, 1629
Oñorbe, J., Boylan-Kolchin, M., Bullock, J. S., et al. 2015, arXiv:1502.02036
Öberg, K. I., Qi, C., Wilner, D. J., & Andrews, S. M. 2011, ApJ, 743, 152
Oesch, P. A., Bouwens, R. J., Carollo, C. M., et al. 2010, ApJ, 709, L21
Offner, S. S. R., Clark, P. C., Hennebelle, P., et al. 2014, Protostars and Planets VI, 53
Oguri, M., & Kawano, Y. 2003, MNRAS, 338, L25
Oguri, M., & Marshall, P. J. 2010, MNRAS, 405, 2579
Oka, A., Inoue, A. K., Nakamoto, T., & Honda, M. 2012, ApJ, 747, 138
Okamoto, Y. K., Kataza, H., Honda, M., et al. 2004, Nature, 431, 660
Olsen, K. A. G., Blum, R. D., & Rigaut, F. 2003, AJ, 126, 452
Onken, C. A., Ferrarese, L., Merritt, D., et al. 2004, ApJ, 615, 645
Ono, Y., Ouchi, M., Mobasher, B., et al. 2012, ApJ, 744, 83
Ono, Y., Ouchi, M., Curtis-Lake, E., et al. 2013, ApJ, 777, 155
Oppenheimer, B. D., Davé, R., Katz, N., Kollmeier, J. A., & Weinberg, D. H. 2012, MNRAS, 420, 829
Osterman, S., Diddams, S., Beasley, M., et al. 2007, in Society of Photo-Optical Instrumentation Engineers (SPIE) Conference Series, 6693, 1
Ouchi, M., Shimasaku, K., Furusawa, H., et al. 2010, ApJ, 723, 869
Ouchi, M., Ellis, R., Ono, Y., et al. 2013, ApJ, 778, 102
Owen, T. 1980, in Astrophysics and Space Science Library, 83, Strategies for the Search for Life in the Universe, ed. M. D. Papagiannis, 177
Packham, C., Young, S., Hough, J. H., Axon, D. J., & Bailey, J. A. 1997, MNRAS, 288, 375
Packham, C., Radomski, J. T., Roche, P. F., et al. 2005, ApJ, 618, L17
Packham, C., Young, S., Fisher, S., et al. 2007, ApJ, 661, L29
Pandey, G., Lambert, D. L., & Rao, N. K. 2008, ApJ, 674, 1068
Pandey, S. B. 2013, Journal of Astrophysics and Astronomy, 34, 157
Parrent, J. T., Thomas, R. C., Fesen, R. A., et al. 2011, ApJ, 732, 30
Paschos, P., & Norman, M. L. 2005, ApJ, 631, 59
Pascucci, I., Herczeg, G., Carr, J. S., & Bruderer, S. 2013, ApJ, 779, 178
Patat, F., Chandra, P., Chevalier, R., et al. 2007, Science, 317, 924
Patat, F., Cordiner, M. A., Cox, N. L. J., et al. 2013, A&A, 549, A62
Paulson, D. B., Saar, S. H., Cochran, W. D., & Henry, G. W. 2004, AJ, 127, 1644
Peña Ramírez, K., Béjar, V. J. S., Zapatero Osorio, M. R., Petr-Gotzens, M. G., & Martín, E. L. 2012, ApJ, 754, 30
Pearson, K. J., Horne, K., & Skidmore, W. 2005, ApJ, 619, 999
Peng, Y.-j., Lilly, S. J., Renzini, A., & Carollo, M. 2012, ApJ, 757, 4
Pentericci, L., Fontana, A., Vanzella, E., et al. 2011, ApJ, 743, 132
Pepe, F., Cristiani, S., Rebolo, R., et al. 2013, The Messenger, 153, 6
Perlmutter, S., Aldering, G., Goldhaber, G., et al. 1999, ApJ, 517, 565
Persic, M., Salucci, P., & Stel, F. 1996, MNRAS, 281, 27
Persson, S. E., Madore, B. F., Krzemiński, W., et al. 2004, AJ, 128, 2239
Pettini, M., Steidel, C. C., Adelberger, K. L., Dickinson, M., & Giavalisco, M. 2000, ApJ, 528, 96
Pettini, M., Rix, S. A., Steidel, C. C., et al. 2002, ApJ, 569, 742

Phillips, J. I., Wheeler, C., Boylan-Kolchin, M., et al. 2014, MNRAS, 437, 1930
Pierce, M. 2014, in Thirty Meter Telescope Science Forum, 28
Pierpaoli, E. 2004, Physical Review Letters, 92, 031301
Planck Collaboration 2014a, A&A, 571, A1
Planck Collaboration 2014b, A&A, 571, A16
Pontoppidan, K. M., Salyk, C., Blake, G. A., & Käufl, H. U. 2010a, ApJ, 722, L173
Pontoppidan, K. M., Salyk, C., Blake, G. A., et al. 2010b, ApJ, 720, 887
Pontoppidan, K. M., Blake, G. A., & Smette, A. 2011, ApJ, 733, 84
Pontoppidan, K. M., Salyk, C., Bergin, E. A., et al. 2014, Protostars and Planets VI, 363
Pontzen, A., & Governato, F. 2014, Nature, 506, 171
Postman, M., Coe, D., Benítez, N., et al. 2012, ApJS, 199, 25
Prantzos, N. 2006, 'On the Early Chemical Evolution of the Milky Way', in Nuclei in the Cosmos IX, Proceedings of Science, IX, see *http://pos.sissa.it/archive/conferences/028/254/NIC-IX_254.pdf* (astro-ph/0612633)
Preibisch, T., Ratzka, T., Gehring, T., et al. 2011, A&A, 530, A40
Price-Whelan, A. M., Johnston, K. V., Sheffield, A. A., Laporte, C. F. P., & Sesar, B. 2015, MNRAS, 452, 676
Prieto, J. L., Garnavich, P. M., Phillips, M. M., et al. 2007, arXiv:0706.4088
Primas, F., Asplund, M., Nissen, P. E., & Hill, V. 2000, A&A, 364, L42
Prša, A., Robin, A., & Barclay, T. 2015, International Journal of Astrobiology, 14, 165
Quimby, R. M., Werner, M. C., Oguri, M., et al. 2013, ApJ, 768, L20
Quimby, R. M., Oguri, M., More, A., et al. 2014, Science, 344, 396
Quinn, S. N., White, R. J., Latham, D. W., et al. 2014, ApJ, 787, 27
Quintana, E. V., Adams, F. C., Lissauer, J. J., & Chambers, J. E. 2007, ApJ, 660, 807
Raghavan, D., McAlister, H. A., Henry, T. J., et al. 2010, ApJS, 190, 1
Rameau, J., Chauvin, G., Lagrange, A.-M., et al. 2013, ApJ, 779, L26
Randall, S. W., Markevitch, M., Clowe, D., Gonzalez, A. H., & Bradač, M. 2008, ApJ, 679, 1173
Rauer, H., Catala, C., Aerts, C., et al. 2014, Experimental Astronomy, 38, 249
Ravindranath, S., Ho, L. C., & Filippenko, A. V. 2002, ApJ, 566, 801
Reddy, B. E., Tomkin, J., Lambert, D. L., & Allende Prieto, C. 2003, MNRAS, 340, 304
Reddy, N. A., Steidel, C. C., Pettini, M., et al. 2008, ApJS, 175, 48
Reddy, N. A., Erb, D. K., Pettini, M., Steidel, C. C., & Shapley, A. E. 2010, ApJ, 712, 1070
Reddy, N. A., Pettini, M., Steidel, C. C., et al. 2012, ApJ, 754, 25
Rees, M. J. 1988, Nature, 333, 523
Regály, Z., Király, S., & Kiss, L. L. 2014, ApJ, 785, L31
Reines, A. E., Sivakoff, G. R., Johnson, K. E., & Brogan, C. L. 2011, Nature, 470, 66
Reinhold, E., Buning, R., Hollenstein, U., et al. 2006, Physical Review Letters, 96, 151101
Ribeiro, F. M. A., & Diaz, M. P. 2008, PASJ, 60, 327
Ribeiro, V. A. R. M., Darnley, M. J., Bode, M. F., et al. 2011, MNRAS, 412, 1701
Richard, J., Jauzac, M., Limousin, M., et al. 2014, MNRAS, 444, 268
Ricker, G. R., Winn, J. N., Vanderspek, R., et al. 2014, in Society of Photo-Optical Instrumentation Engineers (SPIE) Conference Series, 9143, 20
Riess, A. G., Filippenko, A. V., Challis, P., et al. 1998, AJ, 116, 1009
Riess, A. G., Macri, L., Casertano, S., et al. 2011, ApJ, 730, 119
Rix, S. A., Pettini, M., Leitherer, C., et al. 2004, ApJ, 615, 98
Roberge, A., Chen, C. H., Millan-Gabet, R., et al. 2012, PASP, 124, 799
Robertson, B. E., & Ellis, R. S. 2012, ApJ, 744, 95
Rodler, F., & López-Morales, M. 2014, ApJ, 781, 54
Roederer, I. U., Lawler, J. E., Sneden, C., et al. 2008, ApJ, 675, 723

Rubilar, G. F., & Eckart, A. 2001, A&A, 374, 95
Rudie, G. C., Steidel, C. C., Trainor, R. F., et al. 2012, ApJ, 750, 67
Ryan-Weber, E. V., Pettini, M., Madau, P., & Zych, B. J. 2009, MNRAS, 395, 1476
Sahu, D. K., Tanaka, M., Anupama, G. C., et al. 2008, ApJ, 680, 580
Sako, T., Sekiguchi, T., Sasaki, M., et al. 2008, Experimental Astronomy, 22, 51
Salaris, M., Groenewegen, M. A. T., & Weiss, A. 2000, A&A, 355, 299
Salyk, C., Pontoppidan, K. M., Blake, G. A., Najita, J. R., & Carr, J. S. 2011, ApJ, 731, 130
Sanders, D. B., Mazzarella, J. M., Kim, D.-C., Surace, J. A., & Soifer, B. T. 2003, AJ, 126, 1607
Santos, N. C., Israelian, G., & Mayor, M. 2004, A&A, 415, 1153
Sato, B., Ando, H., Kambe, E., et al. 2003, ApJ, 597, L157
Sayanagi, K. M., Dyudina, U. A., Ewald, S. P., Muro, G. D., & Ingersoll, A. P. 2014, Icarus, 229, 170
Scannapieco, E., Madau, P., Woosley, S., Heger, A., & Ferrara, A. 2005, ApJ, 633, 1031
Schaefer, G. H., Brummelaar, T. T., Gies, D. R., et al. 2014, Nature, 515, 234
Schaerer, D. 2002, A&A, 382, 28
Schawinski, K., Justham, S., Wolf, C., et al. 2008, Science, 321, 223
Schenker, M. A., Stark, D. P., Ellis, R. S., et al. 2012, ApJ, 744, 179
Schenker, M. A., Ellis, R. S., Konidaris, N. P., & Stark, D. P. 2014, ApJ, 795, 20
Schlaufman, K. C., Rockosi, C. M., Allende Prieto, C., et al. 2009, ApJ, 703, 2177
Schmidt, M. 1959, ApJ, 129, 243
Scholz, A., Jayawardhana, R., Muzic, K., et al. 2012, ApJ, 756, 24
Schulze, A., & Wisotzki, L. 2014, MNRAS, 438, 3422
Schwab, J., Podsiadlowski, P., & Rappaport, S. 2010, ApJ, 719, 722
Searle, L., & Zinn, R. 1978, ApJ, 225, 357
Seitenzahl, I. R., Cescutti, G., Röpke, F. K., Ruiter, A. J., & Pakmor, R. 2013, A&A, 559, L5
Selsis, F. 2002, in ESA Special Publication, 514, Earth-like Planets and Moons, eds. B. H. Foing, & B. Battrick (ESA-SP 514; Noordwijk: ESA)
Sesar, B. 2010, Mapping the Halo Substructure with SDSS RR Lyrae Stars, PhD thesis, University of Washington (*http://search.proquest.com/docview/814800641*)
Sesar, B., Grillmair, C. J., Cohen, J. G., et al. 2013, ApJ, 776, 26
Setiawan, J., Henning, T., Launhardt, R., et al. 2008, Nature, 451, 38
Shafter, A. W. 1997, ApJ, 487, 226
Shafter, A. W., Darnley, M. J., Hornoch, K., et al. 2011, ApJ, 734, 12
Shafter, A. W., Curtin, C., Pritchet, C. J., Bode, M. F., & Darnley, M. J. 2014, in Astronomical Society of the Pacific Conference Series, 490, Stell Novae: Past and Future Decades, eds. P. A. Woudt, & V. A. R. M. Ribeiro, 77
Shalima, P., Jithesh, V., Jeena, K., et al. 2013, MNRAS, 434, 639
Shao, L., & Wex, N. 2012, Classical and Quantum Gravity, 29, 215018
Shapley, A. E., Steidel, C. C., Pettini, M., & Adelberger, K. L. 2003, ApJ, 588, 65
Shen, K. J., Guillochon, J., & Foley, R. J. 2013, ApJ, 770, L35
Shen, Y. 2013, Bulletin of the Astronomical Society of India, 41, 61
Sheth, K., Regan, M. W., Scoville, N. Z., & Strubbe, L. E. 2003, ApJ, 592, L13
Sheth, K., Elmegreen, D. M., Elmegreen, B. G., et al. 2008, ApJ, 675, 1141
Sheth, K., Melbourne, J., Elmegreen, D. M., et al. 2012, ApJ, 758, 136
Shim, H., Chary, R.-R., Dickinson, M., et al. 2011, ApJ, 738, 69
Shore, S. N. 2013, A&A, 559, L7
Showman, A. P., Fortney, J. J., Lewis, N. K., & Shabram, M. 2013, ApJ, 762, 24
Shvartzvald, Y., & Maoz, D. 2012, MNRAS, 419, 3631
Sicilia-Aguilar, A., Henning, T., & Hartmann, L. W. 2010, ApJ, 710, 597

Simon, J. D., Gal-Yam, A., Penprase, B. E., et al. 2007, ApJ, 671, L25
Simon, J. D., Gal-Yam, A., Gnat, O., et al. 2009, ApJ, 702, 1157
Simpson, J. P., Colgan, S. W. J., Erickson, E. F., et al. 2002, ApJ, 574, 95
Sironi, L., & Spitkovsky, A. 2014, ApJ, 783, L21
Skemer, A. J., Hinz, P. M., Esposito, S., et al. 2012, ApJ, 753, 14
Skemer, A. J., Marley, M. S., Hinz, P. M., et al. 2014, ApJ, 792, 17
Skidmore, W., Horne, K., Pearson, K., et al. 2004, in Revista Mexicana de Astronomia y Astrofisica Conference Series, 20, Revista Mexicana de Astronomia y Astrofisica Conference Series, eds. G. Tovmassian, & E. Sion, 155
Skillman, E. D., & Kennicutt, Jr., R. C. 1993, ApJ, 411, 655
Slosar, A., Iršič, V., Kirkby, D., et al. 2013, J. Cosmol. Astropart. Phys., 4, 26
Sneden, C., McWilliam, A., Preston, G. W., et al. 1996, ApJ, 467, 819
Snellen, I. A. G., de Kok, R. J., le Poole, R., Brogi, M., & Birkby, J. 2013, ApJ, 764, 182
Snellen, I. A. G., Brandl, B. R., de Kok, R. J., et al. 2014, Nature, 509, 63
Snijders, L., Kewley, L. J., & van der Werf, P. P. 2007, ApJ, 669, 269
Soderberg, A. M., Berger, E., Page, K. L., et al. 2008, Nature, 453, 469
Sohn, S. T., Anderson, J., & van der Marel, R. P. 2012, ApJ, 753, 7
Sohn, S. T., Besla, G., van der Marel, R. P., et al. 2013, ApJ, 768, 139
Soltan, A. 1982, MNRAS, 200, 115
Somerville, R. S., Hopkins, P. F., Cox, T. J., Robertson, B. E., & Hernquist, L. 2008, MNRAS, 391, 481
Songaila, A., & Cowie, L. L. 2002, AJ, 123, 2183
Spencer, J. R., Stern, S. A., Cheng, A. F., et al. 2007, Science, 318, 240
Spergel, D., Gehrels, N., Breckinridge, J., et al. 2013, arXiv:1305.5422
Spite, F., & Spite, M. 1982, A&A, 115, 357
Spitler, L. R., Straatman, C. M. S., Labbé, I., et al. 2014, ApJ, 787, L36
Springel, V., Di Matteo, T., & Hernquist, L. 2005, MNRAS, 361, 776
Springel, V., Wang, J., Vogelsberger, M., et al. 2008, MNRAS, 391, 1685
Stark, D. P., Ellis, R. S., Chiu, K., Ouchi, M., & Bunker, A. 2010, MNRAS, 408, 1628
Stark, D. P., Richard, J., Siana, B., et al. 2014, MNRAS, 445, 3200
Starrfield, S., Iliadis, C., Timmes, F. X., et al. 2012, Bulletin of the Astronomical Society of India, 40, 419
Steidel, C. C., Erb, D. K., Shapley, A. E., et al. 2010, ApJ, 717, 289
Strigari, L. E., Bullock, J. S., & Kaplinghat, M. 2007, ApJ, 657, L1
Su, K. Y. L., Rieke, G. H., Stansberry, J. A., et al. 2006, ApJ, 653, 675
Sugai, H., Malkan, M. A., Ward, M. J., & McLean, I. S. 1997, ApJ, 481, 186
Sumi, T., Kamiya, K., Bennett, D. P., et al. 2011, Nature, 473, 349
Suyu, S. H., Auger, M. W., Hilbert, S., et al. 2013, ApJ, 766, 70
Suyu, S. H., Treu, T., Hilbert, S., et al. 2014, ApJ, 788, L35
Tan, J. C., Beltrán, M. T., Caselli, P., et al. 2014, Protostars and Planets VI, 149
Tanaka, H., Takeuchi, T., & Ward, W. R. 2002, ApJ, 565, 1257
Tanaka, M., Kodama, T., Arimoto, N., et al. 2005, MNRAS, 362, 268
Tanaka, M., & Hotokezaka, K. 2013, ApJ, 775, 113
Tanaka, M., Hotokezaka, K., Kyutoku, K., et al. 2014, ApJ, 780, 31
Tanvir, N. R., Fox, D. B., Levan, A. J., et al. 2009, Nature, 461, 1254
Tanvir, N. R., Levan, A. J., Fruchter, A. S., et al. 2013, Nature, 500, 547
Testi, L., Tan, J. C., & Palla, F. 2010, A&A, 522, A44
Tian, L., & Mao, S. 2012, MNRAS, 427, 2292
Tian, F., France, K., Linsky, J. L., Mauas, P. J. D., & Vieytes, M. C. 2014, Earth and Planetary Science Letters, 385, 22

Tissera, P. B., Beers, T. C., Carollo, D., & Scannapieco, C. 2014, MNRAS, 439, 3128
Tolstoy, E., Hill, V., & Tosi, M. 2009, ARA&A, 47, 371
Tominaga, N., Morokuma, T., Blinnikov, S. I., et al. 2011, ApJS, 193, 20
Tong, H., Xu, R.-X., & Song, L.-M. 2011, RAA (Research in Astronomy and Astrophysics), 11, 1371
Totani, T., Aoki, K., Hattori, T., et al. 2014, PASJ, 66, 63
Trainor, R., & Steidel, C. C. 2013, ApJ, 775, L3
Tran, K.-V. H., Franx, M., Illingworth, G., Kelson, D. D., & van Dokkum, P. 2003, ApJ, 599, 865
Tran, K.-V. H., Franx, M., Illingworth, G. D., et al. 2004, ApJ, 609, 683
Tremaine, S., Gebhardt, K., Bender, R., et al. 2002, ApJ, 574, 740
Treu, T., Ellis, R. S., Kneib, J.-P., et al. 2003, ApJ, 591, 53
Treu, T., Trenti, M., Stiavelli, M., Auger, M. W., & Bradley, L. D. 2012, ApJ, 747, 27
Treu, T., Schmidt, K. B., Trenti, M., Bradley, L. D., & Stiavelli, M. 2013a, ApJ, 775, L29
Treu, T., Marshall, P. J., Cyr-Racine, F.-Y., et al. 2013b, arXiv:1306.1272
Trilling, D. E., Stansberry, J. A., Stapelfeldt, K. R., et al. 2007, ApJ, 658, 1289
Trilling, D. E., Bryden, G., Beichman, C. A., et al. 2008, ApJ, 674, 1086
Trippe, S., Davies, R., Eisenhauer, F., et al. 2010, MNRAS, 402, 1126
Tully, R. B., & Fisher, J. R. 1977, A&A, 54, 661
Tully, R. B., & Pierce, M. J. 2000, ApJ, 533, 744
Tumlinson, J. 2007, ApJ, 664, L63
Turner, J. L., Beck, S. C., Benford, D. J., et al. 2015, Nature, 519, 331
Tzanavaris, P., Webb, J. K., Murphy, M. T., Flambaum, V. V., & Curran, S. J. 2005, Physical Review Letters, 95, 041301
U, V., Medling, A., Sanders, D., et al. 2013, ApJ, 775, 115
Udalski, A. 2009, in Astronomical Society of the Pacific Conference Series, 403, The Variable universe: A Celebration of Bohdan Paczynski, ed. K. Z. Stanek, 110
Udry, S., & Mayor, M. 2008, in Astronomical Society of the Pacific Conference Series, 398, Extreme Solar Systems, eds. D. Fischer, F. A. Rasio, S. E. Thorsett, & A. Wolszczan, 13
Uzan, J.-P. 2007, General Relativity and Gravitation, 39, 307
van den Bosch, R. C. E., Gebhardt, K., Gültekin, K., et al. 2012, Nature, 491, 729
van der Marel, R. P., & Guhathakurta, P. 2008, ApJ, 678, 187
van Dishoeck, E. F., Bergin, E. A., Lis, D. C., & Lunine, J. I. 2014, Protostars and Planets VI, 835
van Dokkum, P. G., & Franx, M. 2001, ApJ, 553, 90
van Velzen, S., Farrar, G. R., Gezari, S., et al. 2011, ApJ, 741, 73
Vassiliadis, E., & Wood, P. R. 1994, ApJS, 92, 125
Vegetti, S., Lagattuta, D. J., McKean, J. P., et al. 2012, Nature, 481, 341
Venemans, B. P., Findlay, J. R., Sutherland, W. J., et al. 2013, ApJ, 779, 24
Venn, K. A., Irwin, M., Shetrone, M. D., et al. 2004, AJ, 128, 1177
Viel, M., Lesgourgues, J., Haehnelt, M. G., Matarrese, S., & Riotto, A. 2005, Phys. Rev. D, 71, 063534
Viel, M., Lesgourgues, J., Haehnelt, M. G., Matarrese, S., & Riotto, A. 2006, Physical Review Letters, 97, 071301
Viel, M., Becker, G. D., Bolton, J. S., & Haehnelt, M. G. 2013, Phys. Rev. D, 88, 043502
Vigan, A., Patience, J., Marois, C., et al. 2012, A&A, 544, A9
Vikhlinin, A., Kravtsov, A. V., Burenin, R. A., et al. 2009, ApJ, 692, 1060
Volonteri, M., Lodato, G., & Natarajan, P. 2008, MNRAS, 383, 1079
Walker, M. G., Mateo, M., Olszewski, E. W., et al. 2009, ApJ, 704, 1274
Wang, X., Filippenko, A. V., Ganeshalingam, M., et al. 2009, ApJ, 699, L139
Wang, X., Wang, L., Filippenko, A. V., Zhang, T., & Zhao, X. 2013, Science, 340, 170
Watanabe, M., Nagata, T., Sato, S., Nakaya, H., & Hough, J. H. 2003, ApJ, 591, 714

Watkins, L. L., Evans, N. W., Belokurov, V., et al. 2009, MNRAS, 398, 1757
Webb, J. K., Flambaum, V. V., Churchill, C. W., Drinkwater, M. J., & Barrow, J. D. 1999, Physical Review Letters, 82, 884
Webb, J. K., & Wormleaton, I. 2001, PASA, 18, 252
Webb, J. R., Laurence, D., Bhatta, G., Dhalla, S. M., & Harrington, O. 2013, in American Astronomical Society Meeting Abstracts, 222, #215.03
Weinberg, N. N., Milosavljević, M., & Ghez, A. M. 2005, ApJ, 622, 878
Weinberg, D. H., Mortonson, M. J., Eisenstein, D. J., et al. 2013, Phys. Rep., 530, 87
Weinmann, S. M., Kauffmann, G., von der Linden, A., & De Lucia, G. 2010, MNRAS, 406, 2249
Weinmann, S. M., Lisker, T., Guo, Q., Meyer, H. T., & Janz, J. 2011, MNRAS, 416, 1197
Weinmann, S. M., Pasquali, A., Oppenheimer, B. D., et al. 2012, MNRAS, 426, 2797
Weinmann, S. M., van den Bosch, F. C., Yang, X., & Mo, H. J. 2006, MNRAS, 366, 2
Weisz, D. R., Dalcanton, J. J., Williams, B. F., et al. 2011, ApJ, 739, 5
Wetzel, A. R., Tinker, J. L., Conroy, C., & van den Bosch, F. C. 2013, MNRAS, 432, 336
Wheeler, C., Phillips, J. I., Cooper, M. C., Boylan-Kolchin, M., & Bullock, J. S. 2014, MNRAS, 442, 1396
Whitaker, K. E., van Dokkum, P. G., Brammer, G., et al. 2013, ApJ, 770, L39
Will, C. M. 2008, ApJ, 674, L25
Williams, R. 2013, AJ, 146, 55
Williams, C. C., Giavalisco, M., Cassata, P., et al. 2014, ApJ, 780, 1
Willott, C. J., Delorme, P., Omont, A., et al. 2007, AJ, 134, 2435
Willott, C. J., Delorme, P., Reylé, C., et al. 2010, AJ, 139, 906
Windmark, F., Lindegren, L., & Hobbs, D. 2011, A&A, 530, A76
Wisotzki, L., Koehler, T., Groote, D., & Reimers, D. 1996, A&AS, 115, 227
Woosley, S. E., & Weaver, T. A. 1995, ApJS, 101, 181
Woosley, S. E., & Bloom, J. S. 2006, ARA&A, 44, 507
Woudt, P. A., Steeghs, D., Karovska, M., et al. 2009, ApJ, 706, 738
Wright, S. A., Larkin, J. E., Law, D. R., et al. 2009, ApJ, 699, 421
Wright, S. A., Barton, E. J., Larkin, J. E., et al. 2010, in Society of Photo-Optical Instrumentation Engineers (SPIE) Conference Series, 7735, 7
Wu, Y.-Z., & Zhang, S.-N. 2013, MNRAS, 436, 934
Wuyts, S., Cox, T. J., Hayward, C. C., et al. 2010, ApJ, 722, 1666
Xu, Y., Newberg, H. J., Carlin, J. L., et al. 2015, ApJ, 801, 105
Young, S., Hough, J. H., Axon, D. J., Bailey, J. A., & Ward, M. J. 1995, MNRAS, 272, 513
Yuan, H.-B., Liu, X.-W., Huo, Z.-Y., et al. 2010, RAA (Research in Astronomy and Astrophysics), 10, 599
Yuan, H.-B., Liu, X.-W., Huo, Z.-Y., et al. 2015, MNRAS, 448, 855
Zahn, J.-P. 1992, A&A, 265, 115
Zaritsky, D., Hill, J. M., & Elston, R. 1990, AJ, 99, 1108
Zhang, X., Lu, Y., & Yu, Q. 2012, ApJ, 761, 5
Zhang, K., Pontoppidan, K. M., Salyk, C., & Blake, G. A. 2013, ApJ, 766, 82
Zhang, Y., Tan, J. C., & Hosokawa, T. 2014, ApJ, 788, 166
Zhao, G.-B., Li, B., & Koyama, K. 2011a, Phys. Rev. D, 83, 044007
Zhao, G.-B., Li, B., & Koyama, K. 2011b, Physical Review Letters, 107, 071303
Zhao, H., Peacock, J. A., & Li, B. 2013, Phys. Rev. D, 88, 043013
Zheng, W., Postman, M., Zitrin, A., et al. 2012, Nature, 489, 406
Zhou, Y., Herczeg, G. J., Kraus, A. L., Metchev, S., & Cruz, K. L. 2014, ApJ, 783, L17
Zhu, Q.-F., Lacy, J. H., Jaffe, D. T., Richter, M. J., & Greathouse, T. K. 2008, ApJS, 177, 584
Zhu, Z., Stone, J. M., Rafikov, R. R., & Bai, X.-n. 2014, ApJ, 785, 122
Zinnecker, H., & Yorke, H. W. 2007, ARA&A, 45, 481